Developmental and Evolutionary Consequences of Mutation to Transcription Factor Gli3

Jonathan Thomas Delafield Butt

Thesis submitted for the degree of Doctor of Philosophy
in the College of Medicine and Veterinary Medicine,
The University of Edinburgh

April 2003

Disclaimer

I am responsible for the experiments, preparations, analyses, and interpretations presented in this thesis. All work presented here was performed by myself, except the experiments in Part II of the thesis, which were performed in collaboration with Dr. Paulette Zaki, and the mathematics behind Figure 6.4, which were worked through with Mr. Jeffrey Butt. All work was supervised by Dr. David Price, and anatomical preparations were supervised by Prof. Matt Kaufman.

No part of this work has previously, or will be submitted for another degree.

Jonathan Butt, 18 April 2003

Abstract

Gli3 is a zinc-finger transcription factor homologous to the *Drosophila* segment polarity gene *Cubitus interruptus*. It is expressed early in mouse development in mesoderm and ectoderm, and continues to be expressed during organogenesis of brain, limb, and other structures. In mouse, mutation in *Gli3* produces the *extra-toe* (*Xt*) phenotype. In man, mutation in *GLI3* produces isolate pre- and post-axial polydactylys, and polydactyl complexes associated with craniofacial and neurological abnormalities (Greig's Cephalopolysyndactyly and Pallister-Hall syndrome). *Gli3* function has been well studied in the limb and spinal cord, but little is known about its mode of action in brain.

In this thesis, I examined the function of *Gli3* in murine forebrain development. I employed a primary culture technique to test the survival and gene expression characteristics of neocortical cells from *Xt/Xt*, *Xt/+*, and +/+ mice during mid-neurogenesis (embryonic days (E)14.5, 15.5, and 16.5). I found that the survival of neocortical cells is age and density dependent, and that *Xt/Xt* cells exhibit greater viability than their +/+ counterparts. Furthermore, I found that E16.5 *Xt/+* cells exhibit greater viability than +/+ cells, indicating that a murine *Xt/+* neurological phenotype might exist.

I tested *Xt/Xt* and *Xt/+* telencephalon for disruption to normal cell-type composition using markers of pre- and post-mitotic cell types. Acutely dissociated neocortical and ganglionic eminence cells from E14.5 and E15.5 embryos were immunoreacted with neuronal markers β-tubulin III and microtubule associated protein 2. Proliferating pre-mitotic cell types were labelled with RC2 and nestin. A further BrDU incorporation technique was employed to test for cells in active cell cycle. The results from these experiments suggest that the cell-type composition of *Xt/Xt*

neocortex does not differ significantly from wild-type proportions, though the proportion of cells undergoing proliferation may be increased.

In a separate line of investigation, I examined the neonatal skeleton of *Xt/Xt*, *Xt/+*, and +/+ in a mouse colony derived from the Jackson Laboratory. I found that the skeletal phenotypes were comparable to those reported on a similar *Xt* mouse strain from the M.R.C. Harwell Unit. Furthermore, I crossed the *Xt* mouse onto two other backgrounds and showed that the heterozygote limb phenotype is, in part, dependent on the background.

I also report on the transmission of the *Gli3*(-) allele from one generation to the next. In data collected over two years, I show that the mutant allele transmits at a greater rate than the wild-type allele. Moreover, I show that this behaviour is restricted to a subset of the mice, and in this subset the transmission rate of *Gli3*(-) is two-fold higher than would be expected by Mendelian genetics. I term this bizarre finding *Gli3*(-) positive transmission distortion, and refer to data on the transmission of human *GLI3* to suggest this phenomenon is occurring in other species.

Finally, I present an essay to suggest evolutionary consequences of mutation to *Gli3*. I present an overview of the *Gli3* gene and the effects of *Gli3*-mutation on its function as a regulator of tissue patterning in multiple systems. In conclusion, I attempt to place the role of *Gli3*, and mutations to *Gli3* in a framework that includes modern theories on evolution, and more mature theories on the role of genes and development in evolution.

Acknowledgements

There are a fair few people I would like to thank for their help in preparing the work presented in this thesis, for stimulating my interest in science and in life, and for helping me along in mine. Thanks to my Dad for poking me along since childhood, and to my Mum for her assured comfort and understanding. Thanks to my brother for his unending acceptance and steadfast support. Thanks to Dr. Julie Fisher for pulling me out of mid-west U.S.A. and for transplanting me happily into the heart of socialist Yorkshire. Thanks to Dr. Debra Gawler for my first introduction to research, and thanks also to you for failing to frighten me away. Thanks to those in the Edinburgh Neuroscience community for being educative and genuinely interesting. Thanks to Dr. David Price, of course, for believing in me, and for supporting my unusual interests. Thanks to all those in the laboratory, past and present. Thanks to Pundit and Dave and Julia and Tom, thanks to Theresa and Natasha and Guillermo and Jane. Thanks to Katy and Grace and Vivian. Thanks to the new recruits, the Molecular Biology Crew. Thanks of course to Dr. Paulette Zaki for leading me to the end, and for whisky-fueled inspiration.

Science is a necessary method for the collection of knowledge, and it does go about collecting a knowledge on the material of life, but I especially praise those that have managed to integrate an intuitive *understanding* of nature with a scientific *knowledge*. In this respect, my sincere gratitude for the work and writings of the late C.H. Waddington, your work has been as inspiring as it has insightful. And thanks also to Dr. Jamie Davies for keeping a broad theoretical view and lending this to his students, of which I was one. Thanks to Prof. Matt Kaufman for your friendship and your tutelage, my view of history and of medicine is forever marked by your words. Thanks also to others outside my immediate line of development. Thanks to Dr. Louise Milne and David Connearn for a steady supply of red wine and with it, a steady flow of information, from the heads of artists, to my boggled mind. Thanks

to Duncan for your help and humour in the animal house, and to Dr. Duncan MacGregor for remaining my friend through the bloody mire of Ph.D. life. Thanks also to all of those whom I am happy to call my friends. Thanks to those workers who helped to build The Forest, and to those with whom I spent some precious moments at Beltane. These two activities, above all, have helped me to live a balanced, constructive life during the dry business of science, and have coloured my life with art and simple human love. Oh, and thanks to Nick. Malaka!

Table of Contents

PART 4: DISCUSSION - GLI3 IN EVOLUTION AND DEVELOPMENT

Part 1

Introduction:
the Gli3 Gene and its Mutations in Mouse and Human

Chapter I: Introduction

Objectives

This thesis sets out to define the role of *Gli3* in development, with an eye on its evolutionary potential. *Gli3* is a gene that codes for a zinc-finger transcription factor. The focus of my work is on the function of *Gli3* in the development of the murine telencephalon during neurogenesis, and also on its function in the patterning of the distal limb, namely digit specification. I also include observations on the anatomy of the skeleton in the *Gli3*-mutant neonate, and on the transmission of the *Gli3*-mutant allele from one generation to the next. Together, my data suggest a developmental role for *Gli3* in dorsal telencephalon development and in distal limb development, and point to potential evolutionary consequences that arise from mutation to *Gli3*.

The Basics of Forebrain Development in Mouse

Early Development

The brain first emerges as a morphologically distinct feature on the seventh day of gestation, embryonic day 7 (E7) in mouse, when the rostral portion of the neural tube expands medio-laterally as the neural tube begins to close. Expansion is not uniform, however, and three distinct swellings can be recognised that will eventually form the fore-, mid-, and hindbrain regions. I will focus on the development of the forebrain, the rostral-most tissue, which gives rise to the hypothalamus, the retina of the eye, the diencephalon, and the telencephalon. The telencephalon is formed from the rostral-most tissue of the forebrain and develops into the cerebral cortex, the basal ganglia, and the olfactory bulbs. Early in development, the tissue architecture

and cell-type composition is seemingly homogenous, but the fate of cells composing these structures is already being determined by differential gene expression.

Morphogenesis of the forebrain requires a number of movements that take it from its linear anterio-posterior axis. First, at the late neural plate stage, the rostral-most swelling of the neural tube (the forebrain) expands rapidly and its dorsal portion folds over its ventral tissue in a movement known as the cephalic flexure. The dorsal position therefore becomes the most 'ventral' in relation to the rest of the embryo, and will continue to grow in a caudal 'ballooning' to form the telencephalic vesicles. The position that was formerly ventral will progress to form the diencephalon.

By E9.5, the forebrain is divided into morphologically distinct regions that will continue to expand to fill out their respective structures (Figure 1.1). The neocortex begins to balloon dorsally, laterally, and anteriorly, except for the dorsal midline that remains relatively stationary. This creates the formation of two distinct telencephalic hemispheres invaginated along the midline. The paleocortex and the ganglionic eminences grow with the neocortex but remain in a ventral position.

Signalling Centres

In the telencephalon, there are three known signalling centres (Figure 1.1), though I must emphasise that data on their position, function, and gene expression profiles is limited. The first is a band of ectodermal cells, called the anterior neural ridge (ANR), that lie along the rostral-most surface of the prosencephalon. The ANR in mouse is thought to serve a similar function to the row-1 cells in zebrafish, which are required for forebrain development (Houart et al., 1998). The ANR expresses *Fibroblast growth factor 8* (*FGF8*) which is a strong growth promoter (Grove et al., 1998; Shimamura and Rubenstein, 1997). Furthermore, its position at the rostral-most surface of the forebrain can be considered the leading edge as it grows

Figure 1.1 Morphogenesis (a) and signalling centres (b) of the forebrain. a) Schematic of forebrain morphogenesis from the time of rostral neural tube closure at E9, illustrating the emergence of the telencephalic lobes (arrowheads). At E9 they are not morphologically detectable. By E11, rapid expansion of the telencephalon has begun in all areas but the dorsal midline roofplate, which results in a relative invagination of the telencephalon at the dorsal midline, and apparent cleavage of the telencephalic lobes. The eye primordia and its development are noted (open arrows). b) Schematic of the known signalling centres at E11. Adjacent to the dorsal midline runs the cortical hem (brown region, pictured slightly too lateral) which expresses Wnt's and Bmp's. At the most rostral and ventral position lies the ANR (red region) which expresses FGF8, and just posterior lies the prechordal mesoderm (orange region) which is an area of strong *Shh* expression. b') Cross section of b showing medial and lateral ganglionic eminences (MGE and LGE, repsectively), the cortex (dark blue), and the cortical hem expressing Wnt's (light brown) and Bmp's (dark brown) which act on the adjacent cells of the cortex (dotted arrow). Cells of the ganglionic eminences later migrate into the cortex and are a source of potential patterning information. Sizes are not comparative. Adapted from Monuki and Walsh (2001).

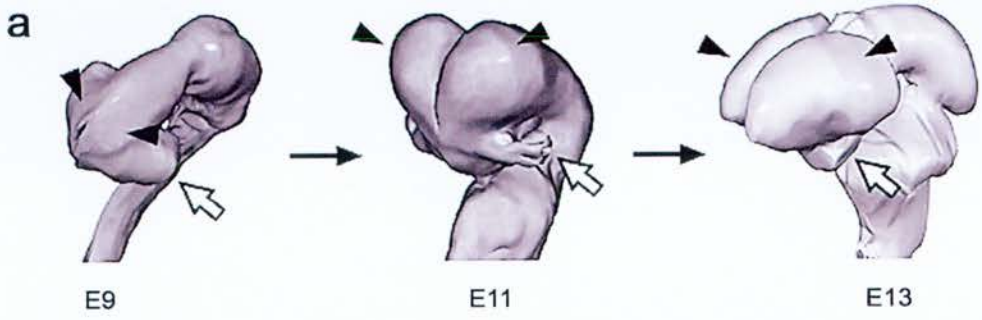
a
E9
E11
E13

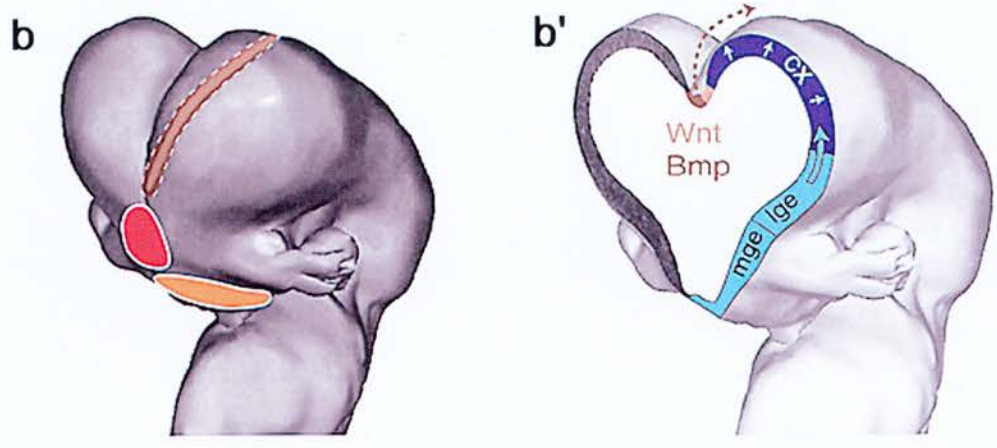
b
b'
CX
Wnt
Bmp
mge
lge

rostrally. This is comparable to the AER in the developing limb-bud which is the leading edge of the developing limb (see below).

The second signalling centre is the cortical hem. The cortical hem lies at the medial edge of the neocortex along the dorsal midline and connects the neocortex to the hippocampus. It expresses *Wnt*'s and *Bone morphogenic proteins* (*Bmp*'s) (Furuta et al., 1997; Grove et al., 1998; Grove et al., 1997) which are soluble signalling molecules thought to signal development of the neocortex, hippocampus, and choroid plexus. *Wnt*'s and *Bmp*'s are also known to influence the pattern of digit formation in the limb (for review see: Capdevila and Belmonte, 2001) and are thought to exert a similar influence on the forebrain.

The third early signalling centre is the *Sonic hedgehog* (*Shh*) expressing domain which runs underneath the ventral diencephalon in the area of the prechordal mesoderm, and then tangentially anterior through the middle of the diencephalon. *Shh* is small secreted protein which induces the formation of the ventral neural tube and ventral mid- and hind-brain structures from its expression in the notocord along the spine and prechordal mesoderm in the head. It is often disregarded as a signalling molecule important in telencephalon development because of the long-range action it would have to yield. However, there are two possibilities by which *Shh* might be important in the patterning of telencephalon. First, the *Shh* signal may initiate a signalling cascade which is passed on from cell to cell by other means, or it may in fact diffuse over long ranges itself (Zeng et al., 2001).

Thus, the developing telencephalon holds potentially three important signalling centres which emit signals to specify areal cell fate. Signalling centres fulfil an essential role in the development of pattern information by supplying fixed points of reference for the cells that are differentiating. It is known that cells of the telencephalon are plastic well into neurogenesis; Fishell (1995) transplanted embryonic striatal cells into the cortex and found they took on a cortical fate, and *vice versa*. Therefore positional information must be provided either by neighbouring cells through cell-cell contact, or by signalling molecules present in the

extracellular matrix. Either way, signalling centres must establish a fixed point by which other cells can interpret their relative position.

Patterning the Forebrain

Evidence suggests that the forebrain is patterned at the level of the VZ where the fate of asymmetrically divided cells is determined before migration. Data from cell lineage studies show that cortical progenitors in the VZ form large columnar 'clones' of neurones which become the glutamatergic projection neurones of the cortex (Mione et al., 1994; Tan et al., 1998; Ware et al., 1999). Glutamatergic projection neurones form the efferent output of the cortex and define areal-specific connectivity. Tangentially migrating neurones, which form large populations of GABAergic interneurones in the dorsal telencephalon, originate from the ganglionic eminences where they migrate over long distances to reach their position sometime after mid-neurogenesis (Tan et al., 1998; Ware et al., 1999). These cells are not thought to contribute to neocortical arealisation because areal pattern must first be defined before they can find their position. Thus, the primary regionalisation, or arealisation, or patterning of the neocortex arises from activity during the cell cycle of cortical progenitors in the VZ.

A number of transcription factors are expressed in the VZ of the neocortex, such as *Pax6*, *Foxg1*, *Emx1*, *Emx2*, *Arx*, *Tbr1*, and *Id2*, which form an overlapping, graded pattern of expression across the neocortex (for review see: Price and Willshaw, 2000). These transcription factors are thought to specify positional information in a quasi-combinatorial manner. If the neocortex is patterned at the level of the VZ, and the VZ is morphologically homogenous, then differences between different regions must come from differential gene expression, and the most likely candidates to influence cell fate are the transcription factors which influence the expression of other downstream genes.

Proliferation, Differentiation, Migration, and Death

Cells within the embryo can proliferate, differentiate, migrate, or die, with an alternative of remaining quiescent. These actions make up the process of morphogenesis. Proliferation increases the number of cells and potential mass of the tissue, differentiation produces the specialised cell types, and migration puts those cells into new positions. These are the progressive events of embryogenesis. The fourth possibility is considered a regressive event; it is cell death. Cell death is an active process in development and is thought to morphologically sculpt the tissues either by regulating cell number in a tissue, or by clearing entire areas of tissue, as in the interdigital sculpting of the limbs. The forebrain requires all four morphogenic events for normal development (Price and Willshaw, 2000).

The cerebral cortex develops from a proliferative sheet of neurepithelial cells which line the ventricular walls, collectively called the ventricular zone (VZ). These cells are attached with processes to the ventricular surface and to the distal edge of the VZ, and perform an interkinetic movement as they proceed through the cell cycle. The cell body moves from the ventricular surface to the distal surface during G1. At the distal surface, the cell duplicates its genome (S-phase) and begins to return to the ventricular wall (G2), where it undergoes mitosis (M-phase).

A dividing cell can either divide symmetrically, with its plane of division perpendicular to the ventricular wall, or asymmetrically, with its plane of division parallel to the ventricular wall. It is possible that symmetric and asymmetric divisions are the first visible sign that cell fate has been determined; there is evidence that a symmetrically dividing cell generates daughters, both of which will continue to cycle in the VZ, and an asymmetric division produces one post-mitotic differentiating cell which will leave the VZ and migrate to form the laminar layers, and another cell which will remain cycling in the VZ (Chenn and McConnell, 1995).

Post-mitotic cells which leave the VZ migrate through a cell-sparse region known as the intermediate zone to form the layers of the cortex. Lamination occurs in an inside-out manner where the earliest migrating cells form what will later be the deepest, most ventral layer of neurones. Subsequently, generated cells migrate through the earlier layers to form the more superficial layers.

Cell death as a morphogenic event in the developing telencephalon is thought to occur primarily in the VZ (Blaschke et al., 1996). The occurrence of cell death in the mitotic zone suggests that cell death may be intimately concerned with the cell differentiation (Blaschke et al., 1998). Furthermore, cell death in proliferating cells may work to regulate cell numbers by curbing the proliferative population.

The Basics of Limb Development

Early Development

Limb bud outgrowth begins when proliferating cells from the lateral plate mesoderm and somites accumulate in pockets under the flank epidermal tissue (at about E8). These proliferating cells express *FGF10* which denotes a future limb field and is thought to initiate the transformation of overlying ectoderm into a ridge of specialised cells called the apical ectodermal ridge (AER) (Ohuchi et al., 1997). Continued mesenchymal proliferation and formation of the AER creates the first morphological sign of the limb bud, a circular bulge of tissue which protrudes from the flank of the embryo. Two pairs of limb buds are formed along the anterio-posterior axis of the embryo, one set at an anterior pectoral position, and the other at a posterior pelvic position. In both sets the limb buds grow in symmetrical left-right opposition to each other and follow the same morphogenetic programme, with only minor differences in gene expression to specify fore- or hind-limb identity (Isaac et al., 1998).

Signalling Centres

The limb bud contains three major signalling centres (Figure 1.2). The first to be induced is the AER. The AER is the primary signalling centre for the developing limb and can be thought of as the leading edge which induces the mesenchyme cells underneath to proliferate in a maintained progress zone (PZ). When the AER is removed, limb bud outgrowth ceases. Furthermore, when the underlying mesenchyme is removed, the AER regresses. Thus, these two tissues are mutually supportive (Harrison, 1918; Saunders, 1948). The AER secretes FGF8 to maintain proliferation and developmental plasticity of the neighbouring progress zone mesenchyme cells, while these cells in turn secrete FGF10 to induce and maintain the AER (Mahmood et al., 1995; Ohuchi et al., 1997; Vogel et al., 1996). As well as directing the proximo-distal outgrowth of the limb bud, the AER is necessary for anterio-posterior and dorso-ventral patterning by supporting the transcription of morphogenic molecules.

The second signalling centre of the limb bud is an area of *Shh* expression that lies at the posterior edge of the AER. This domain is maintained through late limb development and is thought to induce the third signalling centre, the zone of polarising activity (ZPA). The ZPA is a powerful centre responsible for the secretion of *Bmp*'s and *FGF*'s. Together with *Shh*, these genes produce molecules which establish the anterio-posterior positional information required for proper differentiation of the progress zone cells as the limb bud progresses.

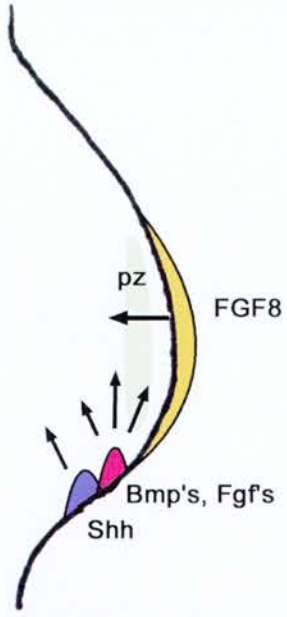

Figure 1.2 Signalling centres of the developing limb. The apical ectodermal ridge (coloured gold) expresses *FGF8*, which promotes rapid proliferation in the progress zone (pz). Progress zone cells are influenced by Shh, Bmp's, and other FGF's expressed in the ZPA and *Shh* expressing centres.

Patterning the Limb

The arrangement of signalling centres established in the early limb bud (AER, ZPA, and *Shh*) (Figure 1.2) is maintained at the distal edge as the limb bud grows distally. Cells of the PZ that have proliferated in response to cues from the AER, differentiate according to cues from the ZPA and *Shh*, and are left behind as the PZ continues to proliferate and push outwards. Cells left behind begin to condense and form the bones of the limb by first differentiating into chondroblasts, which will later ossify. The specification of bone type along the proximo-distal axis is also dependent on *Hoxa* and *Hoxd* gene cluster expression which determines stylopod (humerus or femur), zeugopod (radius and ulna or tibia and fibula), or autopod (carpals, metacarpals, and digits or tarsals, metatarsals, and digits) components (Nelson et al., 1996). *Hoxa* and *Hoxd* gene cluster expression is thought to be involved in anterio-posterior pattern formation, and is thought to be regulated by signals from *Shh* and the ZPA It is therefore intimately connected to the *Bmp* and *FGF* network which originates in the AER and ZPA.

Proliferation, Differentiation, Migration, and Death

As with most developmental systems, proliferation, differentiation, migration and cell death are the major events of morphogenesis. In the limb, primary proliferation is controlled first by the AER which induces rapid proliferation in the PZ. Cells from this zone condense to form the presumptive bones of the limb, under control of secreted factors from the ZPA and AER, and also from the Hox gene cluster expression pattern. Once the bone primordia are specified, proliferation continues in a secondary step at the bone growth plates. The growth plate is a region which contributes to the cartilaginous model of the bone, which then ossifies to form the bone proper.

Differentiation of each particular bone occurs as an interaction of the complex of morphogenic molecules, *i.e. Shh*, *FGF*'s, *Bmp*'s, and by *Hoxa* and *Hoxd* gene expression. Gross differentiation is made at the level of the PZ, which is able to specify the pattern, or position of the bones by determining the position of condensation, subsequent chondrogenesis, and finally ossification.

The effect of migration on pattern formation is generally regarded as secondary to the effects of proliferation and differentiation because, like the forebrain, migration events occur after the tissue has been patterned. In fact, the only migrating cells in the developing limb are those that invade the developing limb from the flank mesoderm to form the muscles. They attach themselves to the differentiated ossified cells which have already undergone the patterning processes of proliferation and differentiation.

The final and most intricate interplay of these process occurs in the patterning of the autopod (for review see: Sanz-Ezquerro and Tickle, 2001). The autopod is the distal-most compartment of the limb, and is also the most complex. It is composed of a delicate array of carpals (forelimb) and tarsals (hindlimb), which form the wrist and ankle bones, respectively. Articulating with the distal-most carpals and tarsals are five metacarpals and five metatarsals, which form the bones of the palm of the hand and the base of the foot, respectively. From these bones extend the pentadactyl array of phalanges, which make up the bones of the fingers and toes.

Patterning of the autopod is thought to be performed in much the same way as for the rest of the limb, though expression of the *Hoxa* and *Hoxd* gene clusters probably plays a more critical role. The first morphological signs of digit formation emerge around midgestation in mouse, when condensing chondroblasts are seen to be forming the skeletal components of the limb, including the digits and major carpal/tarsal bones. As development proceeds and the digits become more defined, *cell death* plays an important role in the sculpting of the digits, by clearing the interdigital areas of tissue.

Commonality in Forebrain and Limb Development

The developing brain and limb share some similarities that warrant their mutual investigation. (1) Central to this thesis, they are both major systems of *Gli3* expression (Schimmang et al., 1992). Concordantly, the brain and the limb are two major system perturbed in development when *Gli3* function is removed (Hui and Joyner, 1993; Johnson, 1967). (2) These structures are also the most distal from the centre-point of the early embryo, and are the regions of maximal *Gli3* expression during early neurulation (Schimmang et al., 1992). Beyond the late neurulation stage, increasing morphological complexity of the brain limits the correlation of the forebrain and limb, which I will describe below.

(3) The developing telencephalon and limb share a similar morphology at their earliest onset of organogenesis (E7.5 in brain and E9.5 in limb). The brain is first formed as a sheet of cells that 'bud' out from the anterior end of the neural tube, while the developing limb bud protrudes from the flank of the embryo. Both are symmetrical structures, both develop away from the centre-point as a semi-circular tissue.

Finally, (4) they share similar signalling centres, that express similar molecules, to presumably enable similar functions. The neural tissue grows laterally and anteriorly, induced by signals that emanate from the anterior neural ridge (ANR), namely *FGF8* (Shimamura and Rubenstein, 1997). The limb-bud also grows away from the embryonic centre-point laterally, while expanding anterio-posteriorly. Limb-bud out-growth is induced by the apical ectodermal ridge (AER), a region similar to the ANR in that it is the most distal rim of cells in a hemispherical 'ballooning' structure. The AER secretes the growth factor *FGF8*, which is required for normal limb development (Lewandoski et al., 2000; Moon and Capecchi, 2000; Sun et al., 2002). Furthermore, both the ANR and the AER are composed of cell types which differ from the underlying tissues they induce.

The developing forebrain and developing limb may share an additional signalling centre found at the medial edge of the ANR in brain, and at the posterior edge of the AER in limb. The signalling centre in the limb-bud is well characterised. It lies at a posterior distal position between a small centre of *Shh* expression and the posterior edge of the AER. It is called the zone of polarising activity (ZPA) because of the positional cues it exerts on the developing limb. In the developing telencephalon, the cortical hem lies adjacent to the medial edge of the ANR, between the future hippocampus and the neocortex. It has been suggested that the cortical hem acts as a signalling centre responsible for patterning the neocortex (Grove et al., 1998). Both the cortical hem and the ZPA express *Bmp's*, *Wnt's*, and *FGF's*, which are known to signal growth promotion and positional information (for review on the ZPA see: Capdevila and Belmonte, 2001) .

The Gli3 Gene

Gli3 Sequence and Homology

Gli3 is a gene that spans a genomic region of 275 kilobases on Chromosome 7 in man (7p13), and 260 kilobases on Chromosome 13 in mouse (13, cM Position 8.0) (Maynard et al., 2002). 5054 genomic base pairs in man (Ruppert et al., 1990) and 5113 genomic base pairs in mouse (Thien et al., 1996) are transcribed to produce Gli3 mRNA. *Homo. sapiens* and *Mus. musculus Gli3* share a high degree of homology (i) in the distribution of introns and exons, (ii) in the mRNA sequence (84% by BLASTn sequence alignment, NCBI), and thus (iii) amino acid sequence. In both man and mouse, *Gli3* produces a protein of 1,596 amino acids (Ruppert et al., 1990; Thien et al., 1996). Between them, 75% of the amino acid sequence is identical (BLASTp, NCBI).

By sequence homology, *Gli3* is a member of the *GLI*-Krüppel family of zinc-finger transcription factors (Kinzler et al., 1987; Kinzler et al., 1988). The first, now *GLI1*, was found in a search for amplified genes in human glioma, hence the name Gli, short for Glioma. *GLI2* and *GLI3* were found by homology to *GLI1* in later experiments (Ruppert et al., 1990). The three *Gli* genes share sequence homology, and therefore protein product homology, and are expressed in concert during mammalian embryogenesis (discussed below).

The mammalian *GLI*-Krüppel family shares homology with the *Drosophila* zinc-finger transcription factor *Cubitus interruptus (Ci)* (Ruppert et al., 1988) *Ci* is known to be involved in segment polarity specification and pattern formation (Hepker et al., 1997; Motzny and Holmgren, 1995). These two initial observation – discovery of *Gli1* expression in glioma and *Gli* gene family homology with *Ci* – produced the hypotheses that the *Gli* genes were involved in oncogenesis and embryonic pattern formation. I will focus solely on its importance as a developmental gene.

Little else is known about the specific functionality of the different domains of *Gli3* sequence, bar the presence of the five zinc-finger domains mentioned above. There is a suggestion that a phenotypic analysis of different genetic mutations in human and murine *Gli3* might yield some clue to the functional significance of parts of the gene.

The Expression Profile of Gli3

Gli3 is expressed throughout embryogenesis in the proliferating and differentiating cells of the mesoderm and ectoderm. Its expression is first detected at early neurulation (E7.5) in the mouse embryo, where it is found in broad domains. As development proceeds, Gli3 expression becomes more restricted. During

neurulation (E8.5), it is found in the migrating cranial mesenchyme which will form parts of the head and in the adjacent anterior central nervous system. In the caudal neural tube, which gives rise to the spinal cord, *Gli3* is expressed in the most dorsal domain, and is also expressed in the somites which flank the dorsal neural tube. *Gli3* expression is also found in the lateral flank mesoderm which will give rise to somatic structures later in development (Hui et al., 1994). As organogenesis commences, *Gli3* expression becomes more restricted and specific to proliferating and differentiating cells.

In the developing brain, *Gli3* expression is restricted to the proliferating neurepithelium of the forebrain, midbrain, and hindbrain (Figure 1.3). At E12.5 in the telencephalon, *Gli3* expression is found the dorsal neurepithelium, ventrally in the corpus striatum, and in the area of the developing olfactory bulbs. In the diencephalon, *Gli3* is found in the dorsal wall and the ventricular floor cells which will give rise to the thalamus. In the mesencephalon, *Gli3* expression is restricted to a region along the roof. In the rhombencephalon, expression is weaker than in the other expressing areas of the brain. Expression is also found in Rathke's pocket (presumptive pituitary gland) and in the anterior hypothalamus (Schimmang et al., 1992). *Gli3* expression is strongly expressed in these areas and is always restricted to the proliferative zones. After E15.5, *Gli3* expression in the telencephalon and mesencephalon diminishes in strength until it becomes undetectable around E17.5. In the hindbrain, its expression follows a similar temporal pattern of expression strength, but is set back by two to three days (Hui et al., 1994). The temporal expression strength of *Gli3* correlates with the peak in organogenesis of the telencephalon, mesencephalon, and rhombencephalon, the last of which lags behind the former by two to three days.

In the developing limb, *Gli3* is expressed in the proliferating and differentiating mesenchyme of the early limb bud. Expression is first noted at E7.5 in the lateral mesoderm before the protrusion of the limb bud proper (Hui et al., 1994; Zuniga and Zeller, 1999). As the limb-bud grows distally, *Gli3* expression becomes restricted to the anterior, proximal half of the tissue. It forms a graded expression pattern that

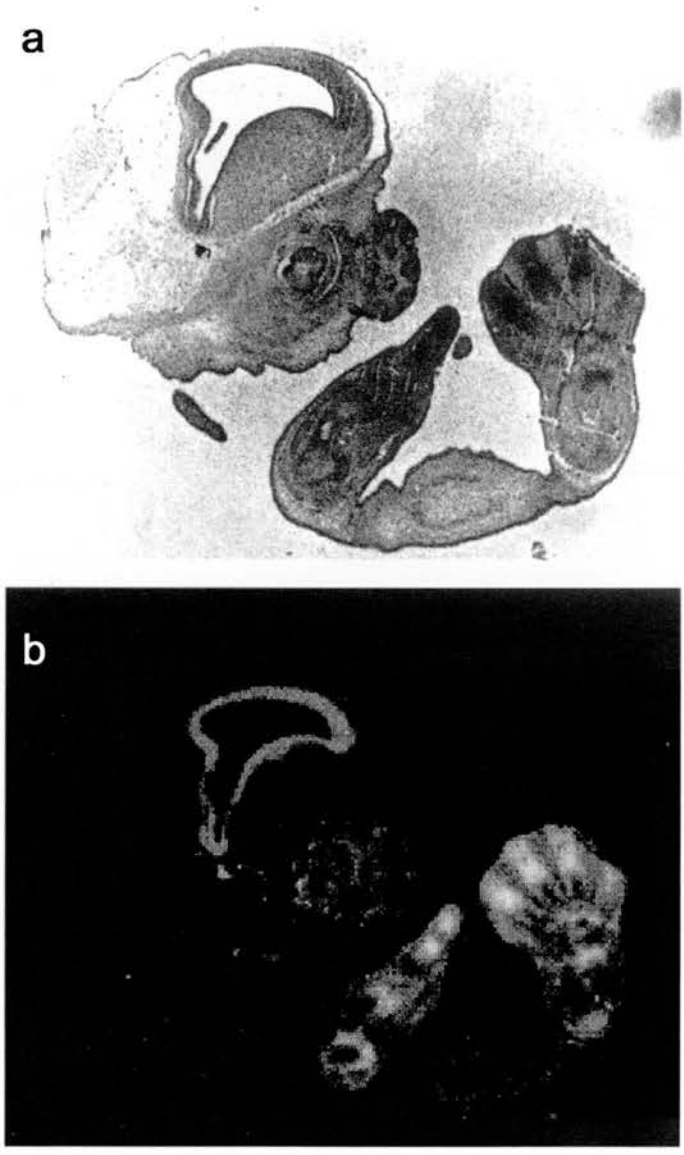

Figure 1.3 *In situ* hybridisation for *Gli3* mRNA in E12.5 mouse. (a) displays the transmitted image of the section and (b) the radioreactivity of the *Gli3* hybridisation. Note Gli3 is highly expressed in the developing distal limb, specifically in the developing digits. Gli3 is also expressed in the neurepithelium of the telencephalon and in the rostral facial mesenchyme. Adapted from Schimmang *et al.* (1994).

declines in strength from its anterior, proximal position, towards the zone of polarising activity (ZPA) at the distal posterior end, where *Shh* is expressed. At E12.5, *Gli3* expression becomes localised to the presumptive digits and is later found in high concentrations in the perichondrium of developing bones (Figure 1.3) (Schimmang et al., 1992).

Gli3 Function in the Cell

The function of Gli3 as a transcriptional regulator of downstream target genes has been modelled on data on from work on its *Drosophila* homologue, Ci (Figure 1.4). Ci is thought to mediate most of the transcriptional outputs of Hedgehog (Hh) signalling in the fly (for review see: Aza-Blanc and Kornberg, 1999) – Hh is the *Drosophila* homologue of the vertebrate Shh. Ci operates in a dual capacity. It is present as either a transcriptional activator or repressor of Hh target genes. In the absence of Hh signalling, a C-terminally truncated form of Ci (Ci^{75}) is produced by a protein kinase A (PKA)-mediated proteolysis, which localises the protein to the nucleus of the cell where it promotes transcriptional *repression* of Hh target genes. In the presence of Hh, cleavage of Ci is prevented, resulting in an accumulation of the full length form of Ci, Ci^{155}. Ci^{155} is predominantly found in the cytoplasm as part of a complex composed of the serine-theonine kinase Fused (Fu), the PEST domain protein Suppressor of Fused (Su(fu)), and the kinesin-related protein Costal2 (Cos2). This complex – Ci^{155}, Fu, Su(fu), and Cos2 – is anchored to microtubules by Cos2 and dissociates from the microtubules upon phosphorylation of Cos2 in response to Hh signalling. Microtubule association is thought to promote Ci^{155} proteolysis to produce the repressor form Ci^{75}. Dissociation from the microtubule may prevent proteolysis of Ci^{155} and promote its transformation into an active, labile form that can act as a transcriptional *activator*, Ci^{act}, of downstream genes.

Gli3 is thought to act in a similar manner to Ci, and there is some evidence to show this. However, the mechanism of Shh signal transduction in vertebrates is more

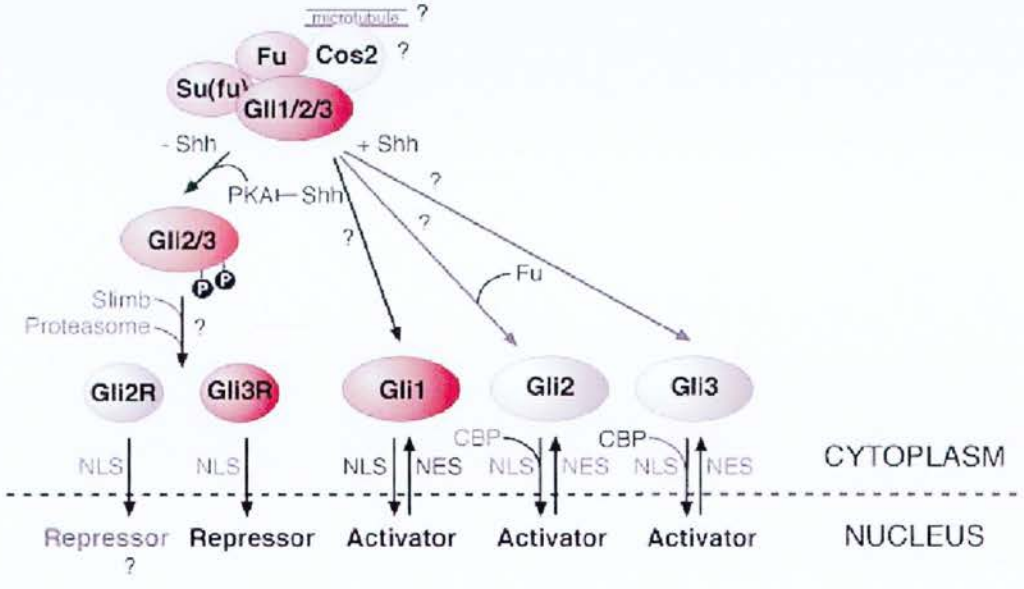

Figure 1.4 Schematic of the proposed model of Gli function in the cell. Those elements that are known are presented in red, while those that are hypothetical, based on evidence of Ci in *Drosophila*, are presented in grey. The nucleocytoplasmic distribution of the Ci^{act} is controlled by nulear import (NLS) and export singals (NES), the same may be true of the Gli proteins. All three Gli proteins can interact with homologues of Su(fu) and Fu. In absence of Shh, Gli3 is processed to generate a repressor form similar to Ci^{75}, Gli3R. Endogenous Gli2-repressor forms have not been identified. Shh inhibits the PKA-mediated phosphorylation and proteolysis of Gli3. The full length forms of Gli1, Gli2, and Gli3 could function as activators. Similar to Ci, Gli1 contains a nuclear export signals (NES) that mediate its nuclear export. Fu positively modulates Gli2 activity. Full length Gli3 has been shown to interact with the transcriptional coactivator Creb Binding Protein (CBP). From Koebernick and Pieler (2002).

complex than that of Hh in fly. It is thought that a single shared ancestral gene has evolved and diverged down the vertebrate lineage to present us with three modern *Ci* homologues, *Gli1*, *Gli2*, and *Gli3*. The function of the *Gli* family as a whole, is thought to be similar to that of Ci in that each protein displays positive and negative functions that correlate with a full-length, predominantly cytoplasmic, and a truncated, predominantly nuclear form (for review see: Koebernick and Pieler, 2002).

In the case of Gli3, there are five major pieces of evidence that support its role as a bipotential transducer of Shh signalling. (1) Full length Gli3 protein has been found to drive the expression of a reporter gene downstream of the *Gli1* and Patched (Ptc) promoters (Dai et al., 1999; Shin et al., 1999), suggesting that it acts as a positive activator of gene expression. (2) Naturally truncated Gli3 is found at high levels in anterior regions of chick limb bud devoid of Shh, and at lower levels in the posterior, Shh rich regions (Wang et al., 2000). (3) Shh inhibits Gli3 proteolysis in chick limb bud cell culture (Wang et al., 2000). (4) Artificially truncated Gli3 appears to act as a repressor form in cultured cells and *Xenopus* embryos; it is present only in the nucleus and represses expression of *Ptc1* and *N-tubulin* (Altaba, 1999; Shin et al., 1999). (5) Gli3 is proteolysed to repress Hh expression in *Drosophila* (Aza-Blanc et al., 2000).

The Gli3 Mutant Mice

One of the most useful approaches in determining the function of a gene is through the use of mice mutant for the gene in question. In a mouse with a single gene deletion, the effect of that gene on development can be discerned by defining the changes that occur to normal development.

There are three mouse lines with spontaneous mutations to *Gli3*, each with a different mutation (Figure 1.5) but a similar phenotype. The *Extra-toes* Harwell (Xt^H) strain was the first to be discovered, and was reported by Johnson in 1967. The *Extra-toes* Jackson (Xt^J) line arose from a spontaneous mutation at the Jackson Laboratory in Bar Harbor, U.S.A. The third is the Polydactyly-Nagoya line (Xt^{Pdn}), which arose spontaneously during a breeding programme (Hayasaka et al 1980).

The Xt^H and Xt^J strains display very similar mutant phenotypes (see below) that are thought to be caused by functionally null mutations, though their genetic mutations are quite different (Figure 1.5). The Xt^H mutation is a deletion of all coding sequence 5' of the zinc-finger domains (Vortkamp et al., 1992). This is thought to remove the promotor region and possibly affect an additional gene 5' of *Gli3*. The Xt^J mutation is the result of a 51.5 k.b. deletion of sequence 3' of the first zinc-finger (Maynard et al., 2002). This effectively removes the zinc-fingers and forms a fusion protein with sequence 3' of *Gli3*. Thus, it is possible that another gene 3' of *Gli3* is also affected in the Xt^J mutation. The Xt^{Pdn} strain displays a milder phenotype, and is caused by the ectopic integration of a retrotransposon into the region just 5' of the zinc-finger domains (Thien and Ruther 1999); the more mild phenotype of the Xt^{Pdn} mouse is due to the production of at least some normal mRNA.

In this thesis I use the Xt^J line for all experimental work, and refer to the Xt^H and Xt^{Pdn} mice for comparative analyses. Unless otherwise stated, *Xt* refers unspecifically to the Xt^J and Xt^H strains.

Overview of the Xt Mouse

The *Xt* mouse was first reported in a comprehensive survey of its developmental anatomy (Johnson, 1967). Evidence that *Gli3* was the gene implicated in this mutant strain came some years later (Vortkamp et al., 1992). Reference to its normal expression profile (Hui et al., 1994; Schimmang et al., 1992) correlates with the

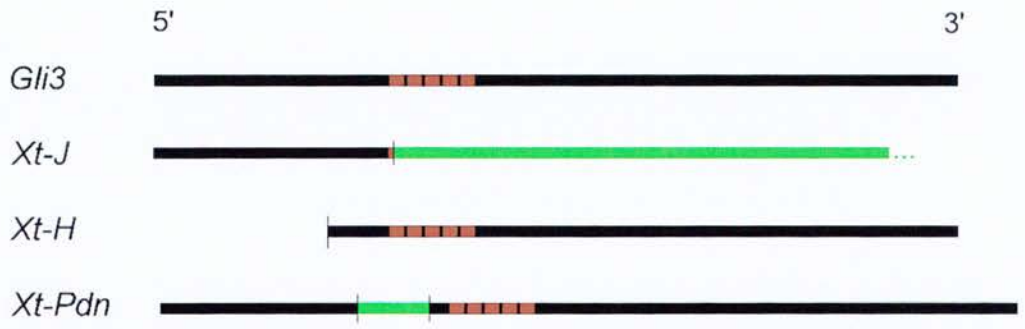

Figure 1.5 Schematic of murine *Gli3* and it's known mutations. *Gli3* is translated into a 1,596 amino acid protein, represented in this figure by the first horizontal bar. The five zinc-finger domains are its most prominent feature and begin at about 400 amino acids from the 5' end (brown shading). In the Xt^{J} mutation, a genomic deletion removes 51.5 k.b. 3' of exon 9 (the start of the code for the zinc-fingers). This effectively deletes the zinc-fingers and creates a fusion transcript with another exon downstream of the *Gli3* gene (green bar). The Xt^{H} mutation is a deletion of all *Gli3* sequence 5' of the zinc-finger domains. This is thought to delete the promoter and prevent transcription. In the Xt^{Pdn} mutation, a retrotransposon has been inserted into the *Gli3* gene just 5' of the first zinc-finger domain (green), leading to different splice variants, some of which may be functional.

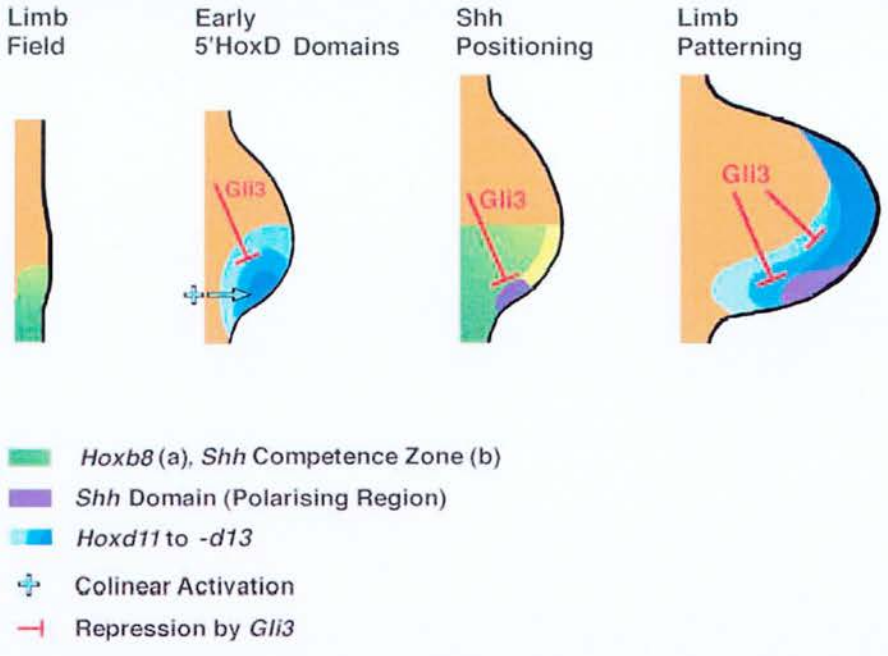

Figure 1.7 The role of *Gli3* in limb development. *Gli3* is part of a genetic network regulating establishment and propagation fo posterior limb-bud identity. Gli3 (orange domains) polarises the early limb field and establishes the early 5'HoxD domains (blue domains). Distribution of Gli3 helps to establish the *Shh* expressing domain, and later Hoxd domains. In the homozygote *Gli3*-mutant, the *Hoxd13* and *Hoxa11* expression expand anteriorly (not shown). Adapted from Zuniga and Zeller (1999).

Figure 1.6 Histology of the developing *+/+* and *Xt/Xt* brain. (A) and (C), sagittal sections of E9.5 and E11.5 wild-type brains compared to (B) and (D) *Xt/Xt* brains of the same age. Note the thickness of the neurepithelium is reduced in the *Xt/Xt* brains, and the rostral facial mesenchyme is also reduced. The dorsal portion of the telencephalon is reduced in size and the di-telencephalic junction (arrowhead) does not form. Dorsal diencephalic structures, the pineal gland (pin) and the posterior commissure (pc), develop normally. (E) and (G), transverse sections of E11.5 and E13.5 wild-type brains compared to (F) and (H) *Xt/Xt* brains of the same age. Note the telencephalic roof-plate (trp) and the adjacent medial cortex (ctx) do not invaginate. Medial structures of the telencephalon such as the hippocampus (hip) and choroid plexus (chp), and cortical hem (adjacent to the hippocampus) fail to form. Ventral (I) and dorsal (J) transverse sections of comparable areas in *Xt/Xt* and *+/+* brain. Note the invaginated cortical neurepithelium (asterisk) of the neocortex and reduction of the ventricular lumen. Note also that medial structures are absent in *Xt/Xt* brain. In the ventral position, the putative cortical tissue is noted (double asterisk). AH, Ammon's horn; BNmntl basal nuclei mantle layer; BNsbv, basal nuclei subventricular zone; CTX, cortex; DG, dentrate gyrus; DOR, dorsal thalamus; HY, hypothalamus; int, internal capsule; ppa, paraphysial arch; PR, palladial (cortical) ridge; SR, striatal ridge. Adapted from Theil et al. (1999).

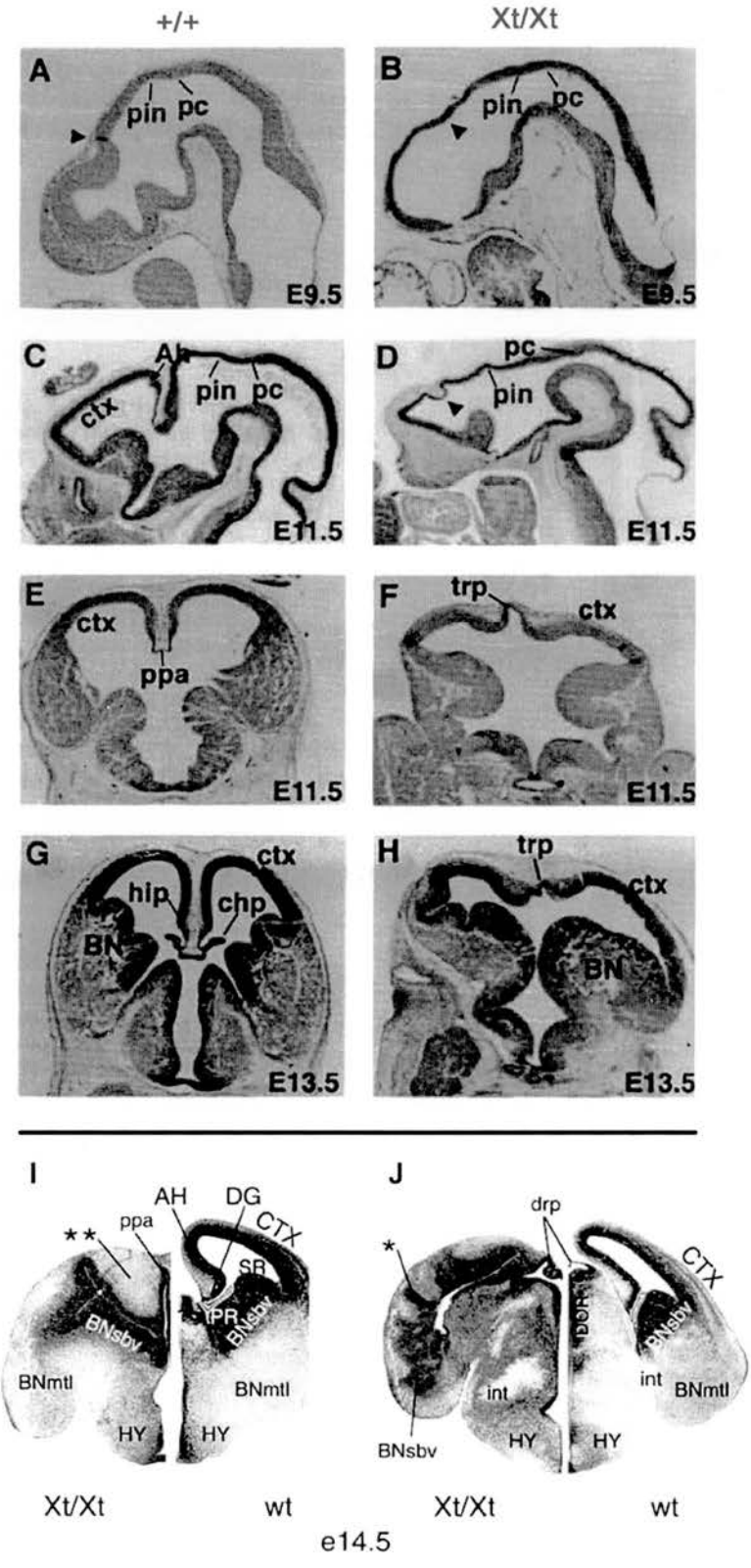
+/+
Xt/Xt
A
pin
pc
E9.5
B
pin
pc
E9.5
C
AH
pin
pc
ctx
E11.5
D
pc
pin
E11.5
E
ctx
ppa
E11.5
F
trp
ctx
E11.5
G
ctx
hip
chp
BN
E13.5
H
trp
ctx
BN
E13.5
I
AH
DG
ppa
CTX
SB
IPR
BNsbv
BNsbv
BNmtl
BNmtl
HY
HY
Xt/Xt
wt
J
drp
CTX
BNsbv
int
int
BNmtl
BNsbv
HY
HY
Xt/Xt
wt
e14.5

phenotypes observed in the homozygous mutant mouse (*Xt/Xt*), where those tissues that normally express *Gli3* are also the tissues that become disrupted during development. The heterozygote mutant (Xt^{H}/+) on the other hand, is believed to develop normally in all respects bar the formation of an additional digit, or digit-like appendage on either the fore- or hindlimbs.

The phenotypes of the *Xt/Xt* embryo are severe and affect multiple systems, including skeletogenesis, neurogenesis, some visceral organogenesis, and development of the gonads. Homozygotes die at birth or are resorbed during gestation. The most prominent defects are found in the distal limb, in rostral portion of the head, including the forebrain and eye, along the ventral midline of thorax where sternal fusion fails, and along the midline of the visceral ectoderm where an umbilical hernia develops. I will discuss the abnormalities found in the limb and in the brain below.

The Basics of Xt/Xt Forebrain Development

Gli3 is expressed in presumptive fore-, mid-, and hind-brain regions from the late neural plate stage (E7.5), and continues to be expressed in the major proliferating regions of the forebrain, *i.e.* the ventricular zone, until neurogenesis is complete (E17.5). The *Xt/Xt* brain fails to develop normally just after the onset of normal *Gli3* expression; this is first detectable at E9.5. As development proceeds, the brain phenotype becomes more and more severe as initial malformations are continually compounded with later ones. The result is a grossly abnormal brain where "a single glance is enough" (Johnson, 1967) to distinguish it from the wild-type brain.

Phenotypic development of the *Xt/Xt* forebrain is first noted at E9.5 when the mutant telencephalon appears retarded due to its abnormally thin epithelial wall, lack of morphological landmarks, and lack of surrounding mesenchymal tissue (Figure 1.6). At E11.5, the cortical primordium is present but morphogenesis is defective and the

medial telencephalic structures which would normally give rise to the hippocampus and choroid plexus have not formed, including the cortical hem. The telencephalic roof plate, which would normally invaginate and form these medial structures, appears to evaginate instead. Continued maldevelopment of midline structures results in the failure of cleavage formation between the two telencephalic lobes. By E13.5, the ventricular layer of the cortex appears folded and poorly differentiated into its cortical layers. Furthermore, there is loss of the dorsal-ventral telencephalic boundary which is normally well-defined in the wild-type animal. At E14.5 and later stages, the ventral telencephalon is seen to progress into the dorsal domain. The olfactory bulbs have also failed to form and instead small nodes of tissue are seen protruding from the normally smooth cortical lobes. By E18.5, the telencephalic lobes form one complete structure lacking any midline component, including the hippocampus and corpus callosum. Neocortical lamination has failed and the VZ has convoluted to form finger-like projections into the more superficial layer of tissue. The ventral telencephalon has moved into space where the neocortex would normally lie, and appears to have squashed the cortex into a confused mass of tissue. (Johnson, 1967; Theil *et al.*, 1999; and my own observations).

The Basics of Xt/+ and Xt/Xt Limb Development

In the heterozygote, the gross development of the limb appears normal, but with the addition of an extra digit or digit-like appendage on the fore and hind limbs. There is no observable difference in the levels of *Gli3* expressed, nor is the expression of the major genes (*e.g. Shh*, *FGF8*, and *BMP4*) disturbed (Zuniga and Zeller, 1999; Zuniga et al., 1997). The extranumerary digit can form on the postaxial (anterior) or preaxial (posterior) border, though in the mouse it is most common on the anterior (Johnson, 1967).

The homozygote limb exhibits extreme abnormalities. Extranumerary anterior digits are formed to give a total of six to eight digits (though in some cases more have been

noted), and digit I (the thumb) is absent. The carpals (wrist bones) and tarsals (ankle bones) are duplicated, and hemimelia (partial formation) of the radius and tibia may occur (Johnson, 1967). These phenotypes are extremely variable.

Gli3 is thought to polarise the limb bud by acting in opposition to *Shh* signalling (Figure 1.7). *Gli3* is expressed in the anterior portion of the developing limb bud – it is this region that is disturbed in the *Xt/Xt* mouse – and *Shh* is expressed in a discrete domain at the posterior. Genetic studies on limb development have shown that *Gli3* acts to inhibit *Shh* expression and *Shh* expression acts to inhibit *Gli3* expression (Welscher et al., 2002). Furthermore, the expression of 5' *Homeobox* (*Hox*) gene clusters are affected in the *Xt/Xt* mouse, suggesting that *Gli3* might act to control their expression pattern (Zuniga and Zeller, 1999). *Hox* gene clusters are known to pattern the skeletal elements of the limb. Thus, *Gli3* appears to act in concert with *Shh* to polarise the limb bud through mutual antagonism and through the control the *Gli3* mediated downstream gene expression, which (directly or indirectly) affects *Hox* gene expression.

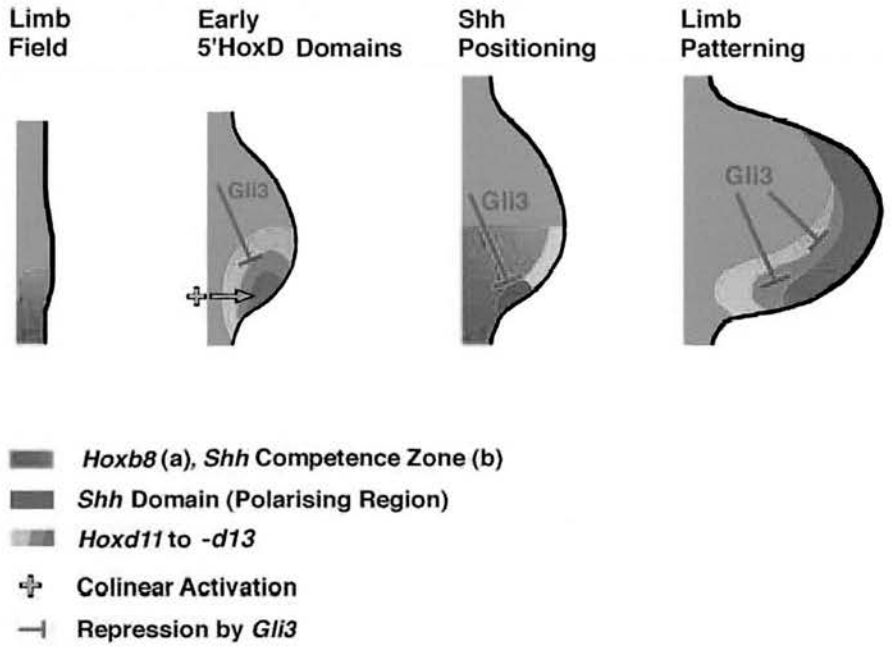

Figure 1.7 The role of *Gli3* in limb development. *Gli3* is part of a genetic network regulating establishment and propagation fo posterior limb-bud identity. Gli3 (orange domains) polarises the early limb field and establishes the early 5'HoxD domains (blue domains). Distribution of Gli3 helps to establish the *Shh* expressing domain, and later Hoxd domains. In the homozygote *Gli3*-mutant, the *Hoxd13* and *Hoxa11* expression expand anteriorly (not shown). Adapted from Zuniga and Zeller (1999).

Chapter II: *GLI3* in Humans

Introduction

This chapter presents the human disorders associated with mutation to the human *GLI3* gene. As in the mouse, mutation to *GLI3* invariably produces polydactyly. Unlike the mouse however, human heterozygote *GLI3*-mutants may also display associated cranio-facial and/or neurological defects. *GLI3* mutations are responsible for two forms of simple polydactyles in human, post- and pre-axial polydactyly. Additionally, the complex phenotypes of Grieg's Cephalopolysyndactyly (GCPS) and Pallister-Hall Syndrome (PHS) are also found to be caused by *GLI3* mutation.

Knowledge of the human phenotypes produced by *GLI3* mutation becomes important later in this thesis when I present data on the phenotypic abnormalities in the *Gli3* heterozygote mouse (Part 3). Furthermore, genetic and phenotypic analysis of human *GLI3* mutants offers some insight into possible activator and repressor functions of the Gli3 protein.

Polydactyly has a long and rich history. The earliest reported case is found in the Old Testament, "And there was again war at Gath, where there was a man of great stature, who had six fingers on each hand, and six toes on each foot, twenty-four in number; and he also was descended from the giants" (Samuel 2 21:20 and Chronicles 1 20:7). Three footprint petroglyphs with postaxial polydactyly, probably of the pedunculated postminimi type were found by Castilla *et.al.* (1973) at Talampaya, La Rioja, Argentina, a ceremonial valley from Aguada Culture, A.D. 1000. The Mayans have also recorded polydactyls in their bas-relief carvings at Pelenque, Mexico (Freidel, 1992), another religious site. The Italian Renaissance painter Raphael depicted several religious figures with polydactyly including Jesus (The Transfiguration, Roma, Pinacoteca Vaticana), John the Baptist (La Belle Jardinière, 1507), and St. Joseph (Marriage of the Virgin, 1504). Raphael also depicted a

number of babies with postaxial polydactyly (Madonna in the Meadow, Wien, Kunsthistorisches Museum; La Madonna del Pez, Madrid, Museo del Prado; and Madonna e Bambino, 15th C fresco). Mother to Queen Elizabeth I, Ann Boleyn had six fingers on each hand, and the American pop icon, Marilyn Monroe, supposedly had six toes before the extranumerary digit was removed. Closer to home, Charles Darwin's friend and publisher, John Murray, was also of six fingers and had an imposing personality to match. He published "*The Origin of the Species*".

The most historic case of polydactyly was reported by Maupertius, the pre-Mendelian geneticist. In 1751, Pierre-Louis Moreau de Maupertius (1698-1759) wrote "*Systeme de la nature*", containing theoretical speculations on the nature of biparental heredity, based on his careful study of the occurrence of polydactyly in several generations of a Berlin family. He demonstrated that polydactyly could be transmitted by either the male or female parent, and he explained the trait as the result of a mutation in the 'hereditary particles' possessed by them. He thus provided the first scientifically accurate record of the transmission of a dominant hereditary trait in humans, which preceded Mendel's well-cited work on peas.

Isolate and Complex Polydactylys Caused by *GLI3* Mutations

Five specific human conditions have been shown to be caused by mutations in *GLI3* explicitly. Medical diagnosis of these conditions, and their characterisation as one syndrome or another is not an easy task because these conditions are extremely variable and the syndromes are not always well defined. There are other conditions with no known aetiology that may also be due to mutations in *GLI3*, but express one or two other phenotypes which place them outside the realm of the *GLI3* related pathologies. A similar situation arises with conditions known to be *GLI3* dependent; an individual may express one or all of the symptoms of a disorder to any degree of severity. Variability of expression is an important feature of both the murine and human *GLI3*-mutant phenotypes.

A lack of formalised criteria that define syndromes hinders the collation of human data on the complex polydactylys. Formalised criteria are necessary to clarify the aetiology of individual cases, and also to allow disparate data sources separated by culture, language, and time to be pooled by researchers. The following description of the *GLI3*-related polydactylys works to help clarify the present diagnostic criteria for these conditions.

Postaxial Polydactyly (PAP)

Overview of PAP

Postaxial polydactyly is the commonest of the *GLI3* related pathologies. It is found across the globe in all races. Frequency estimates calculate PAP incidence at 3.6 per 1000 live births in Africans, and 0.3 per 1000 in Caucasians (Frazier, 1960). The estimate is considerably higher in Nigeria at 22.78 per 1000 live births (Scott-Emuakpor and Madueke, 1976). It is generally considered that PAP expression contains a strong racial component and is far more common in Africans than in Caucasians.

Clinical Diagnosis of PAP

PAP is easy to recognise as the sixth digit is always noticeable. PAP is frequently observed as part of a complex of phenotypes. In these cases, the diagnosis is characterised by the syndrome, not by PAP. A proper diagnosis of PAP is unassociated with any other abnormality.

PAP is subdivided into two types, A and B (Figures 2.1 and 2.2). A third type A/B designates the occurrence of both types, or intermediate phenotypes on the same

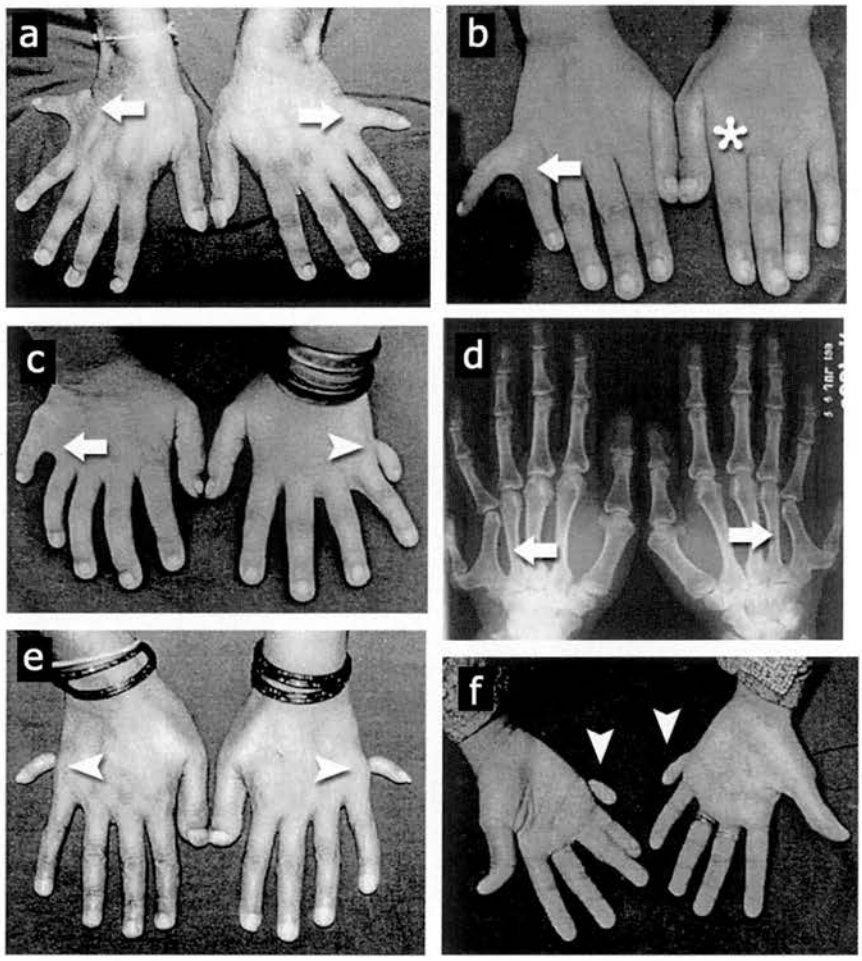

Figure 2.1 Postaxial polydactyly. Examples of hand postaxial polydactyly type A (arrows), B (arrowheads), and A/B of the hands: (a) bilateral PAP type A; (b) unilateral PAP type A, note the broad thumb of the unaffected hand (star); (c) PAP type A/B; (d) radiograph of PAP type A to show bifurcated metacarpal I; (e) PAP type B; and (f) another PAP type B. Adapted from Temtamy and McKusick (1978).

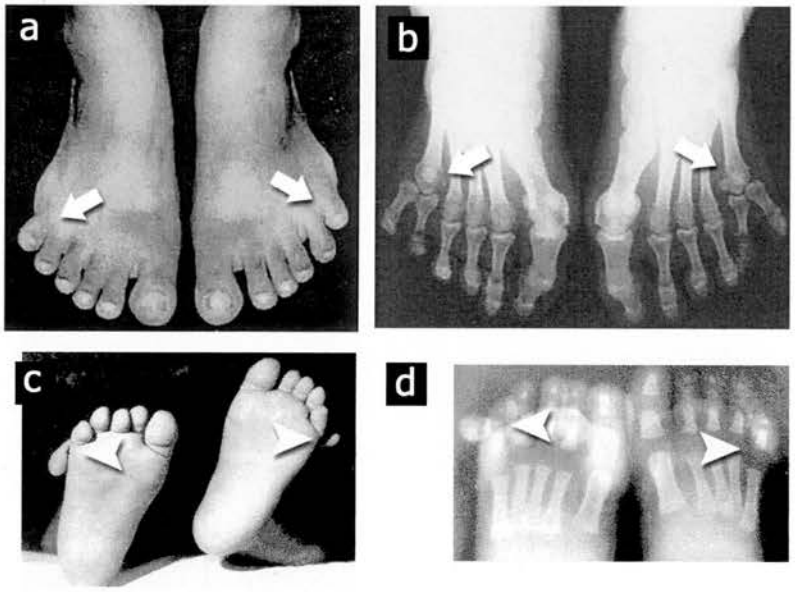

Figure 2.2 Postaxial Polydactyly. Examples of feet postaxial polydactyly types A (arrows) and B (arrowheads): (a) PAP type A; (b) PAP type A roentgenogram; (c) newborn PAP type B; and (d) roentgenogram of (c) PAP type B. Adapted from Temtamy and McKusick (1978).

individual. Sverdrup (1922) delineated the two PAP types now commonly adhered to (Temtamy and McKusick, 1978):

PAP Type A: fully developed extra digits which articulate to a carpal or metacarpal.

PAP Type B: rudimentary extra digits, or pedunculated postminimi which may or may not contain a skeletal element, and which does not articulate with the carpals or metacarpals.

PAP Type A/B: the presence of both type A and type B on the same individual.

There is some discrepancy over PAP type classification when it comes to the feet. Sverdrup's initial classification only considered the hands; the feet did not play a role in type determination. Temtamy and McKusick (1978) also do not make this distinction (their book is on hand abnormalities, not feet). Some reports are more specific and separately classify hands and feet. And individual with type A hands and type B feet would thus be a type A/B individual. This system seems most complete.

Aetiology of PAP

It has been suggested that type A and type B have two different aetiologies (Castilla et al., 1973; Sverdrup, 1922; Woolf and Myrianthopoulos, 1973). The main differences to suggest this theory are: (1) higher incidence of type B in blacks; (2) a greater penetrance in familial cases for type A (0.68) than for type B (0.43); (3) limb preference (left hand only) for type B only; (4) a fourfold higher mutation rate estimate for type B (29.5×10^{-5}) than for type A (7.5×10^{-5}) (Temtamy and McKusick, 1978).

Interestingly, the only gene found to be responsible for PAP is *Gli3*. The gene was found to have different mutations in different families. Families with both type A , A/B, and B had heterozygous mutations in *Gli3*. Thus, heterozygosity of *GLI3* can cause PAP type A or type B.

The important question is, do mutations in other genes cause PAP? As yet, there is no evidence to suggest they do. Could mutations in Gli3 be responsible for all PAP pedigrees? This is unlikely unless *GLI3* exhibits recessive heredity in some races. The effect of genetic background, *i.e.* race in human or strain in mouse, will be discussed in Chapter VII. A mutant *Gli3* allele is commonly thought be expressed in an autosomal dominant manner, though some evidence suggests otherwise (Johnson, 1967). A considerable number of human cases exhibit recessive heredity. This either means that other recessive gene mutations can cause PAP, or that *Gli3*(-) has the potential to transmit in a recessive manner.

Preaxial Polydactyly (PPD) type IV

Overview of PPD

Preaxial polydactyly is thought to be rarer than postaxial polydactyly (Castilla et al., 1973; Woolf and Myrianthopoulos, 1973). Preaxial polydactyly does not exhibit a race bias (Woolf and Myrianthopoulos, 1973). Unlike postaxial polydactyly, PPD has received relatively little attention in the literature.

Clinical Diagnosis of PPD

PPD is broken down into four groups (Temtamy and McKusick, 1978):

PPD Type I: Thumb polydactyly (Figure 2.3). This takes various forms which represent different grades of severity. The mildest form consists merely of

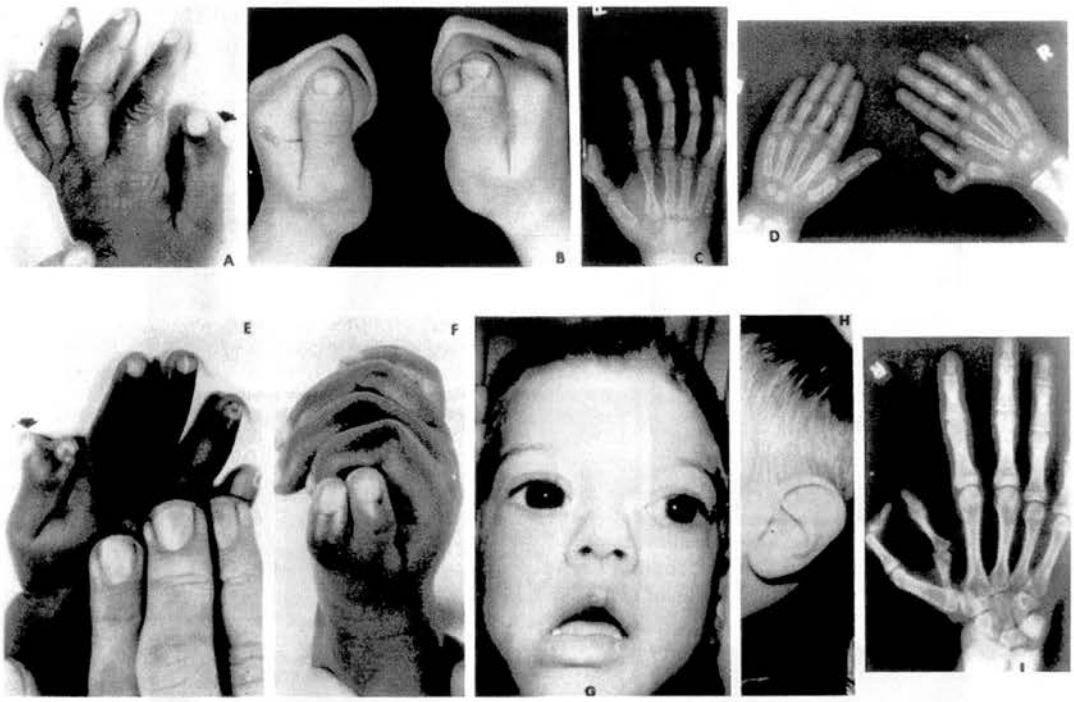

Figure 2.3 Preaxial polydactyly type I. Examples to illustrate the variation in thumb polydactyly. A) left hand with extra nail (arrow). B) Asymmetric PPD-I. C) Radiograph showing rudimentary extra phalanx (arrow). D) Radiograph of a proband, note thickened 1st metacarpal and duplication of the proximal and terminal phalanges of the right thumb. E) Duplication of thumb nail only (c.f. Xt mouse). F) Full duplication of thumb. G) Face of a proband with PPD-I, note the congenital buphthalmos (*cf. Xt* eye phenotypes). H) Left ear of proband in (G) showing malformed helix. I)Radiograph showing full digit I duplication. Reproduced from Temtamy and McKusick, 1978.

broadness of the tip of the distal phalanx, sometimes with a vague suggestion of bifurcation of the tip. A more advanced form shows a distinct bifurcation of the tip with duplication of the distal two-thirds of the phalanx but with a common base (*cf. Xt/+* mouse phenotype, Chapter V). A still more severe degree is duplication of the distal phalanx or both phalanges which attach to the proximal phalanx and/or articulate with the metacarpal head. The most severe form is a duplication of the whole thumb comprising a metacarpal and two phalanges. However, the second thumb is usually rudimentary and receives no tendinous attachment (*c.f.* PAP-B). Aetiology is unclear. Some reported cases are sporadic, others dominantly inherited.

PPD Type II: Polydactyly of triphalangeal thumb (Figures 2.4 and 2.5). This is a rare malformation. In most cases, the extranumerary thumb is opposable and possesses a normal metacarpal. Inheritance is considered autosomal dominant.

PPD Type III: Polydactyly of an digit II (Figure 2.5). This is an unusual form. The thumb is replaced by one or two triphalangeal digits. The extra digits are usually opposable, and share the same configuration as the other digits II-V.

PPD Type IV: Polysyndactyly (Figure 2.6). In the hand, the thumb shows only the mildest degree of duplication, which takes the form of a broad, bifid or radially deviated distal phalanx, and syndactyly of various degrees affects the 3rd and 4th fingers. Hand involvement is variable and mild, in contrast to a constant and near uniform foot phenotype. In the foot, the 1st or 2nd toes are duplicated, and syndactyly affects all the toes, but maximally the 2nd and 3rd. Some families have shown associated postaxial polydactyly in the hands and feet, usually of the pedunculated postminimi type, but also strong type A. PPD type IV is regarded as autosomal dominant with full penetrance.

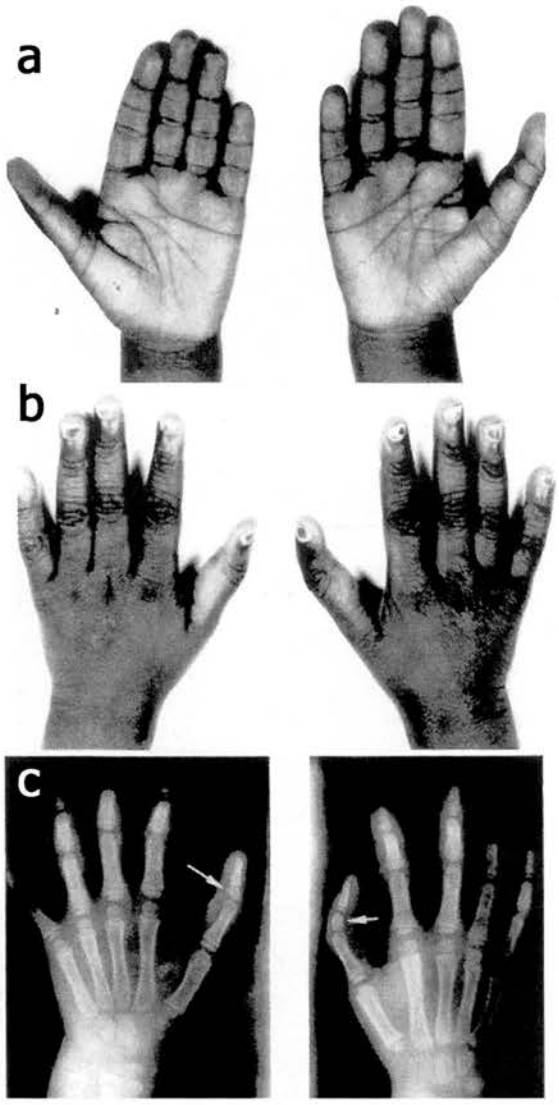

Figure 2.4 Preaxial polydactyly type II. Triphalangeal thumb without extra digit duplication. (a, b) hands of an example proband, (c) radiograph of proband hands. Adapted from Temtamy and McKusic, 1978.

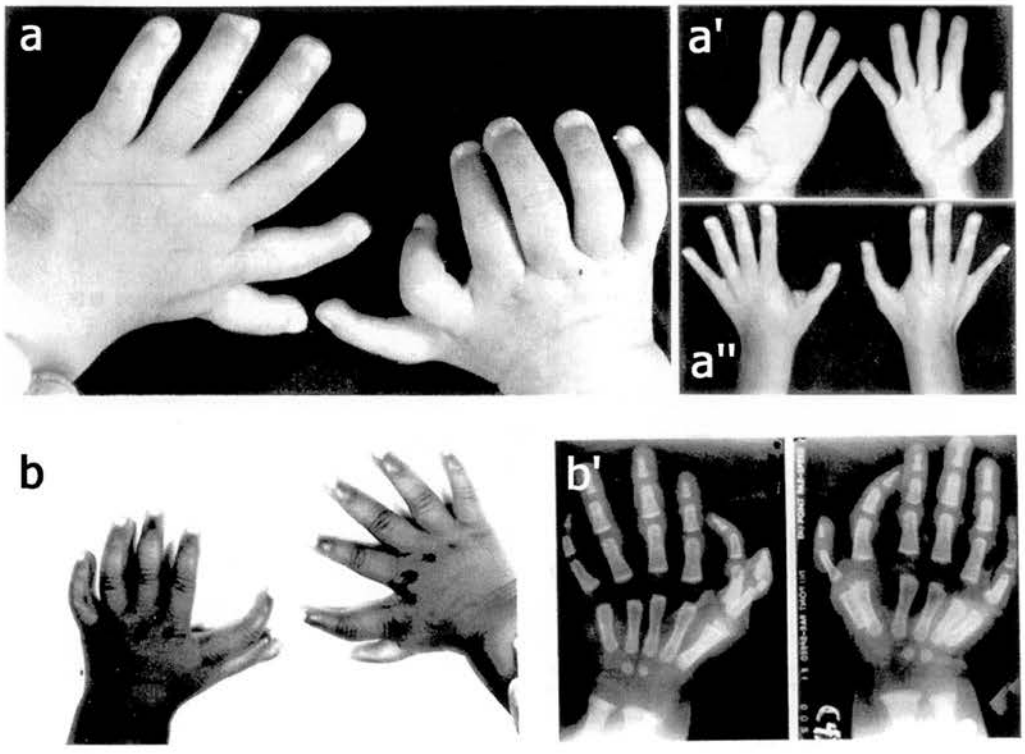

Figure 2.5 Preaxial polydactyly types II and III. (a) preaxial polydactyly type II, duplicated triphalangeal thumb. (a' and a") shows hands after surgery to remove extranumerary digit. (b) preaxial polydactyly type III, duplication of the index finger. Adapted from Temtamy and McKusick, 1978.

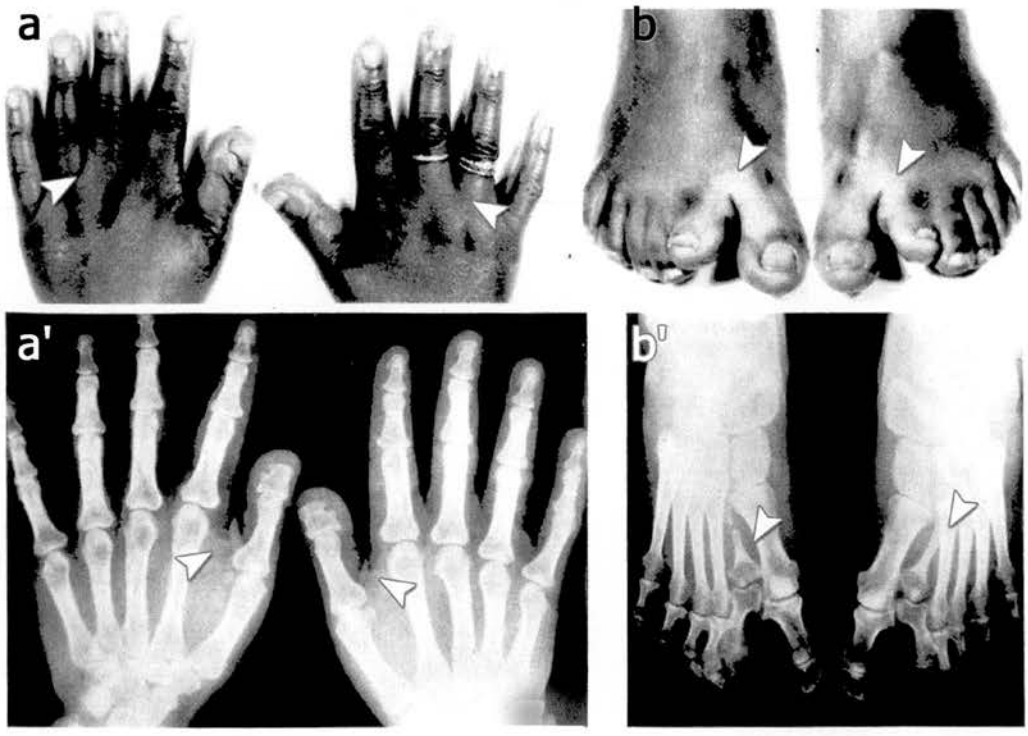

Figure 2.6 Preaxial polydactyly type IV. Hands (a) and feet (b) of a PPD-IV proband showing the characteristic polysyndactyly of digit I and extranumerary digit. In the hands there is mild syndactyly between digits III and IV ((a), arrowheads), and broad thumbs ((a'), arrowheads). The feet display mild soft tissue syndactyly between all toes, and an extranumerary digit inserted between toes II and III. Adapted from Temtamy and McKusick, 1978.

Aetiology of PPD

Mutations in *GLI3* have been shown in some families with PPD type IV (Radhakrishna et al., 1999), the polysyndactyly type also commonly associated with GCPS (see below). Thus, the *GLI3* mutant phenotype in this case completely lacks the craniofacial and somatic affects found in GCPS. No other gene has been implicated in any other form of PPD, though a recent report suggests a novel gene, *Lmbr1*, resides at the same locus as *GLI3* and may be affected in the polydactyl *Hemimelic extra-toes* mouse (*Hx*), and some human PPD types (Clark et al., 2000).

Greig's Cephalopolysyndactyly Syndrome (GCPS)

Overview of GCPS

Greig's Cephalopolysyndactyly Syndrome is the name for the syndrome that follows the seminal publication, Oxycephaly, by David M. Greig in 1926. In this paper, Greig attempted to clarify a group of syndromes which fell under one blanket term 'oxycephaly'[1]. He proposed that oxycephalics fall into one of three categories: true oxycephaly, delayed oxycephaly, and false oxycephaly. The category known today as GCPS is the *true oxycephaly* and is defined as "recognisable at birth and due to general craniofacial synostosis[2]. It is often associated with syndactyly and allied deformities of the extremities.

Delayed oxycephaly, on the other hand, is mild, never congenital, and never leads to exaggerated deformity. Similarly, false oxycephaly is restricted to a localised cranial synostosis, is not congenital, and is not associated with other deformities." (Greig,

---

[1] Oxycephaly is derived from the Greek roots: όευς - sharp, pointed, keen; and κεφαλή - the head. The term 'oxycephalids' was first used in 1830 by the naturalist H. Milne Edwards to designate the genus *Hyperiidea curvicornia* crustaceans where the head is more or less produced into a rostrum.

[2] Synostosis is characterised by complete fusion of the cranial plates and lack of cranial sutures, and can be caused by mutation to *MSX2* (Wilkie and Wall, 1996)

1926) Thus, Greig worked to define and classify the congenital, developmental pathology which today bears his name.

Greig's paper is interesting from a humanist's standpoint. He heavily criticises the behaviour and manner of his patients in a way that would be unacceptable today. In Greig's case, the human element is overwhelmingly clear and the ethics of the day can be seen to echo through his words. However, his descriptive method does not detract from the anatomical precision of his work, but rather adds a behavioural and social aspect. Because those reading this thesis are unlikely to read Greig's work, I must enclose an excerpt from his paper. It is Case Study III of a true oxycephalic:

> Terence M., aged 45 yeas at the time of his death, was a native of Ireland but immigrated to this country when a boy. He was the only member of his family who had any congenital physical defect. His cranial and other deformities had been noticed at birth. He was a Roman Catholic, and had (like his brothers and sisters) received no scholastic training. He could neither read nor write and was uncertain of his age. He was not married. He conformed to the rest of his family by being large in body and of strong physique. Tall, broad-shouldered, ungainly, and slouching, his deformed head and unshapely features rendered him a terrifying object. His employment was the manufacture of stools which he hawked from door to door. He was much given to intemperance and sexual immorality. It was difficult to appraise his mental condition. He refused to have his photograph taken; was sulky, sullen, and stupid, and objected to any examination whatever. His death was due to exposure at the end of a prolonged drunken debauch.
>
> His forehead was flat and almost vertical and his skull culminated in a rounded beak at the bregma. His occiput was small and flattened; the glabella poorly developed and there were no superciliary arches. The eyeballs seemed large as they projected from his shallow orbits and there was a lateral strabismus. The nose was fairly developed but deflected to the left. His upper teeth were irregular and closely packed, his palate was narrow and high, and the pharynx small. Respiration was mostly oral. The mandible, at least towards the chin, was disproportionately large. During life, his protuberant eyes, misshapen head, his open mouth, and his brutish lower jaw, with his head held forwards low between his shoulders, and with his slouching gait making his large arms depend in front of his body, he had a repulsively anthropoid appearance.
>
> There was no internal abnormality except for a large ideal diverticulum. He had symmetrical webbing of his fingers and toes, and in the thumbs and great toes an

interphalangeal (intradigital) synostosis, through in none of the fingers was there an interdigital osseous fusion.

The late Professor A.M. Paterson pronounced the brain to be in no way abnormal except in its shape, that is, it had been moulded to the cranial cavity. [a series of morphometrics follow]

Greig is particularly passionate about this case. It is patent they had a personal clash at some point, probably during an early examination. This man must have irked Greig. He was perhaps the antithesis of Greig: uneducated, poor, inarticulate, uncivilised, and an Irish Roman Catholic. Greig, on the other hand, was a proud Scot, Edinburgh educated, a fellow of the Royal College of Surgeons of Edinburgh and the Royal Society of Edinburgh. Greig was the high and mighty medical establishment, Terence M. was the lowest proletariat. Greig, it seems, took his revenge on the poor fellow, *post mortem*.

Scientifically speaking, Case III is interesting because if it is due to mutation in *GLI3*, it arose from a spontaneous mutation in a germline cell of the parent (neither parents were affected). This produced a severe craniofacial phenotype, but a very mild digit phenotype (fusion of digit I phalanges). It is also possible that other skeletal defects were present. These can be inferred by his posture and gait, which are abnormal and suggestive of subtle limb and spine defects. Such subtle abnormalities will later be shown to be present in the *Gli3*$^{-/+}$ mouse skeleton. This is an important consideration, because subtle changes to the human limb have not been reported in the medical literature, but may be a feature of GCPS or other pathologies caused by *GLI3* mutation (*cf.* murine deltoid tuberosity morphology, Chapter V). Since Greig's initial paper, the exact criteria to diagnose GCPS have been vague and have not well defined. A modern diagnostic criteria is given below (according to this definition, Case III does not have GCPS).

Clinical Diagnosis of GCPS

No published, peer-reviewed phenotypic diagnostic criteria exist for GCPS. The most comprehensive, and to my mind most accurate criteria have been proposed by Leslie G. Biesecker[3] of the National Institute of Health (U.S.A.) and published on the GeneReviews website[4]. According to his report, the major phenotypes for GCPS are:

(1) Polydactyly. Preaxial polydactyly must be present on at least one limb, or digit I must be abnormally wide. Other limbs may display preaxial polydactyly or postaxial polydactyly (PAP) type A, B, or A/B.

(2) Syndactyly. In the hands, syndactyly is present between fingers III and IV, and occasionally I and II. In the feet, syndactyly is present between toes I, II, and III.

(3) Ocular hypertelorism. The interpupillary distance must be greater than the upper limit of normal for age. Increased inner canthal[5] distance (i.e. telecanthus, or apparent hypertelorism) may also be present but is not as distinctive as interpupillary distance. A broad nasal bridge is often associated with these phenotypes.

(4) Macrocephaly. Occipitofrontal circumference must be greater than the upper limit of the 97th centile for age and sex. Some patients may have high, prominent, or bossed forehead.

A diagnosis for GCPS is established if the proband has (1) preaxial polydactyly on at least one limb, (2) syndactyly of toes I-III or fingers III-IV, (3) hypertelorism, and (4) macrocephaly.

---

[3] Biesecker is a clinical geneticist and has worked extensively with international symposia to help define and clarify Gli3 related and other congenital pathologies. Leslie is a man.

[4] GeneReviews is funded by the N.I.H. and supported by the University of Washington, Seattle. It is at present the most accurate and up-to-date database for clinical diagnostic criteria. Access to the database is membership based, which is free for the time being. Biesecker's GCPS diagnotistic criteria are published here, http://www.geneclinics.org/.

Biesecker adds that a first degree relative may be diagnosed if he or she displays pre or postaxial polydactyly with or without the associated craniofacial defects. This is an important note: it suggests the same genetic mutation may be expressed either as GCPS or a simple polydactyly. This issue will be discussed in detail later.

Aetiology of GCPS

A large amount of work has been published on the genetic mutations found in GCPS patients. It is now clear that a number of different mutations to the *GLI3* allele can cause the GCPS phenotype. Known mutations range from large deletions or translocations along the 7p chromosome[6] (OMIM #175700), which can affect multiple alleles, to single point mutations found only in Gli3. Deletions and translocations are known to also affect EGFR, INHBA, IGFBP1, and PGAM2 in some GCPS probands. In all cases, *GLI3* has been suggested or shown to be affected. The more refined point mutations in *GLI3*, on the other hand, demonstrate that (presumptive) haploinsufficiency of GLI3 alone is sufficient to cause GCPS.

Pallister-Hall Syndrome (PHS)

Overview of PHS

Pallister-Hall Syndrome is a severe condition caused by mutation to *Gli3* (Kang et al., 1997b), but the phenotypes observed in head and limb differ remarkably from GCPS. Rather than craniofacial malformation such as frontal bossing, broad nose, and hypertelorism, PHS patients may display reduced ears, nose, and/or jaw. More

---

[5] The inner canthus is the medial corner of eye where eyelids meet

commonly, PHS individuals display defects to midline fusions of the laryngotracheal cleft and epiglottis. The hypothalamus is always found to overgrow during development, and forms an hamartoma. The associated polydactyly is unique, with central and postaxial duplications present. Furthermore, anal, renal, and other visceral abnormalities may occur. As is the case with GCPS and other *GLI3* related pathologies, the spectrum of phenotypic expression is wide and varied.

PHS is a relatively rare condition, less than one hundred cases have been reported since 1980. It was initially thought of as sporadic, but has since been verified to be autosomal dominant. The most severe PHS patients die shortly after birth; these were the initial PHS cases. It is now realised that most PHS is expressed in a very mild way, and can easily be misdiagnosed as postaxial polydactyly.

Clinical Diagnosis of PHS

A peer-reviewed diagnostic criteria for PHS has been established by the N.I.H. Workshop on Pallister-Hall Syndrome and Related Phenotypes (Biesecker, L.G. 1996).

The essential criteria for an affected individual are as follows:

(1) Hypothalamic hamartoma characterised on magnetic resonance imaging (MRI) as a non-enhancing, midline hypothalamic mass that is iso-intense to grey matter on all pulse sequences, or histological confirmation of a hypothalamic hamartoma.

(2) Central polydactyly, most commonly including skeletal polysyndactyly of the third or fourth digit.

Other phenotypes may also be present:

---

[6] *GLI3* is located at 7p13.

(3) Postaxial polydactyly type A, B, or A/B is very common.

(4) Imperforate anus and renal abnormalities including cystic malformations, renal hypoplasia, ectopic uretal implantation, and pulmonary segmentation anomalies such as bilateral bilobed lungs.

(5) Pituitary dysplasia with panhypopituitarism and laryngeal clefts.

(6) Other rare abnormalities such as micropenis, small and rounded ears, short nose, micrognathia, large asymmetric fontanels, short limbs, brachytelephalangy, nail hypoplasia and other hand malformations, kidney adrenal and thyroid dysplasias, and some cardiovascular disorders.

Most PHS patients are mildly affected with polydactyly, asymptomatic bifid epiglottis, and hypothalamic hamartoma. Without careful clinical evaluation, these patients may be diagnosed with PAP-A and suffer no other ill consequences. The most severe cases are rare but may end in neonatal death.

Aetiology of PHS

PHS is largely regarded as an autosomal dominant trait (Biesecker et al., 1994; Kuller et al., 1992; Penman Splitt et al., 1994; Sills et al., 1994a; Sills et al., 1994b; Sills et al., 1993; Thomas et al., 1994), though initial reports suggest cases were sporadic (Finnigan et al., 1991; Hall et al., 1980).

The only gene mutation implicated in PHS is *GLI3* (Kang et al., 1997a; Kang et al., 1997b).

Incidence of Isolate and Complex Polydactylys

The global incidence of polydactylism is 15 in 1000 (Castilla et al., 1996). There is a very distinct difference in the incidence of the various forms of polydactyly. PAP is by far the commonest, and accounts for some 80% of the total polydactyl population (Castilla et al., 1996; Castilla et al., 1998)[7]. PPD type I is the next most frequent, accounting for 15% of the polydactyl population. The other forms of polydactyly, including central digit duplications, polysyndactyly, and PPD type II (digit I triphalangism account for less than 4% (Figure 2.8). However, it is interesting to note that the rare polydactylys such as central polydactyly (duplication of digit III) are most commonly associated with syndromes (65%), while the common polydactylys, PAP and PPD type I, are rarely associated with syndromes (11% and 20%, respectively).

Furthermore, populations studies have shown that there is no evidence to suggest a major gene is acting to produce the commonest form, PAP (Feitosa et al., 1998). Therefore, the only known gene mutation to cause PAP, *GLI3*, cannot be the only gene mutation to cause PAP, or if it is, then it must be inherited in unusual ways. It is also apparent that PAP may simply be an infrequent expression of a normal genotype. These cases will be discussed in Chapter VII.

Similar Human Pathologies

Acrocallosal Syndrome (ACLS)

Acrocallosal Syndrome (ACLS) is a pathology with striking similarities to GCPS. It is defined by postaxial polydactyly type A or B, preaxial polydactyly type I,

---

[7] This is the report of a comprehensive study of over 4,000,000 births in Spain and Latin America.

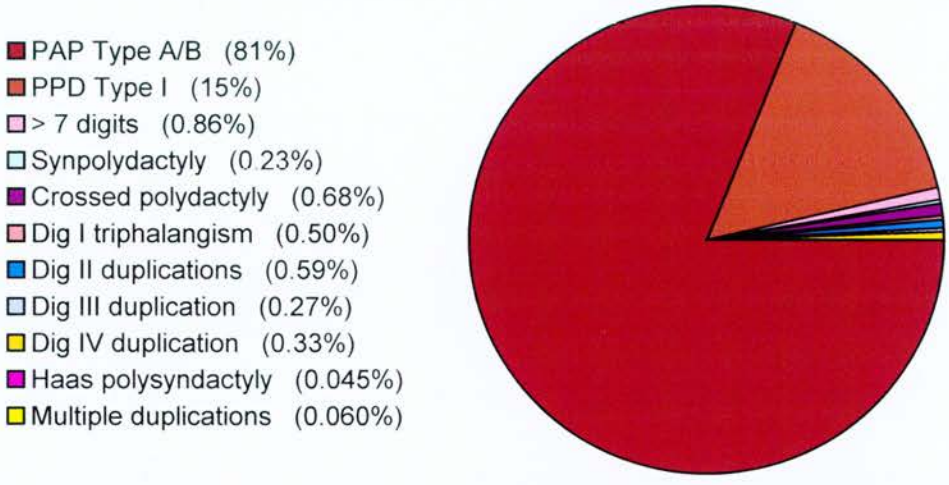

Figure 2.7 Proportional frequency of polydactyly types found by the joint Latin-American Collaborative Study of Congenital Malformations and the Spanish Collaborative Study of Congenital Malformations. Of 4,230,084 near consecutive births, 6599 were found to be polydactyl (15.6 per 1000). The pie chart above is a breakdown of the types of polydactyly found. The majority (81%) is postaxial, followed by preaxial (15%). The other, more rare polydactyl types are frequently (65%) associated with other congenital abnormalities. Preaxial polydactyly displays an intermediate association with other abnormalities (20%), and postaxial polydactyly is least associated (12%). Data acquired from Castilla *et. al.* 1996, 1998.

macrocephaly, large anterior fontanel, absence of the corpus callosum, and severe mental retardation (OMIM #200990: Schinzel and Schmid, 1980). Other similarities to GCPS and PHS include prominent high forehead, malformed ears, strabismus, hypertelorism, optic atrophy, small broad nose, palate defects, heart defects, umbilical hernia, imperforate anus, micropenis, cryptorchidism, brachydactyly, and toe syndactyly (OMIM #200990). The phenotypes which are do not occur in known *GLI3* related pathologies are still closely related to them, but are minor deviations from those typically seen in GCPS or PHS. Such minor deviations include hypoplastic midface, posteriorly rotated ears, cleft palate, cleft lip, and internal genital malformations. The most severe difference is hypoplastic or absent corpus callosum. To my knowledge this has not been observed in any GCPS or PHS patient.

A case was reported (OMIM #200990: Hendriks et al., 1990) which suggests increased birth weight and cerebellar hypoplasia may also be features of the acrocallosal syndrome. This patient had an extra bone within the anterior fontanel. Both are conditions similar to that seen in the *Xt/+* mouse (Chapter V; Johnson, 1967).

ACLS is thought to appear spontaneously or is a recessive mutation (OMIM #200990: Schinzel and Kaufmann, 1986).

Because of its obvious similarity to GCPS, (Brueton et al., 1992) performed linkage analysis in a family with two affected cousins. Using markers known to flank GCPS locus, they found evidence to exclude a translocation or microdeletion of *GLI3*. However, this is not to say a point mutation or frameshift in *GLI3* is not responsible for their patient. The only other genetic analysis revealed a mirror image short-arm duplication of chromosome 12, a *de novo* inverted tandem duplication of 12p13.3-p11.2 (Pfeiffer et al 1992). Similar manifestations of trisomy and tetrasomy 12p show some overlap with ACLS, such as Pallister-Killian Syndrome (OMIM #190070), suggesting disruption to normal gene expression on chromosome 12p may

be responsible for ACLS. No more evidence exists to support either the involvement of *GLI3* or chromosome 12p.

Apert Syndrome

Apert Syndrome is very severe condition with many parallels to GCPS and PHS. It is known to be caused by mutations to *Fibroblast Growth Factor Receptor 2* (*FGFR2*). Several hundred Apert Syndrome cases have been genotyped, all have point mutations in *FGFR2*, most at very specific positions (OMIM #101200: Oldridge et al., 1999; Park et al., 1995; Slaney et al., 1996; Wilkie et al., 1995).

Apert Syndrome is also known as Acrocephalosyndactyly (ACS) type I. ACS type II is unusual and is not strictly Apert Syndrome. Apert Syndrome (ACS type 1) was first characterised by skull malformation (acrocephaly of brachysphenocephalic type) and complete distal fusion of fingers and toes (Apert, 1906). Type II, on the other hand, is characterised by a middigital hand mass with a single nail common to digits II to IV. Type II is a severe and unusual condition. Apert's syndrome is strictly type I.

Common features with GCPS and PHS include large late-closing fontanel, high broad forehead, flat facies, mandibular prognathism, shallow orbits, hypertelorism, depressed nasal bridge, strabismus, narrow palate, heart defects, ectopic anus, cryptorchidism, coronal cranial synostosis, fusion of carpels, syndactyly (though of a more serious type), broad distal digit I on hands and feet, and acne. Apert Syndrome differs most severely in its digit phenotype, and also more severe neurological defects including agenesis of the corpus callosum, ventriculomegaly, absent septum pellucidum, and limbic malformations (OMIM#101200). Similarities between the GCPS and Apert Syndrome suggest that *FGF* signalling may be closely tied to *GLI3* function.

Thesis Overview

Background

When I started work on this Ph.D. thesis in 1998, there was no mention of *Gli3* or *Xt* or anything to do with the material presented here. I began work with my supervisor, Dr. David Price, on the *Pax6* gene, which his laboratory had a certain expertise in. Some time later in 1999, the *Extra-toe* mouse was mentioned and we designed an experiment to test the cell autonomy of the *Gli3* mutation. These experiments failed technically, but they produced unexpected and intriguing data that was replicated. These results were worked up over a two-year period and are presented in Chapter III: Survival of Primary Neocortical Cells.

Needless to say, the *Pax6* experiments were dropped in favour of a more concerted approach to the problem of *Gli3* and its role in forebrain development. I made this decision for two reasons: (1) little was known about the role of *Gli3* – only a small number of publications were available prior to 1999 – and (2) *Gli3* was a widely expressed gene with, what seemed to be pleiotropic function. Unlike *Pax6*, which was restricted to the nervous system and pancreas, *Gli3* affected most regions of developing embryo. This satisfied my desire to explore and understand embryogenesis as a complete system, and not to restrict my attention to one system. I believe I have worked well to this end, and this thesis is the result of my effort.

Thesis Rationale

Throughout my investigations, I have followed an underlying assumption that *Gli3* functions in a similar capacity in the developing limb, developing brain, and developing neural tube (of which the rostral portion gives rise to craniofacial tissue). This assumption rests on observations that (i) the areas of most noticeable *Gli3*-

mutant phenotype are those that most highly express *Gli3*, (ii) *Xt/Xt* forebrain and distal limb are similar in that they both display additional morphological characters, and (iii) comparison to homologue *Ci* shows that *Gli3* may be interpreting extracellular Shh and that this is its primary function in these developing systems. If *Gli3* is acting in a similar manner in these systems, then the findings in one systems should be relevant to the findings in another system. With this in mind, I chose to focus my investigation on one system, the developing forebrain, but also performed an overview of all skeletal defects to the *Gli3*-mutant embryo in order to interpret patterning defects and to find the common, core defects arising in the other systems (developing limb, spinal column, and cranium).

During these investigations, it became apparent that the mutant *Gli3* allele was transmitted at a greater frequency than the wild-type allele. These data were worked up and are presented in Chapter VI. Whether or not this phenomenon is relevant in nature at large, it prompted an investigation into the potential evolutionary benefits of mutation to *Gli3*. I present these benefits in the final part of this thesis, and combine speculations on the advantages of perceived and possible phenotypic changes with the functional significance of transcription factor *Gli3*.

Thesis Plan

The thesis is divided into four parts. The first is background information. This is intended to introduce the reader to the gene, the mutant phenotype, the human pathologies associated with this gene, and to cover some key points about its functional characteristics. First is the notion that the gene is widely expressed during embryogenesis, both in time and space. The second is that the developing brain and the developing limb share some commonality in their initial morphology, more commonality in the signaling molecules used, and finally commonality in *Gli3* expression characteristics. Data on the human *Gli3*-related pathologies has demonstrated the variability of expression of the *Gli3*-mutant phenotypes. These factors will be important when it comes to interpreting the role of *Gli3* in

embryogenesis, and also on speculations of its potential to affect evolutionary morphological change.

The bulk of the experimental work on *Gli3* is presented in Part 2. These experiments focus solely on forebrain development, but discuss data from others on limb and neural tube development that help to shed light on the interpretation of these results.

In the first chapter of Part 2, I present the results from a series of experiments on the properties of *Gli3*(-/-), *Gli3*(-/+), and *Gli3*(+/+) neocortical cells in dissociated cell culture. I focus on neurogenesis of the neocortex at E14.5 to E16.5 because this is the period of time when the defects most obviously arise. These data suggest that a change in either cell death or cell proliferation is a major contributing factor to the *Xt/Xt* forebrain phenotype. I present a number of possible mechanisms for this explanation, and suggest additional upstream, or primary mechanisms that might lead to this dysfunction. These hypotheses are worked up in the second chapter of the section, Chapter IV.

Chapter IV addresses the two hypotheses in a series of smaller experiments: the effect of ectopic ganglionic eminence in the *Xt/Xt* neocortex, a measure of *in vivo* cell death rates, a measure of proliferation rates, and finally an overview of the proportion of pre- and post-mitotic cell types in the neocortex. Together, these results are interpreted and conclusions presented at the end of Part 2. In summary, the mechanism of the *Gli3*-mutant forebrain phenotype is likely to be the result of a disruption to normal cell cycle and cell death dynamics. The cause of this disruption in open to investigation, but may well be a secondary consequence of a primary disruption to the normal expression of key signaling molecules, namely FGF8 and the Bmp's.

Part 3 presents a detailed analysis of the skeletal defects of the *Xt/Xt* and *Xt/+* perinatal animals, and also data on the breeding characteristics of the *Xt* colony. I make the case that the *Xt* colony used for this study, the *Xt-Jackson* strain, is comparable to the strain first reported by Johnson (1967), the *Xt-Harwell* strain.

Only in the region of the base of the skull did I note a difference in mutant phenotype. The cause of this might be due to the specific form of *Gli3* mutation, or due to differences in the genetic background of the two strains.

In Chapter VI I present data on the transmission rate of the mutant *Gli3* gene as it passes from one generation to the next. I show that the mutant form of the gene is preferentially transmitted over the wild-type form, and I prove this observation statistically. It is not possible at this stage to determine the cause of this phenomenon, but I present two most likely hypotheses: either the germ cells are favourably disrupted if they carry the mutant form of *Gli3*, or there is an additional recessive-lethal mutation present in the *Xt* colony.

As I worked on these experiments, I began to piece together an understanding of *Gli3* as a regulator of size and shape. Its mechanism of action was exerted, probably by interpreting Shh signal through it's intra-cellular transduction network (*cf.* *Drosophila* Ci). It seemed intuitively correct that size and shape could be modified by adjusting the sensitivity of the *Gli3* signal transduction network to Shh signal. Furthermore, where the phenotype was most noticeable in the *Gli3*-mutants, I suggest that these areas are those that are less canalized, and so more open to evolutionary change. These areas are craniofacial morphology, brain development, and distal limb development, with some less pronounced changes to other areas such cervical vertebrae and associated spinal cord. This evolutionary function seemed to fit well with the fact that mutant *Gli3* was preferentially transmitted in my *Xt* colony, and that it was those areas most affected by the gene that appeared to me to be those areas that are most diverse between mammalian species. Thus, I present these ideas, in conjunction with a conceptual framework of development and evolution by the late Professor C. H. Waddington.

Part 2

Experimental:
Gli3 in Neocortical Development

Chapter III: Survival of Primary Gli3-mutant Neocortical Cells

Introduction

Hypothesis

Programmed cell death is reduced in the *Xt/Xt* neocortex.

History

The experiments I present in this chapter arose from an observation during a set of separate experiments. I had intended to dissociate and transplant E15.5 *Xt/Xt* neocortical cells into the cerebral vesicles of wild-type rat embryos of a comparable age. These experiments were designed to measure the cell-autonomy of the requirement for normal *Gli3* expression in individual cells by testing the ability of *Gli3*-mutant cells to migrate and differentiate in a wild-type environment. *Xt/Xt* neocortices were dissected out, dissociated, and injected into the cerebral vesicles of the embryonic rats where the cells could theoretically integrate with the wild-type environment of the developing rat cortex. Similar experiments had been performed previously for the *Pax6* mutation (Caric et al. 1997). Because of the extreme experimental conditions, I ran a parallel control group in which dissociated neocortical cells were cultured in an incubator instead of transplanted into brain. The transplantation experiments unfortunately failed, but I noticed that the *Xt/Xt* cells in culture were healthy and had established inter-cellular connections, while the +/+ cells had died. The following chapter is the result of an independent investigation into this serendipitous finding.

Theoretical Considerations

The *Xt/Xt* forebrain phenotype can be produced by disruption to any of the main elements of morphogenesis (cell proliferation, differentiation, migration, and death). However, taken together, the phenotypes – a convolution of the cerebral hemispheres, a lack of normal lamination into the cortical layers, an ill-defined ventricular zone (VZ), and an intrusion of the ventral ganglionic eminences into the dorsal neocortical domain – appear to be the result of an "overgrowth" of the tissue. Convolution of the cerebral hemispheres may arise as a result of an excessive growth of cortical tissue developing in a restricted space. Normal lamination and proper differention of the VZ may also be hindered by spatial restrictions, and arise as a secondary consquence of overgrowth. An over expansion of the ganglionic eminences may also contribute to the overcrowding of dorsal forebrain space.

Overgrowth of the type (suggestively) seen in the *Xt/Xt* forebrain may due to a primary defect, either in normal cell cycle or in normal cell death. Either way, more cells would be produced than normal, and the tissue would expand abnormally to produce the *Xt/Xt* forebrain phenotype.

In this chapter, I focus on the element of cell death as a primary cause of the *Xt/Xt* forebrain because of the overwhelming preliminary *in vitro* observations that showed E15.5 *Xt/Xt* neocortical cells to outlive their wild-type counterparts in culture. These preliminary data raised the hypothesis that normal cell death is disturbed in the *Xt/Xt* forebrain, an hypothesis reinforced by data from three others sources: (i) caspase-3 and caspase-9 knock-outs displayed reduced cell death *and* a forebrain morphology comparable to the *Xt/Xt* forebrain (Haydar et al., 1999); (ii) the Xt^{Pdn}/Xt^{Pdn} mesencephalon and diencephalon displayed abnormal cell death, though here is was suggested to be increased (Keino et al., 1994); and (iii) aberrant cell death could be seen to explain the phenotypes in other developing systems of the *Xt/Xt* embryo, *i.e.* craniofacial, brain, spinal cord, vertebral, and limb phenotypes – this point will be drawn out in the discussion of this chapter.

Cell death in the forebrain is thought to be a key factor in its morphogenesis. Cell death is found widely in the proliferative zones and in the layers of the cortex and is thought to help shape the forebrain by restricting the number of proliferating cells (Blaschke et al., 1996; Blaschke et al., 1998). Inhibition of normal cell death would increase the number of dividing cells in the progenitor pool in the ventricular zone (VZ). This would lead to an expansion of the VZ and of the cortex as a whole. Inhibition at an early age, and continued inhibition, would be catastrophic; an early increase of proliferating cells would create more cells that would continue to proliferate and create more cells that would continue to proliferate, *etc.* If cell death was inhibited, this unchecked proliferation would cause normal development to rapidly deviate from its course. As long as development proceeded, the deviant course would continue to diverge further from its normal trajectory, and a compounding of phenotypes would be observed, as is seen in the *Xt/Xt* forebrain.

Experimental Design

The preliminary *in vitro* observation (that arose as a side-issue from the tranplantation experiments) influenced the design of the subsequent experiments. The *in vitro* technique had its advantages. The procedure challenged the cells and enabled them to be observed with a microscope. Cellular behaviours such as cell death, proliferation, and migration were observable over the course of the culture. This chapter focusses on the observation of cell *survival* in culture. I will discuss these data at the end of this chapter, and will present further experiments in Chapter IV that help to clarify these data and test other possible disruptions to normal developmental mechanisms, *i.e.* that cell cycle, cell differentiation, or cell migration are disturbed in the *Xt/Xt* forebrain.

Primary culture experiments were conducted on E14.5, E15.5, and E16.5 material collected from *Xt/+ x Xt/+* matings. The neocortex of the embryos was removed, and in some experiments also the ganglionic eminences. Neocortical and ganglionic eminence tissue was dissociated into a single cell suspension using mechanical and enzymatic means, and then cultured under standard conditions with serum-free media. Cells were fixed at 24 hour intervals and stained with a nuclear dye to observe nuclear morphology, a determinant of cell viability.

At E14.5, tissue from +/+ and *Xt/+* was pooled to form one population, hereon out referred to as the *control* population. E14.5 *Xt/+* and +/+ cells were pooled because phenotypic differences between the two were unreliable at this age, *i.e.* the extranumerary digit may or may not be noticeable. E15.5 and E16.5 material, on the other hand, was separated into all three phenotypic categories, +/+, *Xt/+*, and *Xt/Xt*. Dissociated cells were plated at different densities, 500, 1000, 2000, and 4000 cells/mm^2. The most informative data were acquired from densities of 1000 and 2000 cells/mm^2.

Materials and Methods

Mouse Matings

The Xt colony was maintained by inbreeding. Mice were housed at room temperature and provided with food and water at liberty. Male *Xt/+* studs (6 weeks to 12 months old) were mated with female *Xt/+* (6 weeks to 6 months old) mice. They were checked each morning for the following three days for the presence of a vaginal plug. The day the vaginal plug was found was considered to be embryonic day 0.5 (E0.5). Once plugged, the male was returned to his cage.

Hysterectomy

Embryos were acquired at E14.5, E15.5, and E16.5 for primary cortical culture experiments. Pregnant mothers were anaesthetised in a halothane (Halothane-Vet Ph.Eur., Merial) gas chamber until unconscious. They were then killed by cervical dislocation and their abdomen cleaned with 70% EtOH. An incision was made through the abdominal wall, and the uterine tubes extracted. Embryos were removed from the uterus and amniotic sac by holding up the organ and allowing the uterus to hang like a string of pearls. Each conceptus was cut with scissors from the bottom, across the tube, as one would open a soft-boiled egg. This allowed the amnion to be punctured and at the same time removed the uterine muscle. The embryo then slid out of the uterus from the natural contraction of the uterine muscle. Embryos were removed in this manner into oxygenated 4°C Earl's Balanced Salt Solution (EBSS) and kept on ice.

Weights

Some litters were weighed at this point. Each embryo was transferred with large forceps cupping the animal from the bottom. It was then touched to a paper towel for three seconds to remove excess EBSS and placed on a balance sensitive to the microgram. Individual embryos were then stored seperatately in 4°C oxygenated EBSS and labelled for phenotype analysis. The course of data collection before phenotyping ensured a blind experimental design. Data from weight measurements are presented in Chapter VI.

Phenotype Sorting

Litters were sorted into the three phenotypes *Xt/Xt*, *Xt/+*, and +/+. *Xt/Xt* embryos were easily recognised as they displayed more than six digits, bent hemimelic hindlimbs, an enlarged maxillary component, and sloped forehead. Other abnormalities were also present but were not necessary for classification. *Xt/+* and +/+ embryos have similar gross morphologies and were distinguished from E15.0 onward by observation of an extranumerary digit or pedunculated postminimus. An extra digit on only one limb was enough for *Xt/+* classification, but more often presence of an extra digit occurred on all limbs. Classification of *Xt/+* before E15.0 was not considered reliable because the preaxial apical ridge extends posterior at this stage and could be mistaken for an extra digit.

Embryos were sorted into groups, transferred to fresh 4°C oxygenated EBSS, and stored on ice. From this point on, all tools were sterile, and all procedures carried out under a Class I flow hood.

Brain Dissection

Heads were removed from the body with a clean incision through the neck using a scalpel blade. The face was then removed by slicing along the coronal plane so that the cut removed the front portion of the calvarium and the bony facial mass, at about

the point of the eye. This opened the cranial vault, and with slight pressure applied to the sides of the head with forceps, and with a gentle push from behind, the brain was eased out of its casing.

Whole brains were then transferred to small bijou containers with fresh oxygenated EBSS and stored on ice.[8] Once all brains had been removed, they were transferred to the Tissue Culture Suite where sterile conditions were maintained.

Neocortical and Ganglionic Eminence Dissection

The telencephalic lobes were separated from the midbrain at the midbrain-forebrain boundary. The anterior and posterior extremes of the telencephalic lobe were removed with a dissecting blade and discarded. The pia was then gently tugged off the surface of the lobe. This had the added benefit of stretching the cortex away from the ganglionic eminences and exposing the striato-cortical boundary. Cortex was then excised from striatum and transferred to bijou with fresh 4°C oxygenated EBSS and stored on ice. Ganglionic eminence tissue was also stored for use in some experiments, presented in Chapter IV.

Dissociation

Dissociation of the brain tissue into a single cell suspension was performed using the Papain Dissociation System (Worthington Biochemical Co., New Jersey, U.S.A.) according to manufacturer's specifications. Briefly, tissue was chopped into 100μm pieces on a Teflon disc using the McIlwain Tissue Chopper (Mickle Laboratory Engineering Co., Surrey). It was then washed to a glass dish with papain-DNAse solution, covered, and incubated at 37°C, 95% CO_2, 5% O_2, 99% humidity for 40 minutes. 500μL papain solution was used for each brain. The mixture was then

[8] Neural tissue is may be preserved on ice in oxygenated EBSS for several hours without damage.

triturated 10 times using a flame-polished glass pipette, transferred to a centrifuge tube and spun at 300g for 5 minutes. Supernatant was removed and the cell pellet resuspended in residual solution by tapping. 200μL of low density ovomucoid inhibitor was added and this placed dropwise atop 500μL high density ovomucoid inhibitor. The bilayer was centrifuged at 70g for 8 minutes and the resulting supernatant removed.[9] The cell pellet was resuspended in 5mL of culture medium (see Appendix A for makeup) and stored at room temperature for the remainder of the protocol.

Plating Density Calculations

Cell density of the suspension was calculated using a standard haemocytometer. About 7μL of the cell suspension was placed on the haemocytometer slide. Using an inverted microscope, the number of cells present in the main 5 x 5 grid square was counted. This gave the number of cells present in 100nL. Multiplication by a factor of 10 gave the number of cells expected in 1.00μL.

The suspension was then diluted to obtain cell densities for plating at 500, 1000, 2000, and 4000 cells/mm^2. For a 96-well flat-bottom plate (Iwaki, Japan, cat. no. 3860-096), 200μL of cell suspension was used for each well. The total bottom surface area per well was 32mm^2. The following formula was used:

$$\text{Dilution Factor} = \frac{\text{number of cells/}\mu\text{L} \quad x \quad \text{volume to be added per well } (\mu\text{L})}{\text{surface area of well } (\text{mm}^2) \quad x \quad \text{plating density } (\text{cells/mm}^2)}$$

[9] The ovomucoid bilayer is intended to remove tissue debris. This step is quite ineffectual and can be omitted.

The dilution factor was then used to calculate the amount of medium to be added to produce, first a plating density of 4000 cells/mm^2, and then lower densities. The calculation can be summarised as:

$$\text{Total Volume} = \text{Volume of cell suspension} \times \text{dilution factor}$$
$$\therefore \text{Volume to add} = \text{Total volume} - \text{Volume of cell suspension}$$

Early experiments involved plating at all four densities. However, it was quickly found that 500 cell/mm^2 was quite uninformative as the cells died very quickly. The density of 4000 cells/mm^2 proved unobtainable for most experiments due to shortfalls in cell number. The results of these experiments are intriguing, but anecdotal.

Initial Cell Viability

Before plating, cells in suspension were tested for viability using a Trypan blue exclusion assay. Trypan blue and the cell suspension were mixed together at a volumetric ratio of 1:1. Cells were then placed into the haemocytometer and observed. Those cells that took up the Trypan blue were considered dead or damaged.

Culture

All tissue culture vessels were treated beforehand with 0.0001% poly-L-lysine (Sigma, cat. no. P-4707) to aid adhesion of cells to the surface. The poly-L-lysine solution was added under sterile conditions to each well, left to incubate at room temperature for 30 minutes, washed three times with dH_2O, and allowed to air dry.

Cell suspension of the appropriate dilution was added to each well using a standard Gilson pipette. Transfer was made as gently and quickly as possible. Denisties and phenotypes were plated in duplicates or triplicates on the same dish, and one dish was used for each day.

Culture plates were then incubated at 37°C, 95% CO_2, 5% O_2, 99% humidity until fixation.

Fixation and Hoechst Staining

At 24 hour intervals, culture plates were removed from the incubator and placed on ice. Half of the medium was removed and replaced with 4% paraformaldehyde (PFA) with 20 μg/mL Hoechst. The culture was then left at room temperature for one hour, and half of the PFA-Hoechst solution removed and replaced with phosphate buffered solution (PBS). This process was repeated until the PFA was reasonably dilute. Care was taken not to disturb the cells.

Cell Death Counts

Viability was determined by nuclear morphology visualised with the Hoechst stain using an inverted fluorescent microscope. Initially, cells were classified as 'healthy', 'early apoptotic', late apoptotic', and 'necrotic'. However, it was difficult to maintain clearly defined categories between the types of cell death, and so these were discarded in favour of a binary 'alive' or 'dead' analysis.

Results

Starting Conditions

After dissociation, cell bodies were round and usually without appendages, though some displayed a small residual process. Cell viability was assayed at 98% or greater by Trypan blue exclusion. Cells were held in suspension as single cells, or less frequently in clumps of two's or three's. A cell's first observed response on being placed into culture was to adhere to the surface of the culture dish. This seemed to be an active reaction, and after about thirty minutes cells were not easily dislodged from the bottom, whereas immediately after plating they would move if the dish was disturbed. At the same time, most cells extended processes away from the cell body.

General Observations

Within 24 hours, processes extended from most cells and connected to other cells in the culture well, and cells had moved together to form small groups of cells. Some of the extending processes displayed a clear growth cone indicating that the process was a neuronal afferent, while others displayed a nondescript terminal foot. Connections between groups of cells were thicker than from single cells, and other processes could be seen extending along the original. These processes did not adhere to the culture floor and would vibrate if the vessels was tapped, indicating that they were held taught. Other process types adhered to the culture floor and branched out in the manner of a dendritic tree. These processes were smaller in diameter than the others and could only be detected if the microscope phase was at an angle.

After two days in culture, the interconnected clusters had grown in size and the areas in between appeared less dense than the initial start conditions. There was some piling of the cells in clusters where cells were seen to overlap each other, but on the whole, cells remained in contact with the culture floor. Cells were also seen to migrate between the clusters along the taught connecting processes.

Classification of Cell Viability

Cell viability was determined by nuclear morphology (Figure 3.1). Healthy cells were those with broad, diffuse staining. Dead cells were those with a clear apoptotic or necrotic morphology.

Neocortical Xt/Xt Viability is Consistently Higher than Xt/+ or +/+ Viability

Dissociated cells of the *Xt/Xt* neocortex consistently displayed greater viability than comparable *Xt/+* and +/+ cultures across the range of densities and embryonic ages (Figures 3.2, 3.3, and 3.4). This increase in viability was least pronounced in E14.5 material where most cell populations survived for more than three days (Figure 3.4). Here, *Xt/Xt* cells followed a trend of increased viability over the *control* (*control*) population (at E14.5, *Xt/+* and +/+ cells were pooled to make the *control* population), but the increase was only statistically significant at three points (Day 1 and Day 3 at low density and Day 4 at high density: Kruskal-Wallis ANOVA, $p<0.05$). *Xt/Xt* increase in viability over the +/+ population became more pronounced in E15.5 cultures (Kruskal-Wallis ANOVA, $p<0.05$) (Figure 3.3), and again more so in E16.5 cultures (Kruskal-Wallis ANOVA, $p<0.05$) (Figure 3.2). At E15.5, +/+ material was 20-26% viable after two days in culture, while *Xt/Xt* material remained 60-70% viable. At E16.5, *Xt/+* and +/+ material was largely dead

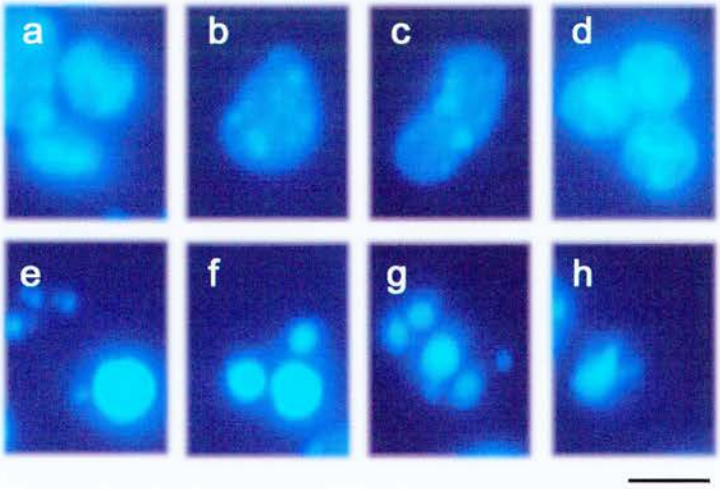

Figure 3.1 Categories of cell viability in primary culture as determined by nuclear morphology. Cells have been fixed in PFA, stained with Hoechst to identify the nucleus, and viewed under epifluorescence microscopy. Cells in M-phase (a) can be identified by a band of intense signal, usually apposing another (in late M-phase), that represents condensed mitotic chromatin. Healthy cells (b and c) in G1 – G2 exhibit broad, diffusely stained nuclei with small pockets of more intense staining. Three examples of early apoptotic cells that are similar to early mitotic cells (d) in appearance; these are excluded from analysis. Apoptotic cells (e – g) display many condensed nuclear compartments which fluoresce intensely. Necrotic cells (h) display a jaded nuclear morphology with diffuse nuclear boundaries. Scale bar measures 10μm.

Figure 3.2. Graph to show the change in viability of E16.5 *Xt/Xt* (circle), *Xt/+* (circle with dot), and *+/+* (triangle) cells cultured in serum-free conditions over a period of days. At an initial plating density of 1000 cells/mm^2 (A), the *Xt/Xt* population is significantly more viable than the others (asterisks), and the *Xt/+* population is significantly more viable than the *+/+* population, after one day in culture (open star). At an initial plating density of 2000 cells/mm^2 (B), the *Xt/Xt* population is significantly more viable than the others after one day in culture (asterisk), and there is a significant difference between the *Xt/+* and *+/+* populations (open star). Note also that the viability of the more densely populated (B) cells decreases more slowly than the sparsely populated (A) population.

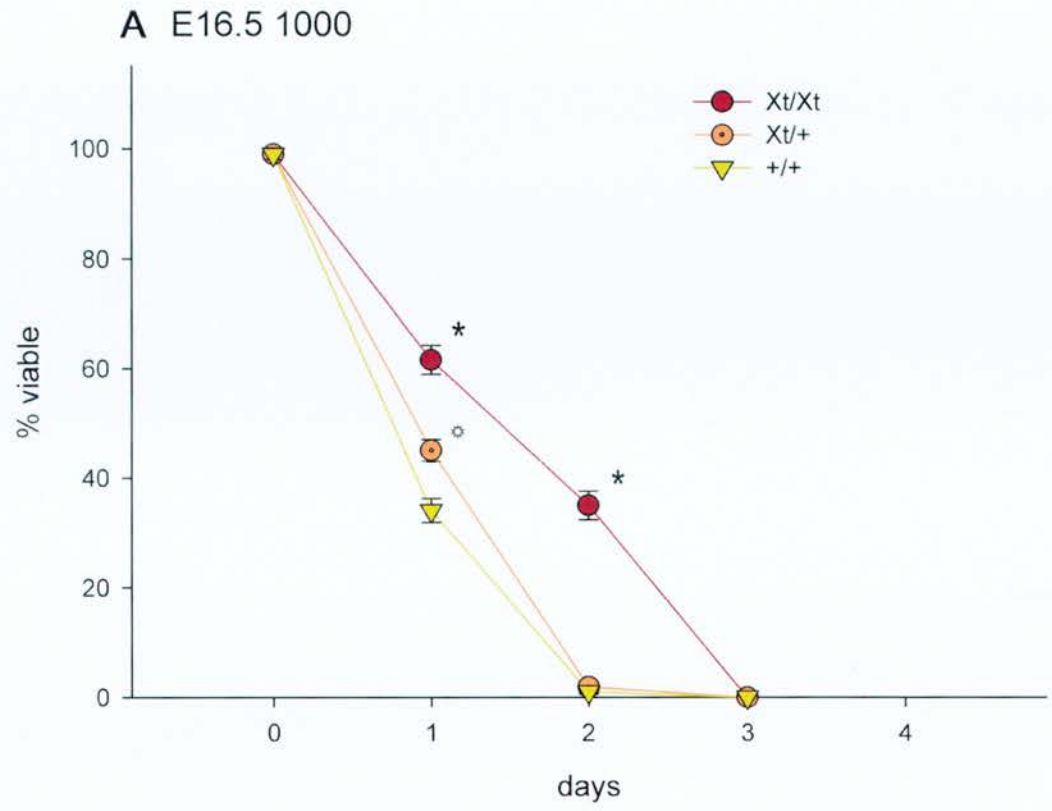
A E16.5 1000
Xt/Xt
Xt/+
+/+
% viable
100
80
60
40
20
0
0
1
2
3
4
days
*
*

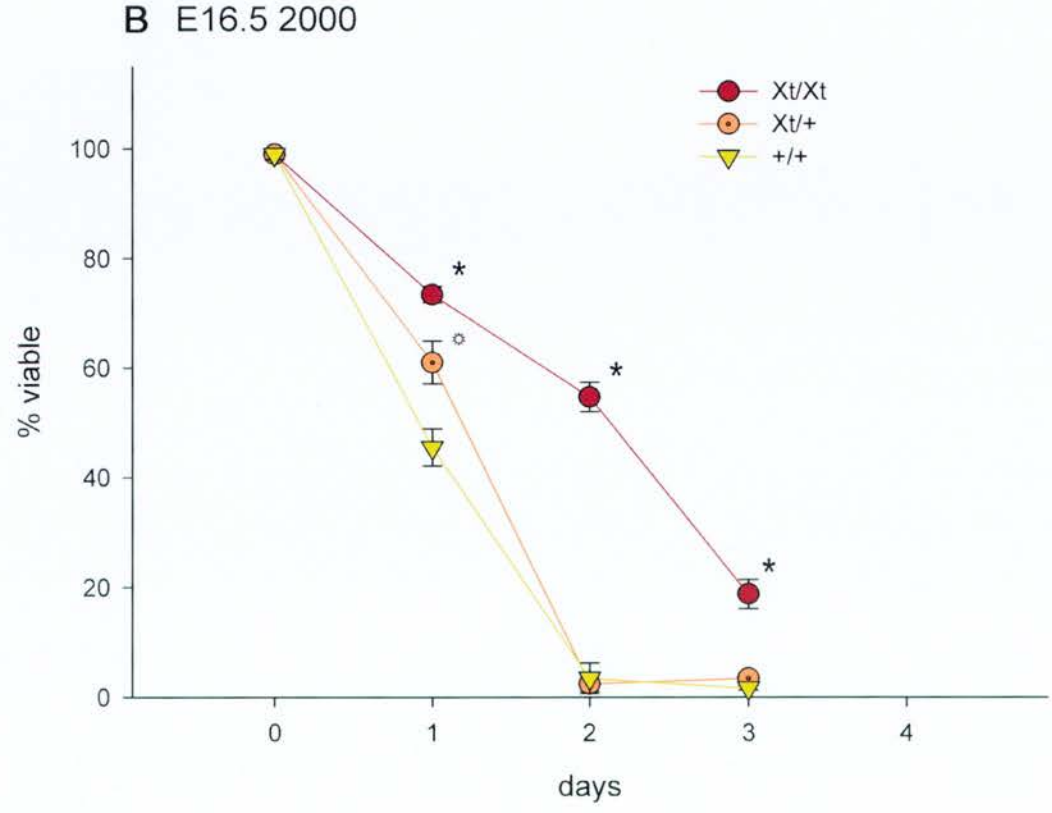
B E16.5 2000
Xt/Xt
Xt/+
+/+
% viable
100
80
60
40
20
0
0
1
2
3
4
days
*
*
*

Figure 3.3. Graph to show the change in viability of E15.5 *Xt* (circle), *Xt/+* (circle with dot), and *+/+* (triangle) cells cultured in serum-free conditions over a period of three days. At the initial plating densities of both 1000 cells/mm^2 (A) and 2000 cells/mm^2 (B), the *Xt/Xt* population is significantly more viable than the other populations by Day 1, and remains so until Day 3 (asterisks), where all cells have died in the less dense cultures (A), and where only *Xt/Xt* cells survive in the more dense cultures (B).

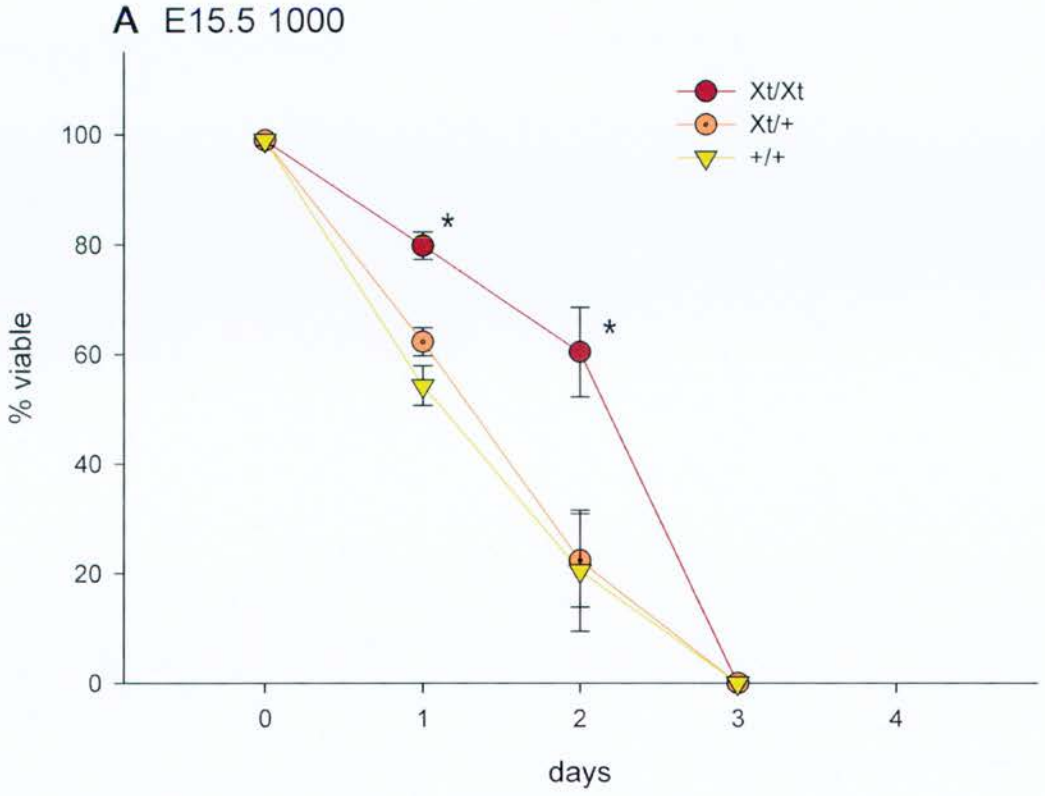
A E15.5 1000
Xt/Xt
Xt/+
+/+
100
80
60
40
20
0
% viable
*
*
0
1
2
3
4
days

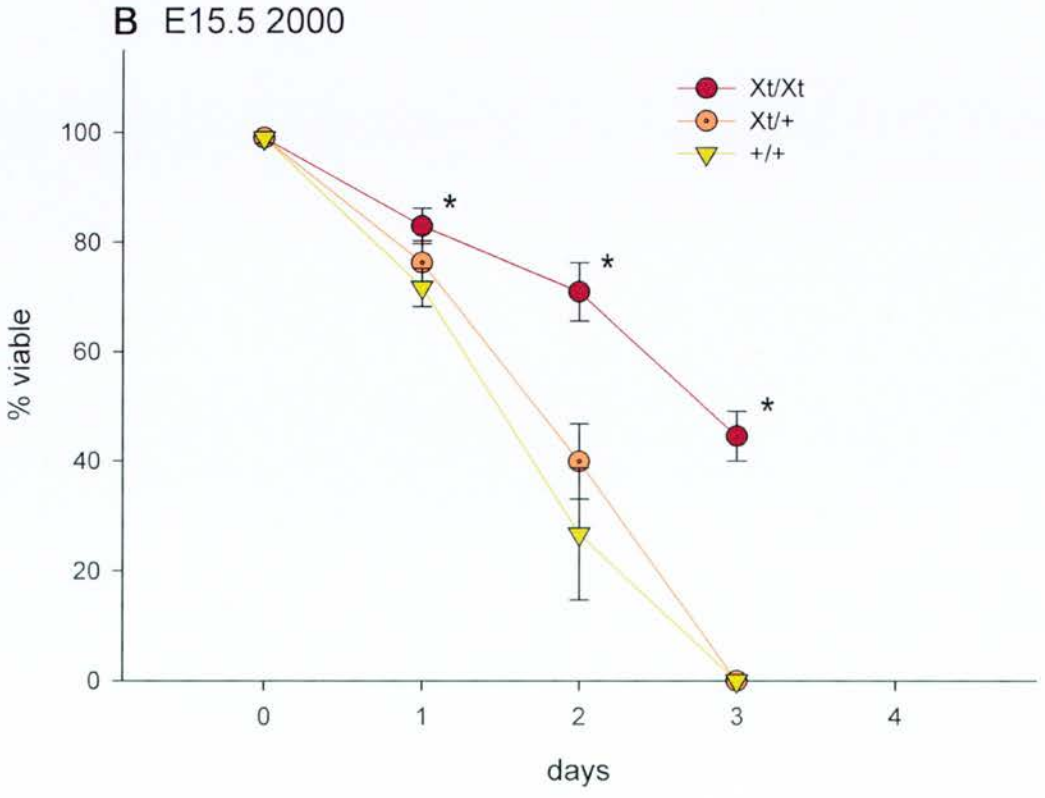
B E15.5 2000
Xt/Xt
Xt/+
+/+
100
80
60
40
20
0
% viable
*
*
*
0
1
2
3
4
days

Figure 3.4. Graph to show the change in viability of E14.5 *Xt/Xt* cortical cells (circle), *+/+* (*control*) striatal and cortical cells mixed (circle with dot), and *+/+* (control) cortical cells (triangle) cells cultured in serum-free conditions over a period of three or four days. At an initial plating densities of (A) 1000 cells/mm^2, the *Xt/Xt* cortical population maintained a trend for greater viability than the *+/+* cortical cells, and was significantly more viable by Days 1 and 3 (asterisks). The *Xt/Xt* cortical population was also significantly more viable than the *control* striato-cortical population by Day 2 (open star). At an initial plating density of (B) 2000 cells/mm^2, the *Xt/Xt* cortical population again maintained a trend for greater viability than *control* cortical cells or the *control* striato-cortical mix. On Day 4, the trend became significantly different (asterisk).

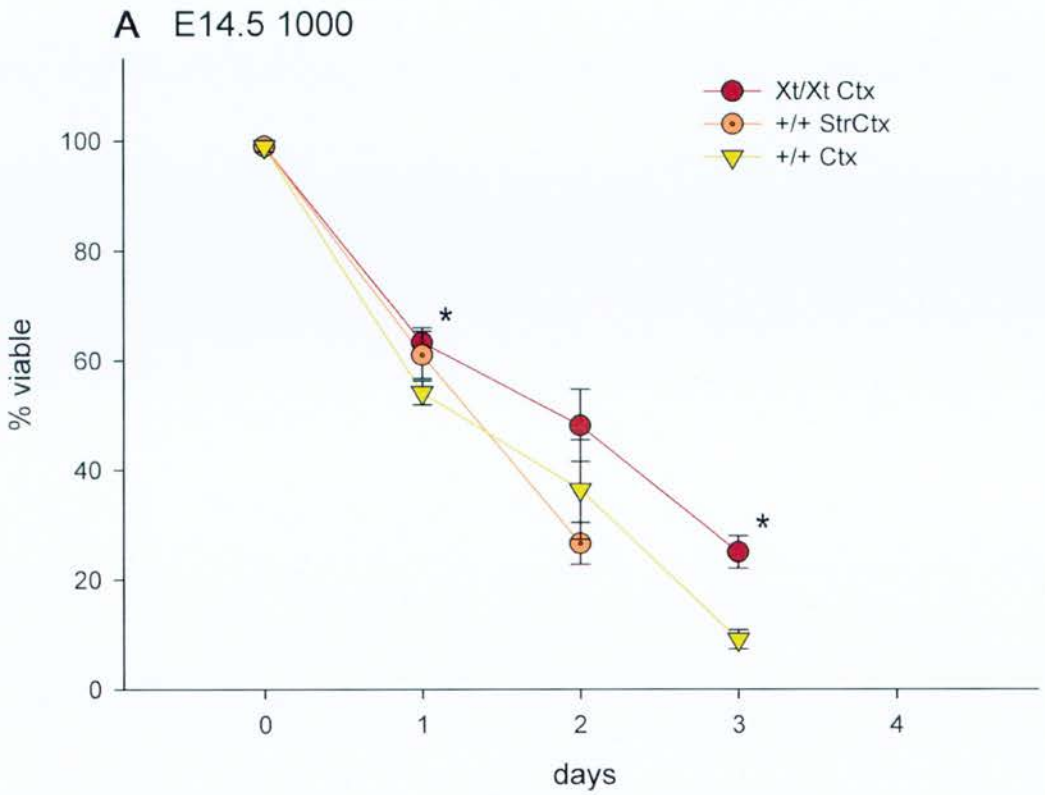
A E14.5 1000
Xt/Xt Ctx
+/+ StrCtx
+/+ Ctx
% viable
100
80
60
40
20
0
0
1
2
3
4
days
*
*

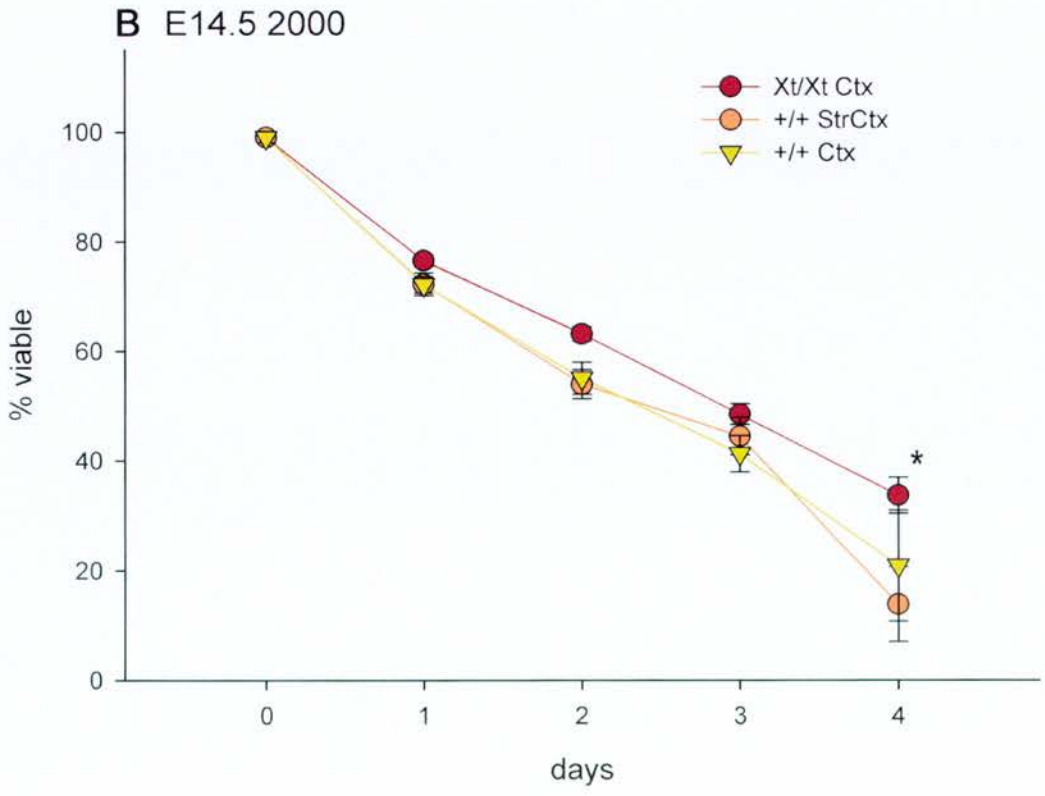
B E14.5 2000
Xt/Xt Ctx
+/+ StrCtx
+/+ Ctx
% viable
100
80
60
40
20
0
0
1
2
3
4
days
*

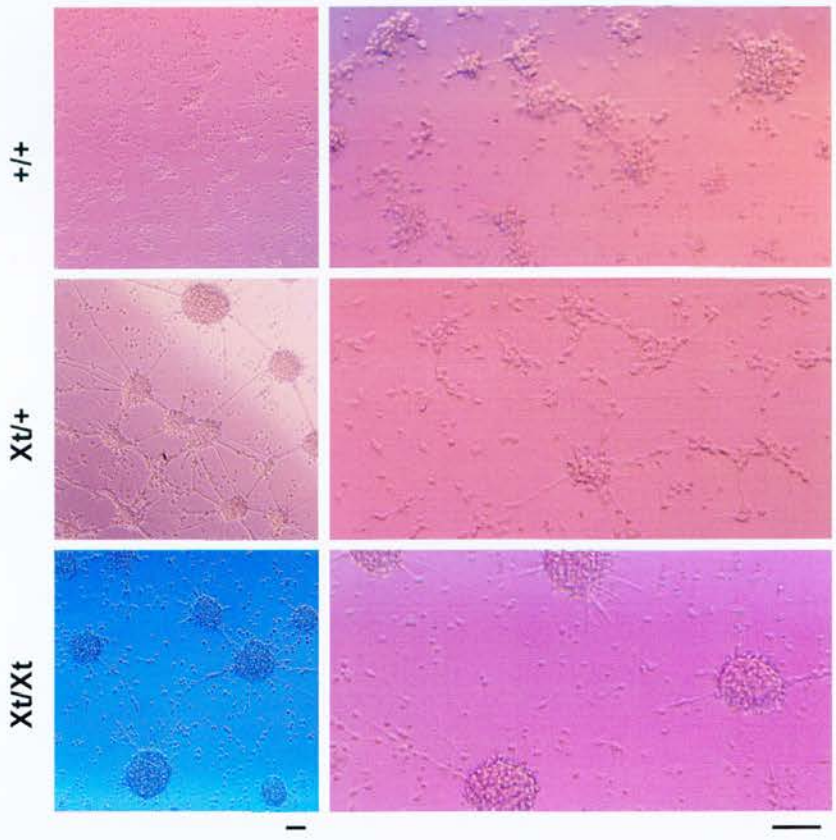

Figure 3.5 Primary +/+, *Xt*/+, and *Xt*/*Xt* neocortical cells from E16.5 embryos cultured for 2 days on vessels not coated with poly-L-lysine. The observed viability (by cell morphology) illustrated in these images show that E16.5 *Xt*/+ and *Xt*/*Xt* neocortical cells exhibited greater viability than their wild-type counterparts. Note the +/+ populations have not formed clusters, and by their morphology appear to be lysed. The *Xt*/+ population had formed clusters and appear viable. The *Xt*/*Xt* population had formed large clusters with fewer cells inbetween than the *Xt*/+ clusters, and appear viable. The clustering effect seen here is more exaggerated than the cell viability assays, which were performed using poly-L-lysine as an adhesive substrate. Scale bars measure 50μm.

on the second day of culture (<3.5%), while *Xt/Xt* material remained viable (>35%). Together, these results suggest that *Xt/Xt* neocortical cultures have an intrinsic property which allows them to survive better than their +/+ counterparts *in vitro*. Furthermore, this property becomes exaggerated as development proceeds from E14.5 through to E16.5.

Xt/+ Neocortex is More Viable than +/+ Neocortex at E16.5

Xt/+ neocortical viability deviated significantly from +/+ viability at E16.5 on Day 1 where it was significantly higher (ANOVA, p=0.004) (Figures 3.2 and 3.5). On Day 2 both populations were dead. This effect was noted at both plating densities. Furthermore, E15.5 *Xt/+* material appears to be more viable than +/+ material (Figure 3.3), though the difference is not significant at this stage.

Younger +/+ Material, but not Xt/Xt Material, is More Viable

+/+ cells cultured at E14.5 were more viable than +/+ cells cultured at E15.5, which were more viable than +/+ E16.5 cells. However, *Xt/Xt* material collected at E15.5 was more viable than *Xt/Xt* material collected at E14.5 and E16.5 (Figure 3.6).

Higher Density Cultures are More Viable than Low Density Cultures

Initial plating density influenced the viability of all cell populations, regardless of developmental age or genotype; the greater the density, the greater the viability of the culture. However, *Xt/Xt* neocortical cells appeared to be less affected by an increase in cell density than +/+ cultures. This was seen by calculating the relative

Figure 3.6. Graph to illustrate the difference between the change in viability of E14.5, E15.5, and E16.5 material after (A) 1 day in culture and (B) two days in culture. Note that at Day 1 (A), the viability of E14.5 and E15.5 *+/+* material remains similar, but the viability of E16.5 *+/+* material is reduced. After two days in culture (B), E14.5 material appears more viable than E15.5 material, that appear more viable than E16.5 material. Compare the change in viability of *+/+* material with *Xt/Xt* material. At Day 1 (A), E15.5 *Xt/Xt* material is more viable than both E14.5 and E16.5 material. This also appears to be the case at Day 2 (B). These data suggest the *in vitro* viability profile from E14.5 to E16.5 of *Xt/Xt* material differs from that of *+/+* material.

A.

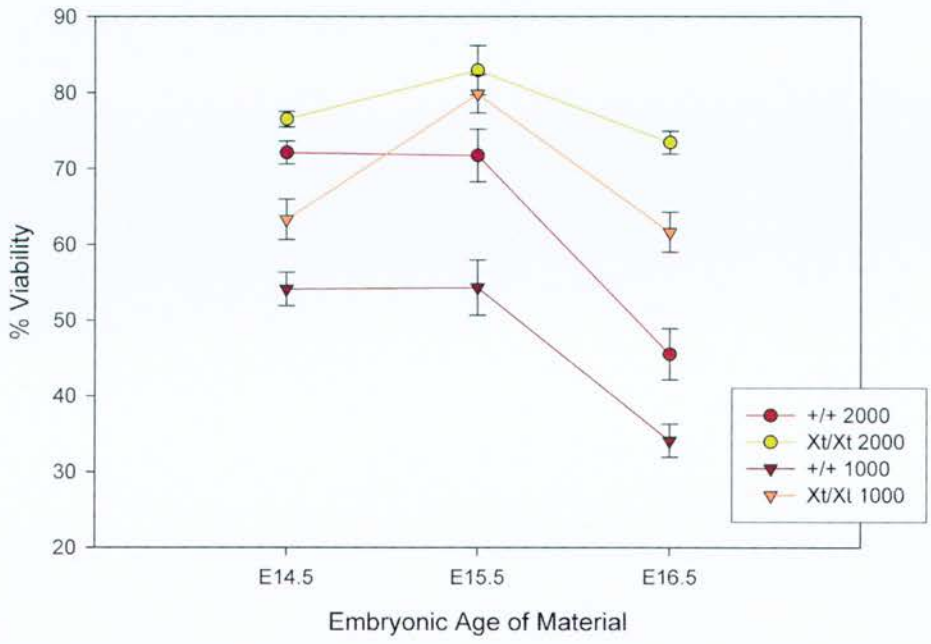
Viability at Day 1 Across the Ages
% Viability
90
80
70
60
50
40
30
20
E14.5
E15.5
E16.5
Embryonic Age of Material
+/+ 2000
Xt/Xt 2000
+/+ 1000
Xt/Xt 1000

B.

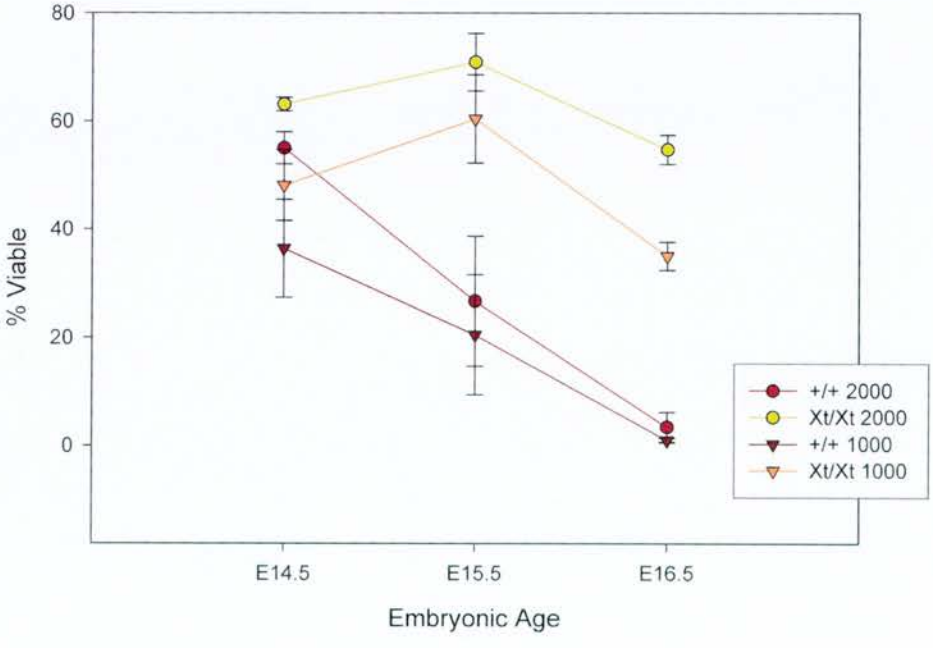
Viability at Day 2 Across the Ages
% Viable
80
60
40
20
0
E14.5
E15.5
E16.5
Embryonic Age
+/+ 2000
Xt/Xt 2000
+/+ 1000
Xt/Xt 1000

change in viability of cultures plated at 2000 and 1000 cells/mm^2, using the equation:

$$\text{relative increase} = (\text{viability}_{1000} / \text{viability}_{2000}) \times 100$$

After one day in culture, +/+ cells cultured at the higher density were 33% more viable than those cultured at the lower density. In *Xt/Xt* cultures, this increase was 20% or less (Table 1).

Table 3.1. *Percent increase in viability of neocortical cells cultured at 1000 cells/mm^2 in relation to those cultured at 2000 cells/mm^2 after 1 day in culture.*

	E14.5	E15.5	E16.5
+/+	33.3	32.0	33.4
Xt/+	-	22.3	35.3
Xt/Xt	20.8	3.88	19.2

Local Cell Densities Do Not Influence Viability

An analysis of local field-of-view densities was performed in order to (i) determine if they were comparable within an experiment between phenotypes, and (ii) to determine if they influenced cell viability, as was seen for global cell plating densities.

Calculation of Local Field-of-View Densities

First, the average field-of-view cell number was calculated by counting the total number of cells counted in an experiment (E16.5, E15.5, and E14.5), for each

phenotype (*Xt/Xt*, *Xt/+*, and +/+ or *control*) at each time-point (Day 1, 2, 3, and 4). The total number of cells was then divided by the total number of field-of-views used to obtain these numbers. This provided an average cell density for the field-of-view for each. The results for these calculations in relation to cell viability are presented in Appendix B, and summarised below.

The average field-of-view cell density was usually comparable between phenotypes for each experiment at each time-point, though some differences were noted.

At E16.5, on Day 2, at the initial plating density of 2000 cells/mm^2, *Xt/Xt* field-of-view density was significantly more dense than *Xt/+* and +/+ (Tukey Test $P < 0.050$). On Day 3 at 2000 cells/mm^2, *Xt/+* was significantly more dense than *Xt/Xt* (Tukey Test $P < 0.050$). The greater density of *Xt/Xt* cells on Day 2 may contribute to an increase in viability. However, the *Xt/Xt* population was also more viable than the other populations on Day 3 when the *Xt/Xt* population exhibited less density. These data suggest local field-of-view densities, though they may differ, do not contribute to the overall viability of a culture.

At E15.5, significant differences between phenotypes were noted, but they did not appear to follow a trend, nor did they correlate with the viability data. Average field-of-view densities were comparable on Day 1. On Day 2, the +/+ population initially plated at 1000 cell/mm^2 was significantly more dense than both the *Xt/Xt* and *Xt/+* populations (Tukey Test, $P<0.050$). At plating density 2000 cells/mm^2, the *Xt/Xt* population on Day 2 appeared more dense than the +/+ population (Tukey Test, $P<0.050$), but not the *Xt/+* population (Tukey Test, $P>0.050$). Here, there is an instance where +/+ field-of-views were more dense, but less viable, and in contrast, another situation where *Xt/Xt* field-of-views were more dense, and more viable. Thus, local-field-of-view densities do not seem to influence viability.

At E14.5, one condition showed a significant difference; *Xt/Xt* Str was more dense than +/+ Str (Kruskal-Wallis ANOVA: $P<0.05$). All other populations exhibited

comparable densities (Kruskal-Wallis ANOVA: P>0.05), which implies that local density was not a contributing factor to differences in viability.

Linear Regression Analysis

Second, a series of linear regressions was performed in order to determine if local field-of-view cell densities, *i.e.* the density measured in one field-of-view, influenced cell viability. Data was analysed for each field-of-view from all experiments. Total cell number per field-of-view (local density) was compared to the viability for that field-of-view and a regression analysis performed to determine if there was a correlation (Figure 3.7). In cultures prepared from E16.5 material, a positive correlation for density and viability was found for +/+ cells on Day1 (R=0.560), and *Xt/Xt* cells on Day 2 (R=0.742), both when plated at 2000 cells/mm^2. In E14.5 cultures, positive correlations were found in the *control* cortical population plated at 1000 cells/mm^2 (R=0.837), and in the *Xt/Xt* cortical populations on Day 3 (R=0.421) and Day 4 (R=0.540), and in the +/+ ganglionic eminence-cortical mix on Day 4 (R=0.876), in cultures plated at 2000 cells/mm^2. A negative correlation was found in the +/+ ganglionic eminence population at Day 3 (R=0.543). No significant correlation was found in cultures prepared from E15.5 material. Together, these data suggest there is a slight positive correlation between local density and viability, but the effect is similar for all phenotypes and thus will not affect difference noted between the phenotypes.

Figure 3.7. Linear regression analyses of E15.5 (A) Day 1 and (B) Day 2 data to show that local field-of-view densities do not correlate with viability at this age. Similar analyses were performed for data from E14.5 and E16.5 material. As illustrated here, these data suggest there is a slight positive correlation between local density and viability, and the effect is similar for all phenotypes.

A. Viability According to Local Density Regression Analyses of E15.5 Day 1 Data

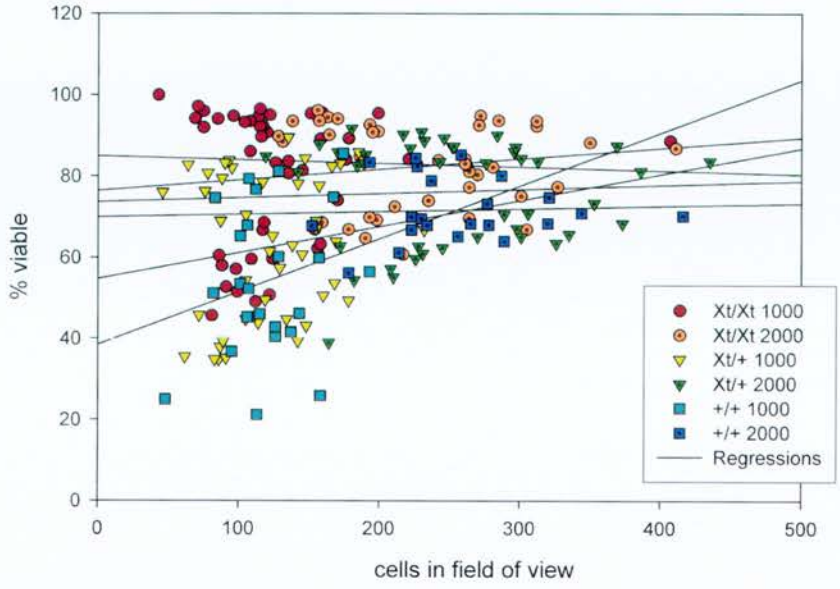

B. Viability According to Local Density Regression Analyses of E15.5 Day 2 Data 1000 and 2000 Plating Densities

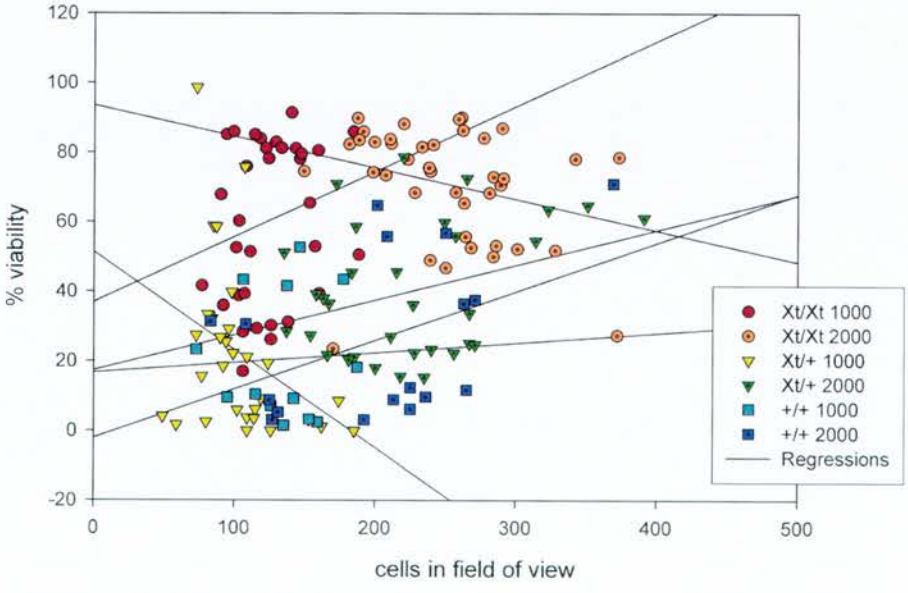

Discussion

The data presented in this chapter tell us that E14.5 to E16.5 *Xt/Xt* neocortical cells outlive their +/+ counterparts in the serum-free *in vitro* conditions mentioned above. The mechanism, or mechanisms behind this phenomenon may be due to a number of different changes that homozygous mutation to *Gli3* creates in the developing mutant brain. In order to pinpoint the function of *Gli3* in normal, wild-type brain, it will help to discuss the results obtained in this chapter and suggest reasons for the observed increase in *Xt/Xt* survival.

I will first discuss the cell culture technique and the factors that are important for primary cell survival. I will then discuss the *Xt/Xt* phenotype and suggest ways in which the *Xt/Xt* brain may be developing to yield the *in vitro* data observed. An analysis of these data will help us to suggest a role for *Gli3* in the development of the forebrain, and help us to suggest which mechanisms are primarily and secondarily disrupted to give rise to the *Xt/Xt* forebrain phenotype. This will provide us with an inferred function of the role of *Gli3* in normal developing brain.

Factors That Influence Cell Survival in Primary Culture

Cortical cells require a number of factors, or conditions for survival. As individual constituents in a tissue, these factors are provided for, and cells undergo a normal developmental process. However, in this culture system the cells have been forcefully removed from their normal environment and placed in an very minimal one. (When we take into account the mechanical and enzymatic treatment that these cells are put through, it is quite amazing that the cells survive at all.) This removes them from their normal matrix of extracellular molecules and neighbouring cells and forces them to adjust to an abstract environment.

The effects of dissociation and culture on the life of neuronal cells has been studied by workers for several decades (for a good review see pg 37-78: Banker and Goslin, 1998). The major criteria for cell survival have been identified, and in this situation, I consider them to be, in no particular order of importance: (i) severity of the dissociation method, *i.e.* mechanical or enzymatic, harsh or mild; (ii) tissue type, *e.g.* cortical, hippocampal, striatal, *etc.*; (iii) age of the tissue, *i.e.* early-, mid-, late-gestation, or postnatal; (iv) cell density of the culture; and (v) media composition, *e.g.* constituent nutrients, growth factors, serum, *etc.* As the culture conditions remain constant between the experimental (*Xt/Xt*) and control (+/+) populations, all of the above factors should remain constant and therefore any change in cell behaviour, *e.g.* cell survival, will be related to the instrinsic differences in the cell population due to presence or absence of the functional *Gli3* gene.

However, the case is not so cut and dry because the morphology of the *Xt/Xt* tissue is so abnormal that it is not clear if the neocortex is indeed neocortex. This provides us with the problem of **cell type**. Is the cell-type composition of the *Xt/Xt* neocortex comparable to that of the +/+ neocortex, *i.e.* does the *Xt/Xt* neocortex contain the same types of cells and the same proportion of those types of cells as the wild-type neocortex? This point is an important consideration because if the cellular composition of *Xt/Xt* and +/+ neocortex is significantly different, then the experimental paradigm used for these experiments may not be testing the effect of *Gli3* in comparable cell populations. If this were the case then we would first and foremost be testing the reaction of different cell types to these culture conditions, and the primary effect of *Gli3* would lie somewhere upstream of this phenomenon.

There are two parts to the issue of cell type. First is the issue of whether the *Xt/Xt* neocortex contains the same proportion of pre- and post-mitotic cell types as normal. The early *Xt/Xt* neocortex is thinner than wild-type neocortex (E12.5), fails to invaginate (E13.5), does not laminate (E14.5 to E17.5), and becomes convoluted (E15.5 to E17.5). These histological phenotypes may have arisen because the tissue is composed of a different proportion of proliferating ventricular zone cells to post-mitotic cortical plate cells than normal. These two cell populations are very different

in structure and behaviour *in vivo*, and probably act very differently in culture. If the *Xt/Xt* neocortex is composed of a greater proportion of ventricular zone cells, for instance, these cells may survive better in culture. Therefore, the increase in viability reported above may be the result of a difference in the proportion of proliferating and post-mitotic cell types in the *Xt/Xt* and +/+ neocortices.

The second issue of cell type is the effect of ectopic ganglionic eminence cells in the neocortex. Theil (1999) and Tole (2000) reported that the *Xt/Xt* forbrain has been 'ventralised', and they point out that some areas of the *Xt/Xt* neocortex contain patches of cells that express ganglionic eminence-specific markers (*Dlx2* and *Isl1*). They suggest that the ventral-dorsal forebrain boundary is broken in the *Xt/Xt* forebrain, a statement supported by the histological appearance of the tissue and the expression of *Dlx2* and *Isl1* in the cortical domain. Further to their report, I have found that the ganglionic eminence-specific marker MASH1 is also found in the neocortex of the *Xt/Xt* embryo (see Chapter IV). It is therefore irrefutable that the *Xt/Xt* neocortex (the *dorsal* forebrain) is partially ventralised. The question then begs to be answered: does the ectopic presence of ganglionic eminence cells in the *Xt/Xt* neocortex affect the *in vitro* (and *in vivo*) viability of neocortical cells? This question is addressed in the next chapter.

Other differences may arise between the composition of *Xt/Xt* and +/+ cultures which may help to account for differences in cell survival. The *Xt/Xt* neocortex may be less advanced than the +/+ neocortex due to **developmental delay**. It is quite clear in the data (Figures 3.2 to 3.4) that wild-type cells from the more advanced neocortical tissue do not survive as well as the wild-type cells derived from less advanced tissue, *i.e.* cells harvested from E16.5 neocortex do not survive for as long in culture as cells harvested from E14.5 neocortex. This is not so much the case for *Xt/Xt* cells. *Xt/Xt* cells remain approximately 60% viable on Day 2 when cultured at 2000 cells/mm^2, whether from E14.5, E15.5, or E16.5 embryos. This is in stark contrast to the rapid decline in viability of Day 2 +/+ cells as the material advances in age from E14.5 to E16.5 (see Figure 3.6). It is possible that between littermates the *Xt/Xt* embryo is less advanced than its +/+ counterpart, and therefore its

dissociated neocortex may exhibit a comparable cell death profile to a younger, wild-type neocortex *in vivo*, and *in vitro*.

The cell viability data shows that there is a smaller difference in viability between *Xt/Xt* and +/+ populations in cells from E14.5 neocortex than there is between these populations in cells from E15.5 and E16.5 neocortex. The data from Day 2 of the 2000 cells/mm^2 cultures most clearly shows this feature (Figure 3.6, B).[10] The wild-type populations drop in survival from 55% viability at E14.5, to 27% at E15.5, to 3% at E16.5; while the viability of the *Xt/Xt* populations remains relatively constant at 63% at E14.5, 70% at E15.5, and 55% at E16.5. This would seem to suggest that from E14.5 (or shortly before, as there is still a slight difference at this age) onwards, the *Xt/Xt* neocortex fails to mature normally, suggesting there might be developmental delay in the forebrain.

Differences in **cell proliferation** may also account for differences in viability. If the *Xt/Xt* population is proliferating at a *greater rate* in culture than the +/+ population, then more cells would be generated. These cells may then survive better *in vitro*, either as an intrinsic property of newborn cells, or because cell-cell contact-mediated survival mechanisms would increase. Cell-cell contact provides vital support, and though the cultures were initially plated at the same cell density, *i.e.* 500, 1000, 2000, or 4000 cells/mm^2, an increase in the rate of proliferation may increase cell density and thus viability. Or, if the *proportion* of proliferating cells is greater in *Xt/Xt* neocortex than in +/+ neocortex, then these proliferating cells may not be damaged as extensively as the post-mitotic cells types, and so overall cellular integrity, and therefore cell viability, may be increased. The latter hypothesis that there is a greater proportion of proliferating cells in *Xt/Xt* neocortex than in +/+ neocortex has been tested using antibodies to mark the proportion of pre- and post-mitotic cell types. The former hypothesis that the rate of cell cycle is increased in

[10] Day 2 data at 2000 cells/mm^2 is the best viability data set for this cross-age comparison because a good proportion of the cells are still healthy at this time (bar E16.5 wild-type), and there is not extensive clumping as there is in time points beyond two days in culture.

Xt/Xt cells has been tested using a BrDU incorporation assay. Both sets of experiments are presented in the next chapter.

The effect of **cell-cell contact** on survival *in vitro* is an interesting feature that appears to be different from normal in the *Xt/Xt* population. If we compare the viabilities of populations cultured at 1000 and 2000 cells/mm^2, we see that in the wild-type cultures viability is increased 33% when we double the density (Table 3.1). This appears to be a robust increase and remains true at E14.5, E15.5, and E16.5. In the *Xt/Xt* cultures, the increase in viability is 20% at E14.5 and E16.5, and only 4% at E15.5, when the density is increased from 1000 to 2000 cells/mm^2. These data would not be so interesting if the wild-type data was less robust, but a consistent increase of about 33% throughout neurogenesis suggests that there is a significant quantifiable relationship between viability and density. Further, this relationship is disturbed in the *Xt/Xt* neocortex to a variable degree. I would suggest that this means *Gli3* is required for normal cell-cell contact-mediated signal transduction, and that without *Gli3*, cells are less sensitive to the signals. I will raise this point again when I consider the development of the limb and other areas affected by a *Gli3* mutation.

Finally, the type and amount of **soluble factors** secreted into the medium may be more favourable in *Xt/Xt* cultures than in +/+ ones. In these experiments, I have used a medium that contains a minimal quotient of nutrients (see Appendix A: Culture Reagents). Most importantly, the medium is serum-free, *i.e.* it does not contain any unknown growth factors, hormones, proteins, peptides or other molecules that may be present in a serum-based medium. This system, then, is clean and well defined. Any additional extra-cellular material that might exist in the medium will and can only come from the cells themselves. This is an important consideration because a primary factor in primary cortical cell survival is the presence or absence of soluble molecules and growth factors in the medium (for example see: Lotto and Price, 1995). These molecules can either be secreted by the cells in culture, or they can be provided through the addition of a serum (serum-enriched medium produces a more viable culture). In my case, any soluble

molecules or growth factors important for survival would have to come from the cells themselves.

In the developing *Xt/Xt* brain, soluble FGF's, Bmp's, and Wnt's are all misexpressed, especially at the cortical hem where the brain would normally invaginate to cleave into two distinct hemispheres (Tole et al., 2000; Theil et al., 1999). The cortical hem also connects the cortex to the hippocampus – another structure missing in the *Xt/Xt* brain. There can be no doubt that **misexpression of key signalling molecules** has downstream effects, and that these downstream effects have contributed to (or are responsible for) the *Xt/Xt* cortical phenotype. I will consider these possibilities below.

Disruption of Signalling Centres May Decrease Cell Death *In Vivo*

Another signalling centre, the anterior neural ridge (ANR) is also disrupted. Recent data shows FGF-8 expression is expanded in the *Xt/Xt* forebrain from E10.5 to E12.5 (Aota et al., 2002). FGF-8 is an important molecule; it is a potent growth factor that is expressed in the AER of developing limb, and the ANR of developing brain. It has been postulated that the molecule has a similar function in both tissues, and that this is to stimulate and maintain proliferation. In the developing *Xt/Xt* embryo, both the ANR and AER are expanded, as defined by the region of FGF8 expression. These data would seem to suggest that the proliferating region underlying the AER in limb would also be expanded, and may contribute to the polydactyl phenotype. In the brain little is known about the role of FGF8, but I have suggested in the Introduction that the signalling centres in the developing brain are comparable to the signalling centres in the developing limb, and that these signalling centres perform similar functions. If we make this supposition, then the principle function of the ANR in the developing brain is to stimulate and maintain cell proliferation, as it is in the AER. An expanded FGF8 domain means an expanded ANR, which we can suppose means a larger area of (more rapidly) proliferating cells.

An expanded FGF8 domain also ties in with a decrease in cell death in the forebrain of the *Xt/Xt* mouse; Aota et al. (2002) also noticed a reduction in cell death in the regions bordering the FGF8-expressing domain. These data were collected in E8.5 and E9.5 embryos, but presumably touch on a common feature of FGF8 expression in the ANR and AER: that it promotes proliferation in cells neighbouring these regions, and also death in regions that border the neighbouring regions. The extent of this effect at the time of my experiments, at E14.5 to E16.5, is unclear, but we can assume with some confidence that FGF8 expression is altered in the developing forebrain nearer to, and probably during neurogenesis, and that this change in expression affects both cell proliferation and cell death in that region.

If cell death is reduced *in vivo* in the *Xt/Xt* neocortex, it can occur at either of the two broad categories of normal PCD in the developing neocortex, (1) ventricular zone cell death and/or (2) cortical pruning of neurones in the cortical layers. Within the ventricular zone of neocortex, the mechanism of an alteration to normal PCD can occur at two levels: (a) disruption of the intracellular signalling pathways, and/or (b) a tissue patterning level where expression of extracellular signals required for normal PCD may be disrupted. In the neuronal layers of the neocortex, cell death may be inhibited by (a) a disruption to the normal neurotrophic signalling pathways, and/or (b) disruption to cell-cell connectivity by way of changes to process extension or aberrant migration of striatal cells into the cortex.

The most likely location of alterated normal programmed cell death in the *Xt/Xt* neocortex is in the VZ. The VZ is the proliferative layer, or pool of cells that gives rise to the (largely) post-mitotic cortical layers. Disruption to cell death in the VZ would yield a compounding phenotypic effect during development, as a reduction of cell death would increase cell number. An increase in the number of cells in the VZ also means an increase in the number of dividing cells, and so as development proceeds, the increase increases and an initially small phenotype is compounded. It is unlikely that the differences in *in vivo* cell death would occur in the laminar layers. This is because a phenotype in the forebrain can be seen before lamination occurs

(<E14.5). Also, cell death in the cortical plates is a matter of cortical pruning, a process that comes into effect in late gestation and early postnatal periods to refine inter-neuronal connectivity; it is not thought to affect the morphology of the tissue.

Thus, it is likely that if normal PCD is disrupted in the forebrain, it is disrupted in the VZ. Furthermore it is probably disrupted from an early age, and continues to be disrupted due to lack of Gli3. A reduction in normal cell death may well be a causal factor of the *Xt/Xt* forebrain phenotype. There is evidence to support this hypothesis. *Bmp2* and *Bmp7* expression is undetectable and *Bmp4* and *Bmp6* expression is reduced to tiny patches in the *Xt/Xt* dorsal telencephalon at E12.5 (Tole et al., 2000). These signalling molecules are known to induce cell death, as well as patterning, in other systems. (1) In the rhombencephalon, Bmp4 signalling was found to induce apoptotic depletion of cranial neural crest cells in a process that precedes their migration to the facial region (Graham et al., 1994). This process helps to sculpt distinct populations of craniofacial progenitors, a process that may also help to explain the craniofacial and cervical phenotypes of the *Xt/Xt* mouse (see Chapter V) (for review see: Graham et al., 1996). Furthermore, the homeobox gene *Msx2* is found to be coincident with *Bmp4* expression in this area and mediates the Bmp-regulated pathway (Marazzi et al., 1997). (2) In the developing limb, *Bmp*'s are important patterning genes that also regulate interdigital cell death (for review see: Capdevila and Belmonte, 2001). When Bmp signalling is prevented, interdigital cell death is downregulated along with the expression of *Msx1*. (3) In other systems, *Bmp4* is found to mediate cell death in the eye (Trousse et al., 2001), and addition of Bmp2 and Bmp4 are found to kill immortalised sympathoadrenal progenitor cells (trunk neural crest derived) in a dose dependent manner, unless there is addition of FGF (Song et al., 1998). (4) These data suggest that *Bmp*'s normally expressed in developing forebrain are also responsible for normal cell death there, though there is no primary data to show this. If *Bmp*'s do induce normal cell death in the developing forebrain as they do in other tissues, and their expression is downregulated as it is in the *Xt/Xt* forebrain, then it is quite probable that cell death is also downregulated, or not induced in *Xt/Xt* forebrain.

Furthermore, the caspase-3 and caspase-9 knock-out mice display a forebrain phenotype comparable to the *Xt/Xt*. Normal cell death is reduced in these knock-outs, an expected pheotype given that the caspases are essential for normal PCD. The brains display an expanded and convoluted cortical plate comparable to the *Xt/Xt* cortex (Haydar et al., 1999; Theil et al., 1999).

Thus, normal cell death may be affected in the *Xt/Xt* forebrain, probably due to lack of *Bmp* expression in the cortical hem, and an increase in the FGF8-expressing ANR. Data presented in this chapter shows that cell death is reduced in primary *Xt/Xt* cells from the neocortex. It is compelling to believe that the *in vitro* effect is reflecting the *in vivo* circumstance.

The *in vitro* data shows a greater difference between *Xt/Xt* and +/+ primary neocortical viability, or cell death rates at older (E16.5) stages than at younger (E14.5) stages. If we consider that *Bmp* expression induces cell death in the neocortex, or primes cells in the neocortex to respond to FGF cues or die, as suggested by Song *et al.* (1998), then this effect must increase in importance as the neocortex matures, or else another mechanism is responsible for the increase in difference between *Xt/Xt* and +/+ cells from E14.5 to E16.5. An *in vivo* investigation into a disruption of cell death in the *Xt/Xt* neocortex was explored, and is the subject of discussion in Chapter IV.

Experimental Cell Damage May Contribute to *in vitro* Cell Viability

Damage to the cells during dissociation may also be a contributing factor to neocortical cell death rates *in vitro*. As I have mentioned earlier, the cells undergo a harsh enzymatic and mechanical treatment and it is surprising that the cells survive at all. It is possible that the *Xt/Xt* cells are less damaged than their wild-type counterparts, and that this is a primary factor in their subsequent increase in *in vitro* viability. Under this interpretation, the data in this chapter can be seen to show that

(i) +/+ neocortex is damaged to a greater extent than *Xt/Xt* neocortex, (ii) older +/+ neocortex is damaged to a greater extent than younger +/+ neocortex, and (iii) the cytological change from E14.5 to E16.5 that is causing increased +/+ cell damage is occurring to a greater extent in +/+ cells than in *Xt/Xt* cells.

The most probable cytological elements damaged during dissociation are the cellular processes, namely the neuronal afferents and dendrites. Thus, the change in viability, or survivability of cell populations from E14.5 to E16.5 may be due to differences in the cell-type composition of the tissue, or the cytoarchitechtonics of the cells in the tissue. There are two possible explanations; either the neocortex in the *Xt/Xt* embryo is composed of a greater percentage of pre-mitotic cell types than in wild-type neocortex, and/or the *Xt/Xt* post-mitotic cell types may have less extensive peripheral appendages.

Development of the neocortex from E14.5 to E16.5 can be divided into the two major layers, each with a different constituent cell type: the 'pre-mitotic', proliferating ventricular epithelium (the ventricular zone, VZ), and the largely post-mitotic laminar cortical plate. The proportion of these layers changes significantly between E14.5 and E16.5. At E16.5, the neocortex is more mature and is composed of a greater percentage of the post-mitotic, differentiated neurones than the E14.5 neocortex. Layers III, IV, V, and VI have formed and cortico-cortical connectivity is being established. The mature neurones have, and are investing in peripheral cytoarchitectonics. Axons are extended away from the cell body and dendrites form to receive afferents. At E14.5 on the other hand, the proliferative ventricular zone accounts for a greater proportion of the total cell population. Ventricular epithelial cells are morphologically simpler than differentiated laminar neurones. They are slender cells with a long bipolar process that touch the ventricular wall at one end, and the border of the subventricular zone at the other. At E14.5, only the first cortical layer has formed and the bulk of the tissue is made of the pre-mitotic, proliferating VZ cells.

The dissociation method of the experiment exposes the cells to a very harsh conditions. Immediately after dissociation the cells can be viewed under the microscope. Most appear as round cell bodies lacking any sign of a peripheral appendage regardless of embryonic age or genotype (though some may exhibit a residual process no longer than 10μm). The peripheral structures have either been forcefully removed or they have been withdrawn. Presumably, the more mature neurones which have invested in peripheral structures such as axons and dendrites, will be more damaged by the procedure. Mature neurones have also finalised their developmental fate, and are less open to change. On the other hand, the epithelial precursor cells in the VZ may be less damaged because of their dynamic cell morphology (they undergo an interkinetic movement) and their relatively simple cytoarchitecture. They are also less specialised, and may be able to cope better with a change in environment. An increase in the amount of overall damage caused to the cells from E14.5 to E16.5 is one factor which may explain the reduction in survivability of older material.

If cell damage is an important factor in the subsequent *in vitro* survival rates, it appears that *Xt/Xt* tissue suffers less damage than +/+ tissue. This may be because (i) *Xt/Xt* neurones have less extensive appendages than +/+ neurones, and/or (ii) *Xt/Xt* neocortex is composed of a greater proportion of ventricular zone cells than +/+ neocortex, and this inter-phenotypic difference increases from E14.5 to E16.5. The former explanation was explored briefly in Chapter IV, and could be examined more closely using the Golgi method to label neurones in the *Xt/Xt* neocortex and their cytoarchitecture compared to wild-type.[11] The latter explanation that the proportion of VZ to cortical plate is greate in *Xt/Xt* neocortex than it is in +/+ neocortex ties in with other hypothesis mentioned above (possible increase in proliferation and inherent survival rates) and is explored using immunocytochemical markers in Chapter IV.

---

[11] This question can be answered using Golgi's Method to stain cortical neurones *in situ*, and the peripheral branches analysed for length and complexity using a computer package such as Neurolucida (MicroBrightField, Inc., Williston, U.S.A.) which will quantitate peripheral development.

A reduction of *Bmp7* expression may affect dendritic outgrowth in the *Xt/Xt* forebrain. *Bmp7* is normally expressed in the cortical hem of the telencephalon, but is not expressed in the *Xt/Xt* telencephalon (Grove et al., 1998). Bmp7 enhances dendritic outgrowth in many neuronal types, including those of the hippocampus and cerebral cortex (Guo et al., 1998; Withers et al., 2000). Without *Bmp7* expression, it is possible that *Xt/Xt* neocortical neurones do not develop extensive dendrites as normal. A lack of normal peripheral appendages may help to preserve the cell's integrity during dissociation, as described.

A Test for Cell Type Composition

The differences between these two major layers of the neocortex, the proliferating VZ and post-mitotic lamination, is crucial because the cell types of each are very different; they have different behaviors, different subcellular components, different architectures, and they have different *requirements for survival.* The hypothesis that the proportion of cell types is abnormal in *Xt/Xt* neocortex has been tested and is reported in the next chapter. I have used immunocytochemical markers to determine the proportion of pre- and post-mitotic cell types in the *Xt/Xt* and +/+ neocortices. A difference in the proportion of the major layers also lends evidence to suggest differences in the amount of proliferation occuring *in vitro*, and indeed *in vivo*. The cell type data obtained from immunochemical methods will be used with data acquired from a BrDU incorporation assay to help answer the question whether or not the rate or amount of proliferation is abnormal in the *Xt/Xt* neocortex. These results are presented in Chapter IV.

Evidence of an Xt/+ Neocortical Phenotype

The *Xt/+* mouse is not known to exhibit any neurological phenotype (Johnson, 1967; Theil 1999). However, some *GLI3*(-/+) humans show levels of mental retardation or low intelligence quotients (IQ) (Williams et al., 1997). The occurrence of an extranumerary digit on *Xt/+* limbs is the only recognised indicator of haploinsufficiency in mouse. Therefore, any evidence that a neurological phenotype might exist in the *Xt/+* mouse is of interest.

Central to this thesis is the suggestion that *Gli3* acts in a similar manner in limb as it does in the forebrain. The fact that no neurological phenotype has been shown in the *Xt/+* mouse does not mean that no neurological phenotype exists, only that one has not been detected. Detection of the *Xt/+* phenotype in limb has the advantage that limb patterning is easily recognised by digit morphogenesis. If a neurological phenotype exists in the cortex of the *Xt/+* mouse, it will be more difficult to discern than the limb phenotype because cortical patterning is not obvious by morphology.

Data on E16.5 *in vitro* viability show a significant increase in the viability of *Xt/+* cells over +/+ cells from the neocortex. Furthermore, the same trend exists for E15.5 material. These data show that when neocortical tissue is challenged with an extreme environment, *Xt/+* tissue is able to survive better than +/+ tissue. Thus, *Xt/+* neocortical cells are inherently different from +/+ neocortical cells. Whether this inherent difference manifests itself *in vivo*, where cells are embedded in an extracellular matrix rich in trophic molecules, is another question. However, these data do show that the potential for *Gli3*-haploinsufficiency exists in neocortex *in vivo*.

Chapter IV: Further Experiments on the Neocortex

This chapter is an account of the experiments undertaken to help explain the data presented in Chapter III. These experiments are smaller and tackle the specific points raised in the discussion. First, I present a set of experiments to test the effect of ganglionic eminence cells in primary neocortical culture. These experiments help to show that ganglionic eminence cells, at E14.5, do not significantly contribute to an increase in primary neocortical survival. This suggests that this effect might be true at E15.5 and E16.5 as well, though this has not been tested.

I then continue with a description of an attempt to catalogue the amount of cell death in the neocortex *in vivo*. These experiments were designed to detect a difference in *in vivo* cell death rates between wild-type and homozygous *Gli3* mutant embryos. As this section will go on to explain, cell death rates in the forebrain of embryonic mice is much lower than expected. Cell death rates are so low, in fact, that a reduction in cell death rates may be inadequate to account the mutant forebrain phenotype.

In light of this result, a late change in tack was performed and an experiment was conducted to determine if cell proliferation rates were altered in the *Xt/Xt* neocortex. A set of experiments using a BrDU inclusion assay is presented. Furthermore, a separate set of experiments using antibodies against proliferative and non-proliferative populations are presented in the final section. Together, these results show than an alteration to cell cycle is observable in cells from the *Xt/Xt* neocortex during neurogenesis, though the exact nature of this alteration will only be defined by future experiments.

Primary Neocortex Co-cultured with Ganglionic Eminence

Does the ectopic presence of ganglionic eminence cells in the neocortex 'rescue' neocortical viability in culture?

The *Xt/Xt* neocortex is composed of normal wild-type neocortical cells, defined by the expression of neocortical markers (*e.g. Emx1, Emx2, Pax6*, and others), and a proportion of cells that are normally only found in the ganglionic eminences (GE), defined by the presence of *Dlx2* and *Isl1* (Thiel et al., 1999; Tole et al., 1999). The ectopic development of ganglionic eminence, or ganglionic eminence-like cells in the neocortex may disrupt the normal development of that tissue. In the wild-type brain, ganglionic eminence cells – expressing *Dlx2*, *Isl1*, and MASH1 – migrate into the neocortex to form a cortical layer of GABAergic inter-neurones (Tan et al., 1998; Ware et al., 1999). These cells connect with other cortical neurones, and in doing so the connected cells are more likely to survive cortical pruning mechanisms due to their established trophic support. Trophic support mechanism are known to encourage the survival of connected cells and discourage the survival of those that are not (Asavaritikrai, 2000). In the wild-type brain, GE cells would normally migrate into the neocortex at about E16.5, and therefore these trophic support mechanisms would not normally be an important factor in cell survival until later in development. However, these mechanism may still be operational at earlier ages, and in the *Xt/Xt* tissue, close proximity of GE cells to cortical cells may allow early GABAergic connectivity and thereby increase the survival rates of those regions.

There is an alternative GE-related hypothesis that might explain the increase in *in vitro* viability of *Xt/Xt* neocortical cells. An inherent property of GE cells may allow them to outlive cortical cells *in vitro*. Thus, it may be the ectopic GE cells present in the *Xt/Xt* neocortical cultures that are surviving for a longer period of time, and possibly the 'normal' *Xt/Xt* neocortical cells in that population are dying at a

comparable rate to wild-type. The ectopic GE cells may simply be masking the results.

Either way, the presence of GE, or GE-like cells, in the *Xt/Xt* neocortex may favourably change the amount of cell death viewed over the time-course of the experiment. If such an effect were happening *in vitro,* it is quite possible that this effect was also present *in vivo*, and that this mechanism may disrupt normal morphological development.

The hypothesis was tested using the *in vitro* system used and described in Chapter III. GE cells from E14.5 *control* (*Xt/+* and +/+ pooled) brains were cultured alone, and with *control* neocortex at a ratio of 1:1. Normal neocortical cultures were run in parallel.

Materials and Method

The methodology is precisely that described in Chapter III. *Control* (+/+ and *Xt/+*) ganglionic eminence cells were dissociated according to the same procedure used for cortical cells. They were then cultured on their own, or in a co-culture with +/+ neocortical cells. Cells were fixed at 24 hour intervals and their nucleus stained with Hoechst. Cell death was analysed according to nuclear morphology.

+/+ Cell Survival is not Increased when +/+ Ganglionic Eminence is Added

The addition of *control* GE cells did not increase the viability of neocortical cultures (Table 4.1). Furthermore, GE cells cultured alone did not exhibit viability greater than neocortex cultured alone. These data suggest that the admixture of striatal cells

in the *Xt/Xt* neocortex does not account for an increase in *Xt/Xt* neocortical viability *in vitro*, by either mechanism described above. However, due to the experimental variation and the small differences in viability normally seen between the phenotypes at E14.5, these results should be interpreted cautiously.

Table 4.1. *Percentage of Cells Viable in* control *Cortex (Ctx),* control *Cortical-Ganglionic Eminence Co-culture (CtxGE), and +/+ Ganglionic Eminence (GE) Cultures from E14.5 Material.*

Density	Day	+/+ Ctx	+/+ CtxGE	+/+ GE
1000	1	54.1	61.0	55.3
1000	2	36.4	26.6	39.8
1000	3	9.06		17.0
2000	1	72.1	72.2	69.1
2000	2	55.0	53.9	50.4
2000	3	41.2	44.4	30.1
2000	4	20.8	13.8	20.5

Discussion

The addition of GE cells to neocortical cultures does not appear to increase the overall survival of those cultures. Also, GE cells cultured on their own exhibit a comparable rate of survival to neocortical cells. These results seem to suggest that ectopic GE does not affect the viablility of neocortical cells in primary culture. However, because these experiments were performed on E14.5 tissue, and because the differences in viability in E14.5 cultures is slight (see Chapter III), these results must be taken as inconclusive. It would be fruitful to repeat these experiments at

E16.5 where the difference in viability between *Xt/Xt* and +/+ populations is more exaggerated, and where GE-type cells are more likely to have an effect on the viability of neighbouring cells *in vitro* and *in vivo*.

An Analysis of *In Vivo* Neocortical Cell Death

Is cell death reduced in the Xt/Xt *neocortex* in vivo*?*

The evidence I have presented so far suggests that normal programmed cell death may be reduced in the neocortex of the *Xt/Xt* brain. The reduction may be due to a direct consequence of the loss of *Gli3*, *i.e.* the Gli3 protein may interact directly with the cell death machinery, or it may be due to secondary consequences such as a change in the expression of *Bmp*'s and *FGF*'s in the dorsal forebrain region, specific combinations of which are known to inhibit or encourage cell death in neurones (Song et al., 1998). Whatever the primary cause of a reduction in cell death in the *Xt/Xt* forebrain, the case remains that an *in vivo* reduction in cell death (whether a primary or secondary effect of the gene) is the most likely explanation of the *Xt/Xt* forebrain phenotype.

In order to show that cell death is reduced in the neocortex of the *Xt/Xt* embryo, it is necessary to show a reduction of cell death *in vivo*. The best approach for this is an histological one. Histology accurately reveals the cellular condition of a tissue, frozen at a particular point in time by the application of a fixative. It is also superior to techniques such as whole mount TUNEL or trypan blue exclusion assays, which suffer from technical complications such as accurate quantitation and tissue penetration problems. It was therefore proposed that an histological examination of the *Xt/Xt* and +/+ forebrain be performed on tissue from E14.5, E15.5, and E16.5 embryos.

The method chosen for this study was based on an analysis of *in situ* cell death detection techniques (*i.e.* the nick-end labelling techniques of TUNEL and ISEL, and the techniques based on nuclear morphology, visualised with Hoechst or Propidium Iodide) used for *in situ* neural material (Asavaritikrai, 2000). It was determined that the simplest and most reliable method was an analysis of nuclear morphology based

on the Hoechst nuclear specific marker. This method allows the visualisation of all nuclei, and the clarity of the stain allows pyknotic and apoptotic cells to be easily distinguished from healthy or dividing cells.

In order then to determine whether or not cell death was affected in the *Xt/Xt* neocortex, a selection of E12.5 *Xt/Xt* and *Control* embryos were harvested and prepared for analysis. A preliminary analysis was conducted on E12.5 material first, because the morphology of this tissue is simpler, and so comparable regions between *Xt/Xt* and *Control* brains were more readily identified.

Materials and Method

The analysis was performed to test the feasibility of the *in vivo* Hoechst cell death detection method. A litter of E12.5 embryos was extracted from the mother of an *Xt/+ x Xt/+* mating. Of these, one *Xt/Xt* and one *control* (*i.e. Xt/+* or *+/+*, see Chapter III Materials and Methods) embryo was embedded in wax and sectioned every 8μm coronally. The tissue was then placed on glass microscope slides and dewaxed by incubation in 100% xylene for ten minutes and then again in fresh xylene for ten minutes. The tissue was then rehydrated by passing it through a series of alcohol baths of increasing water content (100%, 95%, 85%, 75%, 50%, and 30% EtOH in dH_2O) for one minute each. The tissue was then washed in PBS for five minutes and stained with 10μg/mL Hoechst in distilled H_2O for 20 minutes, rinsed twice in distilled water, and preserved in a solution of Vectashield (Vector Labs Inc., U.S.A., Cat. No. H-1000) and glycerol (made at a volumetric ratio of 1:1) by dropwise addition of the preservative. Once the preservative had permeated the tissue, a coverslip was placed carefully on top and the tissue/preservative sealed in with nail varnish. This method provides a remarkably clear visualisation of all nuclei, and after 2 years of storage at 4°C, the material still remained clear and fluorescent.

Results

The nuclei of embryos stained with Hoechst are remarkably clear if the method is properly performed. This technique allows a very resolved visualisation of nuclei, much more so than propidium iodine or ink-based dyes, because Hoechst only chelates with the DNA and does not bind to any other molecule. Thus, under epifluorescent microscopy, the nuclei are clearly visualised and separated by the black, unstained spaces of the cell bodies and extra-cellular spaces, clearly demarcating each nucleus.

The morphology of each nucleus is thereby easily recognised and the state of health of the cell can be reasonably determined. As with the Hoechst-stained nuclei described in Chapter III, healthy cells display broad, diffuse Hoechst staining, and apopototic cells are recognised by their small, dense bodies of Hoeschst-stained chromatin. Cells undergoing mitosis could also be distinguished by their characteristic spindles and chromosomal fingers. Furthermore, different cell types displayed different nuclear morphologies, as would be expected, and the different tissues of the embryo could be discerned accordingly.

Cell death (apoptosis) was clearly recognised at E12.5 in many areas of the embryo. In particular, large regions of cell death were noted within the flank mesoderm, just medial and anterior to the forelimb bud. This region is known as the lateral necrotic zone and provides a good indication that this technique is able to accurately detect apoptotic cells. Furthermore, areas of apoptosis were noted along the midline of the condensing sternabrae, and also within the dorsal root ganglia.

The ventricular zone of the cortex appeared as a densely packed structure with little distance between each nucleus. The nuclei were readily observed, but no apoptotic bodies were detectable. Cells undergoing mitosis were observed along the ventricular edge, but no apoptosis could be detected. At best, a few cells could be categorized as apoptotic, but in these situations the apoptotic body was compressed,

probably due to the compressed nature of the cortical tissue at this age, and the supposed nucleus could be mistaken for the the autofluoresence of a red blood cell.

In light of the low quantity of cell death detectable in the forebrain at E12.5, it was decided that a difference in the quanitity of cell death between *Xt/Xt* and +/+ material would be undetectable. Work by Dr. Pundit Asavaritikrai further showed that only 0.84 cells in every 1000 were apoptotic in the neocortex of E16.5 wild-type mice. This low quantity of cell death remained at E18.5 where he found 0.91 apoptotic cells in every 1000 healthy cells in the cortex. From the preliminary study performed at E12.5 and from Dr. Asavaritikrai's data, it appeared that these low levels of detectable cell death would not reliably detect a difference, if one existed, between *Xt/Xt* and +/+ tissue.

Discussion

These results suggest two things. Either cell death is so low in the developing neocortex (from E12.5 to E18.5) that any further reduction in it could not account for such a dramatic change in morphology as the one we see in the *Xt/Xt* embryo, or that the technique is not reliable. As for terms of technical reliability, the Hoechst technique is almost infallible. The difficulty arises from speculatively high *in vivo* clearance rates where apoptotic bodies are removed quickly by macrophages into the blood stream or resorbed by neighbouring cells. If these process occurred at great speed, then our snap-shot of the tissue may only detect a small proportion of a potentially large pool of dying cells. This question is unanswerable at present and must be addressed by other workers with other experiments. I am left then with a technique that cannot detect enough cell death to reasonably satisfy my hypothesis that cell deat is reduced in the neocortex of the *Xt/Xt* embryo. In this respect, I terminate this avenue of enquiry, and focus instead on the cell-type composition of the mutant and wild-type neocortex, and its levels of proliferation.

A BrDU Analysis of *In Vivo* Neocortical Proliferation

Is cell proliferation increased in the Xt/Xt *Neocortex* In Vivo*?*

The favoured hypothesis up to this point has been the suggestion that the major cause of the neocortical phenotype in the *Xt/Xt* embryo is a reduction in normal cell death in the neocortex during and possibly before neurogenesis. I now consider this hypothesis, though well supported (see Chapter III: Discussion), to be questionable on the grounds that *in vivo* evidence suggests that normal cell death is too low to fully account for the phenotype. There is another explanation, the other side of the coin so to speak: cell proliferation might be increased in the neocortex of the *Xt/Xt* embryo. This fulfills the original explanation that the phenotype is the result of a compounding increase of cell production, only now I am shifting the focus from cell death and placing it on cell proliferation.

As elucidated earlier, the dysmorphology of the *Xt/Xt* forebrain appears to be the result of an overgrowth of the tissue. I have until now discussed cell death as the primary mechanism of this overgrowth. The other possibility is an increase in the *amount* of cell proliferation. If more cells are dividing than normal, if cells are dividing for longer than nomal, or if cells are dividing faster than normal, then more tissue will be generated over the course of neurogenesis than in the wild-type embryo. Presumably this excess in production will upset other developmental processes such as tissue patterning and morphogenesis and a complex phenotype like the one observed in the *Xt/Xt* forebrain might form. A disruption to signal diffusion (patterning) or mechanical problems associated with disproportional growth (morphogenesis) may provide the mechanism that leads to this phenotype. An excessive production of cells can arise from a reduction in cell death, and/or an increase in the amount of proliferation. This section explores the possibility that proliferation is increased in the *Xt/Xt* neocortex.

The proportion of neocortical cells undergoing proliferation was detected using 5-bromo-2'-deoxyuridine (BrDU). The technique labels cells in S-phase during a forty-five minute *in utero* exposure to the chemical prior to dissection. Cells that were undergoing S-phase synthesis of replicant DNA strands preferentially incorporate the BrDU into the new strands instead of endogenous deoxythymidine. Those cells in S-phase during the forty-five minute window are thus labelled with BrDU and are detectable using immunochemistry. BrDU labelling therefore gives a reading of the number of cells that pass through S-phase during the window of BrDU exposure.

Materials and Methods

Pregnant *Xt/+* mothers mated with *Xt/+* males were collected 14.5 days post coitus (E14.5). 0.2mL of 10 mg/mL (in saline) BrDU (Sigma, Cat. No. B-50002) was administered by inter-parietal injection into the abdominal cavity, taking care not to insert into the uterus. The mother was then returned to her cage and left undisturbed for forty-five minutes. After forty-five minutes, the mother was killed by cervical dislocation and her pups extracted into ice-cold PBS. Pups were segregated according to phenotype and their neocortices removed and dissociated using precisely the same methodology described in Chapter III. After plating into culture wells at a density of about 2000 cells/mm^2, cells were left in the incubator for two hours to allow firm adhesion onto the culture floor. At two hours, the cultures were removed, placed on ice, and the cells fixed with Hoechst-PFA according to the protocol laid out in Chapter III. Cells were then rinsed in PBS and stored at 4°C for later immunoreaction.

Immunoreaction against BrDU was carried out as described in the immunocytochemistry section of this chapter. Briefly, cells were permeabilised with Triton X100, blocked in goat serum, and incubated in primary anti-BrDU antibody (Sigma, Cat. No. B2531) at a dilution of 1 in 200 at room temperature for one hour. After washing, the secondary anti-mouse Alexa (Molecular Probes, Cat. No. A-

11001 and A-21043) was applied and left to incubate for 30 minutes before washing. All experiments were conducted with a parallel negative control for the primary and secondary antibodies. Immunoreactivity was visualised using a Leica fluorescent microscope and cell counts were obtained at x200 magnification using a gridded eye-piece graticule.

Results

BrDU uptake was increased in the *Xt/Xt* neocortex compared to +/+ neocortex, at E14.5. In material harvested from mothers that were injected with BrDU forty-five minutes prior to dissection, 8% of *Xt/Xt* and 4% of *control* neocortical cells were immunopositive for BrDU incorporation. This difference is significant (t-test, $p<0.002$). BrDU incorporation was also tested in the ganglionic eminences, where 7% of cells had incorporated BrDU into their DNA. These data suggest that BrDU incorporation is increased in E14.5 *Xt/Xt* neocortex to a level similar to that found in +/+ ganglionic eminences of the same age.

Table 4.2. *Proportion of Dissociated E14.5 Cells Immunopositive for BrDU Incorporation after a 45 Minute* In Utero *Exposure.*

	% BrDU Positive	Total No. of Cells
Xt/Xt Neocortex	7.7	4611
Control Neocortex	4.1	4503
Control Ganglionic Eminence	6.9	4823

Discussion

These results suggest one of two things, either there is a greater proportion of cells that are undergoing cell cycle and are passing through the 45' window of BrDU exposure, and/or the same proportion of cells are undergoing cell cycle but they are taking longer to go through S-phase and so a greater proportion of cycling cells are in S-phase at any one time. It is absolutely not possible to determine which is the truth with the data that I have provided; more experiments are necessary and a time course of BrDU exposures must be performed Further consideration of these results will be discussed in conjunction with data presented in the next section in the Conclusion to this Part.

An Analysis of Cell Types in *Xt/Xt* Telencephalon

Introduction

These experiments were performed to determine the cell type composition of *Xt/Xt*, *Xt/+*, and +/+ telencephalon using molecular markers to recognise neurone- and progenitor-specific proteins. These experiments served to answer the important question: is the *Xt/Xt* neocortex different from the +/+ neocortex in terms of the proportion of neurones and progenitors in the tissue. If there is a difference, this data will help to explain the increase in *in vitro* survivability of *Xt/Xt* neocortical cells.

A number of molecular markers were tested for immunoreactivity in wild-type cortex in order to determine those that would be reliable for experimental purposes. These antibodies are listed in Materials and Methods. To detect the neuronal population, two antibodies were chosen that appeared to react well against the neurone-specific proteins microtubule associated protein 2 (MAP2) and β-tubulin III (β-tubIII). Both of these proteins are found in the cytoskeleton of neurones, and are particularly well represented in the axons and dendrites of these cells. β-tubIII is seen to be expressed in early post-mitotic neurones (Lee et al., 1990) and MAP2 in later postmitotic neurones (Binder et al., 1985; Papasozomenos et al., 1985). Anti-RC2 and anti-nestin antibodies were chosen to mark cells from the proliferative neurepithelium of the cortex. The RC2 antibody reacts with a radial glial cell antigen which is present only in a subpopulation of the neurepithelium (Hartfuss et al., 2001; Misson et al., 1988). Nestin is an intermediate filament protein present in proliferating cells of the neurepithelium, but not the other layers of the cortex (Frederiksen and McKay, 1988).

A total of nine experiments was performed. The first experiment was used to test the immunoreactions and optimise the methodology. Of the subsequent eight

experiments, five produced data. However, not every antibody worked with every experiment. The end result provided data for each antibody, but based on one, or at most two experiments each.

Materials and Methods

Primary Cells from the Telencephalon

Cells for immunocytochemistry were acquired by the same procedure as described in Chapter III. In some cases, the same animals provided material for both cell death and immunocytochemical experiments. In other instances, dissections were carried out solely for the purpose of immunocytochemistry.

Culture vessels for the immunochemistry differed from those used in other cultures because visibility through the bottom of the polystyrene culture plates was poor when trying to detect a weak epifluorescent signal from the fluorophore on the secondary antibody. Instead, circular borosilicate glass coverslips (9mm in diameter, BDH cat. no. 406/0189/04) were treated with poly-L-lysine (as in Chapter III, Materials and Methods) and placed in 48-well flat-bottom culture plates (Corning Costar, U.S.A., cat. no. 3548). This allowed the culturing of cells as normal, after which the coverslip could be removed and placed on a microscope slide for viewing.

Dissociated cells were cultured on the coverslips for 2 hours in the case of acute dissociates, or 24 hours in the case of long-term cultures. A two hour time-point was chosen because this is too short for significant proliferation or changes to the protein composition of the cells, and is thus an accurate representation of the proteins present in the cell types of the various brain areas and ages tested. Cells were fixed by placing the culture plate on ice and removing 50% of the culture medium. Ice-cold 4% PFA was then added to each well and the cells left to fix for thirty minutes. PFA was removed by sequential removal of 75% of the solution and replacement

with ice-cold PBS. Cells were then stored in PBS at 4°C for no more than three days before the immunoreaction was carried out.

After the methodology was optimised, data was acquired from three cultures performed on material from E15.5 *Xt/Xt*, *Xt/+*, and +/+ material, and five performed on material from E14.5 *Xt/Xt* and +/+ material (*Xt/+* and +/+ material were grouped together at this age, see Chapter 3 Materials and Methods). All cultures were fixed at the acute two hour time point. Two E14.5 cultures were cultured for an additional 24 hours.

Antibodies

Primary Antibodies

The following primary antibodies were tested for immunoreactivity with primary wild-type cortical cells harvested at E15.5:

MAP2 (monoclonal IgG_1, Sigma, cat. no. M4403)
β-tubulin III (monoclonal IgG_{2b}, Sigma, cat. no. T8660)
RC2 (polyclonal IgM, DSHB, Iowa, U.S.A.)
Rat-401 a.k.a. nestin (monoclonal IgG_1, DSHB, Iowa, U.S.A.)
lot1 (monoclonal IgG, (Sato et al., 1998))
MASH1 (monoclonal IgG_1, BD PharMingen, cat. no. 556604)
PAX6 (monoclonal IgG_1, DSHB, Iowa, U.S.A.)
R-cadherin (Sigma)
QK1 (Levers, 2000)

Secondary Antibodies

Several fluorescent detection systems were tested for specificity and strength of signal. This included directly conjugated fluorescein isothiocyanate (FITC) and tetramethylrhodamine isothiocynate (TRITC) secondary antibody, and a signal amplification system that used a biotinylated secondary reacted with an ExtrAvidin compound conjugated to FITC or TRITC (Sigma cat. no. E2761 and E3011). However, the best reagent in terms of reliability and signal to noise ratio was found to be the Alexa secondary series produced by Molecular Probes. These antibodies were directly conjugated to a fluorophore, which emitted a very strong epifluorescent signal and left little unspecific binding. To detect primary antibodies made in mouse, Alexa anti-mouse IgG conjugated to a 488nm or 588nm emitting fluorophore (Molecular Probes cat. no. A-11001 and A-21043) or Alexa anti-mouse IgM conjugated to a 488nm emitting fluorophore (Molecular Probes cat. no. A-21042) was used.

Immunochemistry

The cells were treated for 15 minutes with Triton X100 detergent diluted to 0.2% in PBS (PBS-TX) to permeabilise cell membranes. They were then incubated in 10% goat serum in PBS-TX for one hour at room temperature. The primary antibody was added in a solution of 5% goat serum in PBS for one hour at room temperature. The solution was then removed, and the culture washed three times with PBS-TX. The secondary antibody was then added at a dilution of 1:200 in PBS with 5% goat serum, and left to incubate at room temperature for one hour. The solution was removed and the cells washed with PBS three times. They were then incubated in dH_2O with 10% Hoechst for 30 minutes. Cells were rinsed in dH_2O, and the coverslip mounted onto a glass microscope slide. All experiments were conducted with a parallel negative control for the primary and secondary antibody.

Data Collection

Cells were viewed with a Leica DMLB microscope fitted with a Mercury-Argon lamp for fluorophore excitation. Cell counts were obtained using a square grid eyepiece graticule at a magnification of 200x. Fields-of-view were chosen where the fluorescent signal appeared strong and consistent (some areas did not react well and were excluded from analysis). Immunopositive cells were counted first and determined by a clear epifluorescent signal which rose significantly above background – as determined by the negative control. A consistent counting methodology was maintained: cells within the grid, and those touching the top and left border were counted for each field-of-view. The total number of cells in a field-of-view was determined by counting the number of Hoechst-stained nuclei within the grid.

Results

MAP2, β-tubIII, nestin, RC2, and MASH1 Chosen for Analysis

Of the antibodies tested for immunoreactivity, MAP2, β-tubIII, nestin, RC2, and MASH1 reacted well and were chosen for subsequent experimental analysis. BrDU incorporation was also analysed. The R-cadherin and Pax6 antibodies produced very weak signals with a low signal to noise ratios, while the QK1 antibody reacted with a majority of cells and produced a strong, ubiquitous signal. These latter antibodies were rejected on the grounds that the information they would provide was not worthy of the time required to improve their immunoreaction. The lot1 antibody provided a clear, but weak signal in a very low percentage of the cortical cells dissected for this experiment (<1%). lot1 is a protein specific to the flanking cells of the lateral olfactory tract in developing murine telencephalon. This antibody may be of use in future experiments as an *in vivo* marker of a cell and position specific structure.

The Accuracy of the Quantitation

The results I present below are based on cell count data from material obtained from one or two pregnant mothers where the embryos of a phenotype from each mother were pooled to represent that phenotypic population. This material was immunoreacted in several different wells of a culture dish, in parellel, with appropriate controls. Over 1000 cells were counted for each antigen and each phenotype, and more usually this number was in the region of several thousand. The raw data is presented in Appendix F.

The accuracy of these data is, in my mind, questionable. There are a number of technical problems that limit the reliability of the immunopositive cell counts. The first is the nature of the immunochemical reaction, which is not always reliable and can change for unexpected reasons – presumably very subtle differences in temperature, antigen concentration, wash, and block times can influence immunoreaction. Another, more important flaw in the methodology is the final exposure of the fluorophore to fluorescent and normal transmitted light. This causes bleaching and reduces the strength of the signal emission. While the observer is counting cells in a field-of-view, bleaching occurs, and by the end of the field-of-view count the signal strength is significantly reduced. Bleaching affects cell counts, and though measures have been taken to normalise all field-of-view counts, this is a factor that affects the final result. Finally, there is observer error. This is the most significant factor. The threshold between a positive and a negative immunopositive count is an arbitrary, subjective decision. Again, procedure was established to nomalise decision making, but this is still grey area and it must be recognised. It is one I will consider to be present in every experiment of this kind, regardless of the quality of the work or the prestige of the publication.

Thus, in the data analysis below, every well has been treated as a separate experiment and statistically analysed accordingly. I present the results of statistical tests in the text, and show the inter-well standard deviations in Figure 4.2. Presented in this way, the text reveals statistical differences in the data, while the figure allows the reader to question the strength of these results, and indeed whether any other differences might be borne out with a better methodology.

MAP2 Expression

MAP2 was detected only in the cytoplasm of the cell and appeared to be excluded from the nucleus (Figure 4.1). Immunoreaction on acutely dissociated cells (2 hour culture) detected areas of intense immunoreactivity within the cell body at points

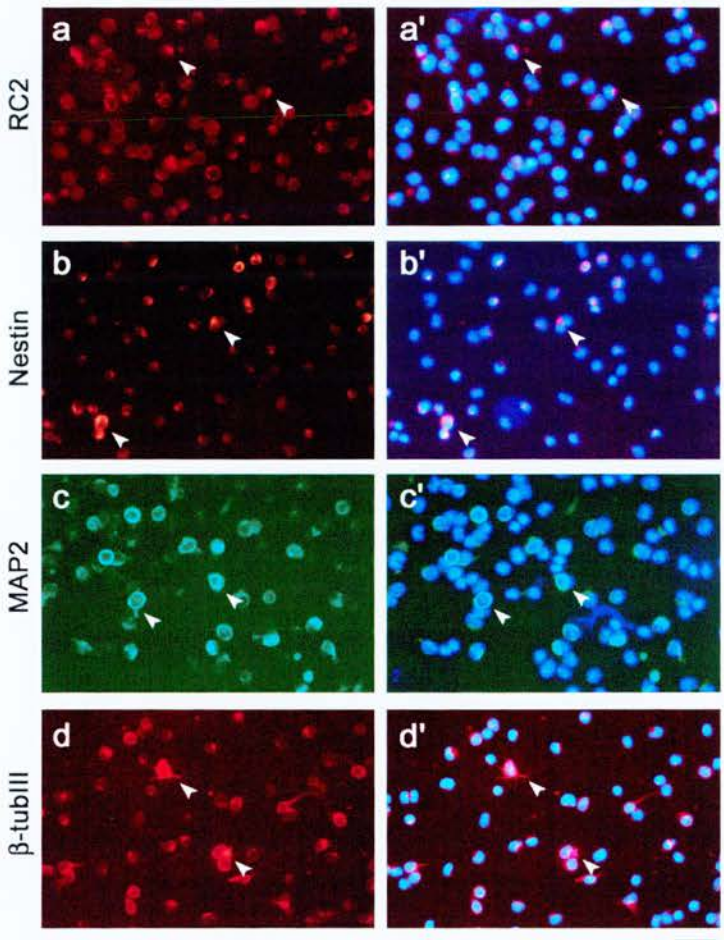

Figure 4.1 Epifluorescence of immunoreactivity against (a) RC2, (b) Nestin, (c) MAP2, and (d) β-tubIII in E15.5 +/+ primary neocortical cultures. Left side (a, b, c, d) immunofluorescence only. Right side (a', b', c', d') immunofluorescence and Hoechst nuclear staining. Arrows indicate example immunopositive cells. Scale bar measures 20μm.

where a process appeared to be extending. If there was no obvious process extension, immunoreactivity was more uniform and present around the edge of the cell body.

A graded level of MAP2 expression was also detected. In some cells, the signal was very strong and obvious. In other cells, the signal was weak but present. An attempt was made to calculate the numbers of 'strong' and 'weak' immunoreactive cells, but this method proved unreliable, and was replaced by a binary positive or negative immunoreactivity count.

MAP2 immunopositivity did not appear to differ between *Xt/Xt* and +/+ neocortical cells at E14.5 or E15.5 (Figure 4.2). At E14.5, 31% of *Xt/Xt* and 27% of *control* neocortical cells were immunopositive for MAP2. These did not differ greatly from the results obtained for E15.5 where 32% of *Xt/Xt* and 31% of +/+ cells were immunopositive for MAP2. Furthermore, 28% of ganglionic eminence cells at E14.5 were immunopositive for MAP2. Thus, these data suggest there is not a great difference in the proportion of MAP2 expressing cells in *Xt/Xt* and +/+ neocortex at E15.5, and that at E14.5, the proportion of MAP2 expressing cells in *Xt/Xt* and +/+ neocortex is comparable to the +/+ striatum.

β-tub III Expression

β-tub III was found to be localised in the cell in very much the same manner as MAP2 (Figure 4.1). β-tubIII immunoreactivity was restricted to the cytoplasm and seemed to be localised in areas where process extension was occurring. β-tubIII also displayed a graded level of expression. In some cells, expression was strong and surrounded the nucleus. In other cells, expression was restricted to a small position in one part of the cell. In the latter case, signal strength was variable and seemed to extend along a continuum from non-existent to weak to strong.

Figure 4.2 Graph to show the proportion of acutely dissociated immunopositive cells at (A) E15.5 and (B) E14.5. At E15.5 (A), a comparable proportion of cells from *Xt/Xt* and *+/+* neocortex reacted with MAP2, β-tubIII, RC2, and nestin antibodies. At E14.5 (B), a comparable proportion of cells from *Xt/Xt* and *control* neocortex immunoreacted with MAP2, and β-tubIII antibodies. However, no cells from *control* neocortex and 9% of cells from *Xt/Xt* neocortex reacted with the MASH1 antibody. *Control* cells from the ganglionic eminences (ge) exhibited a comparable proportion of MAP2 immunoreactivity to *Xt/Xt* and *control* neocortical cells, but exhibited an increase in the proportion of β-tubIII positive cells over *control*, but not *Xt/Xt* neocortical cells. Error bars respresent standard deviations between all field-of-views, indicative of the experimental precision of this technique.

A. E15.5 Acute Cultures

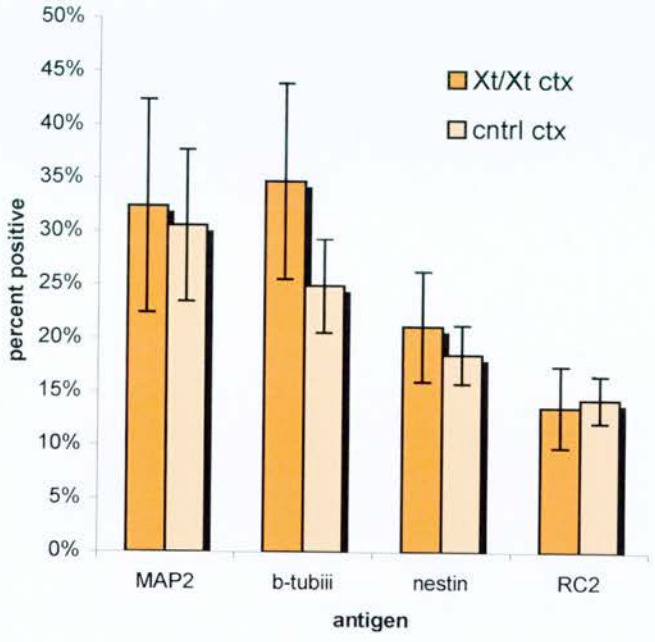

B. E14.5 Acute Cultures

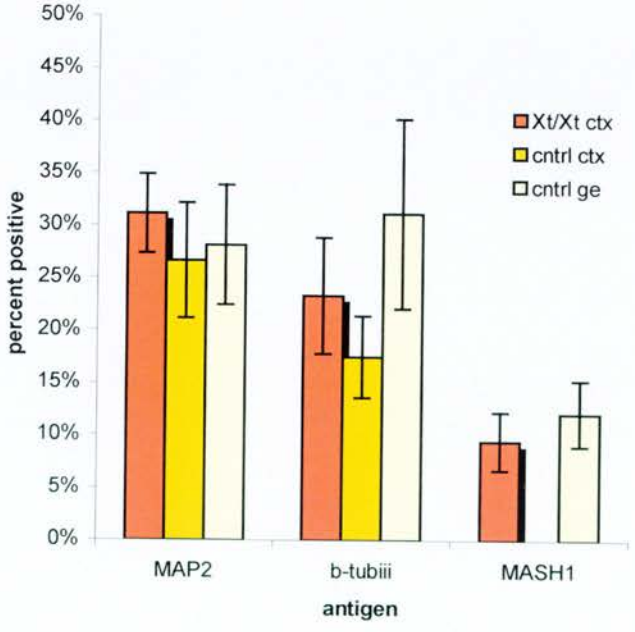

At E14.5 and E15.5, the proportion of β-tubIII immunoreactive cells in the neocortex was similar in material from *Xt/Xt* embryos and *control* embryos. 23% and 35% of cells from *Xt/Xt* neocortex exhibited immunoreactivity at E14.5 and E15.5, respectively. In contrast, 17% and 25% of cells from +/+ neocortex exhibited β-tubIII immunoreactivity. The standard deviation for β-tubIII cell counts is too great to show a significant difference, but these data suggest that the proportion of β-tubIII expressing cells is greater in *Xt/Xt* neocortex than in +/+ neocortex, at both ages. Analysis of the data from individual fields-of-view demonstrates that the proportion of β-tubIII positive cells is greater in cultures from *Xt/Xt* material than from *control* material at either age (t-test, $p<0.005$). Furthermore, at E14.5, the proportion of β-tubIII positive *control* ganglionic eminence cells (31%) is greater than both *Xt/Xt* (23%) and *control* (17%) neocortical cells (t-test, $p<0.005$).

Nestin Expression

Nestin is seen to be expressed in diffuse regions of the cytoplasm of some neocortical cells. The staining is present either in one or two pockets, or is seen to surround the nucleus entirely (Figure 4.1).

At E15.5, there was a similar proportion of cells immunoreactive for nestin in *Xt/Xt* and +/+ neocortical populations (21% and 19%, respectively).

RC2 Expression

The immunopositive RC2 signal was restricted usually to one pocket which sometimes extended in a half-moon around the nucleus (Figure 4.1). It was always specific to the cytoplasm. Because background signal could be quite high with this assay, close comparison to the negative control was emphasised during cell counts.

At E15.5, the population of RC2 immunopositive cells in the *Xt/Xt* cortex did not differ from wild-type cortex (14% and 14%, respectively).

MAP2 and βtubIII Expression after 24 Hours In Vitro

E14.5 cells incubated in culture for 24 hours were tested for immunoreactivity with MAP2 and βtubIII (Figure 4.3). Cells were cultured on glass coverslips and, as a result, migrated to form clumps at a greater rate than would normally occur when cultured on polystyrene (glass is less adhesive than polystyrene).

Both genotypes produced a large number of clusters with a high degree of interconnectivity between them. In both genotypes, connectivity was made with neurites expressing both βtubIII and MAP2. There did not appear to be a difference between the two in terms of length, width, or number of immunopositive processes. Thus, the gross behaviour in terms of migration and neurite extension appears comparable in the *Xt/Xt* and +/+ material of this age.

MASH1 Expression

Cells from the *Xt/Xt* neocortex, +/+ neocortex, and +/+ ganglionic eminences were tested for MASH1 immunoreactivity at E14.5. The *Xt/Xt* neocortex exhibited 9% MASH1 immunoreactivity while the +/+ neocortex exhibited no reactivity at all. Cells from +/+ ganglionic eminences exhibited 12% MASH1 immunopositivity. These data show that ganglionic eminence cells are present in the *Xt/Xt* neocortex, or *Xt/Xt* neocortical cells are expressing the MASH1 gene normally specific to the ganglionic eminences.

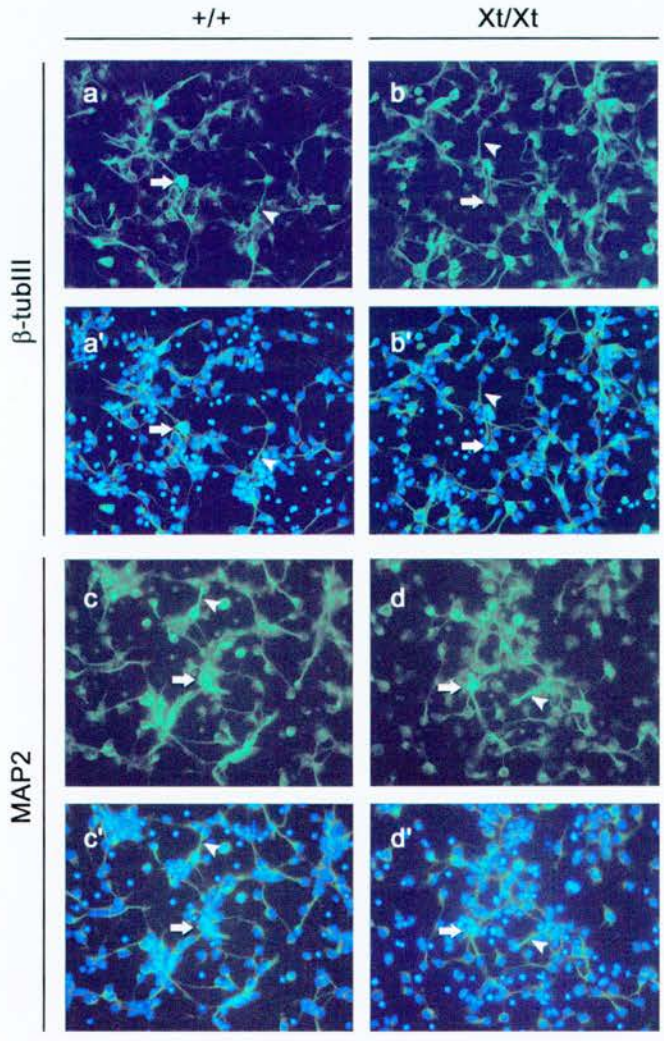

Figure 4.3 β-tubIII and MAP2 immunocytochemistry on dissociated cells from E14.5 +/+ and *Xt/Xt* neocortex after 24 hours of culture. a-b illustrate fluorescent immunoreactivity against β-tubIII. c-d illustrate fluorescent immunoreactivity against MAP2. Cultures have been co-stained with the nuclear marker Hoechst (a'-d'). Note that β-tubIII and MAP2 are expressed in the cell body (but not the nuclues) (arrows) and in cellular process (arrowheads) in both +/+ and *Xt/Xt* neocortical cells. These images also show live and dead cells, recognised by their nuclear morphology (see Figure 1). *n.b.* the clumping characteristics of the cells shown here are not representative of the cultures presented in Chapter III, because the cells here have been cultured on a less adhesive substrate.

Discussion

These data show that the major precursor and post-mitotic cell types are present in the dysmorphic neocortex of the *Xt/Xt* embryo at E14.5 and E15.5. Furthermore, they are present in comparable proportions to those found in the +/+ neocortex at the same age. β-tubIII and MAP2 are markers of neuronal differentiation. β-tubIII is expressed in early post-mitotic neurones (Lee et al., 1990) and MAP2 in more mature post-mitotic neurones (Binder et al., 1985; Papasozomenos et al., 1985). Both cell types form the differentiated layers of the cortex. Nestin and RC2 are markers of cells found in the proliferative neurepithelium (Frederiksen and McKay, 1988; Hartfuss et al., 2001; Misson et al., 1988). Thus, this array of antibodies defines the proportion of differentiated and undifferentiated, proliferating cell types in the neocortex, and from data presented in this chapter, there is no gross disturbance to this balance in *Xt/Xt* neocortex.

This is a surprising finding because the *Xt/Xt* neocortex is convoluted and lamination fails (Chapter I). It was expected that proportions of pre- and post-mitotic cell types would be altered, either as a direct or indirect consequence of homozygous mutation to *Gli3*. However, this was not the case. There is a suggestion in the data that the proportion of β-tubIII-positive cells is increased in the *Xt/Xt* neocortex over wild-type proportions, but this is would require more experiments or an improved technique to determine if it is significant. It is interesting to see, on reference to the histology of the *Xt/Xt* brain (Figure 1.5), that the mechanism for producing and maintaining the balance of proliferating precursor and differentiated post-mitotic cell types is still reasonably in place, in a tissue that bears little morphological resemblance to its wild-type situation.

MASH1 is a marker of ventral telencephalon (Gaufo et al., 2000). MASH1 expressing cells are restricted to the ganglionic eminences of ventral telencephalon until mid-neurogenesis (E15.5) when ganglionic eminence cells migrate tangentially

into the neocortex. Ectopic expression of MASH1 in *Xt/Xt* neocortex is shown above, indicating that normal ventral specification of this cell type is disturbed in the homozygous mutant. This data corroborates with evidence from Theil (1999) and Tole (2000) that show an ectopic expression of other ventral markers, such as *Dlx2* and *Isl1*, in *Xt/Xt* neocortex at E12.5.

A ventralisation of *Xt/Xt* neocortex helps to explain the morphological phenotype of *Xt/Xt* neocortex, but it does not explain the decrease in *in vitro* cell death of primary *Xt/Xt* neocortical cells over wild-type cells. As shown in Chapter III, primary *Xt/Xt* neocortical cells outlive their wild-type counterparts at E14.5, E15.5, and E16.5. In this chapter, I show that E14.5 *Xt/Xt* neocortex is partially ventralised, according to ectopic MASH1 expression. Furthermore, there is a suggestion in the data that BrDU incorporates into a similar proportion of *Xt/Xt* neocortical and +/+ ganglionic eminence cells, which is greater than the proportion that incorporated in +/+ neocortex. The proportion of β-tubIII positive cells in *Xt/Xt* neocortex is also more comparable to +/+ striatum than +/+ neocortex, again indicative that *Xt/Xt* neocortex is exhibiting ventral-like characteristics.

The ectopic location of striatal cells in the *Xt/Xt* neocortex was a plausible explanation for an decrease in *in vitro* (and possibly *in vivo*) cell death because striatal cells make connections with cortical cells, and *vice versa*, in a mechanism that promotes cell survival. An alternative hypothesis suggests that ventral cells, as a rule, display greater viability than neocortical cells. Either way, the ectopic presence of striatal (or striatal-like) cells in the *Xt/Xt* neocortex does not account for the observed improvement in *in vitro* viability over +/+ neocortex, because +/+ ganglionic eminence cells do not survive as well as +/+ cortical cells, nor do they promote an increase in the viability of +/+ neocortical cells when the two populations are co-cultured (see above, this chapter). Thus, from data presented here and data obtained in Chapter III, we can see that although the *Xt/Xt* neocortex expresses some striatal-like characteristics, these do not account for the decrease in *in vitro* cell death.

Conclusions to Part 2

The *Xt/Xt* forebrain phenotype is complex, and though we know in the first case that its aetiology is an homozygous mutation in *Gli3*, we do not know what the function of this gene is, and what principle mechanisms of brain development are affected when this gene is not expressed properly. By extracting *Xt/Xt* and +/+ neocortical cells from the developing embryo and growing them *in vitro*, I found that the *Xt/Xt* cells outlived their wild-type counterparts by several days. Thus, I obtained a phenomenal result that could be used as a conceptual insertion point into the complexity of the forebrain phenotype.

The result, as I have explained it, may be due to an inherent reduction in cell death or an inherent increase in proliferation. As the investigation into *in vivo* cell death turned up a very low level of normal, wild-type cell death, this explanation does not seem as promising as was first thought. Instead, further experiments with BrDU suggested that there was a larger proportion of proliferating cells in *Xt/Xt* neocortex than in +/+ neocortex. This result corroborates with the basic hypothesis that growth of the forebrain is affected in some way, only now it seems more likely that proliferation is increased, rather than cell death decreased.

Immunochemical evidence confuses the matter again. Using a selection of pre- and post-mitotic markers, I have shown that there is not a great deal of difference in the proportion of these cell types between *Xt/Xt* and +/+ tissue. This runs counter to the suggestion that proliferation is increased *in vivo*, the logical explanation of the phenotype if we discount a reduction in cell death. The BrDU data must therefore indicate that cell cycle is stalled in S-phase, or is slowed altogether, but in light of the nestin and RC2 results (markers of proliferating cells) that show no significan difference between *Xt/Xt* and +/+ material, it is not very likely that the proportion of proliferating cells is increased. Thus, we have a situation where one hypothesis kills the one before it and the next kills the one before that.

Conclusions to Part 2

The *Xt/Xt* forebrain phenotype is complex, and though we know in the first case that its aetiology is an homozygous mutation in *Gli3*, we do not know what the function of this gene is, and what principle mechanisms of brain development are affected when this gene is not expressed properly. By extracting *Xt/Xt* and +/+ neocortical cells from the developing embryo and growing them *in vitro*, I found that the *Xt/Xt* cells outlived their wild-type counterparts by several days. Thus, I obtained a phenomenal result that could be used as a conceptual insertion point into the complexity of the forebrain phenotype.

The result, as I have explained it, may be due to an inherent reduction in cell death or an inherent increase in proliferation. As the investigation into *in vivo* cell death turned up a very low level of normal, wild-type cell death, this explanation does not seem as promising as was first thought. Instead, further experiments with BrDU suggested that there was a larger proportion of proliferating cells in *Xt/Xt* neocortex than in +/+ neocortex. This result corroborates with the basic hypothesis that growth of the forebrain is affected in some way, only now it seems more likely that proliferation is increased, rather than cell death decreased.

Immunochemical evidence confuses the matter again. Using a selection of pre- and post-mitotic markers, I have shown that there is not a great deal of difference in the proportion of these cell types between *Xt/Xt* and +/+ tissue. This runs counter to the suggestion that proliferation is increased *in vivo*, the logical explanation of the phenotype if we discount a reduction in cell death. The BrDU data must therefore indicate that cell cycle is stalled in S-phase, or is slowed altogether, but in light of the nestin and RC2 results (markers of proliferating cells) that show no significan difference between *Xt/Xt* and +/+ material, it is not very likely that the proportion of proliferating cells is increased. Thus, we have a situation where one hypothesis kills the one before it and the next kills the one before that.

I believe the truth of the matter lies somewhere in the midst of this data. We know with reasonable certainty that the signalling centres are disrupted in the *Xt/Xt* mouse, and that these signalling centres pattern the neocortex with signalling molecules. We also know that these signalling molecules can affect both cell proliferation and cell death. It is thus likely that both cell proliferation and cell death are affected in the *Xt/Xt* neocortex, and that they may be affected to differing degrees depending on their spatial position. With a shift in the expression pattern of *FGF8*, *Bmp2*, *Bmp4*, *Bmp6*, and *Bmp7*, most of which have been implicated in one way or another to either proliferation or cell death, it is likely that disruption to the normal expression of these genes subsequently affects normal control of both proliferation and cell death. Furthermore, these genes are probably disrupted from a very early age, as the data by Aoto and others (2002) has shown (changes to *FGF8* is shown, changes to the *Bmp*'s are speculative). Thus, the effect we are observing during neurogenesis in the mouse is most likely the late result of a very early defect to patterning and subsequent proliferation and cell death rates, altered in their spatio-temporal dimensions due to a change in the position and strength of the signalling centres.

Part 3

Observations:
Skeletal Anatomy, Weights, and Inheritance in the Xt Colony

Chapter V: Skeletal Phenotypes of the *Xt* Mouse

Introduction

The phenotype of the homozygous and heterozygous *Xt* mouse was first reported by Johnson (1967). He conducted a meticulous analysis of the mouse strain *Extra-toes* (*Xt*) that arose in the control series of an irradiation experiment at the M.R.C. Radiobiological Research Unit at Harwell (Xt^H). Molecular work conducted many years later defined this mutation as a deletion in the *Gli3* gene 5' of the zinc-fingers domain (Schimmang et al., 1992). Another mouse *Xt* line arose spontaneously in the Jackson Laboratory (Xt^J) (Maine, USA) some years later. This mouse mutation displayed a similar phenotype to the Harwell strain (MGD, 2002). Mutation in the Jackson *Xt* mouse has been localised to a 51.5 kb deletion 3' of the first zinc-finger domain (Maynard et al., 2002).

Although the phenotypes of the Xt^J and Xt^H lines are thought to be comparable, they differ noticeably in the number of viable homozygous mutant embryos produced. The Jackson line produces a substantial number homozygous mutant embryos that are viable late into gestation, while the Harwell line exhibits marked resorptions. No resorptions are observed in the *Xt*-Jackson line, and homozygous mutants appear to remain healthy despite their obvious defects. Homozygous mutants from the Harwell strain, on the other hand, suffer a 30% resorption rate by E14.5 (Johnson, 1967). A Harwell colony housed in Edinburgh exhibited complete *Xt/Xt* resorption by E16.5 (personal observation). For this reason, it seems the *Xt* Jackson strain has replaced the *Xt* Harwell strain as the mouse model of choice in many laboratories around the world.

In this chapter, I present a detailed analysis of the skeletal abnormalities observed in *Xt/Xt* and *Xt/+* mice of the Jackson line, in order to determine if the Harwell and Jackson phenotypes are comparable. For clarity and for reasons that will become apparent later, the Xt^{J} line housed in Edinburgh will hereon out referred to as the Xt Jackson-Edinburgh strain (Xt^{JEd}).

Materials and Methods: Skeletal Preparations

Mice

Litters were produced by crossing *Xt/+* males with +/+ or *Xt/+* female mice. Heterozygote males and females always originated from the inbred Xt colony. +/+ females were usually obtained from the *Xt* inbred colony, except in some instances where F1 outbred +/+ mothers were used.

Collection of Mice

Litters of mice were collected from E18 to P0.5. For *in utero* collections, the mother was anaesthetised in a Halothane (Merial) gas chamber and subsequently killed by cervical dislocation. Her pups were removed by Caesarean section, washed in PBS, and placed on ice for one hour to ensure death. For neonatal mice, pups were collected from the mother's cage and killed by a sharp blow to the head.

Individual mice were stored in glass[12] bottles and labelled appropriately.

[12] Glass should be used as plastics tend to degrade during maceration in potassium hydroxide.

Body Weight

Litters were weighed using a Sartorius B120S closed-chamber balance sensitive to one microgram.

Skeletal Preparation

The following method was devised by the author and is an amalgamation of methods previously published (Burdi, 1965; Patton and Kaufman, 1995; Wassersug, 1976). The methodology established here allows for the clear visualisation of both cartilage (blue) and bone (red) and the preservation of this material for years to come.

Collected litters were either prepared immediately or frozen (-20°C) for future study.

Each animal was skinned, eviscerated, washed in water, and placed in rapid fixative (formaldehyde, acetic acid, and ethanol at a volumetric ratio 1:1:8) before staining. The skinning of an animal is a most important step; cutaneous epithelium will prevent Alcian blue from penetrating the subcutaneous tissue, and so prevent the visualisation of any underlying cartilage. This is not a problem for most of the animal, as the skin is readily removed. It is the carpal and tarsal regions as well as the digits of the hands and feet where care and attention is needed most. If the 'glove' is removed too forcefully, the digits will rip off, or even the whole hand. In the case of *Xt/+* and *Xt/Xt* animals, the supernumerary digits are particularly fragile and liable to damage. Where investigation demanded resolution of hand and foot cartilage, extreme care was taken to remove this skin. Otherwise, the glove was left on.

Once skinned, the animal was eviscerated completely. All organs were removed from an incision in the abdomen and discarded. The diaphragm was punctured from below, at the abdominal cavity, and the thoracic contents removed. It is said in the

literature (Burdi 1965, Wassersug 1976) that chemicals from the kidneys and liver may inadvertently stain bone brown. Evisceration also allows fixatives and stains to penetrate the thoracic body wall.

The remaining animal, consisting of bone, brain, and musculature, was washed in running tap water and placed in formaldehyde-acid-alcohol (FAA: formaldehyde : glacial acetic acid : 70% EtOH in a volumetric ratio of 1:1:8.) rapid fixative for forty minutes. The fixative was then replaced with distilled water (dH_2O) and washed three times.

The eviscerated and skinned animal was blot dried and placed in Alcian blue solution (9% Alcian blue in acid-alcohol, consisting of 60% absolute alcohol (EtOH) and 40% glacial acetic acid) for two to ten days, depending on the size of the animal and the strength of staining required. Excess incubation in Alcian blue tended to produce a deeper and darker stain with little effect on soft tissue. Once the stain was satisfactory, the Alcian blue solution was replaced with Industrial Methylated Spirits (IMS) or 100% EtOH, and the solution changed daily for three days[13] to ensure complete dehydration.

Maceration was performed with potassium hydroxide (1% $KOH_{(aq)}$). To prevent distortion of the tissues, the material was brought from 100% alcohol to distilled water in a graded manner by stepwise addition of water carried out at intervals over a period of at least one day. The material was then incubated in 1% $KOH_{(aq)}$ for three days or until the soft tissue was sufficiently transparent to allow analysis of the bony and cartilaginous elements to be performed.

Skeletal material was then washed in dH_2O and Alizarin red solution (0.001% Alizarin red in dH_2O) added. Skeletons were usually incubated for at least three days, but occasionally it was necessary to incubate them for as long as one week.

---

[13] This step dehydrates the material and fixes the Alcian blue into the cartilage. It was noted that if the material was dehydrated before Alcian blue incubation, the cartilage would not take up the stain.

Excess incubation in Alizarin red solution stains the soft tissue a light pink, which can be beneficial.

At this stage, all cartilage is stained blue and all ossified bone red. The appearance of the material was further improved by taking it through a graded series of glycerol solutions (20%, 40%, 60%, 75%, 95% glycerol in distilled water). This preserves the material and increases the transparency of the soft tissues.

Method of Observation

The stained material was examined under low (x10 to x40) magnification with a Leica MS5 dissecting stereo-microscope with side illumination. Each of the skeletons isolated from mice in the first six litters was examined thoroughly and without bias to individual features. Specimens were set side-by-side for comparative analysis of individuals within litters, between litters, and between phenotypes. All characters with different morphologies were noted, and examined sequentially, so that all abnormal features present would be noted. A table was drawn up detailing the following morphological features: eye, interfrontal ossification, fronto-nasal ossification, interparietal ossification, Meckel's cartilage, supraoccipital morphology, vertebral elements, rib elements, sternum, pelvic position, deltoid tuberosity morphology, and finally a detailed examination of the carpal and metacarpal bones of the forelimb. All individuals were analysed according to this regimen and a record produced for each.

Photography of Material

Material was photographed using a 35mm Wild (Heebrugg, Switzerland) MPS15 Semiphotomat mounted on a Wild Makroskop M420 with a deep field Apozoom lens. Tungsten Type II slide film (Kodak or Fujifilm) was always used. Developed slides were digitised using a Nikon Coolscan 2000 slide scanner and stored as tagged

image format (tif) uncompressed binary files on a standard personal computer. Images were enhanced and annotated using Adobe Photoshop.

Morphometric Analysis

The forelimb bones of one litter of newborn mice (6 +/+ and 6 *Xt*/+) were measured using a digital morphometric protocol. The skeletal material was photographed under exact and unaltered conditions. Digitised photographs were then measured using Image Tool version 3.0 (http://ddsdx.uthscsa.edu/dig/itdesc.html). Three measurements were taken for the length of each longbone, and the average of the three measurements used for calculations. The ossified element of each metacarpal was measured five times at regular intervals along its width, and three times along its length. The average length multiplied by the average width provided a total area. Experimental error was calculated by repeating the measurements for each metacarpal on one hand four times.

Results - Gross Anatomy of the Skeleton

The Skull

The skull of the mouse is composed of three major regions: (1) the calvarium, or vault of the skull, which consists of the membranous neurocranium; (2) the viscerocranium, or facial skeleton, which is composed of a number of bones of varying morphologies; and (3) the chondrocranium, or cartilaginous base of the skull.

The *calvarium* consists of a number of 'flat' or 'dermal' bones that constitute the neurocranium. These elements surround and cover the superior, lateral, and posterior portions of the brain. These plates of bone are derived from mesenchyme cells that are thought to originate from the scelerotome component of cranial paraxial mesoderm. They form the frontal, parietal, interparietal, and temporal bones and the tympanic 'ring' that together form the vault of the skull.

The *viscerocranium* is the facial skeleton and consists of the mandible and maxilla, which make up the jaw, the lacrimal, nasal, and ethmoid bones, which make up the nasal capsule, and others that make up the facial skeleton. Except for the nasal turbinate adjacent to the ethmoid bones, which are believed to develop from the primitive cartilaginous nasal capsule, all of the other skeletal elements of the face are believed to be derived from cranial neural crest derived 'dermal' bones and consequently ossify in membrane. The nasal capsule extends forward from the ethmoid bones of the anterior cranial vault to balloon at its most anterior part and form the nose. Cartilaginous turbinate projections line the inside of the nasal cavity, extending from the ethmoid bones towards the anterior end. These bones increase the surface area for nasal epithelium.

The *chondrocranium* makes up the cartilaginous base of the skull. The major bones in this region are (moving anterior to posterior), the sphenoid, basisphenoid, basiocciput, exoocciput, and supraocciput.

The *Xt/Xt* mouse exhibits severe defects to (in decreasing order of severity) the viscerocranium, calvarium, and chondrocranium. The only abnormality noted in the *Xt/+* mouse is a minor increase in ossification of the interfrontal bone above the base of the nasal bones. These observations have been noted by Johnson (1967) and myself.

Calvarium

Xt/Xt Jackson-Edinburgh Data

The *Xt/Xt* calvarium generally showed a high degree of abnormality that was variably expressed. If the embryo appeared healthy with no signs of resorption, hydrocephaly, or exencephaly, and its growth was not impaired, then the calvarium appeared to be larger both transversely and antero-posteriorly than wild-type skulls. The ossified plates of the calvarium were also less well defined, the peripheral margins of the areas of ossification being more diffuse. The *Xt/Xt* calvarium also commonly displayed an 'ectopic' interfrontal bone that was considerably larger than those seen in *Xt/+* and +/+ animals.

Exencephaly is also a common feature of *Xt/Xt* embryos. In these cases, the brain protrudes from its cranial vault through the midline and expands outwards; the calvarium is unable to form due to excessive evagination of the brain. Some *Xt/Xt* embryos displayed complete lack of calvarial bones but were not exencephalic. The brain was instead held in a transparent membrane that was continuous with the

cranial epidermis. The brains of these animals were normally abnormal and hydrocephalic.

No mention was made of the *Xt/Xt* Harwell calvarium because this material was examined before membranous ossification (E15.0). The only calvarial feature noted was the supraoccipital bone, which consists of the most superior parts of the squamous part of the occipital bone (the first membranous bone above the back of the neck). In the Harwell *Xt/Xt* mice, this cartilaginous element appeared jagged with many holes or inlets, protruding into the unossified membranous precursor.

Xt/+ Jackson-Edinburgh Data

The ectopic centre of ossification between the two frontal bones observed by Johnson (1967) was also present in the *Xt* Jackson-Edinburgh strain (Figure 5.1). Furthermore, anomalous staining was present in association with the sagittal sutures of the frontal and parietal bones in some animals. These appeared as a collection of small blue 'blebs', or areas of intense red stain, most commonly at the parietal suture. Quantification concluded that these marks were not dependent on the *Xt* phenotype.

A scaling system was employed to measure the frequency and size of ectopic ossification or anomalous staining for each region, *i.e.* ectopic interfrontal ossification and sagittal parietal suture staining. A number from 0 to 4 was assigned according to the degree of ossification or cartilaginous spotting: 4 being the most severe or largest ossification site, and 0 representing no ossification at all.

Interfrontal Bone

These data show an increase in the frequency and extent of ectopic interfrontal ossification at birth in the *Xt*/+ mouse compared to the +/+ mice. While these elements were occasionally observed in the latter, they were almost always small in

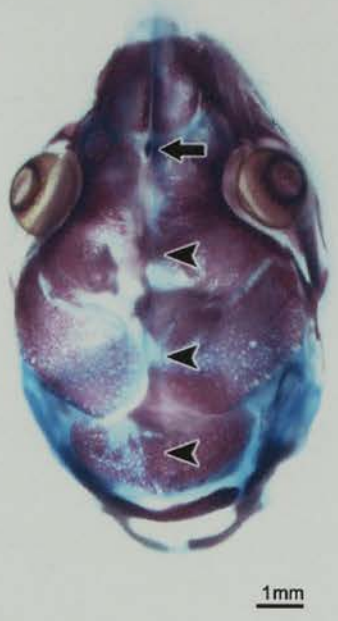

Figure 5.1 Cranium. Dorsal view of a neonatal *Xt*/+ cranium. An interfrontal ectopic centre of ossification (a score of 2) can be seen along the midline just posterior to the nasal bones (arrow). This region is larger in *Xt*/+ animals than in +/+ animals. Other areas were examined for midline ossification: frontal, parietal, and interparietal (respectively, arrowheads descending a-p). These areas varied considerably, but there was no correlation specific to *Xt*/+ mutants. The ethmoidal region lies below the interfrontal area and was also inspected but found to be normal in *Xt*/+ animals.

size. These data agree with Johnson's original findings (1967) where he reported 26 *Xt/+* animals out of 29 had an interfrontal bone, in contrast to only 6 out of 29 in the +/+ mice.

Table 5.1. *Interfrontal ossification size in 29 +/+ and 31 Xt/+ neonates.*

ossification strength	0	1	2	3	4
+/+	23	3	2	1	0
Xt/+	4	2	6	18	1

Midline Parietal

Spots of ectopic blue or red stain were sometimes noted along the midline between the parietal plates (Figure 5.1). Analysis revealed that this ectopic marking is independent of the *Xt/+* phenotype (Table 5.2).

The staining pattern observed appears to be dependent on the background of the litter. Of seven litters analysed, only two showed midline parietal ossification. Within these two litters, every animal showed regions of ectopic stain.

Table 5.2. *Midline interparietal staining in 29 +/+ and 31 Xt/+ neonates.*

stain size	0	1	2	3	4
+/+	23	1	3	2	0
Xt/+	22	4	2	2	0

Viscerocranium

Xt/Xt Jackson-Edinburgh Data

Nasal Capsule

In the *Xt/Xt* condition, the nasal capsule is collapsed. It fails to balloon in a rostral direction, away from the ossified maxillary component (Figure 5.2b), and in a lateral direction to expand away from the midline (Figure 5.2a). The anterior opening thus fails to form.

Ethmoid and Turbinate Array

More posteriorly, towards the ethmoid, the nasal cartilage expands quite dramatically to interface with the space of the cranial vault where the olfactory bulbs normally project from the telencephalon. This is the region of the turbinate projections. *Xt/Xt* turbinate projections are sometimes more numerous, smaller, and less well defined than their +/+ counterparts. The +/+ turbinate array is composed of a series of clean bars which extend from an arch and project deep into the nasal cavity. The *Xt/Xt* array exhibits more numerous, shorter bars that are closer together and extend from the arch into a mass of cartilage. Also, *Xt/Xt* projections do not appear to extend into the nasal capsule as the +/+ projections do.

Others

Other bones of the viscerocranium appeared surprisingly normal in the *Xt/Xt* animal. Most importantly, the morphology of the mandible and maxilla appeared to be normal, though they differed frequently in size.

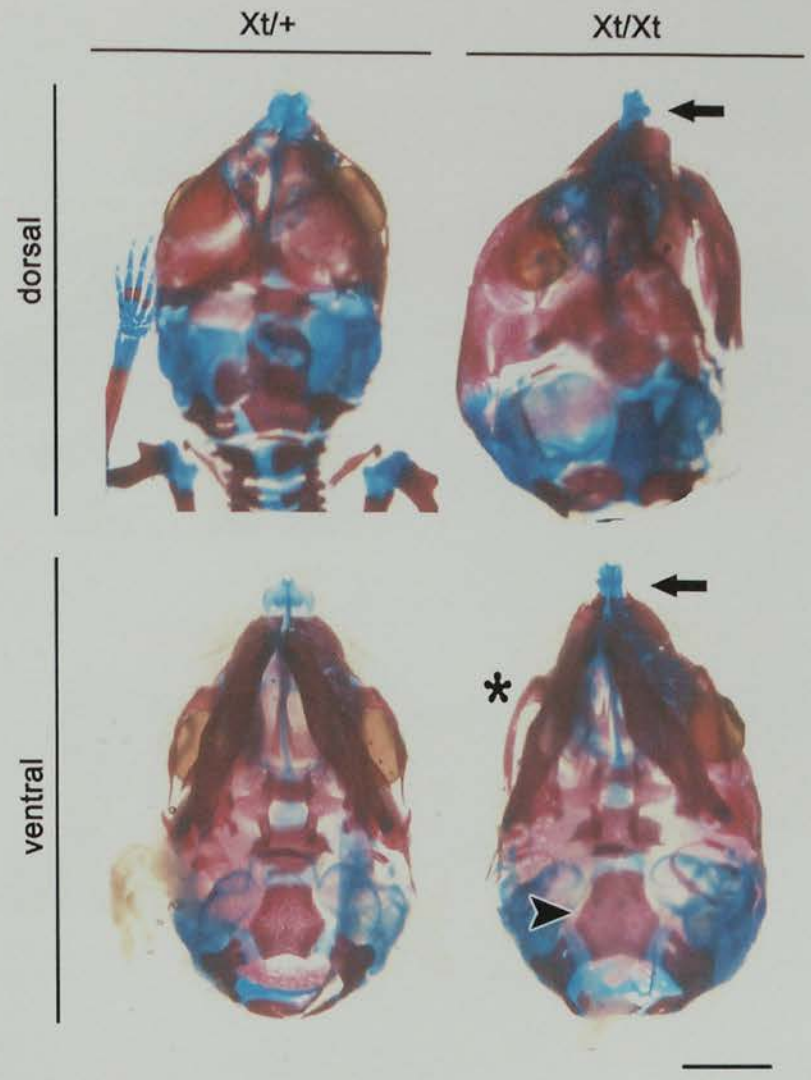

Figure 5.2a Dorsal and ventral cranium. The *Xt/Xt* nasal cartilage fails to expand in a medial-lateral (arrows) and rostral-caudal direction (see Figure 5.2b). *Xt/Xt* basioccipital bone is increased in size (arrowhead). Interestingly, the infraorbital bone adjacent to the right deformed eye retains normal morphology (asterisk). Specimens are littermates and the same individuals as in Figure 5.2b. Scalebar measures 1mm.

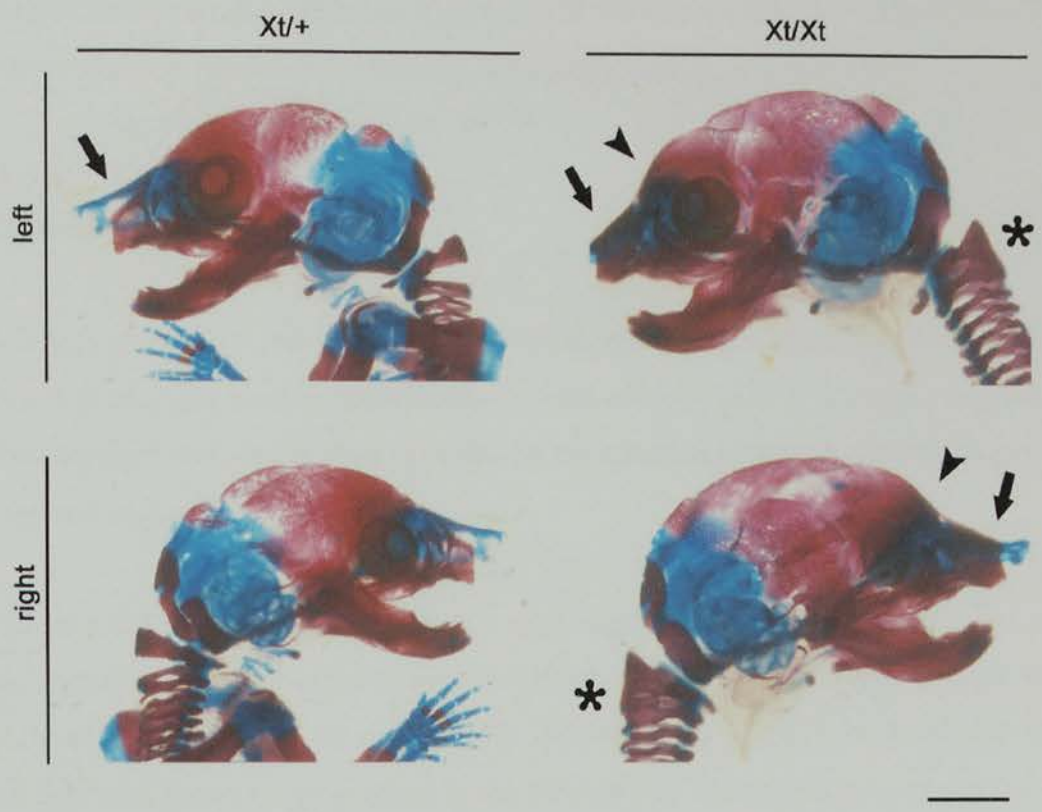

Figure 5.2b Lateral view of the head. The *Xt/Xt* skull displays multiple abnormalities. In this example, the head is larger than its *Xt/+* littermate. The most prominent features of the *Xt/Xt* phenotype is failure of the nasal cartilage to expand away from the membranous ossification of the premaxilla (arrows), causing changes to prefrontal curvature (arrowheads), expansion of the cranial plates along the antero-posterior axis, and eye defects (present only on the right side of this specimen). Dorsal fusion of the cervical vertebrae is also illustrated (asterisk). Specimens are littermates and the same individuals as in Figure 5.2a. Scalebar measures 1mm.

Xt/+ Jackson-Edinburgh Data

An extensive investigation of viscerocranial morphology in *Xt/+* and +/+ neonates was performed. The viscerocranium is a complicated structure composed of many bones of diverse morphologies. Specimens were laid side-by-side for an in-depth comparative analysis. The following features were concentrated on: the ethmoid, infraorbital component of the maxilla, the symphis menti, and mandible.

Ethmoid

Analysis of the *Xt/+* and +/+ ethmoidal region proved to be quite difficult because this is an area that must be accessed through the cranial vault. It is also an area that does not stain well and is often occluded by the calvarial plates. Four litters were analysed successfully.

The ethmoid is a region of cartilage that ossifies to become the most anterior part of the cranial vault. It is formed by fusion of prechordal cartilage with the superior part of the olfactory capsule. As stated earlier, this area is disturbed in the *Xt/Xt* animal, but data here shows no gross affect in the *Xt/+* animal. Ectopic masses of Alcian blue stain, or "blebs" not dissimilar from those seen at the medal parietal suture were noted in some animals (Table 5.3).

Table 5.3. *Ectopic "blebbing" adjacent to the ethmoid seen in 10 +/+ and 10 Xt/+ neonates.*

"blebbing" strength	0	1	2	3	4
+/+	4	0	2	3	1
Xt/+	2	1	3	4	0

Symphis Menti of Meckel's Cartilage

Meckel's cartilage ossifies to form the mandible, the malleus, and incus, although in this study only the mandible was examined in detail. At birth, only the most anterior portion remains in cartilage. This cartilaginous component stretches forward and into the midline to meet its contralateral partner, in the region of the symphysis menti. Analysis showed the mandible to be quite normal in all phenotypes. The *Xt/Xt* mandible may be distorted to a slight degree, but not in comparison with the severity of defects seen elsewhere. The *Xt/+* mandible appeared normal and could not be distinguished by eye from wild-type morphology.

A further quantitative analysis involved counting the number of animals with fused or separate symphysis menti. Meckel's cartilage was found to vary significantly in two litters. There was a tendency for the cartilage to be fused in *Xt/+* when wild-type littermates showed an entirely separate symphysis menti.

Chondrocranium

Johnson surveyed the chondrocranium at E14.5 and found some striking differences between *Xt/Xt*, *Xt/+*, and +/+ mouse embryos. The pattern of his *Xt/Xt* chondrocranium was distorted and asymmetric in appearance. Where there were openings in the bone to allow the passage of blood vessels or nerves, these openings were sometimes duplicated. This is the case at the base of the skull close to the foramen magnum, the foramen lacerum posterius, and where the jugular vein emerges from the skull with cranial nerves IX, X, and XI at the jugular foramen. Duplication is also seen to occur at the pterygoid hamulus (formerly known as the processus alaris).

Xt/Xt Jackson-Edinburgh Data

In contrast to the phenotypes observed in the viscerocranium and the calvarium, the *Xt/Xt* skulls prepared for this analysis appeared relatively normal (Figure 5.2a, dorsal view). The abnormalities illustrated by Johnson were not observed. The primary abnormality of the *Xt/Xt* Jackson-Edinburgh chondrocranium lay in the region of the sphenoid. The basiocciput, basisphenoid, and sphenoid are the three primary centres of ossification along the basal midline of the skull. All three of these were present and apparently normal in most *Xt/Xt* animals. However, one exencephalic newborn lacked evidence of ossification in the region of the sphenoid, although its cartilaginous precursor was present in rudimentary form. In other *Xt/Xt* animals, the sphenoid was present but appeared smaller and less well defined than in their *Xt/+* or +/+ littermates, suggestive of developmental delay. Other features of the chondrocranium appeared normal.

Xt/+ Jackson-Edinburgh Data

The *Xt/+* chondrocranium appeared to be normal.

The Vertebral Column and Bones of the Thoracic Region

The vertebrae are formed from the scleretome component of somites. The more anterior somites from the cervical vertebrae, the medial form the thoracic vertebrae and ribs, and the posterior form the presacral and sacral vertebrae.

Cervical Vertebrae

Xt/Xt Jackson-Edinburgh Data

There was a tendency for the cervical vertebrae of the *Xt/Xt* animal to bifurcate and fuse (Figure 5.3). Cervical vertebrae 1 and 2 (C1 and C2) most commonly bifurcate and fuse together. More caudally, C5 and C6 may also fuse together. Fusion of cervical vertebrae was limited to the dorsal side. The ventral aspect of the vertebrae was never seen to be altered.

Xt/+ Jackson-Edinburgh Data

No abnormality was noted

Note

Extra cervical elements have been noted in the Xt colony (Figure 5.4). This feature occurs in equal proportions in both +/+ and *Xt/+* animals, and is therefore considered Gli3-independent.

The Sternum and Rib Cage

The ribs and costal cartilages characteristically form as lateral extensions of the transverse processes of the thoracic vertebrae. The growing ends of the costal elements make contact with the sternal bars which at this stage, are mesenchymal condensations. At the rostral end of the presumptive sternum, its mesenchyme is in contact with the body wall, which by this stage should be complete, and will form the manubrium. The most rostral elements (the pair extending from thoracic vertebrae) meet and fuse across the midline to form an unpaired rudiment, the precartilage primordium of the manubrium. Midline fusion of the other thoracic costal cartilages occurs in this way, in sequence from cranial to caudal, until the 6th

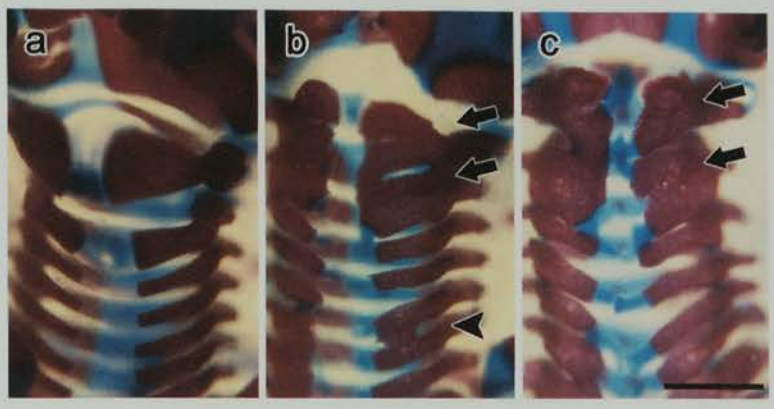

Figure 5.3 Cervical Vertebrae. +/+ (a) and two *Xt/Xt* (b,c) preparations at P0 showing the dorsal views of the cervical vertebrae. Note C1 is bifurcated in both instances and fused to C2. C2 is also bifid (arrows). In b, C5 is fused to C6.(arrowhead). Scalebar measure 1mm.

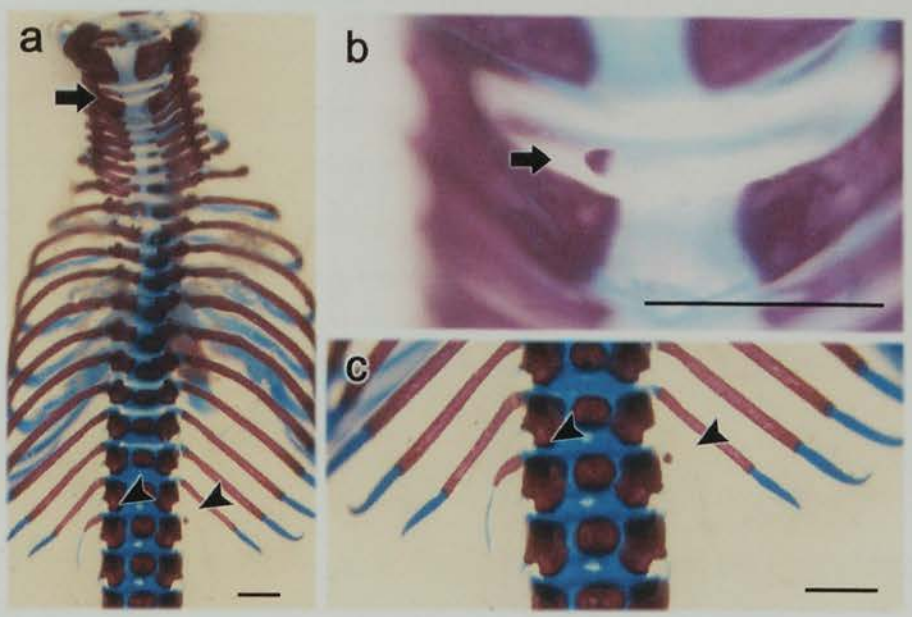

Figure 5.4 Extra Cervical Vertebrae and Ribs. Dorsal view of a +/+ neonate (a), with enlarged views of (b) the cervical vertebrae and (c) thoracic/lumbar vertebrae. An extra cervical element seen at C2 (a and b, arrow), and extra rib elements at L1 (a and c, arrowheads). These anomalies are independent of the *Xt*/+ phenotype and arise in 1/3 all animals in the *Xt* colony. Scalebars measure 1mm.

rib which joins together with the 7th and 8th to form a cartilaginous intersection which will become the xiphisternal joint. These fused elements are termed the sternebrae.

Xt/Xt Jackson-Edinburgh Data

Johnson initially reported failure of midline fusion in the sternum of the *Xt/Xt* embryo. The same condition can be seen in the neonatal material illustrated here (Figure 5.5). Furthermore, there is a failure of the costal cartilages to insert properly into the sternum, probably due to an inability to fuse across the midline with each another. In some cases, the cartilage appears to form a hole, an area of cartilage within the ossified bone of the sternum.

Xt/+ Jackson-Edinburgh Data

Three observation were noted: (i) asymmetric ossification of the sternum, (ii) inferior ossification along the midline, and (iii) extra rib elements. None of these proved to be Gli3-dependent.

Asymmetric ossification was seen in 11/29 +/+ animals and 14/31 *Xt/+* animals. These numbers suggest asymmetry in ossification is a phenomenon of the *Xt* colony as a whole and is not related to the *Xt/+* phenotype in particular (Figure 5.5).

Sternal midline fusion was thought to be attenuated in the *Xt/+* neonate, but subsequent analysis did not verify this. In the neonate, a thin gap runs along midline of the sternum, through its ossified inter-costal regions. The gap can only be seen if the sternum is viewed from directly above. The gap seemed to be more pronounced in *Xt/+* animals than in +/+ animals, but this feature was very subtle and did not differ sufficiently to be considered an abnormal trait.

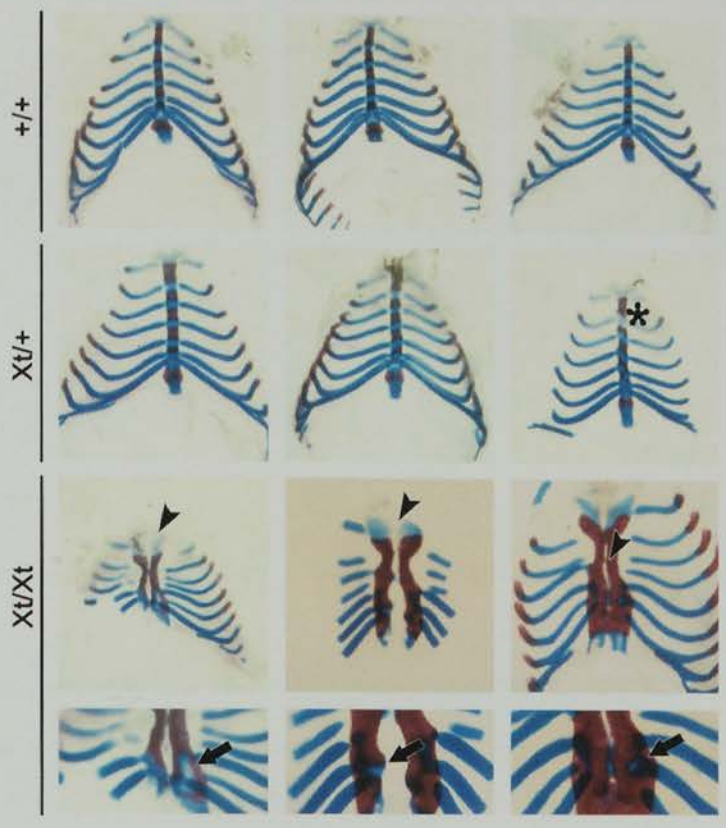

Figure 5.5 Sternum. The sternum is a bilateral character fused along the midline. Asymmetries (asterisk) are present in both +/+ (11/29) and *Xt*/+ (14/31) animals. In *Xt/Xt*, midline fusion fails (arrowheads) and rib costal cartilage fails to insert into the sternum properly (arrows). Specimens on yellow background are littermates. Specimens on pink background are of another litter. Scale between the two litters is not exact.

Extra rib elements were found either at the level of cervical vertebrae 7 (C7), or at lumbar vertebrae 1 (L1) just below the final rib. The extra elements were commonly asymmetric in size, or present on only one side. There was no left-right bias, and the presence of an extra rib was found both in +/+ and *Xt*/+ neonates (Table 5.4).

Table 5.4. *Incidence of extra rib elements noted in 29 +/+ and 31 Xt/+ neonates.*

	cervical 7		lumbar 1		
	left	right	left	right	total elements
+/+	3	2	4	3	12
Xt/+	4	4	3	5	16

The Pelvis

Xt/+ Jackson-Edinburgh Data

The pelvic elements are attached to the vertebral column immediately after the most caudal lumbar vertebrae (L6), at sacral vertebrae 1 to 3 (S1, S2, and S3). Of the 29 *Xt*/+ and 31 +/+ animals analysed, 3 *Xt*/+ and 4 +/+ animals had a displaced pelvis (Figure 5.6). Of these, 3 animals (1 +/+ and 2 *Xt*/+) showed asymmetric displacement of the *right* pelvic cartilage shifted to position L6, S1, and S2 while the left side remained at its normal attachment S1, S2, and S3. No asymmetric left side displacements were noted. More common was a symmetrical shift to fuse at L6, S1, and S2 (2 +/+ and 2 *Xt*/+). In one case (+/+), the pelvic elements shifted down to attach at S2, S3, and S4.

Attachment of the pelvic elements is unaffected by the *Xt*/+ phenotype.

Figure 5.6 Pelvis. Anterior pelvic elements normally fuse with sacral vertebrae 1,2, and 3. Here it has fused to Lumbar vertebrae 6 and Sacral vertebrae 1 and 2. Small arrowheads show Lumbar vertebrae 1-5. Large arrowhead shows the first pelvic attachment at L6. This alteration is independent of *Xt*/+ phenotype.

The Skeletal Elements of the Limbs

There are three major axes of the appendage. The first is the proximal to distal axis. Along this axis extends the length of the limb which can be divided into three compartments. The most proximal compartment is referred to as the stylopodium and contains one skeletal element, the humerus (forelimb) or femur (hindlimb) (Figure 5.7). The medial compartment is the zeugopodium with a set of paired bones, the radius-ulna (forelimb) and tibia-fibula (hindlimb). Most distally is the autopodium which contains the wrist and ankle bones (carpals and tarsals respectively), and the pentadactyl carpal-finger and tarsal-toe array. The second axis is anterior to posterior, sometimes called preaxial to postaxial (in reference to the proximal-distal axis). In the hand, the little finger (digit V) lies at the (postaxial) posterior ulnar end, while the thumb is at the most (preaxial) anterior radial end. The third axis is the dorsal-ventral axis, the palm of the hand being ventral and the "knuckles" the dorsum of the hand.

The limb phenotype is the most obvious of the Xt skeletal abnormalities in both the hetero- and homozygous mutants. The *Xt/Xt* limb is highly abnormal while the *Xt/+* limb appears comparable to +/+ with the addition of an extra pre- or postaxial digit. The hindlimb of the Jackson-Edinburgh strain is comparable to that reported by Johnson, and therefore not described further. The forelimb of the Jackson-Edinburgh strain has been investigated in some detail.

Stylopodium

The humerus is the skeletal element of the stylopodium of the forelimb. Along the anterior border of the humerus lies the deltoid tuberosity which is a notch of bone extending to meet the deltoid muscle. It is formed by a secondary centre of ossification which gives rise to the protuberance. The deltoid muscle is one of the

more prominent of the muscles associated with the pectoral girdle and on contraction flexes the humerus medially.

Xt/Xt Jackson-Edinburgh Data

The skeletal growth of the *Xt/Xt* humerus is retarded. Its most obvious defect is lack of, or severe displacement of the deltoid tuberosity. The deltoid tuberosity may be represented by a small sliver of cartilage that protrudes, not from the middle of the humeral shaft, but from the proximal cartilage (Figure 5.7). The sliver may not even be attached, but may instead form as an independent structure. In its most mild form, the *Xt/Xt* deltoid tuberosity has the appearance of a ridge that extends from the proximal cartilage onto the ossified shaft. It then slopes down to meet the shaft proper, rather than forming the characteristic notch. The degree of variation will be discussed at the end of this section.

Xt/+ Jackson-Edinburgh Data

Xt/+ and +/+ humeri are comparable in size (see below), but differ in the morphology of the deltoid tuberosity. The appearance of the notch associated with the tuberosity extends along a continuum from sharply notched to rounded. +/+ deltoid tuberosities display a sharp distal notch of bone at birth. *Xt/+* animals display a flattened, or rounded notch of bone. +/+ animals occupy the sharp end of the spectrum while in *Xt/+* animals the tuberosity is more rounded (Figure 5.7).

Morphometrics

The ossification length, total length, and area of the humerus were measured. No significant differences were found (Table 5.5).

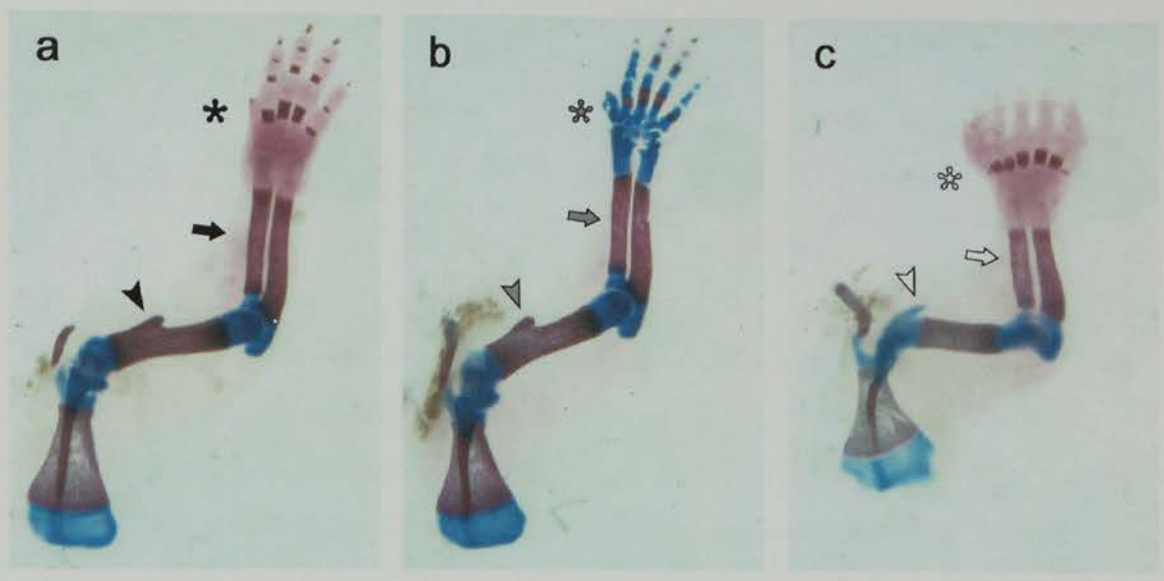

Figure 5.7 Right forelimbs from (a) +/+, (b) *Xt*/+, and (c) *Xt*/*Xt* neonates. In the stylopodium, the deltoid tuberosity lies along the anterior border of the humerus (arrowheads). The tuberosity is notched in the +/+, not notched in the *Xt*/+, and rudimentary in the *Xt*/*Xt* humerus. In the zeugopodium (arrows), the dimensions of the radius are altered in the *Xt*/+ and *Xt*/*Xt* animals, though morphology remains comparable. In the autopodium (asterisk), *Xt*/+ neonates exhibits an extra digit, and *Xt*/*Xt* neonates lack a thumb (digit I) and exhibit multiple extranumerary digits. The epidermal 'gloves' of the autopodia in a and b were not removed, and cartilage staining was prevented.

Table 5.5. *Measurements of humerus ossified length, total length, and total area in one litter.*

	+/+			Xt/+			
	No.	Mean (mm)	S.E.M.	No.	Mean (mm)	S.E.M.	t-test
Ossified Length	4	2.657	*0.0799*	4	2.647	*0.0214*	P=0.90
Total Length	4	4.352	*0.0919*	4	4.471	*0.0130*	P=0.67
Total Area	4	361.2 sq	*16.8*	4	389.4 sq	*2.89*	P=0.15

Zeugopodium

The radius and ulna make up the skeletal elements of the zeugopodium forelimb. These bones articulate with the distal head of the humerus and with the major carpal bones, the radius with the scaphoid-lunate and the ulna with the triquetral. The bones are long and smooth with no major sites of muscle attachment along the shaft.

Xt/Xt Jackson-Edinburgh Data

The gross morphology of the skeletal elements of the forelimb zeugopodium is normal in *Xt/Xt* animals, unless hemimelia (partial formation) of the radius occurs. In this case, the distal half of the radial shaft does not form, leaving the proximal half to taper off; a lack of skeletal support at the anterior autopod causes the forepaw to bend inward anteriorly. A shortened humerus, hemimelic radius, and malformed paw creates a broad arch around an anterior midpoint, giving the *Xt/Xt* forelimb a very dramatic phenotype.

Xt/+ Jackson-Edinburgh Data

No gross morphological abnormalities were observed in the skeletal elements of the zeugopodium of the *Xt*/+ forelimb, though morphometric analysis detected a difference between *Xt*/+ and +/+ radial and ulnar dimensions. The proximal cartilaginous model, the ossified shaft , and the distal cartilaginous model were measured in both bones. The sum of the three components produced the total bone length. Left-right differences were insignificant (t-test, $p>0.05$), allowing data from both the left and right to be pooled.

Radius

Xt/+ proximal and distal cartilage elements were longer than +/+ elements (Table 5.6). *Xt*/+ ossification lengths, on the other hand, were shorter than +/+ ossification. This suggests that the cartilage models were formed according to normal parameters. It is the process of ossification which was changed.

Table 5.6. *Measurement of radial proximal cartilage, ossified component, distal cartilage, and total length in one litter.*

	+/+			*Xt*/+			
	No.	**Mean (mm)**	***S.E.M.***	**No.**	**Mean (mm)**	***S.E.M.***	**t-test**
Proximal cart.	6	0.273	*0.0128*	6	0.324	*0.0486*	*p=0.047* *
Ossified	6	2.343	*0.0462*	6	2.224	*0.0177*	*p=0.037* *
Distal cart.	6	0.690	*0.0157*	6	0.742	*0.0127*	*p=0.026* *
Total Length	6	3.304	*0.0486*	6	3.280	*0.0171*	p=0.651

Ulna

The distal cartilage was found to be significantly longer in the *Xt/+* forelimb (t-test, p=0.047). The other components were comparable in length, and the overall length was similar.

Table 5.7. *Measurement of ulnar proximal cartilage, ossified component, distal cartilage, and total length in one litter.*

	+/+			Xt/+			
	No.	Mean (mm)	S.E.M.	No.	Mean (mm)	S.E.M.	t-test
Proximal cart.	6	0.790	*0.0255*	6	0.807	*0.0111*	p=0.557
Ossified	6	2.870	*0.0467*	6	2.807	*0.0222*	p=0.254
Distal cart.	6	0.614	*0.0151*	6	0.687	*0.0284*	*p=0.047* *
Total Length	6	4.280	*0.0482*	6	4.300	*0.0083*	p=0.690

Autopodium

The forelimb autopodium consists of ten small carpal bones which form the wrist, four metacarpals which articulate with the carpals and phalanges to form the palm, and five sets of phalanges to form the digits. The normal wild-type hand has an arrangement of five digits (Figure 5.8). Digits II through V are similar in size and shape. Each is composed of a metacarpal and three phalanges. As in the human, digit III is the longest and digit V the shortest. Digits II and IV are similar in size and shape. The odd one out is digit I, the thumb.

Digit I is the smallest of the digits because it possesses one less phalangeal element. Traditional nomenclature labels the most proximal bone as metacarpal I. It is

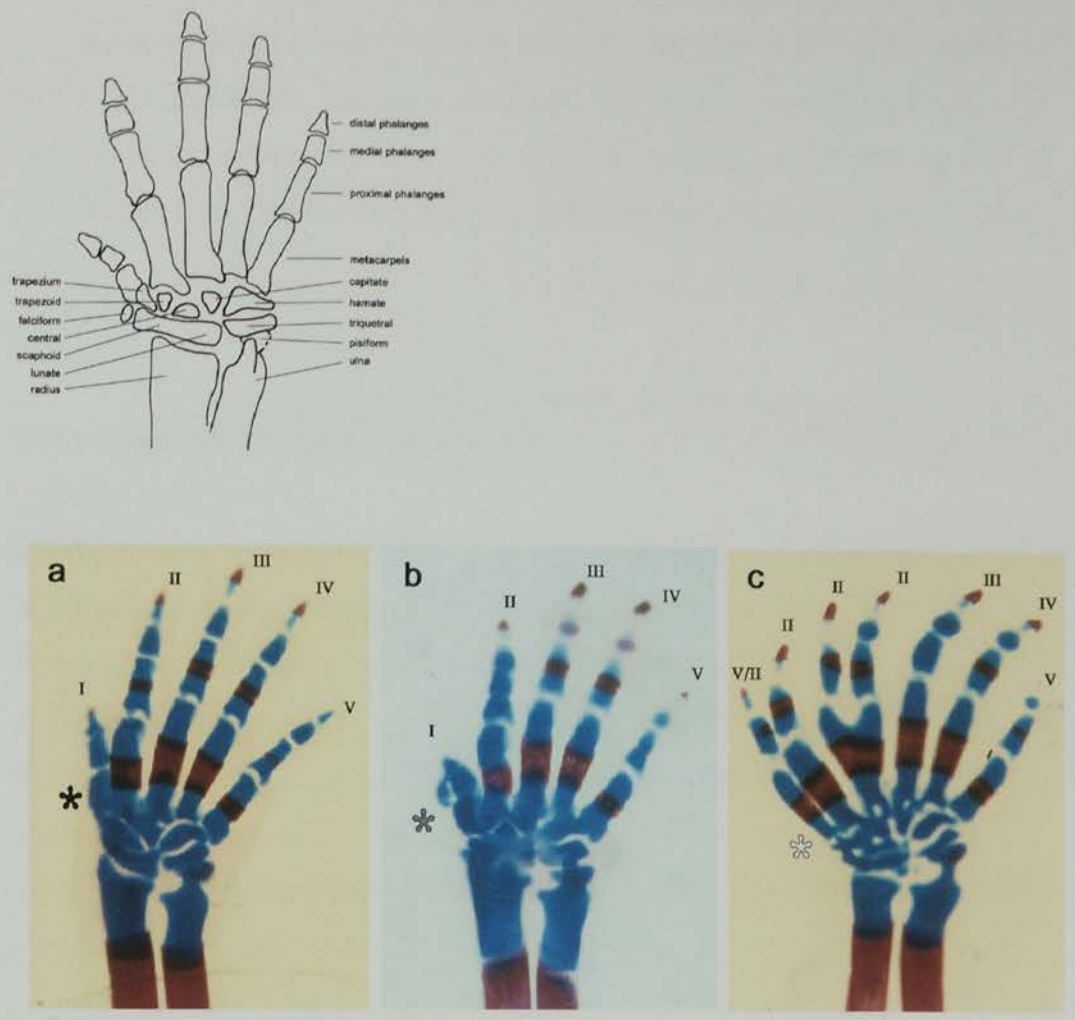

Figure 5.8 Right forelimb autopodia from (a) +/+, (b) *Xt*/+, and (c) *Xt*/*Xt* neonates. Digits are numbered I-V. The anterior border is marked (asterisk). Note the extra digit I phalangeal cartilage in the *Xt*/+ (b). In the *Xt*/*Xt* (c), digits are numbered confidently from the posterior end towards the anterior, until the extranumerary duplications are met. These are labelled digit II because their morphology and dimensions most closely approximate that of digit II. The most anterior digit resembles a hybrid of digits II and V, and bears no resemblance to the digit I noted in (a) +/+ and (b) *Xt*/+.

however, more like a phalanx in shape and developmental characteristics. A more accurate nomenclature would therefore designate the three bones of the thumb as proximal, intermediate, and distal phalanges, thereby acknowledging the possible evolutionary loss of a metacarpal. The thumb lacks a metacarpal, not a phalanx. This feature is of importance when considering the mutant phenotypes described below.

Xt/Xt Jackson-Edinburgh Data

The *Xt/Xt* hand is highly abnormal (Figure 5.8). It exhibits six to eight digits instead of the usual five, displays brachydactyly and syndactyly, and completely lacks a thumb. The phenotype of the *Xt/Xt* hand is the most accessible of the systems disrupted by this mutation. Digit patterning is also a very obvious system with very obvious end products, fingers. This is not the case in the structure of the viscerocranium, which is quite complicated, nor is patterning obvious in the relatively homogeneous tissue of the neocortex. To understand the change to pattern formation in the *Gli3*$^{-/-}$ mutant, digital and carpal morphology and pattern were carefully analysed in the autopod.

A detailed description of one *Xt/Xt* autopod is summarised below as a sample illustration of the defects observed.

Anatomy of the Xt/Xt Carpals

The most dramatic changes here is an increase in both the width and length of the trapezoid bone which curves and extends into two digits instead of only into digit I. The trapezoid looks more like a mirror image hamate. The hamate itself is relatively normal though an extra carpal underlies it which seems to be a replication (mirror image) of the lunate and scaphoid. The triquetral is oddly placed and lies perpendicular to the ulna rather than at an angle. Extra carpals are also seen along

the midline above and below the lunate, and others just above the capitate. These abnormalities are most severe in the anterior portion of the unit where they can be described as a composite of their normal morphologies blended with the mirror-image morphologies of the posterior half.

Anatomy of an Xt/Xt Hand

This hand has six metacarpals and seven digits - the third metacarpal bifurcates to articulate with two fingers. The first point to note is a complete absence of digit I, the thumb. There is no sign of this unit. In its place at the anterior (preaxial) end is a digit that closely resembles posterior digit V. This digit shows the same ossification characteristics as the other phalanges - an ossification centre in the proximal phalanx and one at the tip of the distal phalanx - but the intermediate phalanx is missing. Like the thumb, this digit is made of three elements, but unlike the thumb, it has retained a proper metacarpal. The neighbouring ectopic anterior digits have also lost their intermediate phalanx, but are otherwise similar in shape and size to digit II (Figure 5.8). It is not until the fourth phalange that an intermediate phalanx is formed. Here it is present, but malformed in the shape of a round mass of cartilage rather than the slender conical shape necessary for proper digit morphology. These intermediate phalangeal cartilaginous masses are present in phalanges, 4, 5, 6, and 7. Thus, the *Xt/Xt* digital array is missing a thumb and in its place has formed a mirror image duplication of digit V and adjacent duplications of digit II, and all preaxial digits lack an intermediate phalanx. Verification of the type of extranumerary hybrid digits has been made by comparing their metacarpal dimensions to normal wild-type dimensions (Figure 5.8).

The *Xt/Xt* digit pattern is variable but shows consistent features in line with those observed above. (1) Digits III through V are relatively normal, though they may show brachydactyly (absence or shortening of an intermediate phalanx), probably due to retarded growth at this late stage. (2) Replication of digit II by bifurcation of metacarpal II, and by complete replication of the associated metacarpal and

phalanges. The most anterior of these is often smaller and reminiscent of digit V. (3) Complete absence of digit I.

Xt/+ Jackson-Edinburgh Data

The *Xt*/+ hand is a fine example of a patterning system haploinsufficient for the *Gli3* component (Figure 5.8). Like its homozygous counterpart, phenotypic variation is considerable. The phenotypes seen in the *Xt*/+ forelimb autopodium follow.

Anatomy of Xt/+ Carpals

Particular attention was given to carpal morphology and arrangement in the *Xt*/+ and +/+ animals. In *Xt*/+ animals, lateral elongation of the trapezium, trapezoid, and central carpal was noted in most animals. The carpals also appeared to be larger than their wild-type counterparts with more space between the characters, though this feature has not been quantitated. In one animal, a small ectopic carpal was seen between the lunate and triquetral. This is the middle of the palm where ectopic carpals are common in the *Xt/Xt* forelimb autopod.

Morphometrics of Xt/+ Metacarpals

Length and width of the ossified component of the forelimb metacarpals were measured, plotted (Figures 5.9 and 5.10), and analysed for differences between +/+ and *Xt*/+. Left-right sides revealed no significant difference, allowing these populations to be pooled. No significant differences were found in digits III, IV, and V.

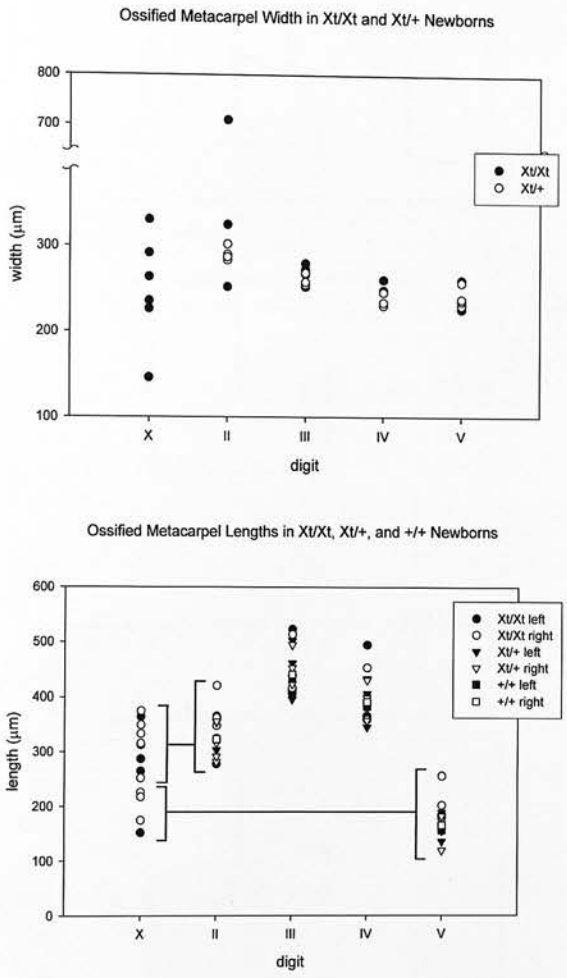

Figure 5.9 Scatter plots to show individual **metacarpal measurements** in one litter of +/+, *Xt/+*, and *Xt/Xt* neonates. Note the wide spread of *Xt/Xt* metacarpels. Bands group ectopic *Xt/Xt* digit measurements with the comparable +/+ and *Xt/+* digits. Digit V is replicated at the anterior side of the *Xt/Xt* hand, and digit II is duplicated in the *Xt/Xt* hands of this litter.

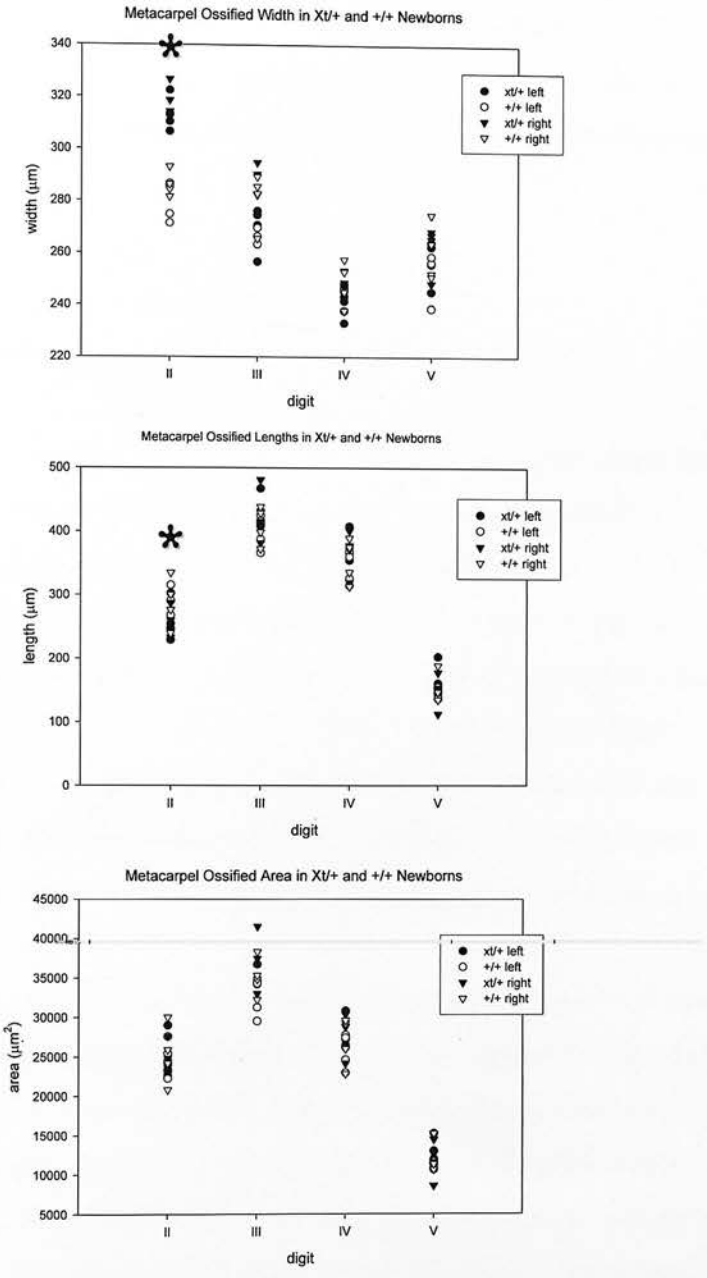

Figure 5.10 Scatter plots to show the individual **measurements of each metacarpal** in one litter. The ossified component of digit II metacarpal in the *Xt*/+ mouse is wider than +/+ ($P < 0.001$). Conversely, *Xt*/+ ossified digit II metacarpal is shorter than +/+ ($P = 0.034$). The total area of digit II ossified metacarpal is comparable in both *Xt*/+ and +/+ neonates. All other measurements yield comparable results.

Xt/+ digit II ossification was found to be shorter (t-test, $p=0.034$) and wider (t-test, $p<0.001$) than ossification in the wild-type. Together, these dimensions produced the same overall area observed in the +/+ animal. Thus, ossification in digit II of this litter is the same overall size, and may have contained the same number of cells, but the bone is narrower along its proximo-distal axis, and widened along its anterio-posterior axis.

Anatomy of Xt/+ Digits:

The most common anomaly is the formation of extra skeletal elements fused to digit I (preaxial polysyndactyly). As most of the analysis was conducted on perinatal material, the elements at this stage are still in their cartilaginous form. However, from observations on *Xt/+* adult phenotypes, these arrangements persist into adulthood. The elements take on a number of different arrangements which include duplication and fusion of any combination of the digit I elements. That is, a lateral extension of the distal element to form a partially duplicated distal phalanx with additional medial element, a lateral extension and duplication of the medial and proximal element, and a lateral extension and duplication of the all three elements.

An unusual phenotype was observed in offspring produced by outbred wild-type F1 mothers crossed with inbred *Xt/+* males. The *Xt/+* offspring developed an additional digit II. In these cases, the proximal phalanx bifurcated to articulate with two medial phalanges, which in turn articulate with their distal elements. This effectively created two digit II. Digit I duplication was also seen in these animals, comparable to the phenotypes listed above for the inbred *Xt/+* phenotype. Because duplication of digit II has not been seen in any inbred heterozygote (more than 300 observed), this unusual phenotype must be due to a change in genetic background. This consideration is of extreme importance when considering the role of the *Xt/+* phenotype in nature. It will be discussed later.

In rare cases, an additional ectopic skin tag is found on the ulnar (postaxial) side of the hand usually attached to digit V.

Triphalangism of Digit I.

The preaxial extranumerary digit sometimes formed with three phalanges, instead of the normal two. This feature has been noted in two heterozygote animals out of the hundreds generated in for the breeding and analysis programmes It is therefore a rare manifestation of *Gli3* haploinsufficiency. Presence of a triphalangeal digit I in the mouse suggests human PPD Types II and III may also be caused by *GLI3* mutation.

Phenotypic Variance in the Limb

Deltoid Tuberosity Morphology

The morphologies of the deltoid tuberosity of +/+, Xt/+, and Xt/Xt neonates exhibited marked variation which appeared to be expressed across a phenotypic range (Figure 5.11). In +/+ neonates, the deltoid tuberosity appeared notched, where the bone protruded from the medial anterior border of the humerus and swept distally to produce a slight overhang. Within this phenotype, the degree and sharpness of the notch was variable, but always maintained the basic notch-like morphology. In the Xt/+ neonate, the tuberosity protruded from the medial anterior border of the humerus, but did not sweep distally to produce an overhang, which makes the notch-like appearance. Like the +/+ phenotypic range, variation was observed within the phenotype, but the basic morphology remained hump-like rather than notch-like. The deltoid tuberosities of Xt/Xt perinatal animals were considerably different from the +/+ or Xt/+ morphologies. In these animals, the deltoid tuberosity appeared at the proximal end of the humerus rather than along the medial border. Here, the

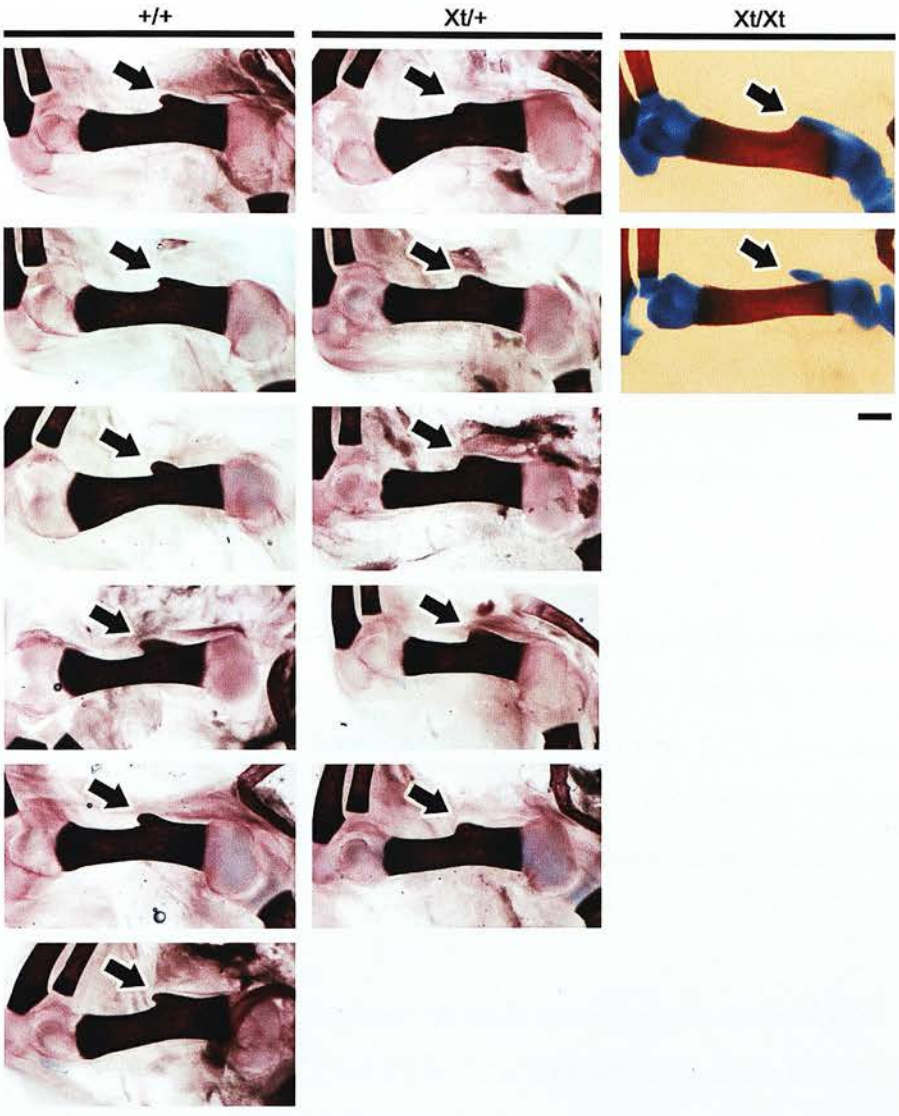

Figure 5.11 Deltoid Tuberosity. Forelimb humeri of +/+, *Xt*/+, and *Xt/Xt* animals. Note the difference in the morphology of the tuberosities (arrows). They appear to extend along a continuum: +/+ tuberosity morphology appears sharp and notched with an overhang extending distally towards the stylopodium; *Xt*/+ tuberosity morphology is rounded with no notched overhang; and *Xt/Xt* tuberocities vary from a sloped appearance, to a rudimentary nub present at the proximal cartilage. All +/+ and *Xt*/+ material are from the same litter. *Xt/Xt* material is from another litter of comparable age. Scalebar measures approximately 0.5mm.

tuberosity was connected to the proximal cartilage and extended into the ossified shaft to where the tuberosity was seen to slope posteriorly into the shaft proper. In some cases, no protrusion was evident on the shaft and the tuberosity was identified as an ectopic mass of cartilage which sometimes was not attached to the humerus at all.

Extranumerary Digits and Genetic Background

The extranumerary digit phenotype in Xt/+ and Xt/Xt neonates displayed considerable variation (for an example the variation in one litter, see Figure 5.12). In contrast, the +/+ animals were always seen to be pentadactyl and displayed no signs of extranumerary digit formation.

The Xt/+ forelimb phenotype was seen to be expressed in five broad categories: (1) the presence of a preaxial skin tag, or "nubbin", which may or may not contain bone; (2) complete duplication of digit I not fused to the original digit I; (3) duplication of one or more bones of digit I, fused to digit I; (4) bifurcation of proximal phalanx II with duplicated intermediate and distal phalanges; and (5) postaxial nubbins which may or may not contain bone.

Background appeared to be a contributory factor in the expression of the Xt/+ extranumerary digit phenotype (Figure 5.13). In a series of eight litters studied, five were produced by crossing inbred Xt/+ and +/+ animals, and three were produced by crossing an Xt/+ stud with an outbred F1 +/+ female. The inbred litters displayed polysyndactyly of digit I, predominantly duplication of the distal element. There was a higher degree of inter-familial variation than intra-familial, *e.g.* one litter displayed an incidence of postaxial (digit V) extranumerary nubbin formation (three times), while no other matings produced this phenotype. Moreover, the litters produced by a cross onto the outbred background all displayed the most severe digit I phenotype (both proximal and distal duplications) and an incidence of digit II

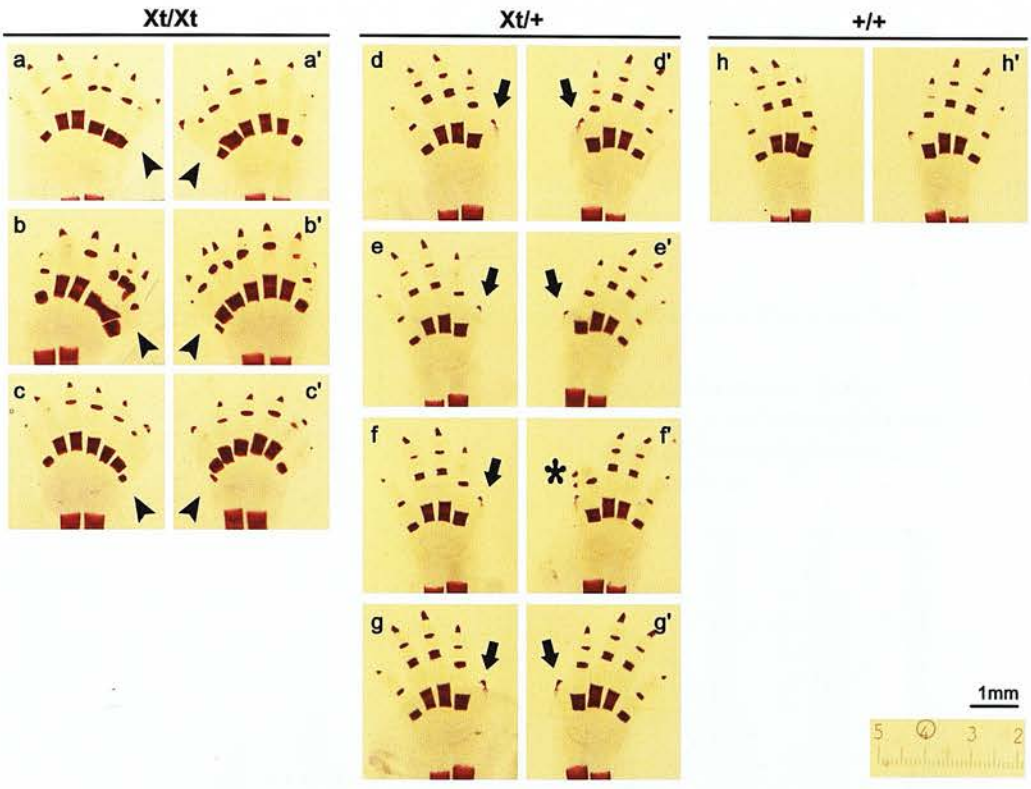

Figure 5.12 Forelimb autopods of a typical litter produced by inbreeding an *Xt/+* male with an *Xt/+* female. Tissue has been cleared and the bones stained with Alizarin red. The cartilage was not stained. Left hands are on the left, right on the right. Note the slight intrafamial variation. In the case of *Xt/Xt*, digit duplications extend from digit III toward the preaxial (arrowheads). A thumb is never present. In this family, the most common *Xt/+* phenotype is extension of the distal phalanx on digit I (arrows). The proximal phalanx may also show some alteration, but this is unlikely to be as severe as the distal duplication/extension because of the shadow of soft tissue visible in this area. One anomaly is present in the form of ectopic ossification along the anterior border of digit II (asterisk).

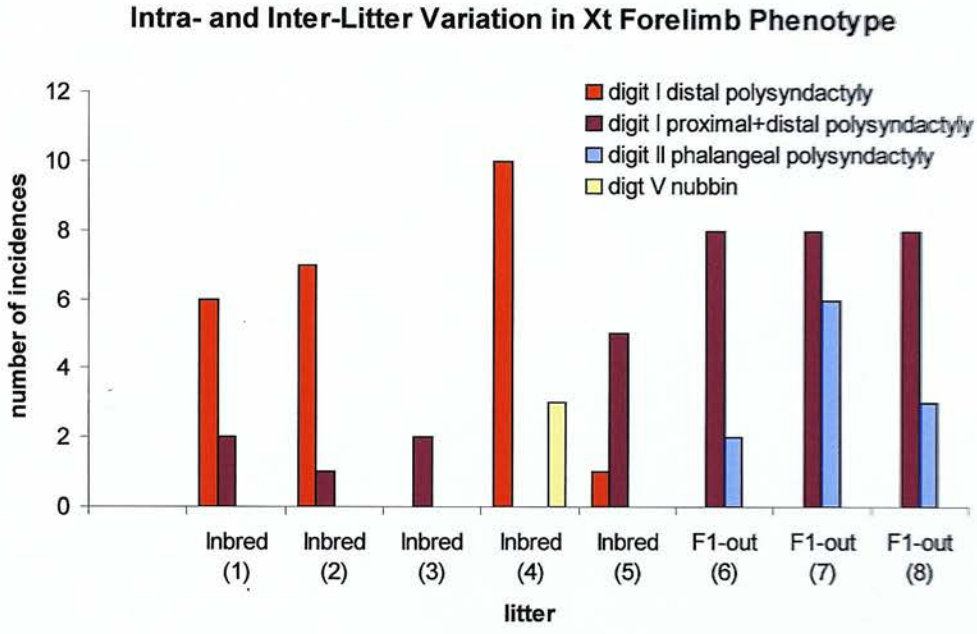

Figure 5.13 Influences of Background on *Xt*/+ Hand Phenotype. Inbred litters 1-5 display a similar phenotypic spectrum (duplication of digit I elements). When an *Xt*/+ stud is mated with an outbred F1 +/+ mother, the phenotypic range appeared to change (litters 6-8), both proximal and distal phalanges of digit I were duplicated, and some animals displayed digit II duplications.

duplication. Bifurcation of the proximal digit II element and duplication of the intermediate and distal phalanges is a phenotype that has been noted in these outcrossed litters and has not been seen in the inbred Xt colony.

The Xt/Xt phenotype was found to be the most variable. The autopod in this animal displayed 6-8 digits with different degrees of bifurcation and/or brachydactyly. However, two aspects of the phenotype are consistent across the phenotypic range: (1) Xt/Xt autopodia were never seen to exhibit a thumb, and (2) the posterior portion of the autopod remained comparable to wild-type, leaving the phenotypic alterations to the anterior portion.

Discussion

Phenotypic Comparison of the Xt^{Jed} Strain with the Xt^{H} Strain

The calvarium and viscerocranium of the Xt^{Jed} and Xt^{H} homozygote mutants appears to differ to some degree, though it is not clear whether this difference is due to the age of the material examined (Johnson examined the skull of the Xt^{H} mouse at E14.5 and I examined the Xt^{Jed} at E18.5-E19.5), or whether it is due to their genetic differences. In the Xt^{Jed}/Xt^{Jed} mouse, I have observed an enlarged calvarium and one where the plates fail to differentiate fully at their borders. There is also an enlarged ectopic interfrontal bone which is a more severe version of that found in the heterozygote. There has been no comparable report on calvarial defects in the Xt^{H}/Xt^{H} mouse; Johnson examined embryonic material before the calvarial plates had ossified. Thus, the phenotypes I present here may or may not be present in the Xt^{H}/Xt^{H} cranium. Severe defects *were* reported in the *chondrocranium* of Xt^{H}/Xt^{H} mice. Johnson reported several morphological defects to the parachordal cartilage that resulted in a division of the chondrocranium into an anterior and posterior part. This phenotype was not noted in Xt^{Jed}/Xt^{Jed} material. A discrepancy in the age of the material examined in the two lines (E15 and E19, respectively) raises the possibility that Xt^{Jed}/Xt^{Jed} chondrocrania may have undergone corrective measures between E15 and the time of observation, but corrective measures are unlikely to reform a break in the cartilage of the type reported by Johnson. Other phenotypes found in the Xt^{Jed}/Xt^{Jed} line are comparable to those reported by Johnson, *i.e.* sternal fusion and ossification, cervical vertebrae bifurcations and fusions, and limb phenotypes. This suggests then that the major skeletal difference between the two lines lies in the region of the head, and specifically the parachordal region that forms the chondrocranium.

The Xt^{Jed} heterozygotes share similar skeletal phenotypes as Xt^{H} heterozygotes (Table 5.8). In these animals, the deltoid tuberosity phenotype and minor changes to the carpels are novel abnormalities that have not previously been reported in the Xt^{H} line, or any other *Gli3*-mutant mouse. The subtle shift of carpal morphologies may have been overlooked by Johnson – this is quite likely because the digit phenotypes between the two lines are comparable. Furthermore, his sketches suggest a change in deltoid tuberosity morphology in the heterozygote, but he made no comment on this feature in the text.

Table 5.8. *Summary of the phenotypes observed in the* Xt^{Jed} line and the Xt^{H} *line* (according to Johnson 1967). + *(mild) to* ++++ *(severe) denotes degree of severity.*

Character	Xt^{Jed}/Xt^{Jed}	Xt^{H}/Xt^{H}	$Xt^{Jed}/+$	$Xt^{H}/+$
calvarium	+++	?	+	+
viscerocranium	++++	++++	-	-
chondrocranium	+	++++	-	-
ribs	++	++	-	-
pelvis	-	-	-	-
sternum	++++	++++	+	-
deltoid tub	++++	++++	+	?
digits	++++	++++	++	++

In conclusion then, the Xt^{H} and Xt^{Jed} lines display comparable phenotypes in all regions but the head, where the Xt^{H}/Xt^{H} cranium is more severely disrupted along the base of the skull, in the area of the parachordal cartilage. This data, together with the observation that the Xt^{H} line exhibits marked *in utero* resorptions, suggests that the Xt^{H} mutation more severely disrupts normal development than the Xt^{Jed} mutation.

Genotypic Comparison of the Xt^{Jed} Strain with the Xt^{H} Strain

The functionality of different coding regions of the *Gli3* gene has been the object of recent investigation and speculation by some authors (Altaba, 1999; Aza-Blanc et al., 2000; Kang et al., 1997a; Koebernick and Pieler, 2002; Sasaki et al., 1999). The nature of the *Gli3* mutations in the Xt^{H} and Xt^{J} mice has been described in the Introduction. The Xt^{H} mutation is a delation 5' of the zinc-finger DNA-binding domains that removes the *Gli3* promotor and may potentially disturb another/other genes 5' of *Gli3*. The Xt^{J} mutation is a deletion 3' of the first zinc-finger domain that effectively removes the zinc-fingers and creates a fusion transcript with another, unknown exon 3' of the *Gli3* gene. Thus, the Xt^{J} mutation may also affect another gene, albeit 3' of *Gli3*.

There is another genetic difference between the two strains, genetic background. The Harwell line was produced by parents from C3H/HeH *x* 101/H backgrounds and the Xt^{J} was produced on a B6.C3 background and later crossed to a CBA to produce the Xt^{Jed} strain. Differences in genetic background are known to alter the expression of mutant and/or wild-type phenotypes (this is discussed in more detail in Chapter VII). *Gli3*-mutant phenotypes are also affected by genetic background. A novel *Gli3*-mutant mouse on an inbred 129 background exhibited a 6% occurrence of postaxial polydactyly in the forelimb (Bose et al., 2002). When this line was crossed to a C57/BL6 background, the appearance of postaxial polydactyly was reduced to 3%. In an *Xt* Jackson line, Tomioka *et. al.* (2000) report a frequent occurrence of exencephaly in Xt^{J}/Xt^{J} embryos bred on a C3HeB/Fej background. When this line was crossed with C57BL/6 mice, exencephaly vanished completely. Genetic background can be seen to be a major determinant of *Xt/Xt* and *Xt/+* phenotypic expression.

The differences between the phenotype of the Xt^{H} and Xt^{Jed} mice may therefore be the result, either of a difference in the genetic mutations of the *Gli3* gene, or as a

result of differences between the genetic background of the two strains. It is not possible at this stage to be certain which is the more important factor.

Xt Phenotypes are Expressed only in *Gli3* Expression Domains

Xt/Xt and *Xt/+* phenotypes arise in areas where *Gli3* would normally be expressed during development, or in tissues derived from earlier *Gli3* expressing cells. The severity of the phenotype appears to be related to the strength of normal gene expression in that region; areas of peak gene expression show the most severe abnormalities when the gene is mutated. This is found in the distal limb and in the head, where *Gli3* expression strength is seen to be at its greatest during the last quarter of embryogenesis (Schimmang et al., 1992).

The correlation between normal *Gli3* expression and areas of *Xt/Xt* and *Xt/+* phenotypic expression indicates that *Gli3* acts on cells in which it is expressed and not on others. In a system such as the migrating facial mesenchyme or the developing limb, this implies that Gli3 functions in a *responsive* manner, and does not extend its domain of influence outside of the cell in which it is expressed. This feature is illustrated below.

Cranial Neural-Crest-Cell-Derived Structures

Cranial neural crest cells give rise to the mesenchyme which migrates to form the complex structures of the facial skeleton, and also the dermal bones of the calvarium (Jiang et al., 2002). *Gli3* is expressed in cranial neural crest cells, and also in the dorsal neural tube which first gives rise to the neural crest. The formation the facial skeleton is a complex process that forms a complex structure and is not well understood, though some basic processes are coming to light.

In early development, *Shh* is expressed in the notochord which runs along the anterio-posterior axis subjacent to the ventral neural tube. *Shh* works with *Gli1, Gli2, and Gli3* to pattern dorsal and ventral domains (Altaba, 1998). Homozygous mutation to *Gli3* causes *Gli1 and Gli2* expression domains, which normally lie ventral and intermediate, to shift dorsally. Thus, *Xt/Xt* neural tube is ventralised, as seen in the forebrain (see Chapter III). Early ventralisation of the neural tube may help to explain skeletal defects such as the bifurcation of the dorsal cervical vertebrae and the failure of normal sternal and rib formation (neural-crest-derived structures).

Cranial neural crest cells from the rhombomeres migrate to contribute to craniofacial mesenchyme. The production of neural crest cells from the rhombomeres is discontinuous, and crest cells destined for different pharangeal arches, carrying different positional cues, are separated by regions of apoptosis centred on rhombomeres 3 and 5 (Graham et al., 1996). Cell death here is found to be regulated by *Bmp4* and *Msx2*, both of which are expressed in the apoptotic foci, and both of which are regulated by neighbouring rhombomeric signalling. The role of *Gli3* in this system is not known, but evidence presented in Chapter III, and data shown in the forebrain (Tole et al., 2000), suggest loss of *Bmp4* expression and/or inhibition of normal cell death in the rhombomeric neural crest may be a feature of *Xt/Xt* maldevelopment. Lack of normal separation of the rhombomeric crest cells by cell death would inhibit the discontinuous production of neural crest cells and potentially lead to a mixing of migratory streams into the craniofacial region, thus disrupting normal pattern formation. Inhibition of normal cell death would also lead to an increase in the number of cells, and overgrowth would be observed; the first obvious sign of the *Xt/Xt* embryo is observed at E9.5 when the pharangeal arches are seen to be larger than wild-type, indicative of an increased cell population.

Furthermore, *Gli3* continues to be expressed in the craniofacial mesenchyme late in development. Its expression pattern at this stage is not well known and not been well studied – the only expression data in this region were produce by a radio-labelled *in situ* hybridisation probe (see Chapter I) (Hui et al., 1994; Schimmang et

al., 1992). It is probable *Gli3* continues to interact with signalling molecules in the viscerocranium in an interpretive manner, as in the limb (see below).

Cervical Vertebrae and Thoracic Ribs

The cervical vertebrae and thoracic vertebrae are formed from somite precursors which flank the neural tube. *Gli3* expression is found in the somites as well as presomitic mesoderm (Hui et al., 1994). The cervical vertebrae of the *Xt/Xt* mouse bifurcate and fuse at their dorsal, but not ventral borders. The thoracic vertebrae give rise to the ribs, which fail to fuse along the midline and fail to form a normal sternum in the *Xt/Xt* embryo. The common *Xt/Xt* phenotypic feature in these two regions is the distance of the phenotype from *Shh* expression. In the cervical vertebrae, the point furthest from *Shh* expression is the dorsal border, where the phenotype is expressed. In the thoracic vertebrae, the distal-most point is the leading edge of rib development, which extends around the thoracic wall to meet at the ventral midline, where sternal fusion fails. It is becoming apparent that most *Xt/Xt* phenotypes lie in opposition to *Shh* expression, a feature that will be discussed later.

Limb

As described in the results, changes occur to the anterior half of the limb in the *Xt/Xt* mouse, but the posterior half remains normal. Basic limb patterning (formation of stylopodia, zeugopodia, and autopodia) is preserved, but anterior positional information is disrupted by loss of *Gli3*. This can be seen in the aberrant deltoid tuberosity of the stylopodium (the anterior structure), in the occasional hemimelia of the radius, and in the aberrant patterning of the anterior autopod. The anterior-most character of the *Xt/Xt* autopod, the thumb, is lost. Furthermore, extranumerary anterior digits appear to be a partial mirror image replication of the posterior digits (the same is true for the carpals). The midline axis runs through the middle digit,

digit III; anterior digits I and II appear morphologically similar to IV and V, but not absolutely. It would seem that enough information remains for the extranumerary anterior digits to attempt to form normal anterior digit morphologies, while also under the influence of mirror-image replication from the posterior. As a result, a confused development of anterior digits I and II produces a hybrid of posterior digits IV and V (by morphological and ossification characteristics), but they are reduced from three phalangeal elements to two – reminiscent of the wild-type thumb. Thus, digits V, IV, III and II can be confidently labelled, but the extranumerary digits dissolve into posteriorised hybrids.

Loss of anterior positional information and an extension, or partial mirror-image replication of the posterior *Xt/Xt* domain, can be explained by an abnormal response of the anterior limb bud to *Shh* signalling. *Gli3* and *Shh* are two key regulators of the anterio-posterior positioning network. *Shh* acts in a proactive manner by secreting Shh signalling molecules that may act directly on cells receiving Shh, or indirectly through the establishment and maintenance of the FGF and Bmp expression domains. *Gli3* appears to act in a responsive manner by enabling the cell to interpret the positional information caused by the *Shh*-induced signalling system. Because *Gli3* acts responsively, it is only the cells in which it would normally be expressed that are affected by its mutation.

In the (haploinsufficent) heterozygote, a potential decrease in the expression strength of *Gli3* either shifts the entire *Gli3* expression domain toward the anterior, or simply reduces the maximum possible expression strength in the anterior region. Either way, an effect is only produced at the anterior border of the limb bud, where an ectopic digit later forms. There is enough leeway within the rest of the haploinsufficient *Gli3* expression domain to produce a normal digit pattern.

The role of *Gli3* in limb development is two-fold. First, it patterns the early flank outgrowth prior to *Shh* expression to establish broad anterio-posterior domains (Welscher et al., 2002). Then, a gradient of *Gli3* expression strength extends from a high point at the proximal anterior, declining slowly towards the distal posterior,

where the *Shh* expression domain lies (Zuniga and Zeller, 1999). As development proceeds, *Gli3* expression is restricted to the anterior. Graded *Gli3* expression establishes a position dependent cellular response to *Shh* or the *Shh*-induced signalling network.

Structures Near Shh Expression Domains Remain Unchanged

There is one over-riding rule observed in *Xt/Xt* and *Xt/+* phenotypes: areas in the vicinity of normal *Shh* expression are unaffected. In the skull, the most severe abnormalities are located in the viscerocranium and in the calvarium. The area adjacent to the *Shh*-expressing region of the floorplate of the skull, the intermediate and posterior chondrocranium, appears normal. The *Xt/Xt* skull phenotype is comparable to the *Xt/Xt* autopod phenotype in that it is the areas in opposition to *Shh* expression which are aberrant, and not the areas close to *Shh* expression. This is also true of the brain phenotype in *Xt/Xt* animals where the morphology of the ventral mesencephalon, diencephalon, and telencephalon remains relatively unchanged compared to the aberrant morphology of the dorsum of these structures. Vertebral and limb phenotypes also follow this general rule, and have been discussed above. Thus, it would seem that a primary function of *Gli3* is to lie in opposition to *Shh* in order to respond to patterning cues downstream of that gene. Furthermore, it appears that *Gli3* function is only important in areas where the concentration of Shh is presumably low due to a significant distance from *Shh* expression.

Chapter VI: Transmission of the *Gli3*(-) Allele

Introduction

History

This chapter describes an analysis of two phenomena observed during the course of the corticogenesis (Part 2) experiments that were subsequently worked up in additional experiments to provide the data presented here. First, it appeared that more *Xt/Xt* and *Xt/+* embryos were produced than predicted by Mendelian genetics, and second, *Xt/Xt* and *Xt/+* mutant embryos appeared to be larger than wild-type homozygotes.

Mendelian Inheritance

Mendelian law stipulates that each copy of a gene, from either the father or mother, will be transmitted to the next generation with equal probability. If one parent has an heterozygous mutation for a gene, *e.g. Gli3*(-/+), and the other parent is homozygous wild-type for that gene, *e.g. Gli3*(+/+), then an equal number of heterozygous and homozygous wild-type offspring will be produced (Table 6.1). Likewise, if both parents carry one copy of a mutated gene, *e.g. Gli3*(-/+), then the expected genotype ratio of the offspring will be 1 homozygous mutant to 2 heterozygotes to 1 homozygous wild-type (Table 6.2).

Table 6.1. *Mendelian gene transmission from one Xt/+ parent and one +/+ parent (in bold) to produce the classic 1:1 ratio of Xt/+ : +/+ offspring (in italics).*

	Xt	**+**
+	*Xt/+*	*+/+*
+	*+/Xt*	*+/+*

Table 6.2. *Mendelian gene transmission from two Xt/+ parents (in bold) to produce the classic 1:2:1 ratio of Xt/Xt : Xt/+ : +/+ offspring (in italics).*

	Xt	**+**
Xt	*Xt/Xt*	*Xt/+*
+	*+/Xt*	*+/+*

Insufficient numbers of wild-type embryos from *Xt/+ x Xt/+* matings complicated the corticogenesis experiments and prompted investigation into this phenomenon. A record keeping system was established to count the litter sizes and phenotypic segregation. A further investigation was established to record the segregation of offspring produced by the breeding pairs of the animal colony (*Xt/+ x +/+*). Additional litters were produced by mating *Xt/+* studs with *+/+* females from other strains, CD1 inbreds and F1 outbreds.

Body Weights

Xt/Xt embryos appeared to be larger than *Xt/+* embryos, and *Xt/+* embryos appeared to be larger than their +/+ counterparts. This observation was supported by Johnson's (1967) data which show a slight increase in birthweight of *Xt/+* animals over +/+. A protocol to measure the weights of embryos from *Xt/+ x Xt/+* matings was inserted into the standard protocol when collecting embryos for the corticogenesis experiments (Part 2). Further weights were obtained from newborn litters, and some late postnatal litters, produced by *Xt/+ x* +/+ crosses, *i.e. Xt/+ and* +/+ pups only.

Materials and Methods

The Xt^J Animal Colony

The Price Lab Extra-toe colony was derived from a colony managed by Dr. Bob Hill's group (M.R.C. Human Genetics Unit, Western General Hospital, Edinburgh). The colony originated from a spontaneous mutation found at the Jackson Laboratory (Bar Harbor, Maine, USA) which was inbred to produce Stock #000026, and later designated B6.C3-Gli3 Xt^J. Bob Hill's group crossed these animals with wild-type CBA mice to increase the vitality and yield of litters. I acquired the animals in 1999 and have since maintained the colony by inbreeding. For one year, *Xt*/+ males were mated with *Xt*/+ females to form breeding pairs. After 2000, breeding pairs were formed by mating *Xt*/+ males with +/+ females.

Mating Regimes

Two mating systems were used to produce mutant offspring, (1) *Xt*/+ studs were mated with *Xt*/+ females to yield *Xt*/*Xt*, *Xt*/+, and +/+ embryos, and (2) *Xt*/+ studs were mated with +/+ females to yield *Xt*/+ and +/+ offspring. Data on the *Xt*/+ x +/+ matings were obtained over eighteen months from July 1999 to January 2002. Most litters were extracted before birth and used for corticogenesis experiments (see Part 2). Those litters that were extracted near or at birth were used for skeletal analysis and have been preserved in glycerol (see Chapter V).

Two additional wild-type strains were used to provide females for *Xt*/+ x +/+ matings, a CD1 inbred strain and an F1 outbred strain. These matings were performed as a separate experiment.

Phenotype Criteria

Phenotype analysis of embryos was performed using a Leica dissecting microscope with magnification at x16 and x40. *Xt/Xt* embryos were reliably phenotyped from E13.5 onward. They always displayed digits in excess of six, an enlarged maxillary component, and sloped forehead. Other abnormalities were also present but were not necessary for classification. *Xt/+* and +/+ embryos have similar gross morphologies. *Xt/+* phenotypes were reliably distinguished at E15.0 onward from their +/+ littermates by observation of an extranumerary digit or pedunculated postminimus. An extra digit on only one limb was enough for *Xt/+* classification, but more often the presence of an extra digit occurred on all limbs. Classification of *Xt/+* before E15.0 was not considered reliable because the preaxial apical ridge extends posterior at this stage and could be mistaken for an extra digit.

Postnatal animals were considered *Xt/+* if they displayed one or more preaxial digits and/or pedunculated postminimi. The hindlimbs displayed the most obvious phenotype and this was often sufficient to classify the animal as *Xt/+*. If an *Xt/+* phenotype was not seen on either hindlimb, the forelimbs were examined with great care for the presence of an extra digit or pedunculated postminimi. Animals with normal pentadactyly were considered +/+.

Genotype Analysis

Genotype analysis for the Xt^J mutation was carried out using a modified version of the Polymerase Chain Reaction (PCR) genotype method devised by Maynard et al. (2002). Two sets of primers were used, one set to recognise the full-length *Gli3* sequence (C3FOR and C3REV, see below) and another to recognise the $Gli3^{Xt\text{-}J}$

sequence (580FOR and 580REV, see below). DNA was obtained from earclips and purified according to standard procedure. The PCR reaction mixture was prepared as follows:

2.0µL	DNA (approximately 10mg/mL) dissolved in ddH_2O
2.0µL	10X Reaction Buffer
0.5µL	C3 FOR (Forward primer) 5' – GGC CCA AAC ATC TAC CAA CAC ATA G – 3'
0.5µL	C3 REV (Reverse primer) 5' – GTT GGC TGC TGC ATG AAG ACT GAC – 3'
0.5µL	580 FOR (Forward primer) 5' – TAC CCC AGC AGG AGA CTC AGA TTA G – 3'
0.5µL	580 REV (Reverse primer) 5' – AAA CCC GTG GCT CAG GAC AAG – 3'
0.4µL	10mM dNTP mixture
13.4µL	ddH_2O
0.2µL	Taq E polymerase

The reaction mixture was placed in ultra-thin walled eppendorfs and the following PCR program cycle used:

1. 95°C 2'00"
2. 94°C 0'20"
3. 63°C 0'20"
4. 72°C 0'50"
5. Goto 2., 34 times
6. End.

10µL of each PCR product was then run on a 1% Agarose gel at 50Vfor about one hour.

Weights

Litters were weighed either at an embryonic age (during the course of neocortical culture experiments – see Chapter III) or just after birth. For embryonic material, each embryo was removed from the mother and stored in EBSS on ice, as described in Chapter III. Embryos were then transferred with large forceps cupping the animal from the bottom, touched to a paper towel for three seconds to remove excess EBSS,

and placed on a balance sensitive to the microgramme (Sartorius B120S closed-chamber balance). Individual embryos were stored seperatately in 4°C oxygenated EBSS and labelled for phenotype analysis. The course of data collection before phenotyping ensured a blind experimental design. Neonatal animals were collected from the nest, weighed, and then phenotyped. These pups were either used for skeletal preparations, or were returned to the nest.

Results

Xt/+ x Xt/+ Litter Segregations Suggest Transmission Distortion

Xt/+ x Xt/+ matings yielded a greater proportion of *Xt/Xt* and *Xt/+* embryos than would be expected by normal Mendelian segregation (Table 6.3). Of 36 litters, 327 offspring were produced. 83 were *Xt/Xt*, 177 *Xt/+*, and 67 +/+. The expected Mendelian ratio of 1:2:1 had been skewed to 1.24 : 2.64 : 1.00. The average litter produced 9.1 offspring which segregated to give average yields of 2.3 *Xt/Xt* embryos, 4.9 *Xt/+* embryos, and 1.86 +/+ embryos. Raw data for each litter is presented in Appendix C.

Table 6.3. *Segregation of Extra-toes from Xt/+ x Xt/+ matings.*

no. of litters	total offspring	mean litter size	expected Mendelian *Xt/Xt:Xt/+:+/+*	observed *Xt/Xt:Xt/+:+/+*	χ^2
36	327	9.1	82:164:82	83:177:67	p=0.15

These data suggest the *Gli3*(-) allele is transmitted at a greater frequency than would be predicted by Mendelian genetics. Analysis by the chi squared test gives us a p value of 0.15, not a significant result. However, the chi squared test operates on the assumption that we are interested in two degrees of freedom. This does not test the hypothesis that the *Gli3*(-) allele is preferentially transmitted regardless of whether it ends up in a homo- or heterozygote conceptus. To test this hypothesis, I have pooled the *Xt/Xt* and *Xt/+* data to determine if the *Gli3*(-) allele is transmitted at a greater frequency than *Gli3*(+).

This creates a situation with only one degree of freedom and more accurately tests our hypothesis that *Gli3*(-) is more frequently transmitted. In this situation, 260 *Xt/Xt* and *Xt/+* embryos, and 67 +/+ embryos were produced. A chi squared test demonstrates a p value of 0.060, not significant but a probable trend (Table 6.4).

Table 6.4. *Segregation of Extra-toes from Xt/+ x Xt/+ matings - Xt/Xt and Xt/+ populations pooled.*

expected Mendelian *Xt/Xt* and *Xt/+* : *+/+*	observed *Xt/Xt* and *Xt/+* : *+/+*	X^2
245¼ :81¾	260:67	p=0.06

Finally, I have omitted the *Xt/Xt* data on the grounds that some embryos may have reabsorbed. In this case, we only compare the *Xt/+* to the +/+. This produces a chi square p value of 0.052 (Table 6.5).

Table 6.5. *Segregation of Extra-toes from Xt/+ x Xt/+ matings: Xt/+ and +/+ populations only*

expected Mendelian *Xt/+* : *+/+*	observed *Xt/Xt* and *Xt/+* : *+/+*	X^2
162.6 : 81.3	177 : 67	p=0.052

The result from this method does not differ significantly from the situation demonstrated in Table 6.4, which suggests that the *Xt/Xt* resorption rate is not significant, and that a trend does exists for more *Xt/+* embryos than +/+.

Xt/+ x +/+ Litter Segregations Show Gli3(-) Positive Transmission Distortion

To test the hypothesis that *Gli3*(-) transmits at a greater frequency than the *Gli3*(+) allele, *Xt/+* studs were mated with +/+ mothers. This provided a simpler system that was not complicated by developmental extremes or stresses to the mother that may occur *in utero* due to the presence of the highly abnormal homozygous mutants. Mating heterozygotes with wild-types also produces a situation that is closer to a 'natural' setting where heterozygotes in the wild do have a chance to breed with wild-type mates.

Breeding pairs were established by mating *Xt/+* males with +/+ females. Each newborn litter was counted just after birth, and phenotyped within the first few days of life. If a discrepancy arose between the number born and the number phenotyped, this was noted. Raw data for this experiment is presented in Appendix D.

Of 43 litters born between February 2001 and 2002, 378 offspring were produced. 210 were *Xt/+* and 168 +/+. The expected Mendelian ratio of 1:1 had been skewed to 1.25 to 1. The average litter contained 8.8 offspring, which segregated to give average yields of 4.9 *Xt/+* and 3.9 +/+ (Table 6.6).

Table 6.6. *Segregation of Extra-toes from Xt/+ x +/+ matings.*

no. of litters	total offspring	mean litter size	expected Mendelian *Xt/+*:+/+	observed *Xt/+*:+/+	X^2
44	378	8.8	189:189	210:168	p=0.03

These data show that the *Gli3*(-) allele is transmitted at a greater frequency than would be predicted by Mendelian genetics. I have phrased this phenomenon positive

transmission distortion (PTD) of the *Gli3*(-) allele. Statistical analysis by the chi squared test gives a p value of 0.03, a significant result.

Of minor note, a slight sex bias was also observed. A total of 275 newborns were sexed. 144 pups were male, and 131 were female. Of the males, 82 were *Xt*/+ and 64 +/+. Of the females, 67 were *Xt*/+ and 61 +/+. These data were not significant in this case (p=0.22), but the potential for a sex bias is worth noting, as we will see a similar phenemenon in the transmission of polydactyly in man (see below).

Gli3(-) Positive Transmission Distortion Occurs Only in a Subset of the Xt^{Jed} Colony

Further investigation of the data set revealed two distinct subsets. Of the total fourteen breeding pairs, one subset of six pairs exhibited a remarkably high *Gli3*(-) PTD ratio of 2 : 1 (*Xt*/+ : +/+). The second subset of eight breeding pairs exhibited the expected Mendelian ratio of 1 : 1 (Table 6.7). Furthermore, both breeding pairs subsets (those with high PTD and those with no PTD) produced comparable litter sizes, which implies that the observed PTD is not the result of a recessive *Gli3*(-) allele carried by a phenotypic wild-type mother (see Discussion).

Table 6.7. *Segregation of Xt/+ and +/+ Newborns Grouped by PTD Subset.*

PTD	no. of breeding pairs	no. of litters	mean litter size	total *Xt*/+	total +/+	ratio	χ^2
Yes	6	16	8.8	101	49	2 : 1	p<0.01*
No	8	27	8.4	109	119	1 : 1.1	p=0.51

Gli3(-) PTD Does Not Occur in CD1 and F1 Backgrounds

To determine if positive transmission distortion of the *Gli3*(-) allele was background dependent, *Xt*/+ studs were mated with random-bred CD1 and inbred F1 +/+ females. Seven litters were obtained from CD1 mothers, and eighteen litters obtained from F1 mothers. Neither strain exhibited PTD of *Gli3*(-) (Table 6.8).

Table 6.8. *Segregation of Extra-toes from Xt/+ x* CD1 and F1 +/+ *matings.*

+/+ strain	no. of litters	total offspring	mean litter size	expected Mendelian *Xt/+*:+/+	observed *Xt/+*:+/+	χ^2
CD1	7	82	11.7	41 : 41	35 : 47	p=0.19
F1	18	152	8.9	76 : 76	81 : 71	p=0.42

The *Xt/+* Phenotype is Due to the *Gli3*$^{-/+}$ Genotype

Animals phenotyped as *Xt*/+ and +/+ were genotyped as *Gli3*$^{Xt\text{-}J/+}$ and *Gli3*$^{+/+}$, respectively (Figure 6.1). DNA from *Xt*/+ animals produced two PCR products: one that appeared to be the 193 b.p. amplicon from the full-length wild-type *Gli3* sequence, and another that appeared to be the 580 b.p. amplicon from the *Xt*-Jackson sequence. DNA from +/+ animals (from the *Xt* colony) and from a *Small eye* mouse (*Pax6*$^{-/+}$/*Gli3*$^{+/+}$) produced a single 193 b.p. amplicon. These data confirm that the mutation in the *Xt* colony is indeed the *Xt*-Jackson mutation, a 51.5 kb deletion in the *Gli3* gene (Maynard et al., 2002) . It is unfortunate that this protocol was not developed earlier, before the animals that produced the PTD data were destroyed. Nevertheless, these data do confirm the presence of the *Xt*-Jackson mutation in the *Xt* colony housed in Edinburgh, and they show that phenotypic analysis is a reasonable determinant of the animals' genotype.

Figure 6.1 Ethidium bromide stained agarose gel with the PCR *Gli3* geneotype product from eight animals. Lanes 1 and 10 contain a 100 b.p. and 1 k.b. DNA ladder, respectively. Product run in lanes 2, 5, and 7 was obtained from +/+ animals. Product run in lane 10 was from a *Sey/+* animal, and product run in lanes 3, 4, 6, 8, and 9 is from *Xt/+* animals. The 193 b.p. product is indicative of wild-type *Gli3*, while the 580 b.p. product is indicative of the *Gli3-Xt-J* mutation. It is clear that DNA from those animals with an *Xt/+* phenotype produce both PCR products.

Gli3(-) Increases Embryonic Mass in a Dose Dependent Manner

Xt/Xt embryos weigh more than *Xt/+* embryos, and *Xt/+* embryos weigh more than +/+ embryos (Figure 6.2). This was observed from E14.5 to E18.5, and proven to be significant using a ranking method which rated the relative weights of the phenotypes within age groups, and then tallied the results to present overall rank of all litters between E14.5 and E18.5 (Snedecor's F-test, $p<0.05$) After E18.5, *Xt/Xt* embryonic mass tended to be less than the other phenotypes, probably due to developmental stall or partial resorption. Postnatally, *Xt/+* pups were seen to be heavier than +/+ pups at 28 days (P28) (t-test, $p=0.04$), after which the mass of postnatal animals appears comparable (Table 6.9).

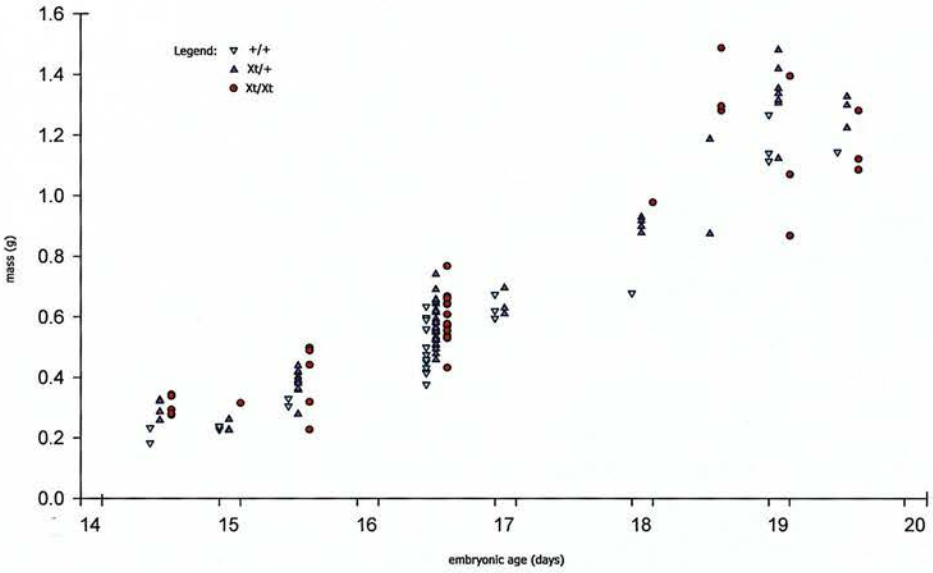

Figure 6.2 Graph to compare the weight of individual +/+, *Xt/+*, and *Xt/Xt* embyos over the course of development. Each age is represented by one litter except E15.5 with two litters, E16.5 with six litters, and E19.0 with two litters. Note that *Xt/Xt* most commony exhibits the greatest mass, and that *Xt/+* are usually heavier than +/+.

Table 6.9. *Embryonic and Postnatal Weights of +/+, Xt/+, and Xt/Xt Animals.*

		+/+			Xt/+			Xt/Xt		
Age	No. of Litters	No.	Mean Wt. (g)	*S.E.M.*	No.	Mean Wt. (g)	*S.E.M.*	No.	Mean Wt. (g)	*S.E.M.*
E14.5	1	2	0.208	*0.0253*	4	0.298	*0.0158*	5	0.306	*0.0145*
E15.0	1	3	0.234	*0.0033*	3	0.238	*0.0117*	1	0.315	-
E15.5	2	2	0.318	*0.0126*	10	0.384	*0.0141*	5	0.395	*0.0527*
E16.5	6	13	0.498	*0.0229*	30	0.576	*0.0120*	16	0.601	*0.0196*
E17.0	1	3	0.631	*0.0231*	3	0.646	*0.0260*	0	-	-
E18.0	1	1	0.680	-	6	0.906	*0.0074*	1	0.981	-
E18.5	1	0	-	-	2	1.034	*0.1560*	4	1.344	*0.0495*
E19.0	2	3	1.178	*0.0471*	7	1.339	*0.0423*	3	1.115	*0.1540*
E19.5	1	1	1.149	-	4	1.273	*0.0265*	3	1.167	*0.0600*
P28	1	*6*	*12.333*	*1.272*	*6*	*15.725*	*0.684*	-	-	-
P42	1	7	18.093	*1.108*	5	18.442	*1.721*	-	-	-
P56	1	2	25.235	*0.245*	5	26.172	*1.165*	-	-	-

Discussion

Positive Transmission Distortion of *Gli3*(-) in Mouse

Summary

Positive transmission distortion (PTD) of the *Gli3*(-) allele was an unexpected finding in the *Xt/+ x Xt/+* mating regimen. Further matings with *Xt/+ x* inbred +/+ parents show that this phenomenon is significant. More surprising still was the finding that PTD occurs only in a subset of the breeding pairs, and in this subset PTD is found at a remarkably high level (2 *Xt/+* to 1 +/+). These data imply that PTD is dependent on the genetic background of the parents. Furthermore, *Xt/+* males mated with other strains (CD1 and F1) did not produce PTD. Thus, *Gli3*(-) PTD is restricted to a subset of animals in the inbred *Xt* colony.

Qualifying Argument

These data rest on the assumption that *Gli3(-)* is fully penetrant. If it were not, some animals that appear to be wild-type may be heterozygous for the *Gli3*(-) allele. This presents the possibility that some phenotypic wild-type mothers may in fact be *Gli3(-)* heterozygotes, and any offspring would be produced at a normal *Xt/Xt*:*Xt/+*:+/+ segregation ratio of 1:2:1. The subset of breeding pairs which exhibit PTD (see Appendix D: BP 544, 547, 548, 550, 556, and 557) display an *Xt/+*:+/+ segregation ratio of 2:1, raising the possibility that the +/+ mothers are recessive carriers of the *Gli3*(-) allele. This cannot be the case: (1) The average litter size for these breeding pairs is the same as produced by the normal subset (8.8 and 8.4, respectively). If the PTD subset was from *Xt/+ x Xt/+* matings where one

parent was recessive for the *Gli3*(-) allele, then the average litter size should be reduced by 25% to account for the homozygous mutants. It is not. Furthermore, (2) there were no signs of homozygous mutant remains. Litters were always counted within twelve hours of birth, and usually within a few hours. In the case of *Xt*/+ *x* *Xt*/+ matings that came to term, remnants of the homozygous mutants would remain in the cage for several hours to half a day before being eaten by the mother. These two points suggest that homozygous mutants were not produced. Finally, (3) an incidence of six recessive carriers of *Gli3*(-) in a population of fourteen implies a *Gli3*(-) penetrance of 57% (8/14). That is, 57% of *Gli3*(-/+) animals would exhibit polydactyly. If this is the case, then the segregation data from *Xt*/+ *x* *Xt*/+ matings must be adjusted to account for poor penetrance. Adjusting these data provides a significant result ($p<0.01$) where before only a trend was observed. Either way, the *Gli3*(-) allele exhibits significant PTD.

I would like to suggest that the *Gli3*(-) allele is not recessive in the *Xt* colony, or is in the very least semi-dominant, and that *Gli3*(-) segregates to a high degree in a subset of the animals in the *Xt* colony.[14]

Comparison With Human Transmission of *GLI3*(-): Sverdrup's Postaxial Polydactyly

In 1922, Sverdrup reported on a similar occurrence of transmission in a pedigree of postaxial polydactyl humans; some parents produced a dramatic overabundance of polydactyl children while others produced the expected Mendelian ratio. I will explore this in some detail.

---

[14] In order to prove this point unequivocably, a genotype assay of future *Xt*/+ and +/+ offspring will need to be performed. This is possible according to the protocol set out by Maynard (2002).

Sverdrup performed an analysis of twenty-three individuals in a family of fifty-seven spanning six generations. He reports and defines the two classifications of postaxial polydactyly still in use today, and which are now known to be caused by heterozygous mutation in *GLI3* (Radhakrishna et al., 1997). PAP type A is characterised by an articulated extra digit, and PAP type B by a loose pedunculated postminimi, both present along the ulnar (postaxial) border of the hand. A further classification of type A/B has more recently been introduced use to define those phenotypes which fall somewhere between full digit duplication and postminimus. Because *Gli3* is the only gene known to be responsible for this condition[15], I will make this assumption that Sverdrup's pedigree is comparable to the *Xt* mouse colony.

PAP, like the *Xt* phenotype, is known to be extremely variable. Sverdrup's original report notes a great deal of variation: the postaxial extra digit was commonest when exhibited on both feet and hands, but in some cases the polydactylism was seen to be restricted to one hand and both feet, or one hand and one foot, or only the hands and so on. Unilateral affection appeared on either side with equal frequency; asymmetries were unbiased. Thus, the phenotypic range and degree of asymmetry of Sverdrup's pedigree is comparable to that observed in the Xt^{Jed} colony (Chapter V).

Sverdrup's most intriguing finding is a bizarre pattern of inheritance similar to that reported above. Before discussing his data, Sverdrup makes it clear that no peculiar matings have occurred, such as intermarriage within the family or the marriage between two polydactylous individuals. For all intents and purposes then, his data are comparable to *Xt*/+ *x* +/+ breeding pair dataset above.

The inheritance of PAP found in his pedigree is shown in Table 6.10. The ratio between normal and affected individuals differs greatly from the expected Mendelian. Among 57 children from 12 marriages in which one of the parents has

---

[15] An abstract was published by Akarsu *et al* (1997) to report a mapping of PAP-A to chromosome 13q21-q32 in a Turkish pedigree. This abstract was not peer reviewed and has not subsequently been published in a peer reviewed journal. I consider these results to be unsubstantiated and possibly incorrect.

supernumerary fingers, there are 34 polydactylous and 23 normal individuals. This ratio of 34:23 is far from the expected 1:1, though it is not significantly different (chi squared, $p = 0.15$). Sverdrup continues to make a distinction between lines 1 and 3 of his pedigree, which represent two distinct lineages with a common first generation ancestor (Figure 6.3). Line 1 gives a conspicuous excess of polydactylous individuals, the ratio being 17 polydactylous to 8 normal ones (2 : 1), while line 3 yields an excess of normal individuals, there being 8 polydactylous and 14 normal ones. Neither of these figures present a statistically significant result (chi squared test, $p = 0.07$ and 0.20 respectively), but I agree with Sverdrup that "these differences are too large to be considered accidental". There is an important other consideration. The A-type polydactylism that covers all the most pronounced cases of the abnormality has only been seen in line 1. All polydactylous individuals in line 3 are of the B-type. This finding suggests that A-type PAP is transmitted with greater frequency, and B-type with less, though subsequent reports fail to prove this.

Table 6.10. *Numbers of affected and normal individuals from the family studied (Sverdrup 1922).*

	Normals	Polydactylous
From generation II, one family	1	9
From line 1, including four generations and six families	8	17
From line 3, including three generations and five families	14	8
Totals.	23	34

Earlier reports lend some support to his idea that PAP is not transmitted according to strict Mendelian genetics: (1) Carlisle (1814) reports on 3 PAP-A families with 23 children, 19 polydactylous and 4 normals; (2) Smith and Norwell (1894) describe a strong polysyndactylism where 5 marriages produced 27 individuals, 20

Figure 6.3 PAP pedigree family tree showing transmission along two lineages, lines 1 and 3. Note the presence of only PAP type A in line 1 until the final generation when it type A/B is expressed. Reproduced from Sverdrup (1922).

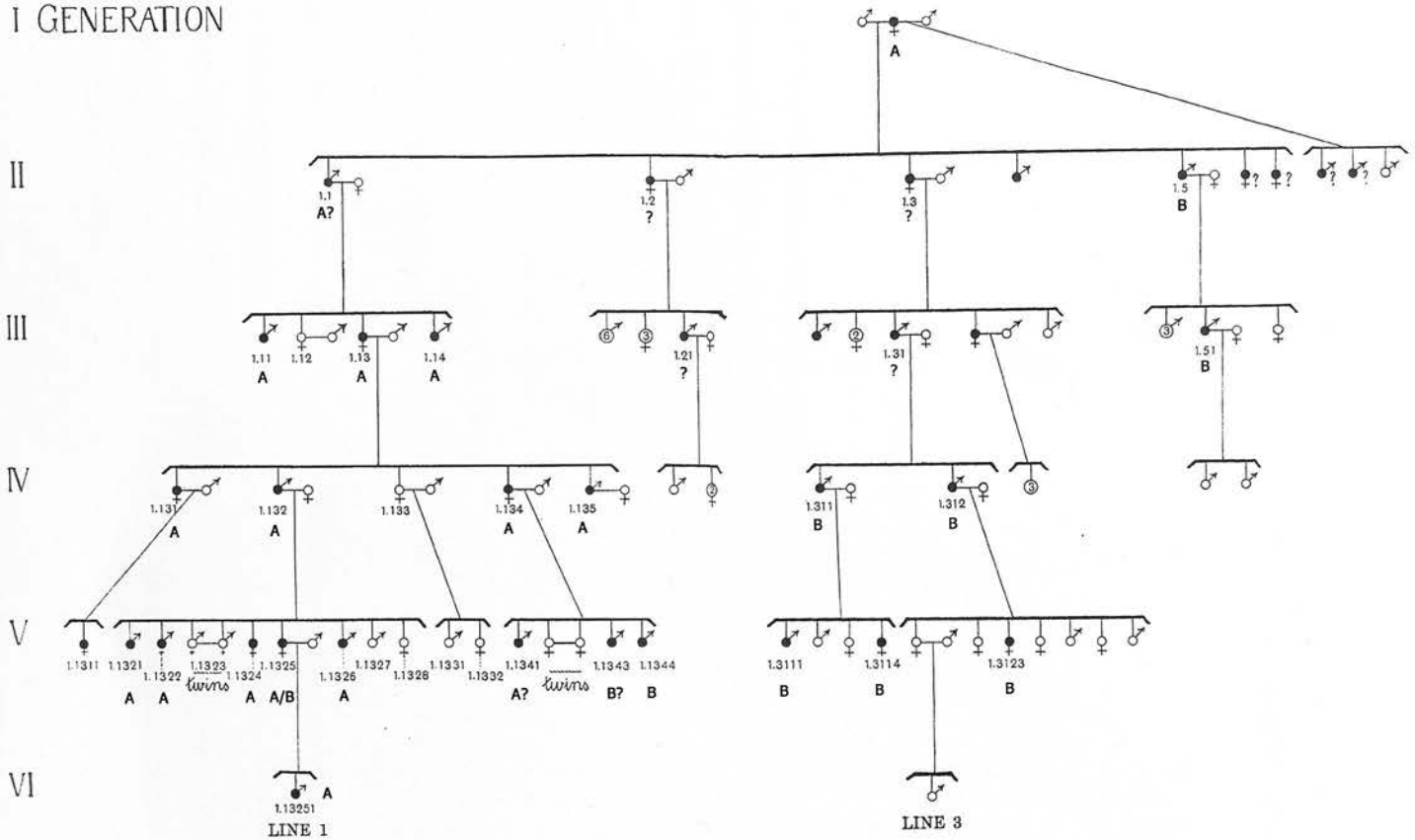
I GENERATION
II
III
IV
V
VI
A
1.1 A?
1.2 ?
1.3 ?
1.5 B
1.11 A
1.12
1.13 A
1.14 A
1.21 ?
1.31 ?
1.51 B
1.311 B
1.312 B
1.131 A
1.132 A
1.133
1.134 A
1.135 A
1.1311
1.1321 A
1.1322 A
1.1323 twins
1.1324 A
1.1325 A/B
1.1326 A
1.1327
1.1328
1.1331
1.1332
1.1341 A?
1.1343 twins
1.1344 B? B
1.13251 A
1.3111 B
1.3114 B
1.3123 B
LINE 1
LINE 3

polydactylous and 7 normals; (3) Nylander (1904) reports a preaxial polydactyl pedigree with bifurcation of digit I, 23 polydactylous to 14 normal offspring were produced. Each of these conditions can and may have been caused by mutation to *GLI3*. Sverdrup suggests PTD and strongly expressed polydactyly share a close correlation. In contrast, individuals with a weak polydactyly, for instance PAP-B, will not exhibit PTD but are more likely to exhibit neutral or negative transmission for the phenotype.

Human Transmission: General Rules

Subsequent reports on PAP paint a very unclear picture, though it seems transmission distortion does play a consistent role. The medical literature is fragmented with no well defined procedure for the reporting of, and the collection of data on congenital abnormalities. From a thorough review of the available literature, I have observed these general rules:

(1) PAP-A is the 'stronger' form of PAP
(2) a PAP-A parent can produce PAP-A, B, or A/B children
(3) a PAP-B parent can only produce PAP-B children
(4) males are more likely to be affected than females

These rules are consistent, yet there are always rule breakers. Recessive behaviour crops up from time to time (Ventruto et al. 1980; Kucheria et al. 1981). This has lead some to suggest that a second modifier gene may also be present. A secondary modifier, or accessory gene would account for recessive behaviour and might also account for PTD (Walker 1961).

Whether we are looking at a single dominant gene with a modifier component, or a single gene with variable expressivity, PTD seems to be a consistent feature of strongly expressed PAP. Data collated from pedigrees with known *GLI3* mutations

Table 6.11. *Collated data from families with* GLI3 *mutions.*

Refs.	Syn.	Fam.	Total	Mutant	Norm	♂	♀	♂ Mut	♀ Mut
[1]	PAP-A/B	UR014	13	**6**	**7**	7	6	3	3
[1]	PAP-A/B	UR015	27	**15**	**12**	19	8	10	5
[1]	PAP-A/B	UR016	10	**6**	**4**	6	4	4	2
[1]	PPD-IV	UR003	26	**21**	**5**	12	14	9	12
[2]	PAP-A	UR004	16	**11**	**5**	4	12	4	7
[3]	GCPS	1	11	**6**	**5**	4	7	2	4
[3]	GCPS	2	3	**2**	**1**	1	2	1	2
[3]	GCPS	3	2	**2**	**0**	1	1	1	1
[4]	GCPS	1	15	**9**	**6**	10	5	6	3
[5]	GCPS	1	17	**12**	**5**	7	10	5	7
[6]	PHS	1	49	**22**	**27**	22	27	6	16
[6]	PHS	2	20	**11**	**9**	14	6	8	3
sums			209	**123**	**86**	107	102	59	65
expected sums				**104.5**	**104.5**				
chi squared p value					**0.01**				

References: [1] (Radhakrishna et al., 1999), [2] (Radhakrishna et al., 1997), [3] (Baraitser et al., 1983), [4] (Temtamy and McKusick, 1978), [5] (Kruger et al., 1989), and [6] (Kang et al., 1997a).

reveal a significant incidence of *GLI3*(-) PTD (Table 6.11). The majority of these data were acquired from families where genotyping has been performed (Table 6.11 references 1, 2, and 6) to show a mutation in *GLI3*. The other pedigrees display transmission of GCPS, which is only known to be caused by mutations in *GLI3*, and it is reasonable to assume that *GLI3* mutations were the cause of GCPS in these pedigrees.

In the above dataset (Table 6.11), there are some pedigrees that exhibit a marked PTD ratio of 2:1, others that display a slight PTD, and others that display no PTD. In two recent papers on two PAP type A/B pedigrees, a ratio of 13:7 and 8:9 was reported (Kucheria et al., 1981; Ventruto et al., 1980). I mention these latter pedigrees because these are the largest (after Sverdrup's) available in the literature, and they reinforce the notion that PTD can occur at a 2:1 ratio, or not at all.

PTD cannot be a sustained phenomenon

PTD of the *Gli3*(-) allele cannot be sustained in any population without rapidly becoming the dominant genotype (Figure 6.4). If we suggest that the *Gli3* allele is transmitted at an average ratio of 1.25 *Gli3*(-) to 1.00 *Gli3*(+) offspring, then after successive generations the *Gli3*(-) allele gains predominance until the majority of animals carry the *Gli3*(-) allele.

I have mapped the effect of PTD in a closed system with an initial population of one million wild-type animals. In this model, if one animal were to develop a spontaneous mutation in *Gli3*, and the animal mated to produce 5 *Gli3*(-/+) offspring and 4 *Gli3*(+/+), then after twenty-three generations at least 50% of the population would be *Gli3*(-/+) (Figure 6.4). This is quite obviously not the case in nature.

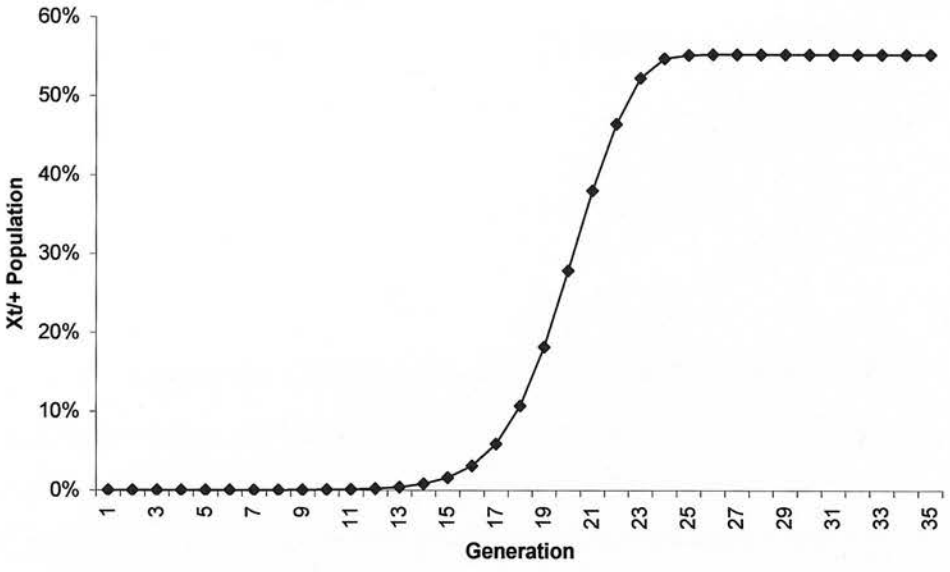

Figure 6.4 A graph to illustrate the rapid domination of the Gli3(-/+) genotype if PTD is maintained. The graph shows the percentage of Gli3(-/+) animals in a population starting with 1 Gli3(-/+) animal and 999,999 Gli3 (+/+) animals. The rules state that half (sex segregated) of the Gli3(-/+) animals mate with half of the Gli3(+/+) animals to produce 5 additional Gli3(-/+) and 4 additional Gli3(+/+) animals. This is reiterated for each generation. The graph plateaues once the 5:4 ratio is obtained and ignores the possiblility of Gli3(-/+) animals mating with other Gli3(-/+) animals.

Possible Mechanisms of Gli3(-) PTD

The mechanism of a *Gli3*(-) positive transmission distortion is open to speculation. There are four stages at which the effect might happen, if the effect was due to the mutant *Gli3* gene: sperm production, pre-fertilization, fertilization, and early *in utero* competition. There is an alternative explanation that has nothing to do with the functionality of the *Gli3* gene product. I will discuss this alternative hypothesis at the end. For now I will consider a mechanism of PTD that is due directly to the gene mutation. I suggest that this mechanism of *Gli3*(-) PTD probably occurs before implantation, and will discuss this below.

Mutant Sperm

As demonstrated in Chapter III, *Gli3*(-/-) neocortical cells exhibit increased viability over their wild-type counterparts, *in vitro*. It is possible that *Gli3*(-) sperm also exhibit an increase in survivability over normal *Gli3*(+) sperm. During sperm production, consecutive cell proliferations of the diploid spermatogonia ends with a final meiotic divisions to produce the haploid spermatids. At this point, the newly formed spermatid is still a round cell, connected to the colony of spermatogonia through syncytial channels, which allow the passage of gene products. It is there that the haploid cell undergoes dramatic rearrangements to its cytoarchitecture and constructs it trademark organelles, an acrosomal cap and flagellum. The nucleus also begins major changes and the transcription of genes for protamines begins. When this transcription is finished a few days later, protamines replace histones and virtually all transcription ceases. Sperm ready.

If *Gli3* is to have an effect on the sperm, it will occur before cessation of transcription, and after meiosis. *Gli3* is known to fulfil a cytoplasmic role as part of a complex of molecules (fused and costal) attached to the microtubules of somatic cells (Altaba, 1999). *Gli3* function there is not well understood, but its association

with cytoarchitectonics suggests that it may play a role in the compacting of the spermatid and the construction of the (microtubule-rich) flagellum. Further *Gli3*-dependent transcription may also be disturbed in the *Gli3*(-) spermatid during the final replacement of histones with protamines.

The presence of a *Gli3*(-) allele may disrupt these systems, and give the *Gli3*(-) sperm a competitive advantage (i) in maintaining its prostitution in the testes, *i.e.* inhibition to apoptosis and resorption, (ii) during the journey through the harsh environment of the female genital tract, and/or (iii) during final penetration of the ovum. If *Gli3* is involved in the cytoarchitectonic changes during the construction of the flagellum, then *Gli3*(-) sperm might produce faster, more motile flagella. This would allow the sperm to travel more quickly through the uterus and meet with the expecting ova. It is also possible that *Gli3*(-) sperm are more able to withstand the harsh environment of the female genital tract than normal *Gli3*(+) sperm. Evidence from the corticogenesis experiments (Chapter III) suggest that *Gli3*(-/-) cells might withstand extremes of environment better than *Gli3*(+/+) cells. If this were the case, then *Gli3*(-) spermatids might not die as quickly *in utero* as *Gli3*(+) spermatids. Finally, *Gli3*(-) sperm may have a more potent potion in their acrosomal cap, enabling them to penetrate the ovum with more efficiency than their *Gli3*(+) counterparts.

Thus, the mechanism of *Gli3*(-) PTD at the level of the sperm probably exerts itself during the final stage of spermatogenesis as the haploid cell is compacting and the spermatic organelles are being produced. I have refrained from making mention of competitive advantages on the side of the female, because the strongest data in this chapter is from *Xt*/+ males breeding with +/+ females.

Post-fertilisation Competition

Another plausible mechanism is a post-fertilisation, pre-implantation competition of *Xt*/+ and +/+ conceptuses to implant. This mechanism is possible, but there is no

evidence to link the function of *Gli3* with implantation, nor is it thought that embryos compete to implant (Prof. Matt Kaufman, personal communication). Post-implantation competition, where mutant embryos might sequester more of the uterine blood supply or otherwise inhibit growth of +/+ embryos is also unlikely on the grounds that litter sizes between *Xt/+ x Xt/+* and *Xt/+ x +/+* are comparable, where one would expect more +/+ embryos to resorb or abort on the grounds that there are more mutants present to cause harm to the wild-types.

Additional Recessive Lethal Mutation

There is an alternative explanation independent of the hypotheses proposed above. The hypothesis, put forward by Prof. Ian Jackson (MRC-HGU, Western General Hospital, personal communication), suggests that there is an additional mutation on the chromosome carrying the wild-type *Gli3* allele, at or near the *Gli3* gene. This novel mutation is a recessive lethal that has arisen spontaneously in the $Xt^{Jackson-Edinburgh}$ stock. The novel mutation might be segregating through the stock so that it is only present in some individuals. Thus, some of the breeding pairs might contain the recessive lethal gene in both animals. These crosses would produce 25% offspring homozygous for the lethal mutation, resulting in a 2:1 ratio *Xt/+*:+/+ (which is seen in the crosses I have labelled the PTD breeding pairs). Those crosses that do not show PTD would not have both parents with the lethal gene.

This hypothesis is further supported by data on the transmission of the *Xt* allele onto different strains. When *Xt/+* males were crossed with +/+ females, not PTD was observed (Table 6.8). According to the hypothesis, the other strains do not contain the recessive lethal, and so PTD would not be observed until the second generation, when it would be possible for two parents with the recessive lethal gene to mate.

PTD of Other Genes

There are two well known situations in the literature that have demonstrated a mechanism for mammalian PTD of a mutant allele.

The first is disruption to the meiotic drive of the oocyte. This produces a classic segregation distortion where an unequal meiotic segregation affects allelic frequency. During meiosis, an aberrant Chromosome 1 is preferentially transmitted (*ca.* 85%) to the secondary oocyte and then to the egg (rather than to either polar body), leading to a distorted allelic frequency of that female's offspring. This has been noted in females of wild mouse populations carrying an aberrant form of Chromosome 1 (Agulnik et al., 1990; Ruvinsky, 1995).

The second mechanism is a consequence of post-meiotic, but pre-fertilisation effects on gamete functionality. This well-studied phenomenon occurs in the *t*-haplotype system on mouse Chr 17 (Schimenti, 2000; Silver, 1985). Spermatids bearing the variant *t*-haplotype form of this chromosome post-meiotically inactivate their wild-type competitors and, as a consequence, gain a relative advantage in fertilising ability (Silver, 1993).

Other cases also exist, most of which are the result of disruption to the meiotic division in the oocyte (for review see: de Villena and Sapienza, 2001). This is not the case with *Gli3*(-) PTD, as it occurs when the male is the mutant allele carrier.

Gli3 Expression in the Genitals

The genetic network governing external genitalia development in the mouse is remarkably similar to that expressed in developing limb bud. The same network, based on an acute *Shh* polarising centre, with known downstream *Hox* targets d-11, -12, -13, and a-13 (Zakany et al., 1997), *Fgf8*, *Fgf10*, *Bmp4*, and *Ptch1* (Haraguchi

et al., 2001), is expressed in murine external genitalia as it is in developing limb bud. Moreover, *Gli3* is expressed in concert with these genes and the other *Gli* family members (Haraguchi et al., 2001). Retinoic acid (RA) and its usual cohort of receptor and receptor-mediated molecules RAR's RXR's, RALDH2, and CYP26 are also present (Ogino et al., 2001).

The evidence for *Gli3* involvement in genital development, and the presence of the same genetic network known to be disrupted in the hand of *Gli3* mutants, suggests that phenotypic differences are also present in heterozygote genitals. This is indeed the case in the external genitalia of the *Xt* mouse (Zakany et al., 1997), and may also be the case in the internal genitalia of human PHS patients (Verloes et al., 1995a; Verloes et al., 1995b).

The collection of molecules involved in external genital formation are the same in limb and brain. The triad of brain, limb, and genitalia maintains the same genetic network to create morphologically and physiologically distinct systems. It is unlikely such homology would remain for long, especially in such diverse structures, unless there was an evolutionary advantage to connect these structures. I believe the importance lies in a shared coevolution of these structures, and the favoured mechanism to change this system is through perturbations in *Gli3*. This will be explained in Chapter VII.

Part 4

Discussion: Gli3 Mutations in Evolution and Development

Chapter VII: Gli3 Mutations in Evolution

Introduction

This final chapter will explore the potential evolutionary consequences of mutation to the transcription factor *Gli3*. Evolutionary developmental biology is presently resurfacing to the foreground of academic thought, after several neglected decades while developmental genetics took precedence. Evolutionary developmental biology, or 'evo-devo' in the parlance of modern workers, attempts to place the mechanisms of development in an evolutionary context and, to determine the genetic and developmental systems that have changed, or have been changed by evolution. The field shares early roots with developmental biology, as first illustrated by von Baer's (1828) laws which recognise that early vertebrate embryos are very similar, and that the specialised features of the various vertebrates arise later in embryogenesis; general embryological features of large groups of animals, *e.g.* tetrapods, appear earlier in development than do the specialised features of a smaller groups, *e.g.* rodents. In the present day, developmental biology is working to understand the role of genes in the formation of generalised and specialised structures, and evo-devo is working to understand the role of the same genes to create different structures, and different species.

I take time to explore the potential evolutionary implications of mutation to *Gli3* because, unlike most other gene mutations, mutation to *Gli3* appears to induce positive, potentially beneficial changes to the final form of the (heterozygous) newborn. Furthermore, the mutated *Gli3* allele appears to be inherited, or transmitted at a greater frequency than its wild-type allele (positive transmission distortion: Chapter VI). *Gli3*(-) mediated positive phenotypic change, coupled with

Gli3(-) positive transmission distortion (PTD), may create a system to promote the rapid morphological change of *Gli3*-affected areas within a population of animals. This chapter will focus on the immediate benefits of such morphological change, and will discuss the potential of genetic background to affect that morphological change. Furthermore, it will present the phenomenon of PTD as a possible evolutionary accelerator, which may act to produce an unusually large proportion of animals with a wide variety of *Gli3*-mutant phenotypes. The morphogenetic mechanisms of *Gli3*-expressing systems will be discussed, as will the effect of *Gli3* and *Gli3*-mutations on these genetic networks. Finally, to better understand the role of genetic networks in development and evolution, I present the epigenetic landscape model to help clarify the role of developmental potential, probability, and history in the development of evolution.

Gli3 Mutations

The transcription factor *Gli3* is a large gene that appears to have a high propensity to mutate. The average gene in the human genome is made up of 30,000 nucleotides (Lander et al., 2001). Human *GLI3* spans 260,000 nucleotides, and murine *Gli3* spans 275,000 (Maynard et al., 2002). The fact that *Gli3* covers a genomic extent almost 10-fold longer than the average gene suggests that *Gli3* will mutate, on average, 10 times more than the average gene. A high frequency of spontaneous *Gli3* mutation in man and mouse has been observed, and has prompted some authors to suggest that "the sequence of the *Gli3* region is somehow [prone] to genomic rearrangements" (Maynard et al., 2002).

Several spontaneous mutations in murine *Gli3* have been recorded (*Xt*-Jackson, *Xt*-Polydactyly Nagoya, and seven *Xt* mutations reported by Harwell, at least one of which was spontaneous). In man, *GLI3* has been found to be responsible for conditions of PAP, PPD-IV, GCPS, and PHS (Kalff-Suske et al., 1999; Kang et al.,

1997b; Radhakrishna et al., 1999; Radhakrishna et al., 1997; Sobetzko et al., 2000; Vortkamp et al., 1991; Wild et al., 1997). Furthermore, mutations to *GLI3* may be responsible for other congenital polydacytylys such as PPD-II and III (Chapter V), and there is a good chance that *GLI3*-mutations are the sole cause of isolate PAP's and PPD's (no other gene mutations are known to cause these conditions, see Chapter II). Other animals also show an incidence of polydactyly (Figure 7.1). It is not presently known if *Gli3*-mutations are the cause, but conventional wisdom suggests that developmental genes play a similar role in most mammals. Thus, *Gli3* mutations may be the cause of common polydactylys in many species.

Gli3 in Morphogenesis

Gli3 is expressed in mid and late development in a wide variety of ectodermal and mesodermal tissues (Hui et al., 1994; Schimmang et al., 1992). These tissues give rise to the craniofacial region, the brain, the cervical vertebrae, the ribs, some visceral organs, and the limb. Homozygous mutation in *Gli3* affects all of these systems (Johnson, 1967). Heterozygous mutation to *Gli3* noticeably affects the craniofacial region (human PHS and GCPS), the brain (human PHS and GCPS, and Chapter III) and the distal limb, namely digit patterning (Chapters II and V).

Here I review the observed phenotypes in the *Xt/Xt* and *Xt/+* mouse in order to illustrate the potential competitive advantages the heterozygote form may present.

The Limb

The limb of *Gli3* heterozygotes is normal in most respects, but exhibits subtle skeletal changes to the wild-type form. In the *Xt/+* animal, the autopod exhibits an

Figure 7.1. Polydactyly is common in many animals. Chickens, hamsters, rats, mice, humans, and cats all exhibit polydactyly. Cats are particularly popular polydactyls and are a registered breed defined by an extranumerary digit that "may be polydactyl on only front, only hind, or both. Some cats display the 'thumb' shape on front or hind while others have almost double feet, *i.e.* a 4 toed foot and a smaller 3 toed foot. 'Mitten', 'double foot' or 'snowshoe' shaped front feet are acceptable." (American Association of Polydactyl Breeders).

extranumerary digit, the carpals are altered slightly, the radius exhibits a subtle change in size, and the stylopod displays an aberrant deltoid tuberosity. For comparative purposes, the homozygote mutant displays a number of deformities including six to eight digits, extra and altered carpals/tarsals, potential hemimelia of the radius and tibia, and a misplaced deltoid tuberosity.

Changes to wild-type autopodial architecture may present novel forms of movement and dexterity that allow the animal to explore environmental domains inaccessible to the wild-type. The forepaw is composed of three compartments of bone, the phalanges, metacarpals, and carpals. The anterior of these compartments is altered slightly in the *Xt*/+ animal to present morphological changes to digits I and II, and to adjust carpal morphology (Chapter V). Alterations to these structures may affect the function of the forepaw. In particular, alterations to the carpel region determines the degree of flexibility, or range of movement open to that paw. The potential for a beneficial alterations to the skeletal structure of the autopod exists in the heterozygote mutant, although the extranumerary digits, as it is observed in the animal house, do not appear to come into use when the animal is climbing or holding onto bars. In the wild, the paws are used to navigate terrain, *e.g.* climbing and walking, and to manipulate objects found in the environment, *e.g.* digging and manipulating food. Adjustments to the skeletal structure of the paw might affect the type of range of action available to the animal, enable it to explore novel environments, and so help to confer evolutionary success.

In the humerus, deltoid tuberosities of wild-type animals display a distinct sharp notch of bone at birth, while *Xt*/+ animals display a flattened, or rounded notch of bone at birth. Sharpness of the notch is dependent on the *Gli3* genotype and extends along a continuum from sharply notched to rounded. +/+ animals occupy the sharp end of the range while *Xt*/+ animals occupy the rounded (Chapter V).

The deltoid muscle and geometry of tuberosity provide lateral flexion to the forelimb. Changes to wild-type deltoid tuberosity morphology may affect the strength and range of movement of the forelimb, thus affecting the animal's gait.

This in turn may affect the variety of terrain over which the mouse is able to navigate. There is no literature source to help define the exact changes to locomotion that a change to wild-type tuberosity morphology may cause, but it is conceivable that in some heterozygote situations this change may be advantageous, while in others it may be disadvantageous. The fact remains that heterozygosity produces novel variation to wild-type morphology that may promote an advantageous use of the limb in the environment.

Brain and Skull

Facial tissue, brain, and limb are dramatically different structures, yet they share a basic underlying signalling system for positional information. Craniofacial morphogenesis and limb development share a common *Shh* signalling pathway to induce polarising activity (Schneider et al., 1999). In brain, Shh is thought to lay out the ventral position in mesencephalon , and in telencephalon this may act by long-range *Shh* signalling (Gritli-Linde et al., 2001; Zeng et al., 2001). In the *Gli3* homozygote mutant, these structures are probably affected by a disruption to the underlying *Shh* signalling network. In limb it is lack of posterior repression that allows posterior digit pattern to be reiterated anteriorly (Zuniga and Zeller, 1999). In brain, lack of dorsalisation causes ventral expression domains to move dorsally (*cf.* posteriorisation in *Xt/Xt* limb), which disturbs ventral and dorsal morphological structure (Tole et al., 2000). Thus, *Gli3* may act to repress ventral domains in dorsal brain, in the same way that it represses posterior domains in anterior limb.

The homozygous *Gli3* mutant mouse suffers from a number of dramatic craniofacial defects. The first, seen at E9.5, is an enlarged pharangeal arch. As development proceeds, craniofacial defects become compounded and more severe, resulting in a defects to all facial features: jaw, teeth, nose, vibrissae, eye, and craniofacial skeleton. On the other hand, the *Gli3* heterozygote appears normal with only a small

centre of ectopic ossification noticed between the frontal plates of the skull (Chapter V and Johnson, 1967).

If one considers that the spectrum of *Gli3* phenotypes lies on a continuum from severe phenotypes in the homozygote mutant to normal phenotypes in the wild-type, it seems probable that additional craniofacial and neurological phenotypes are present in the *heterozygote* mouse that have not yet been recorded. This reasoning prompted a detailed analysis of the *Xt/+* newborn cranium. The most obvious phenotype was seen in only 2 out of 60 animals. This was a lateral extension of the infra-orbital bone. Other changes were hard to identify with certainty because, like the carpels, the alteration is subtle and morphology complex. In human *GLI3* heterozygotes, craniofacial defects are a common feature of patients suffering from GCPS. Human GCPS patients display frontal bossing (high forehead), hypertelorism (increased distance between the eyes), and a broad nose (Greig, 1926). One is able to detect these anomalies in man because our visual perception is highly attuned to facial recognition. Changes in murine *Xt/+* facial morphology can be inferred from (1) the severity of *Xt/Xt* facial changes, (2) the human GCPS (*Gli3-/+*) facial change, and (3) exhibition of murine *Xt/+* ectopic interfrontal ossification.

Changes to wild-type craniofacial morphology may be advantageous in an evolutionary setting. Lateral displacement of the orbitales, which house the eye, may increase the visual range of the animal and increase detection of predators. Changes to dental morphology have been noted, and may affect the types of food the animal is able to masticate (Hardcastle et al., 1998). Displacement of the otic capsule toward the anterior (*cf. Xt/Xt*) may increase auditory perceptual range. Furthermore, changes to the structure of the brain may promote beneficial cognitive changes.

Cervical and Thoracic Vertebrae

The cervical and thoracic vertebrae are also affected in the *Xt/Xt* mouse, but are not altered not a noticeable degree in the heterozygote. This suggests that if evolutionary changes by *Gli3*-mutation do occur in these regions, they are likely to be less affected than changes to the other structures, such as the limb and craniofacial morphology, where phenotypes have been observed. Changes to the morphology of wild-type cervical vertebrae may affect the range of motion of the neck, and changes to wild-type thoracic vertebrae may affect the animal's posture.

Phenotypic Range

An important consideration of the role of *Gli3* heterozygote phenotypes is the amount, or degree of variation within each phenotype. Variation may be a key to the evolutionary success of a new genotype, because it produces the range of new 'prototypes' to be tested in Darwinian survival of the fittest. Those prototypes that succeed in the environment will continue to breed and the genotype will be transmitted to the next generation. Part and parcel of this process is the influence of genetic background to adjust the phenotypes produced by the mutation, *e.g. Gli3* mutations. I will first explore the phenotypic range of each *Gli3* mutant phenotype, and then discuss the possible and observed affects of genetic background on the phenotypic range.

The phenotypic spectrum of *Gli3*-mutant mice extends from severe (*Xt/Xt*), through mild (*Xt/+*), to normal (+/+). Within each phenotype, the phenotypic spectrum is distributed across a range of possibilities that produces a bell curve probability distribution (Figure 7.2). The probability distribution of the phenotypic range of *Xt/+* and +/+ animals overlaps to form a continuous spectrum of phenotypic

Figure 7.2 The phenotypic range of some features in *Xt/Xt*, *Xt/+*, and +/+ mice in the Xt^{Jed} colony (Chapter V). (A) The frequency of the sizes of interfrontal ossification as observed in *Xt/+* and +/+ animals in the Xt^{Jed} colony. Distribution of *Xt/Xt* ossification sizes are inferred by the large variation noted in the hand and deltoid tuberosity. (B) A schematic of the interfrontal ossification (red region) found in *Xt/Xt*, *Xt/+*, and +/+ animals. The distribution of interfrontal ossification sizes noted in these phenotypes may be indicative of the general distribution of variance noted in the other phenotypes of Xt^{Jed} colony. Illustrated here are (C) the morphologies of the deltoid tuberosity. *Xt/Xt* tuberosities show great variation. Illustrated here is one that slopes onto the humeral shaft. *Xt/+* tuberosities are present, but not notched as they are in +/+ animals. (D) Digit and carpal patterning of the forelimb autopodia (see below for key to colour coding), and (E) a graph to represent the difference in mass of *Xt/Xt*, *Xt/+*, and +/+ embryos, where *Xt/Xt* > *Xt/+* > +/+ (Chapter VI).

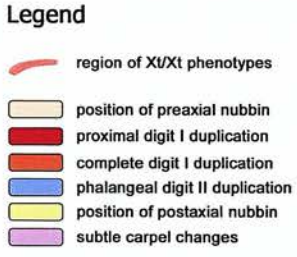

A.

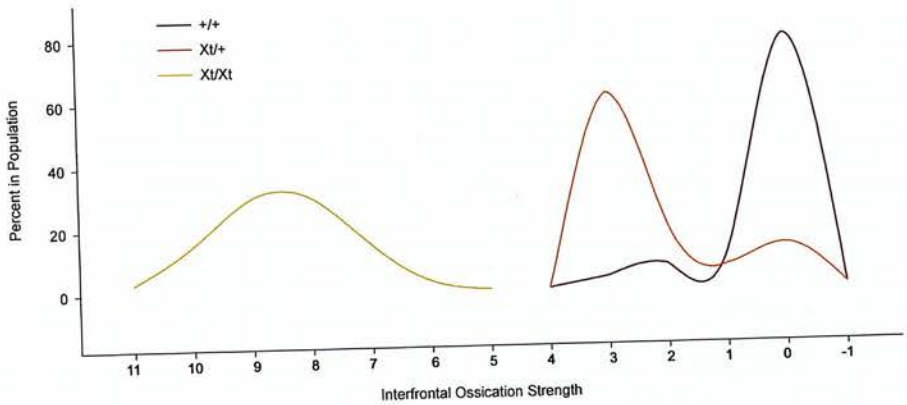
+/+
Xt/+
Xt/Xt
Percent in Population
80
60
40
20
0
11
10
9
8
7
6
5
4
3
2
1
0
-1
Interfrontal Ossication Strength

B.

C.

D.

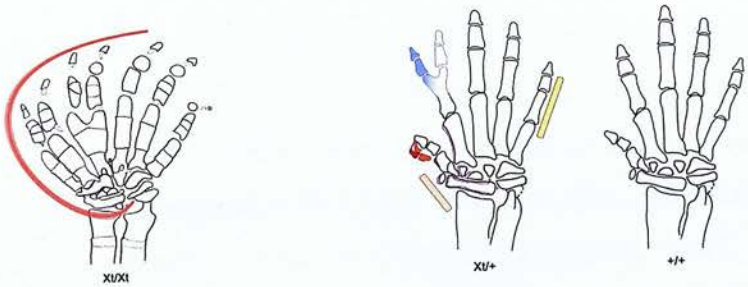
Xt/Xt
Xt/+
+/+

E.

expression, whereas the *Xt/Xt* phenotypic range is separated from the others due to its extreme severity, but nevertheless represents an exaggeration of those phenotypes observed in the heterozygote.

The phenotypic spectrum of *Xt/Xt* neonates illustrates the developmental systems that are affected by *Gli3* mutation (*e.g.* craniofacial, neural, *etc.*). The phenotypic spectrum of the *Xt/+* neonate illustrates the most affected developmental systems of the heterozygote animal, the systems that are most susceptible to change by *Gli3* mutation, the systems that exhibit the *observed* phenotypic change. It is also possible that the *Xt/+* animal displays some unobserved phenotypes, such as an adjustment in the brain (Chapter III), or novel adjustments to limb morphology (Chapter V). By examining both genotypes, we are able to detect the systems that are potentially affected in the *Xt/+* animal, and observe the phenotypic range of those that are noticeably affected.

Distribution of Interfrontal Ossification

The size and frequency of occurrence of the interfrontal bone of the cranium are increased on mutation to one allele of *Gli3*, and increased further on mutation to both alleles (Figure 7.2). Interfrontal ossification is a good measure of the probability distribution, or phenotypic range of an *Xt/+* (and +/+) phenotype; quantitated data is available on this feature from two studies (Chapter V and Johnson, 1967), and the expression of interfrontal ossification is not meristically restricted as it is in the digits, but is expressed across a continuum. Wild-type animals present a 21% incidence of an interfrontal bone at birth, whereas *Xt/+* animals display an interfrontal bone in 88% of the cases observed. Furthermore, the mean size of the bone is increased in the *Xt/+* animals; the bell curve median has shifted towards a larger phenotype. In *Xt/Xt* animals where the calvarium develops normally, interfrontal ossification is always seen (3/3) and is much larger than the largest observed *Xt/+* interfrontal bone.

Spectrum of Hand Phenotypes

The autopodial phenotypic range is distributed across the phenotypes in a similar manner to interfrontal ossification, but with meristic restrictions (Figure 7.2). Distribution within the *Xt/+* phenotype is centred on the commonest phenotype, duplication of the distal digit I phalanx (24/37), with less common possibilities of full digit I duplication (to varying degrees of size and syndactyly), and postaxial nubbin formation. There is some overlap between the heterozygote and homozygote wild-type phenotypes. Some limbs on some *Xt/+* animals do not display an extranumerary digit. The incidence of this occurrence is quite low (<10%) in the Xt^{Jed} colony. Furthermore, in some strains wild-type animals have been to display a very low incidence of extranumerary digit formation, without gene mutation (Grüneberg, 1963). The *Xt/Xt* phenotypic range does not overlap with the *Xt/+* range, but is similar in that it is a more severe expression of preaxial polydactyly, *cf.* interfrontal ossification.

Spectrum of Deltoid Tuberosity Morphology

In +/+ animals, deltoid tuberosities display a distinct sharp notch of bone at birth. *Xt/+* animals display a flattened, or rounded notch of bone. Sharpness of the notch is dependent on *Gli3* genotype and extends along a continuum from sharply notched to rounded. +/+ animals occupy the sharp end of the range while *Xt/+* animals occupy the rounded (Figure 7.2). In *Xt/Xt* animals, the tuberosity has been shifted proximally and displays a wide range of expression from a gentle slope to an isolated mass of cartilage.

I have shown above the major phenotypic features of the *Xt/+* animal, and the range of variation they display. Furthermore, I have suggested possible competitive

advantages that these features might lend to an animal in the wild. I would now like to introduce the epigenetic landscape model to help explain the function of probability in development as the source of phenotypic variation, and then continue with a discussion on genetic background as a source of phenotypic change to change mutant, as well as wild-type phenotypes.

The Epigenetic Landscape

Waddington formed the epigenetic landscape model (Figure 7.4) to depict the branching patterns of development[16] and at the same time portray the different stabilities of these pathways by depth and contours. Waddington's conceit is introduced as a representation of development "not as a branching line on a plane but by branching valleys on a surface" (Waddington, 1939). The depth and contours of the "geological model represent probability, so that the valley bottom is really a representative of an equilibrium." The totipotent cell falls into valleys of specialisation, where contours and depth represent probability and population. Movement is accompanied by proliferation, forming a wave of cells moving *en masse*, gathering in number and diversity as they proceed through the landscape, until embryogenesis is complete and the system cessates.

The trajectory a particular cell line takes during this process is affected by its developmental history and its present position in the developing system. A cell's history defines its genetic and molecular components at any point in the epigenetic landscape; its history reflects the path the of its lineage as it has progressed through

---

[16] Embryogenesis is the process of repeated cell divisions that progress along avenues of specialisation. At each branch of specialisation a 'decision' is made to proceed down one avenue or the other. A cell's fate decision depends on the its history and cues in the immediate external environment. The first diploid cell, the fertilized ovum, undergoes many cell division to create the tissues of the neonatal mouse. At points during this process, cells differentiate to follow a particular specialisation. Each avenue of specialisation restricts the future possibilities for that cell and it's future progeny. The branches of specialisation, forming the tissues and specialised cell types of the organism, are usually mapped out in the form of a cell lineage diagram drawn with lines (Figure 7.3).

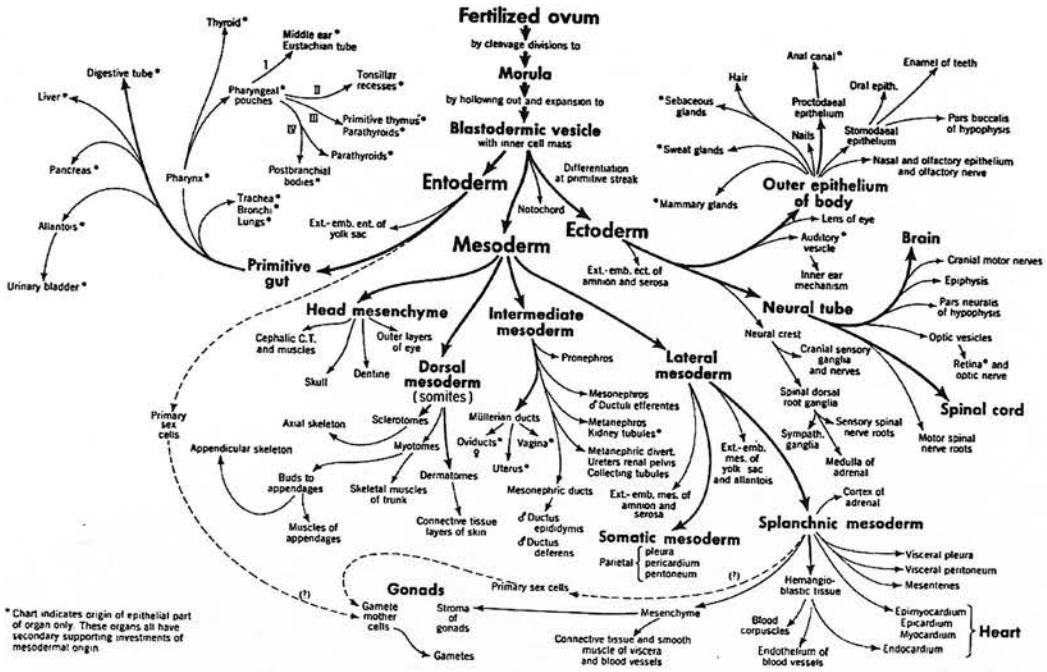

Figure 7.3 Standard Lineage Diagram. A standard lineage diagram uses lines to depict the developmental tree. Cell fate choices are made at each branch of the cell lineage diagram. Once a cell proceeds down an avenue of specialisation, it can only further specialise down that particular avenue. Endodermal gut cells, for instance, cannot later become mesodermal somitic cell, but are restricted to further specialisations of the gut. Transdifferentiation, the jumping from one lineage to another, is known to occur only in very exceptional circumstances. This diagram is intended for illustrative purposes only and may not be accurate by modern standards. (Reprinted from Pattern and Carlson, 1974.)

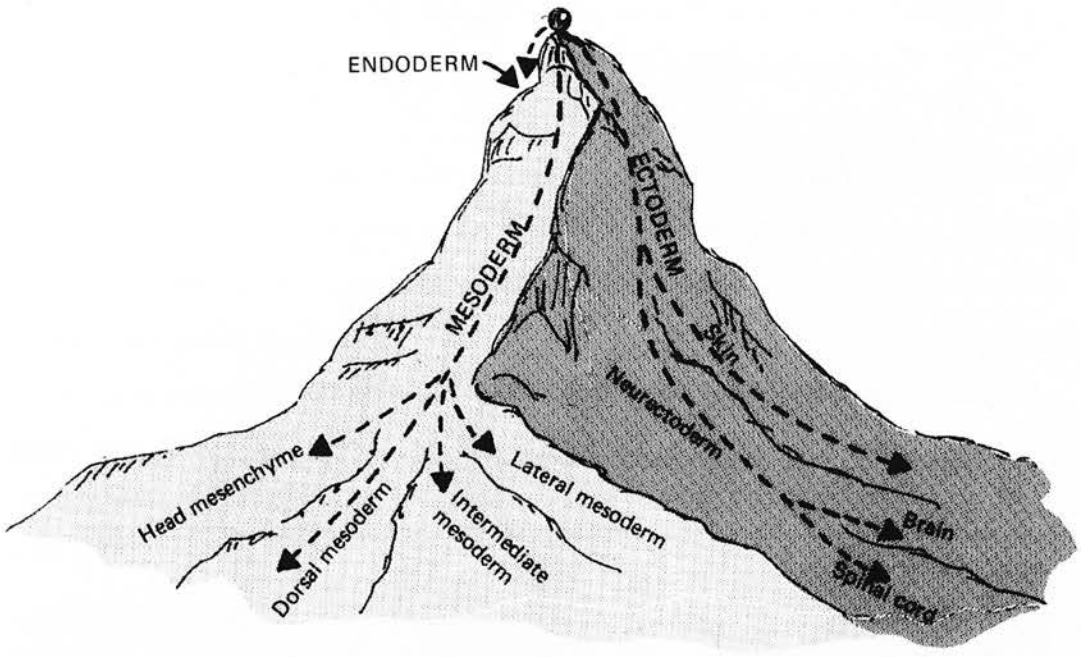

Figure 7.4 The Epigenetic Landscape. Waddington's developmental model represented the lineage diagram "not as a branching line on a plane but by branching valleys on a surface". The depth and contours of the "geological model represent probability, so that the valley bottom is really representative of an equilibrium." The totipotent cells on the mountain's peak is able to take any valley of specialisation. Indeed, once it has proliferated sufficiently, it will tumble down all valleys, and as development proceeds, a wave of proliferation and differentiation will descend.

development. In the early embryo, neural tissue of the forebrain will have had a similar gene expression profile, and so a similar history. It is a degree of chance that determines its flow down one line or the other, and this is in part reflected by the position of the cell in the tissue. Cells in some positions will come under the influence of inducers and cells in other positions will be affected by signalling molecules of another type. A combination of positional information, current gene expression, and cellular composition determines the possible future trajectories for that cell's further development. Altogether, the many branching lines fulfil the epigenetic possibilities of the genome, and a whole embryo is formed.

This process forms a robust developmental network which is able to, generation after generation, produce organisms of like form. The network of inter-relating genes and their products forms the epigenetic landscape. At points during development a cell will proceed down one or other valley of specialisation. At these points, some genes are thought to weigh more heavily, "and genes like [the Drosophila eye pigment gene] vermillion which have their effects at certain branching points are like intrusive masses that can direct the course of the developmental process down a side valley," (Figure 7.5). Other genes, like the *Drosophila Hsp90*, buffer the developmental 'canals' to ensure that development proceeds down tried and tested paths. A cell's network of gene expression lies underneath the epigenetic landscape to give rise to the mountain valleys.

Our knowledge of gene interactions is growing, but it is still very crude; only gross effects can be recognised, which is why there has been no need for Waddington's more 'organic' model of development. The subtle effects of chance and probability, which differentiate Waddington's model from a lineage diagram, are today not accounted for. Interestingly, it is the subtle variations caused by chance, or stochastic effects, which are likely to influence evolutionary change.

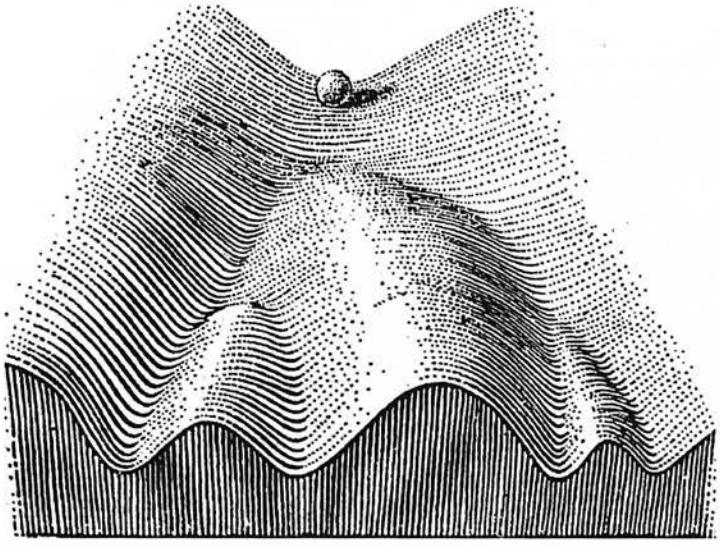

Figure 7.5 Representation of the epigenetic landscape. The ball represents cell fate. The valleys are the different fates the cell might roll into. At the beginning of its journey, development is plastic, and a cell can become many fates. However, as development proceeds, certain decisions cannot be reversed. From Waddington 1956, Principles of Embryology, p. 412

Within systems, we are beginning to understand the role of key molecules in the epigenetic process. In the forebrain, for example, one sees a number of transcription factors differentially expressed across the tissue. *Otx1*, *Emx1*, *Emx2*, *Arx*, *Pax6*, *BF1*, *Dlx5*, *Trbr1*, and *Id2* are a handful of the genes we know to be intimately involved in the specification of forebrain cell fate (Price and Willshaw, 2000). Each forebrain cell will express a combination of these genes, dependent on its history and positional information. That combination sets out, or lays down the epigenetic possibilities available to the cell, presumably to refine neural fate.

Waddington's epigenetic landscape incorporates the notion of canalisation, which reflects both the probability of a particular trajectory, and also the evolutionary stability of that trajectory. He stated that "developmental reactions... are in general canalised. That is to say, they are adjusted so as to bring about one end result regardless of minor variations in conditions during the course of the reaction." (Waddington, 1941). Canalisation is necessary if the developing system is to buffer itself from developmental noise, *i.e.* changes in the uterine environment (nutrition supply, temperature, pathogens, *etc.*), changes in the genome from sexual recombination and mutation, and also local variation in the molecular composition of cells and tissues. If a developmental trajectory is not heavily canalised, then phenotypic variation in form may arise, because the walls of the valley are lower and chance may allow cells to spill over into another valley. A poorly canalised developmental system is also thought to be one open to evolutionary change, because this is one that has not been heavily selected for, and so genetic 'buffers' or canalising genes have not evolved to raise the walls of the valley and restrict development to a particular phenotype.

The endpoint of Waddington's epigenetic landscape presents us with a graph of contours which represent the final product of embryogenesis; it represents the total collection of cells at their fully matured state. The final graph is the complete set of an organisms phenotypes, and can be visualised by taking the last contour from the skirt of the mountain (see Figures 7.4 and 7.5), and unwrapping it onto a standard two-dimensional plane. Thus, each trough represents individual phenotypes toward

which many cells have travelled. Time then, exists along the z-axis and travels back from the final point of embryogenesis. Some small, shallow valleys may not be expressed, because the developmental trajectories were such that no cell travelled into it. Such valleys may reflect developmental abnormalities. In our case, I refer to the formation of a sixth digit, which may not form from genetic mutation, but by chance (Grüneberg, 1963). Other valleys will form deep gorges and are the heavily canalised valleys imperative for survival.

Alteration of Gli3 Morphologies by Genetic Background

Background on Genetic Background

The *Gli3*-mutant phenotypes are, in part, dependent on the genetic background of the animal (Chapter V). To understand how genetic background might influence the phenotypes, it is important to define what is mean by 'background', because there is no clear definition of the concept. Presently, developmental biology is concerned with the role of major transcription factors and other genes which, when they are removed, cause a noticeable and consistent disturbance to development. The number of genes known to fit into this category is very small, especially when considered as a percentage of the total genome. There are 30-35,000 genes in the human genome, each with an average length of 30 kilobases (kb) and an average exon content (translated region) is 1.4 kb (Lander et al., 2001). Thus, only 4.5% of the 'gene' is transcribed into protein. Genes represent about 1/3 of the entire genome, so, 1.5% of the entire genome is used to make protein. If we take a dictionary definition of background as "the ground or surface lying behind... the chief objects of contemplation" (O.E.D., 2002), then we can see that genetic background in fact accounts for most (98.5%) of the genome.

Grüneberg, in his authorative publication "The Pathology of Development" (1963), is more specific by what he terms genetic background:

> "Such genes which modify the manifestation of a mutant gene without having an obvious effect on the normal condition are known under the name of 'modifying genes'. Modifying genes for mutants are extremely common in all genetically mixed populations; indeed, they are ubiquitous. This does not mean that the whole of this variation is under the control of modifiers. Part of it is commonly due to the environment or to chance... However, the fact remains that the manifestation of genes is largely under the influence of modifiers which are collectively referred to as the 'genetic background' in which the gene finds itself."

Thus, to Grüneberg, modifier genes represented the major component of genetic background, though the presence of modifier genes in the genome has yet to be established. In the early days of developmental genetics (*circa* 1950), modifier genes were regarded as important components of development, and the epigenetic landscape was key to Waddington's understanding of the effect of modifier genes on development. Modifier genes were thought to help canalise developmental trajectories by 'building' the walls of the valley. Modifier genes were also thought to move the valleys, so that a new organism's final developmental trajectory may differ from that of its parents, due to a novel background created by sexual recombination.

Thus, modifier genes, or genetic background, affect the final morphology of an individual by adjusting developmental trajectories. If one considers that each species is similar in terms of its genomic sequence, then genetic background may be largely responsible for the morphological variation within a species. In *Homo sapiens*, we can most readily see morphological differences between races. Consider, for example, the difference between a Negro and an Asian. Negroes have broader faces, are taller, and more muscular than their Asiatic counterparts. Even within races one can often determine an individual's geographic origin by their facial, and other characteristic features, *e.g.* the aristocratic nose.

The exact composition of genetic background is still unclear. Variation in gene structure, such as polymorphisms, probably contribute to genetic background. The presence or absence of some minor genes may also contribute to genetic background. But perhaps the most intriguing source of genetic background lies in the untranscribed regions of DNA. Here lie stretches of code which affect the binding properties of transcription factors, and either increase or decrease the expression of genes within their locus. These sites, called enhance and silencer regions, are most likely to affect the phenotypic differences we see as a result of genetic background, because it is these regions that are free to change without adverse effect to development.

The effect of genetic background (untranslated regions in a modern sense, or modifier genes in Gruneberg's opinion) on specific traits has been studied by comparing differences between inbred mouse strains. Grüneberg (1963) reviews a number of publications on the level of pelvic attachment to the vertebral column, and compares the differences according to the strain of mouse.

Pelvic level is defined by the number of presacral vertebrae, the first sacral vertebrae being the point of attachment to the pelvis. The following table gives an indication of the degree of variation and of the influence of genetic background on pelvic level:

Some strains are nearly constant (P, C3H, and NB) while others have considerable phenotypic variance (DBA/2L, BALB/c, and SEC/2) despite their near genetic homogeneity. The aetiology of this variance became a topic of debate. Nutritional studies, strain crosses, and zygote transplantation studies were carried out to determine the cause. Grüneberg (1963, pg. 250) concluded that pelvic attachment is "a continuously varying entity (like stature in man) which is determined by genes with additive effects." These genes make up the genetic background of the strains. How many 'genes' were involved in the effect was unclear, "it is virtually certain that several gene pairs are involved whose number remains uncertain and which is likely to be different from cross to cross." This suggests that background may not be 'genes' at all, but may be collective effects of the unexpressed genome.

Table 1. *The pelvic level in seven inbred strains of mice. From E.L. Green (1954), with Xt colony addition in italics.*

Strain	Presacral vertebrae					total
	25.0	25.5	26.0	26.5	27.0	
P	92.2	4.4	3.4	-	-	384
C3H	92.6	6.4	1.0	-	-	203
DBA/2L	77.7	9.4	12.9	-	-	139
C57BL/10	3.6	6.7	89.7	-	-	419
NB	-	-	99.2	0.8	-	245
BALB/c	-	-	52.0	24.3	23.6	296
SEC/2 and 2d	0.1	-	14.7	17.3	67.9	941
B6.C3/CBA		*11.4*	*88.6*	-	-	*60*

As shown above, genetic background skews the developmental canal to produce variety. It seems to do this by adjusting the thresholds for phenotypic expression (Figure 7.6). In mutant animals, this may determine whether or not a particular phenotype is expressed. Grüneberg suggests that background may act accumulatively, even to the extent of producing a 'phenocopy' of a mutant phenotype. Or it may act diminutively by reducing the expression of a mutant phenotype. Thus, background is an important determinant of phenotypic expression.

Background Dependence of *Gli3*(-/+) Phenotypes

Phenotypic expression of the *Gli3*-mutants (hetero- and homozygotes) is affected by background (Chapter V and VI). Background can affect the type of phenotype produced, and can determine whether or not the phenotype is expressed. A mutant gene which does not always produce a mutant phenotype is considered non-

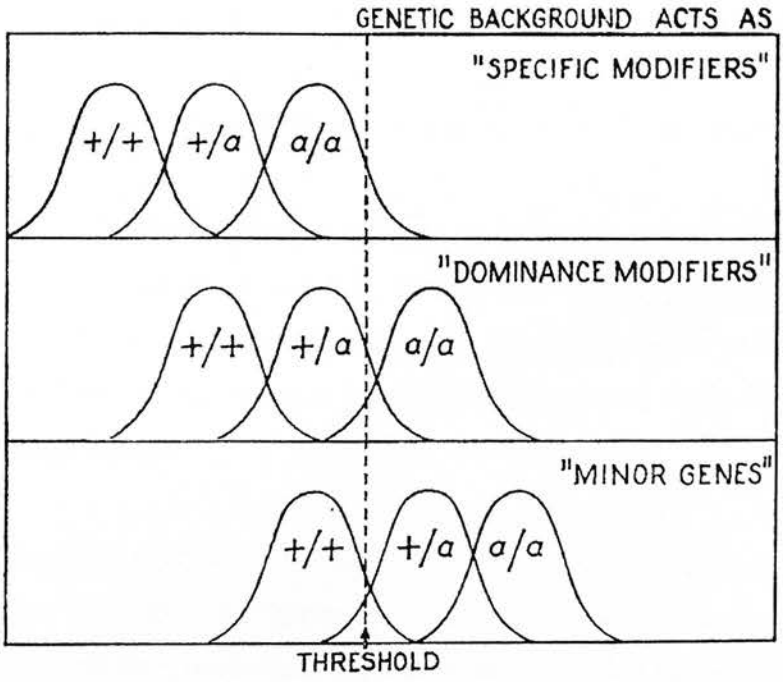

Figure 7.6 The Threshold Effect. A threshold exists for the expression of any phenotype. Threshold reflects the probability distribution within the epigenetic landscape. Genetic background adjust threshold levels, and can affect the phenotype of wild-type animals, sometimes acting cumulatively as 'minor genes'. On heterozygotes, background may affect penetrance and act as 'dominance modifiers'. Finally, background may affect the type of phenotype produced by a mutation, as shown by 'specific modifiers'. From Grüneberg 1963.

dominant. Background therefore affects the penetrance of a gene.[17] *Gli3* is considered a semi-dominant gene (near 100% penetrance), but this feature may also be dependent on background. The possibility exists that *Gli3* heterozygosity may be present in some phenotypic wild-type animals. Taken to an extreme, *Gli3* heterozygosity may be present on a background that inhibits obvious phenotypic expression, and a subpopulation of heterozygous animals may exist unnoticed. It is only when these heterozygous animals breed with animals of another background, that penetrance is uninhibited and expressed as a polydactyl phenotype.

In the *Xt* mouse, background is seen to affect the type of polydactyly expressed. This is seen within familial lines where *intra-familial* variation is present, but as variable as *inter-familial* variation (Chapter V). The occurrence of variation within the inbred Xt^{Jed} colony indicates that phenotypic expression is highly variable, even within an inbred colony.

Then there is the level of *strain*, or race. When *Xt* studs impregnated F1-outbred wild-type females, *Gli3*(-/+) offspring exhibited a novel phenotype, digit II polysyndactyly. Digit II polysyndactyly has not been noted in any animal within the Xt^{Jed} colony. Other examples of background dependence have been reported. A novel Gli3-mutant mouse (Bose et al., 2002) exhibited 6% occurrence of forelimb postaxial polydactyly on an inbred 129 background. When this line was crossed to a C57/BL6 background, the appears of postaxial polydactyly was reduced to 3%. In another Xt^{J} colony, exencephaly was a common occurrence when bred on a C3HeB/Fej background (50%) (Tole et al., 2000), but completely vanished when crossed to a C57/BL6 background (Tomioka et al., 2000).

The pattern of background-dependent *Gli3*(-/+) phenotypic expression is common to both humans and mice. Radhikrishna (1999) agrees "the *Xt* spontaneously induced mutation that occurred in a (C3Hx101)F2 mixed background shows variable

---

[17] The degree of penetrance is defined as the percentage of genotypically affected individuals which are phenotypically abnormal.

expressivity and severity in affected homozygous and heterozygous mice. It is likely that the genetic background may contribute to the modification of the phenotype." He comments that inter-famial variation is less than intra-familial.

It is not clear how background and phenotypic variance interact to produce novel forms, nor how this might influence the evolution of form, but it is possible that the two interact under the influence of *Gli3* mutations to produce novel, variable, and viable animals with structural differences that promote survival, and evolutionary success.

The Shh-Gli3 Axis in Morphogenesis

Signalling by Shh

In the wild-type and heterozygote embryo, *Gli3* is expressed in apposition[18] to *Shh* (Chapter I). In the developing limb bud, *Gli3* is expressed in a broad anterior domain and *Shh* in a discrete posterior region. In the rostral portion of the neural tube that gives rise to cranial neural crest (craniofacial precursors), trunk neural crest and somites (somatic organ and rib precursors), *Shh* is expressed in the notochord and prechordal mesoderm which lies ventral to the spinal cord and brain. In apposition, *Gli3* is expressed in the dorsal neural tube, dorsal rhombencephalon, and dorsal mesencephalon. Where *Shh* expression terminates under the diencephalon, *Gli3* expression extends anteriorly to be expressed in the telencephalon, which is the

[18] Apposition means 'placing side by side; juxtaposition, or 'the placing of a word next to another... in order to qualify or explain the first' (O.E.D.). I refer to the expression of *Gli3* in *apposition* to *Shh* expression in the gramatical sense that *Gli3* appears to be used to *qualify or explain* Shh *expression* by acting as the mediator of Shh signal. Thus, in the grammar of developmental gene expression, *Gli3* is expressed in apposition to *Shh* expression to qualify or explain it.

most anterior neural structure. Thus, in the developing limb, spinal cord, and brain regions, *Gli3* expression remains in apposition to *Shh* expression.

Furthermore, *Gli3*'s primary function in the cell is probably to mediate Shh signalling and activate or repress the expression of downstream Shh-signalling targets. *Gli3*'s mode of action in the cell supports this hypothesis. Like its *Drosophila* homologue, Ci, Gli3 protein is found in two forms, a full-length version and a truncated version. Full-length Gli3 is found predominantly in the cytoplasm in a Cos-Fu-Su(Fu) complex. Full-length Gli3 is also found in small quantities in the nucleus where it is thought to activate transcription of (unknown) downstream targets (presumably amongst others, *Bmp*'s, the vertebrate homologue of *Drosophila decapentapalegic*, which is regulated by Ci). When Shh binds to the Patched cell surface receptor, *Gli3* is thought to be proteolysed into its truncated form which translocates to the nucleus to repress the transcription of downstream targets (Chapter I).

Data on this process is not complete, but the assumption that Gli3 mediates Shh signalling is well founded (for review see Koebernick and Pieler, 2002). Its bipotential function as both a repressor and activator of Shh signalling is seen to pattern the anterio-posterior axis in vertebrate limb bud (Wang et al., 2000; Zuniga and Zeller, 1999) and spinal cord (Altaba, 1998; Altaba, 1999), in response to Shh signalling. In the telencephalon, cells of the cortical hem, cortex, and early striatal regions, are proposed to be too far away from the nearest *Shh* expressing domain (the prechordal mesoderm under diencephalon) to be affected by *Shh* signalling. However, recent evidence suggests that *Shh* can have similar, long-range effects through the a modification of its cholesterols (Goetz et al., 2002; Zeng et al., 2001). This recent discovery suggests that in the telencephalon, like developing limb and spinal cord, *Gli3* may be mediating a Shh signalling patterning network, by interpreting extracellular Shh (with the Patched-Cos-Fu-Su(Fu) system) and activating or repressing downstream gene expression accordingly.

Mutations to *Gli3* may alter the balance of repressor and activator forms in the cell. Some studies have suggested that mutations to *Gli3* in different parts of the gene may promote one form over the other, or produce a functionally-null protein. A change in the balance of one form over the other, or simple haploinsufficiency, may lead to the distinct phenotypes observed man (PHS, GCPS, PAP-A, or PPD-IV) (Wessling et al., 2000a; Wessling et al., 2000b), and suggested ones in mouse (Xt^{H}, Xt^{Jed}, Xt^{Pdn}, Xt^{PHS}) (Bose et al., 2002).

The phenotypes described above may contribute to the evolution of form, if heterozygous mutation in *Gli3* is creating a *deconstrained* system that allows phenotypic variation to be expressed, then fixed when wild-type homozygosity is restored through subsequent matings. This suggestion is borrowed from work on the *Drosophila Heat shock protein 90* (*Hsp90*), where a mutation in *Hsp90* allows 'cryptic' genetic networks to express novel phenotypes that are then 'solidified', or maintained on reintroduction of wild-type homozygosity (Rutherford, 2000; Rutherford and Lindquist, 1998). *Gli3* mutations might act is a similar way, but with less dramatic effects than those observed by *Hsp90* mutation in fly. This hypothesis would help to explain the unusual transmission characteristics of the mutant allele, as this feature might have evolved to promote evolution (the evolution of evolvability).

However, a more likely hypothesis exists, and that is: the mutations that successfully pass through the sieve of survival are those that produce subtle (potentially unobserved) phenotypes that yield an competitive advantage^{-} to the organism. These mutations would probably occur in the introns of the gene, possibly to adjust levels of *Gli3* expression by altering the sequence of (presumptive) enhancer or silencer regions. If we consider that the known *Gli3* mutations are the ones that produce *observable* phenotypes, then there may be many other mutations that cause more subtle, unobserved phenotypes.

In this thesis, I have shown the morphological changes that occur to the skeletal system when one copy of the *Gli3* gene is mutated (in what is considered a functionally-null transcript). These phenotypic changes are brought about by

haploinsufficiency of the Gli3 protein, presumably because wild-type levels of Gli3 protein are reduced in the heterozygote *Gli3*-expressing tissues. Reduction of the normal wild-type level of protein present in the cell may alters that cell's mediation of Shh signalling, which results a change of regional interpretation of Shh signalling to produce the mutant phenotype.

Altered Patterning by Gli3 Mutation

The downstream targets of Gli3 repressor and activator forms are not known. *Ptc1* and *n-tubulin* expression are repressed by ectopic expression of artificially truncated *Gli3* (Altaba, 1999). Furthermore, *Ci* is known to affect the expression of *decapentapalegic* (*dpp*), the *Drosophila* homologue of vertebrate *Bmp*'s. However, the most interesting genes affected by *Gli3* mutation are the *Hox* gene clusters found in limb and spinal cord. It is adjustment to *Hox* gene cluster expression that is thought to affect morphological evolution. In the *Gli3* homozygous mouse mutant, *Xt/Xt*, *Hoxd13* expression is altered, and it is this alteration that is thought to induce the extranumerary digit phenotype (Moribe et al., 2000; Zuniga and Zeller, 1999).

If *Gli3* affects the expression profile of the *Hoxa* and *Hoxd* clusters, as indicated by their changed expression pattern in *Gli3*-mutant limb, then mutations to *Gli3* may alter their expression during the course to evolution to produce novel forms, probably by change to Shh responsiveness in the cell The expression profiles of the *Hox* clusters and *Gli3* correlate. In the limb, *Gli3* is expressed along a gradient from a high level (where most protein exists as the full-length activator form) in the anterior portion of limb bud, to a low level of expression at the posterior portion of limb bud (where a higher proportion of the truncated repressor protein is found). *Hoxa* and *Hoxd* gene cluster expression extends in a 'rainbow', which runs just distal of the ZPA and *Shh* expression domain (Figure 1.5). *Gli3* repression of *Hox* cluster expression is thought to pattern the digits (Moribe et al., 2000; Zuniga and Zeller, 1999).

In the anterior neural tube, regionalisation of the brain and spinal cord is dependent on *Hox* gene expression pattern, and the regional specification of the somitic segments depends on the expression of the paralogous *Hox* gene clusters. It is evident that homozygous *Gli3* mutation affects *Hox* gene expression in the limb, but it has yet to be shown whether this is also the case in the spinal cord. However, the correlation between *Gli3* expression and *Hox* gene expression, and the alteration of *Hox* gene expression by *Gli3* mutation in the limb, suggests that *Gli3* may be upstream of *Hox* expression to control its expression domains. Mutation to *Gli3* may therefore shift the expression patterns of the *Hox* genes to produce novel form.

Mechanism of Morphological Evolution by Mutating Gli3?

In this chapter, I have discussed the variation produced by mutation to *Gli3*, and suggested how this variation might produce advantageous phenotypes in the wild. I have further discussed the influence of background on variation and its ability to change phenotypic expression to yield different phenotypes. The interaction between genetic background, phenotypic expression, and evolution is not known, but these features may act with mutation to *Gli3* to produce novel phenotypes, some of which confer evolutionary success.

I have further touched on the evidence that *Gli3* is acting as a mediator of *Shh* signalling, and that mutations to *Gli3*, whether major mutations that produce noticeable phenotypes, or minor mutations that produce subtle phenotypes, may alter the mediation of *Shh* signalling to shift downstream gene expression patterns. This may, either directly or indirectly alter gene expression patterns of other patterning genes, such as the *Hox* gene clusters – known 'regulators' of evolutionary change.

I have also presented the epigenetic landscape model to help understand the role of probability in development, and to help visualise the phenotypic range presented on

mutation to *Gli3*. It is possible that some systems that *Gli3*-mutant phenotypes are more heavily canalised than others, and so do not display noticeable phenotypes in the heterozygote. The concept of canalisation is understood to reflect evolutionary potential (Møller and Swaddle, 1997), and implies those systems that express a *Gli3* heterozygote phenotype are more open to evolutionary change.

Finally, the phenomenon of *Gli3*(-) PTD (Chapter VI) might act as a rapid accelerator of morphological change in evolution by producing large numbers of variable *Gli3*-mutant mutant forms. Variation of form probably arises from the type of *Gli3*-mutation, in conjunction with genetic background, to sometimes produce a form that survives the sieve of competitive selection.

Concluding Remarks

In this thesis I have presented a number of data that reveal the effect of mutation to transcription factor Gli3. I have shown that this gene can affect multiple systems, the developing forebrain, craniofacial region, cervical vertebrae, and limbs. I have asked the question, 'how does the mutation affect forebrain development?', and have presented a series of experiments to suggest that disruption to programmed cell death or cell proliferation rates may be a causal factor in the dysmorphogenesis of forebrain. I have further referenced research by others to suggest that disruption to the signalling centres of the developing telencephalon may be the initial phenotype that then causes a decrease in programmed cell death or an increase in proliferation.

I continue my line of investigation by comparing the signalling centres in developing forebrain with those in the developing limb. I suggest that the two systems share similar properties and reference literature to compare the molecular expression of some *BMP*'s, *FGF*'s and *Wnt*'s to suggest that the two tissues are patterned by a similar patterning network. With this in mind, I examine the skeleton of the *Gli3*-mutant mice and comment on the patterning systems that seem to be going awry when one, or both copies of *Gli3* is mutated. I further observe some novel, subtle phenotypes of the heterozygote and suggest that some of these features might be advantageous in the wild. A later finding gives credibility to the thought that *Gli3* mutations may be an integral mechanism of evolutionary change: the mutant *Gli3* allele appears to transmit at twice its expected frequency, thereby suppressing proliferation of wild-type mice and increasing the number of heterozygotes.

I conclude my thesis with an overview of the changes to the morphology of the homozygous and heterozygous mutants. This is important because it discusses the range of phenotypic possibilities available to the genome in its wild-type and mutant states, when it is expressed in a normal uterine environment. Mutation to *Gli3*

increases the range of phenotypic possibilities in multiple systems. This is suggested by the variation observed in human and mouse *Gli3*-related polydactylys, and by the variation observed in the mutant skeletons.

The effect of genetic background on the expression of phenotypes is also quite remarkable, and I have suggested this is an important factor in the function of *Gli3* mutations on evolution. If background can increase the severity of a phenotype, as shown by an increase in the severity of polydactyly on outbred F1 mutants, then background can also decrease the severity of a phenotype until the phenotype is no longer noticeable, *i.e.* not a phenotype. This might be the case in the 'wild-type' females that produced the positive transmission distortion data. Probability weighs against this hypothesis, but it may still be true. If that's the case, then it's a matter of plain bad luck. Everything feasible in the time allowed has been done to ensure against it, but it may be true. Only a genotype analysis will tell us the truth. But I digress. Whether these animals exhibit PTD or simply do not express the mutant allele is not the point. The point is that genetic background, even within an inbred colony, is important in the expression of a phenotype. If we find that these six PTD-expressing mothers are wild-type, then it suggests recessivity is more common than thought. No other gene mutation has been found to cause isolate polydactylys in humans. The incidence of PAP and PPD may therefore be a direct measure of the incidence of *GLI3* mutations in the human population. This speculation is interesting because it suggest that the incidence of *Gli3* mutation in many species is quite high, a suggestion also proposed from its large genomic size and high incidence of mutation in mouse. *Gli3* mutation may persist, possibly as a function to allow morphological change in *Gli3* expressing systems - a mechanism of evolutionary development.

Gli3 is involved in the patterning of several different systems, all of which change in unison during evolution. Now I know that the entire body changes during evolution, and that all systems are intertwined, but it may be possible to dissect out evolutionary 'compartments'. The *Gli3-Shh* axis may be one such compartment. There is an obvious clue to suggest that this is so: the limbs of *Shh*(-/-)*Gli3*(-/-) mice

are normal, but polydactylous in an identical pattern to the *Gli3*(-/-) mice (Litingtung et al., 2002), and *Gli3*(-/-) limbs display a comparable digit pattern to that of *Acanthostega*, one of the first tetrapods (*ca.* 360 MYA) (Clack, 1989). Could it be that this early creature did not express *Gli3*, *i.e. Gli3* had not 'evolved'? Or was it that both *Shh* and *Gli3* had not evolved, or not evolved expression in the limb? I would suggest that *Shh* was present in the limb, and that *Gli3* was not far behind.

Let us look at what happens to the limb when one copy of the gene is mutated. The deltoid tuberosity morphology fails to form the wild-type notch-like characteristic. On mutation to one copy of *Gli3*, the deltoid tuberosity appears 'held back'; it does not extend forward distally. Likewise with the formation of an extra digit, it seems that the anterior-most border is 'held back' and as a result it trips and stumbles and two digits or two bones are formed where there should only be one. If we remove *Gli3* altogether, the system is held back fully and the deltoid tuberosity is formed most proximally and loses its ability to integrate with the shaft. The digits too are left unchecked and they proliferate to for a pattern that is more 'natural' to them, that is more *primitive*. *Gli3*, then, is a surge forward along the anterior rim of the limb. A half compliment of *Gli3* pushes the tuberosity onto the medial shaft, and quells the proliferation of digits, limiting their number to five or six, and in the process forming an unusual one, the thumb. A full compliment of *Gli3* settles the number at five and adds the finishing touch to the tuberosity.

In the brain, a similar effect can be seen. It is obvious in the homozygote mutant that tissue patterning has been left unchecked, but the patterning system of the brain is more complex than that of the limb. I have attempted to define the dysmorphology of the homozygote mutant brain as a result of signalling centre misexpression and consequential cell death and proliferation changes. The dysmorphology of the *Xt/Xt* may be comparable to the extranumerary digit formation in the limb. The developed murine cortex is divided into 'fingers' of functional specification that extend along the anterio-posterior axis. Thus, moving from the cortical hem laterally, the different fingers are crossed (Ragsdale and Grove, 2001). If, in the brain, the morphological features of bone and digit development in the limb have been replaced by functional

Figure 8.1 Macroevolution of tetrapods. Comparative skeletal anatomy of (a) *Acanthostega*, (b) *Xt/Xt* and (c) *+/+* forelimbs. Note that the *Acanthostega* ulna is hemimelic whereas in *Xt/Xt* the radius is hemimelic (arrowheads). Digit patterning is analysed more clearly in (b') and (c'). Note that digits III through V are comparable in *Acanthostega* and *Xt/Xt*; it is digits I and II that evolve into the modern pentadactyl pattern. *Acanthostega* and *Xt/Xt* show a similar arrangement of multiple digit I (arrows), composed of one less element than digits II through V. In *+/+* mouse, this has evolved to form a pollex (thumb) with no associated metacarpal. Recent work has shown that the double homozygous mutant *Shh*$^{-/-}$;*Gli3*$^{-/-}$ exhibits the same skeletal morphology and digit pattern as the *Gli3*$^{-/-}$ animal (Litingtung et al., 2002). Thus, *Shh* and *Gli3* may have evolved in concert in the limb to present modern pentadactyly.

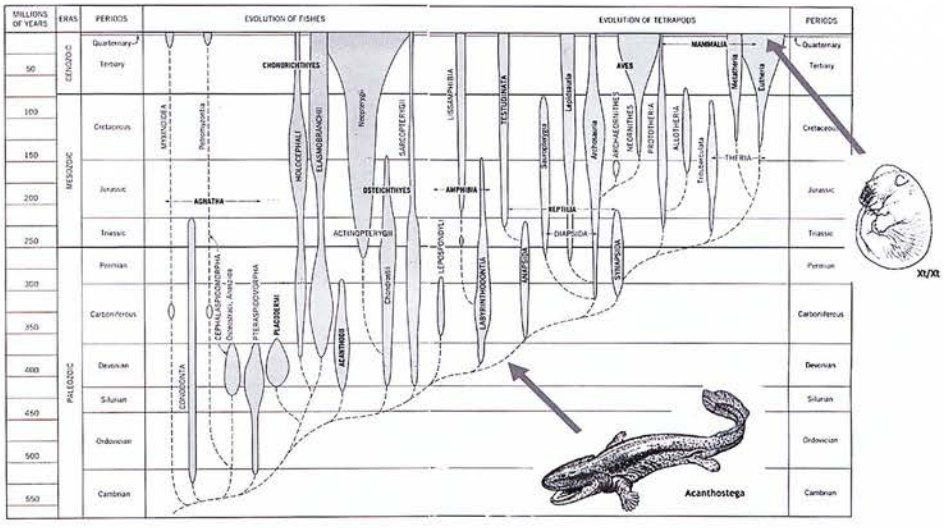
MILLIONS OF YEARS
ERAS
PERIODS
EVOLUTION OF FISHES
EVOLUTION OF TETRAPODS
PERIODS
CENOZOIC
MESOZOIC
PALEOZOIC
Quaternary
Tertiary
Cretaceous
Jurassic
Triassic
Permian
Carboniferous
Devonian
Silurian
Ordovician
Cambrian
MYXINOIDEA
Petromyzontia
CONODONTA
CEPHALASPIDOMORPHI
Osteostraci, Anaspida
PTERASPIDOMORPHIA
PLACODERMI
ACANTHODII
CHONDRICHTHYES
HOLOCEPHALI
ELASMOBRANCHII
Neopterygii
OSTEICHTHYES
ACTINOPTERYGII
SARCOPTERYGII
Dipnoi
LEPOSPONDYLI
LISSAMPHIBIA
AGNATHA
AMPHIBIA
LABYRINTHODONTIA
TESTUDINATA
ANAPSIDA
Squamata
Lacertilia
Archosauria
REPTILIA
DIAPSIDA
SYNAPSIDA
AVES
ARCHAEOCETHES
NEOCETHES
PROTOTHERIA
ALLOTHERIA
Triisodontia
THERIA
Metatheria
Eutheria
MAMMALIA
Acanthostega
X1/X1

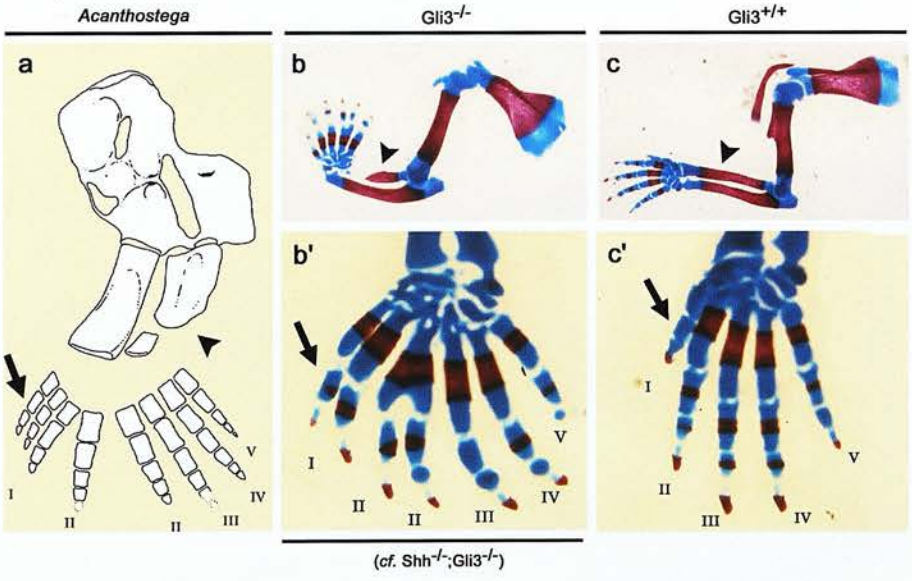
Acanthostega
Gli3-/-
Gli3+/+
a
b
c
b'
c'
I
II
II
III
IV
V
(cf. Shh-/-;Gli3-/-)

neural features, then the same patterning system may be used for both limb and brain, with different *Gli3*-output genes expressed for each tissue. I suspect this is an accurate generalisation, and that the role of *Gli3* in both limb and brain is the same (as it may be in the spinal cord too), and it is the output of the *Shh-Gli3* system that is changed between these tissues.

References

Agulnik, S. I., Agulnik, A. I. and Ruvinsky, A. O. (1990). Meiotic drive in female mice heterozygous for the HSR inserts on chromosome 1. *Genet Res* **55**, 97-100.

Altaba, A. R. I. (1998). Combinatorial Gli gene function in floor plate and neuronal inductions by sonic hedgehog. *Development* **125**, 2203-2212.

Altaba, A. R. I. (1999). Gli proteins encode context-dependent positive and negative functions: implications for development and disease. *Development* **126**, 3205-3216.

Apert, M. E. (1906). De l'acrocephalosyndactylie. *Bull. Mem. Soc. Med. Hop. Paris* **23**, 1310-1330.

Asavaritikrai, P. (2000). Regulation of Programmed Cell Death in the Developing Thalamus, pp. 189. Edinburgh: Edinburgh University.

Aza-Blanc, P. and Kornberg, T. B. (1999). Ci: a complex transducer of the hedgehog signal. *Trends Genet* **15**, 458-62.

Aza-Blanc, P., Lin, H. Y., Altaba, A. R. I. and Kornberg, T. B. (2000). Expression of the vertebrate Gli proteins in Drosophila reveals a distribution of activator and repressor activities. *Development* **127**, 4293-4301.

Baer, K. E. v. (1828). Entwicklungsgeschichte der Thiere: Beobachtung und Reflexion. Konigsberg: Bornträger.

Banker, G. and Goslin, K. (1998). Culturing Nerve Cells. Cambridge, Massachusetts: The MIT Press.

Biesecker, L. G., Topf, K. and Graham, J. M., Jr. (1994). Familial Pallister-Hall syndrome. *J Med Genet* **31**, 740.

Binder, L. I., Frankfurter, A. and Rebhun, L. I. (1985). The Distribution of Tau in the Mammalian Central Nervous-System. *Journal of Cell Biology* **101**, 1371-1378.

Blaschke, A. J., Staley, K. and Chun, J. (1996). Widespread programmed cell death in proliferative and postmitotic regions of the fetal cerebral cortex. *Development* **122**, 1165-1174.

Blaschke, A. J., Weiner, J. A. and Chun, J. (1998). Programmed cell death is a universal feature of embryonic and postnatal neuroproliferative regions throughout the central nervous system. *Journal of Comparative Neurology* **396**, 39-50.

Bose, J., Grotewold, L. and Ruther, U. (2002). Pallister-Hall syndrome phenotype in mice mutant for Gli3. *Human Molecular Genetics* **11**, 1129-1135.

Brueton, L. A., Chotai, K. A., van Herwerden, L., Schinzel, A. and Winter, R. M. (1992). The acrocallosal syndrome and Greig syndrome are not allelic disorders. *J Med Genet* **29**, 635-7.

Burdi, A. R. (1965). Toluidine Blue - Alizarin Red S staining of Cartilage and Bone in Whole-Mount Skeletons In Vitro. *Stain Technology* **40**, 45-48.

Capdevila, J. and Belmonte, J. C. I. (2001). Patterning mechanisms controlling vertebrate limb development. *Annual Review of Cell and Developmental Biology* **17**, 87-132.

Carlisle, A. (1814). An account of a family having hands and feet with supernumerary fingers and toes. *Phil. Trans. Roy. Soc.* **Part I**.

Castilla, E., Paz, J., Mutchinick, O., Munoz, E., Giorgiutti, E. and Gelman, Z. (1973). Polydactyly: a genetic study in South America. *Am J Hum Genet* **25**, 405-12.

Castilla, E. E., Lugarinho da Fonseca, R., da Graca Dutra, M., Bermejo, E., Cuevas, L. and Martinez-Frias, M. L. (1996). Epidemiological analysis of rare polydactylies. *Am J Med Genet* **65**, 295-303.

Castilla, E. E., Lugarinho, R., da Graca Dutra, M. and Salgado, L. J. (1998). Associated anomalies in individuals with polydactyly. *Am J Med Genet* **80**, 459-65.

Chenn, A. and McConnell, S. K. (1995). Cleavage Orientation and the Asymmetric Inheritance of Notch1 Immunoreactivity in Mammalian Neurogenesis. *Cell* **82**, 631-641.

Clack, J. A. (1989). Discovery of the earliest-known tetrapod stapes. *Nature* **342**, 425-7.

Clark, R. M., Marker, P. C. and Kingsley, D. M. (2000). A novel candidate gene for mouse and human preaxial polydactyly with altered expression in limbs of Hemimelic extra-toes mutant mice. *Genomics* **67**, 19-27.

Dai, P., Akimaru, H., Tanaka, Y., Maekawa, T., Nakafuku, M. and Ishii, S. (1999). Sonic hedgehog-induced activation of the Gli1 promoter is mediated by GLI3. *Journal of Biological Chemistry* **274**, 8143-8152.

de Villena, F. P. M. and Sapienza, C. (2001). Nonrandom segregation during meiosis: the unfairness of females. *Mammalian Genome* **12**, 331-339.

Feitosa, M. F., Castilla, E. E., da Graca Dutra, M. and Krieger, H. (1998). Lack of evidence of a major gene acting on postaxial polydactyly in South America. *Am J Med Genet* **80**, 466-72.

Finnigan, D. P., Clarren, S. K. and Haas, J. E. (1991). Extending the Pallister-Hall syndrome to include other central nervous system malformations. *Am J Med Genet* **40**, 395-400.

Fishell, G. (1995). Striatal precursors adopt cortical identities in response to local cues. *Development* **121**, 803-12.

Frazier, T. M. (1960). A note on race-specific congenital malformation rates. *Am. J. Obstet. Gynec.* **80**, 184-185.

Frederiksen, K. and McKay, R. D. G. (1988). Proliferation and Differentiation of Rat Neuroepithelial Precursor Cells Invivo. *Journal of Neuroscience* **8**, 1144-1151.

Freidel, L. S. a. D. (1992). The Forest of Kings: The Untold Story of the Ancient Maya: Quill.

Furuta, Y., Piston, D. W. and Hogan, B. L. (1997). Bone morphogenetic proteins (BMPs) as regulators of dorsal forebrain development. *Development* **124**, 2203-12.

Gaufo, G. O., Flodby, P. and Capecchi, M. R. (2000). Hoxb1 controls effectors of sonic hedgehog and Mash1 signaling pathways. *Development* **127**, 5343-54.

Goetz, J. A., Suber, L. M., Zeng, X. and Robbins, D. J. (2002). Sonic Hedgehog as a mediator of long-range signaling. *Bioessays* **24**, 157-65.

Graham, A., Francis-West, P., Brickell, P. and Lumsden, A. (1994). The signalling molecule BMP4 mediates apoptosis in the rhombencephalic neural crest. *Nature* **372**, 684-6.

Graham, A., Koentges, G. and Lumsden, A. (1996). Neural crest apoptosis and the establishment of craniofacial pattern: An Honorable death. *Molecular and Cellular Neuroscience* **8**, 76-83.

Green, E. L. (1954). Quantitative genetics of skeletal variations in the mouse. I. Crosses between three short-ear strains (P, NB, SEC/2). *J. Nat. Cancer Inst.* **15**, 609-624.

Greig, D. M. (1926). Oxycephaly. *Edinburgh Medical Journal* **33**, 189-218.

Gritli-Linde, A., Lewis, P., McMahon, A. P. and Linde, A. (2001). The whereabouts of a morphogen: direct evidence for short- and graded long-range activity of hedgehog signaling peptides. *Dev Biol* **236**, 364-86.

Grove, E. A., Tole, S., Limon, J., Yip, L. W. and Ragsdale, C. W. (1998). The hem of the embryonic cerebral cortex is defined by the expression of multiple Wnt genes and is compromised in Gli3- deficient mice. *Development* **125**, 2315-2325.

Grove, E. A., Tole, S., Yip, L., Limon, J. and Ragsdale, C. W. (1997). A role for Wnt genes in patterning the mouse telencephalon. *Developmental Biology* **186**, A95-A95.

Grüneberg, H. (1963). The Pathology of Development: a study of inherited skeletal disorders in animals. Oxford: Blackwell Scientific Publications.

Guo, X., Rueger, D. and Higgins, D. (1998). Osteogenic protein-1 and related bone morphogenetic proteins regulate dendritic growth and the expression of microtubule-associated protein-2 in rat sympathetic neurons. *Neuroscience Letters* **245**, 131-134.

Hall, J. G., Pallister, P. D., Clarren, S. K., Beckwith, J. B., Wiglesworth, F. W., Fraser, F. C., Cho, S., Benke, P. J. and Reed, S. D. (1980). Congenital hypothalamic hamartoblastoma, hypopituitarism, imperforate anus and postaxial polydactyly--a new syndrome? Part I: clinical, causal, and pathogenetic considerations. *Am J Med Genet* **7**, 47-74.

Haraguchi, R., Mo, R., Hui, C., Motoyama, J., Makino, S., Shiroishi, T., Gaffield, W. and Yamada, G. (2001). Unique functions of Sonic hedgehog signaling during external genitalia development. *Development* **128**, 4241-50.

Hardcastle, Z., Mo, R., Hui, C. C. and Sharpe, P. T. (1998). The Shh signalling pathway in tooth development: Defects in Gli2 and Gli3 mutants. *Development* **125**, 2803-2811.

Harrison, R. G. (1918). Experiments on the development of the forelimb of *Ambystoma*, a self-differentiating equipotential system. *Journal of Experimental Zoology* **25**, 413-461.

Hartfuss, E., Galli, R., Heins, N. and Gotz, M. (2001). Characterization of CNS precursor subtypes and radial glia. *Developmental Biology* **229**, 15-30.

Haydar, T. F., Kuan, C. Y., Flavell, R. A. and Rakic, P. (1999). The role of cell death in regulating the size and shape of the mammalian forebrain. *Cerebral Cortex* **9**, 621-626.

Hendriks, H. J., Brunner, H. G., Haagen, T. A. and Hamel, B. C. (1990). Acrocallosal syndrome. *Am J Med Genet* **35**, 443-6.

Hepker, J., Wang, Q. T., Motzny, C. K., Holmgren, R. and Orenic, T. V. (1997). Drosophila cubitus interruptus forms a negative feedback loop with patched and regulates expression of Hedgehog target genes. *Development* **124**, 549-58.

Houart, C., Westerfield, M. and Wilson, S. W. (1998). A small population of anterior cells patterns for forebrain during zebrafish gastrulation. *Nature* **391**, 788-792.

Hui, C. C. and Joyner, A. L. (1993). A Mouse Model of Greig Cephalopolysyndactyly Syndrome - the Extra-Toes(J) Mutation Contains an Intragenic Deletion of the Gli3 Gene. *Nature Genetics* **3**, 241-246.

Hui, C. C., Slusarski, D., Platt, K. A., Holmgren, R. and Joyner, A. L. (1994). Expression of three mouse homologs of the Drosophila segment polarity gene cubitus interruptus, Gli, Gli-2, and Gli-3, in ectoderm- and mesoderm-derived tissues suggests multiple roles during postimplantation development. *Dev Biol* **162**, 402-13.

Isaac, A., Rodriguez-Esteban, C., Ryan, A., Altabef, M., Tsukui, T., Patel, K., Tickle, C. and Izpisua-Belmonte, J. C. (1998). Tbx genes and limb identity in chick embryo development. *Development* **125**, 1867-75.

Jiang, X. B., Iseki, S., Maxson, R. E., Sucov, H. M. and Morriss-Kay, G. M. (2002). Tissue origins and interactions in the mammalian skull vault. *Developmental Biology* **241**, 106-116.

Johnson, D. R. (1967). Extra-Toes - a New Mutant Gene Causing Multiple Abnormalities in Mouse. *Journal of Embryology and Experimental Morphology* **17**, 543-&.

Kalff-Suske, M., Wild, A., Topp, J., Wessling, M., Jacobsen, E. M., Bornholdt, D., Engel, H., Heuer, H., Aalfs, C. M., Ausems, M. et al. (1999). Point mutations throughout the GLI3 gene cause Greig cephalopolysyndactyly syndrome. *Human Molecular Genetics* **8**, 1769-1777.

Kang, S., Allen, J., Graham, J. M., Jr., Grebe, T., Clericuzio, C., Patronas, N., Ondrey, F., Green, E., Schaffer, A., Abbott, M. et al. (1997a). Linkage mapping and phenotypic analysis of autosomal dominant Pallister-Hall syndrome. *J Med Genet* **34**, 441-6.

Kang, S., Graham, J. M., Olney, A. H. and Biesecker, L. G. (1997b). GLI3 frameshift mutations cause autosomal dominant Pallister- Hall syndrome. *Nature Genetics* **15**, 266-268.

Keino, H., Masaki, S., Kawarada, Y. and Naruse, I. (1994). Apoptotic degeneration in the arhinencephalic brain of the mouse mutant Pdn/Pdn. *Brain Res Dev Brain Res* **78**, 161-8.

Kinzler, K. W., Bigner, S. H., Bigner, D. D., Trent, J. M., Law, M. L., O'Brien, S. J., Wong, A. J. and Vogelstein, B. (1987). Identification of an amplified, highly expressed gene in a human glioma. *Science* **236**, 70-3.

Kinzler, K. W., Ruppert, J. M., Bigner, S. H. and Vogelstein, B. (1988). The GLI gene is a member of the Kruppel family of zinc finger proteins. *Nature* **332**, 371-4.

Koebernick, K. and Pieler, T. (2002). Gli-type zinc finger proteins as bipotential transducers of Hedgehog signaling. *Differentiation* **70**, 69-76.

Kucheria, K., Kenue, R. K. and Taneja, N. (1981). An Indian family with postaxial polydactyly in four generations. *Clin Genet* **20**, 36-9.

Kuller, J. A., Cox, V. A., Schonberg, S. A. and Golabi, M. (1992). Pallister-Hall syndrome associated with an unbalanced chromosome translocation. *Am J Med Genet* **43**, 647-50.

Lander, E. S. Linton, L. M. Birren, B. Nusbaum, C. Zody, M. C. Baldwin, J. Devon, K. Dewar, K. Doyle, M. FitzHugh, W. et al. (2001a). Initial sequencing and analysis of the human genome. *Nature* **409**, 860-921.

Lee, M. K., Tuttle, J. B., Rebhun, L. I., Cleveland, D. W. and Frankfurter, A. (1990). The Expression and Posttranslational Modification of a Neuron- Specific Beta-Tubulin Isotype During Chick Embryogenesis. *Cell Motility and the Cytoskeleton* **17**, 118-132.

Lewandoski, M., Sun, X. and Martin, G. R. (2000). Fgf8 signalling from the AER is essential for normal limb development. *Nature Genetics* **26**, 460-463.

Litingtung, Y., Dahn, R. D., Li, Y., Fallon, J. F. and Chiang, C. (2002). Shh and Gli3 are dispensable for limb skeleton formation but regulate digit number and identity. *Nature* **418**, 979-83.

Lotto, R. B. and Price, D. J. (1995). The stimulation of thalamic neurite outgrowth by cortex-derived growth factors in vitro - the influence of cortical age and activity. *European Journal of Neuroscience* **7**, 318-328.

Mahmood, R., Bresnick, J., Hornbruch, A., Mahony, C., Morton, N., Colquhoun, K., Martin, P., Lumsden, A., Dickson, C. and Mason, I. (1995). A role for FGF-8 in the initiation and maintenance of vertebrate limb bud outgrowth. *Curr Biol* **5**, 797-806.

Marazzi, G., Wang, Y. Q. and Sassoon, D. (1997). Msx2 is a transcriptional regulator in the BMP4-mediated programmed cell death pathway. *Developmental Biology* **186**, 127-138.

Maynard, T. M., Jain, M. D., Balmer, C. W. and LaMantia, A. S. (2002). High-resolution mapping of the Gli3 mutation Extra-toes(J) reveals a 51.5-kb deletion. *Mammalian Genome* **13**, 58-61.

MGD, J. L. (2002). Mouse Genome Database, Mouse Genome Informatics, vol. 2002 (ed. Bar Harbor: The Jackson Laboratory.

Mione, M. C., Danevic, C., Boardman, P., Harris, B. and Parnavelas, J. G. (1994). Lineage analysis reveals neurotransmitter (GABA or glutamate) but not calcium-binding protein homogeneity in clonally related cortical neurons. *J Neurosci* **14**, 107-23.

Misson, J. P., Edwards, M. A., Yamamoto, M. and Caviness, V. S. (1988). Identification of Radial Glial-Cells within the Developing Murine Central Nervous-System - Studies Based Upon a New Immunohistochemical Marker. *Developmental Brain Research* **44**, 95-108.

Møller, A. P. and Swaddle, J. P. (1997). Asymmetry, developmental stability, and evolution. Oxford ; New York: Oxford University Press.

Moon, A. M. and Capecchi, M. R. (2000). Fgf8 is required for outgrowth and patterning of the limbs. *Nature Genetics* **26**, 455-459.

Moribe, H., Takagi, T., Kondoh, H. and Higashi, Y. (2000). Suppression of polydactyly of the Gli3 mutant (extra toes) by delta EF1 homozygous mutation. *Development Growth & Differentiation* **42**, 367-376.

Motzny, C. K. and Holmgren, R. (1995). The Drosophila cubitus interruptus protein and its role in the wingless and hedgehog signal transduction pathways. *Mech Dev* **52**, 137-50.

Nelson, C. E., Morgan, B. A., Burke, A. C., Laufer, E., DiMambro, E., Murtaugh, L. C., Gonzales, E., Tessarollo, L., Parada, L. F. and Tabin, C. (1996). Analysis of Hox gene expression in the chick limb bud. *Development* **122**, 1449-66.

Norwell, S. a. (1894). Hereditary malformations of hands and feet. *British Medical Journal* **II**.

Nylander. (1904). Bidrag til laaran om aarftlig polyactyli. *Hygiea.*

Ogino, Y., Suzuki, K., Haraguchi, R., Satoh, Y., Dolle, P. and Yamada, G. (2001). External genitalia formation: role of fibroblast growth factor, retinoic acid signaling, and distal urethral epithelium. *Ann N Y Acad Sci* **948**, 13-31.

Ohuchi, H., Nakagawa, T., Yamamoto, A., Araga, A., Ohata, T., Ishimaru, Y., Yoshioka, H., Kuwana, T., Nohno, T., Yamasaki, M. et al. (1997). The mesenchymal factor, FGF10, initiates and maintains the outgrowth of the chick limb bud through interaction with FGF8, an apical ectodermal factor. *Development* **124**, 2235-2244.

Oldridge, M., Zackai, E. H., McDonald-McGinn, D. M., Iseki, S., Morriss-Kay, G. M., Twigg, S. R., Johnson, D., Wall, S. A., Jiang, W., Theda, C. et al. (1999). De novo alu-element insertions in FGFR2 identify a distinct pathological basis for Apert syndrome. *Am J Hum Genet* **64**, 446-61.

Papasozomenos, S. C., Binder, L. I., Bender, P. K. and Payne, M. R. (1985). Microtubule-Associated Protein-2 within Axons of Spinal Motor Neurons - Associations with Microtubules and Neurofilaments in Normal and Beta,Beta'-Iminodipropionitrile-Treated Axons. *Journal of Cell Biology* **100**, 74-85.

Park, W. J., Theda, C., Maestri, N. E., Meyers, G. A., Fryburg, J. S., Dufresne, C., Cohen, M. M., Jr. and Jabs, E. W. (1995). Analysis of phenotypic features and FGFR2 mutations in Apert syndrome. *Am J Hum Genet* **57**, 321-8.

Patton, J. T. and Kaufman, M. H. (1995). The timing of ossification of the limb bones, and growth rates of various long bones of the fore and hind limbs of the prenatal and early postnatal laboratory mouse. *J Anat* **186 (Pt 1)**, 175-85.

Penman Splitt, M., Wright, C., Perry, R. and Burn, J. (1994). Autosomal dominant transmission of Pallister-Hall syndrome. *Clin Dysmorphol* **3**, 301-8.

Price, D. J. and Willshaw, D. J. (2000). Mechanisms of Cortical Development. Oxford: Oxford University Press.

Radhakrishna, U., Bornholdt, D., Scott, H. S., Patel, U. C., Rossier, C., Engel, H., Bottani, A., Chandal, D., Blouin, J. L., Solanki, J. V. et al. (1999b). The phenotypic spectrum of GLI3 morphopathies includes autosomal dominant preaxial polydactyly type-IV and postaxial polydactyly type-A/B; No phenotype prediction from the position of GLI3 mutations. *American Journal of Human Genetics* **65**, 645-655.

Radhakrishna, U., Wild, A., Grzeschik, K. H. and Antonarakis, S. E. (1997b). Mutation in GLI3 in postaxial polydactyly type A. *Nature Genetics* **17**, 269-271.

Ragsdale, C. W. and Grove, E. A. (2001). Patterning the mammalian cerebral cortex. *Current Opinion in Neurobiology* **11**, 50-58.

Ruppert, J. M., Kinzler, K. W., Wong, A. J., Bigner, S. H., Kao, F. T., Law, M. L., Seuanez, H. N., O'Brien, S. J. and Vogelstein, B. (1988). The GLI-Kruppel family of human genes. *Mol Cell Biol* **8**, 3104-13.

Ruppert, J. M., Vogelstein, B., Arheden, K. and Kinzler, K. W. (1990). GLI3 encodes a 190-kilodalton protein with multiple regions of GLI similarity. *Mol Cell Biol* **10**, 5408-15.

Rutherford, S. L. (2000). From genotype to phenotype: buffering mechanisms and the storage of genetic information. *Bioessays* **22**, 1095-105.

Rutherford, S. L. and Lindquist, S. (1998). Hsp90 as a capacitor for morphological evolution. *Nature* **396**, 336-42.

Ruvinsky, A. (1995). Meiotic drive in female mice: an essay. *Mamm Genome* **6**, 315-20.

Sanz-Ezquerro, J. J. and Tickle, C. (2001). "Fingering" the vertebrate limb. *Differentiation* **69**, 91-99.

Sasaki, H., Nishizaki, Y., Hui, C. C., Nakafuku, M. and Kondoh, H. (1999). Regulation of Gli2 and Gli3 activities by an amino-terminal repression domain: implication of Gli2 and Gli3 as primary mediators of Shh signaling. *Development* **126**, 3915-3924.

Sato, Y., Hirata, T., Ogawa, M. and Fujisawa, H. (1998). Requirement for early-generated neurons recognized by monoclonal antibody Lot1 in the formation of lateral olfactory tract. *Journal of Neuroscience* **18**, 7800-7810.

Saunders, J. J. W. (1948). The proximal-distal sequence of origin of the parts of the chick wing and the role of the ectoderm. *Journal of Experimental Zoology* **108**, 363-404.

Schimenti, J. (2000). Segregation distortion of mouse t haplotypes the molecular basis emerges. *Trends Genet* **16**, 240-3.

Schimmang, T., Lemaistre, M., Vortkamp, A. and Ruther, U. (1992). Expression of the Zinc Finger Gene Gli3 Is Affected in the Morphogenetic Mouse Mutant Extra-Toes (Xt). *Development* **116**, 799-804.

Schinzel, A. and Kaufmann, U. (1986). The acrocallosal syndrome in sisters. *Clin Genet* **30**, 399-405.

Schinzel, A. and Schmid, W. (1980). Hallux duplication, postaxial polydactyly, absence of the corpus callosum, severe mental retardation, and additional anomalies in two unrelated patients: a new syndrome. *Am J Med Genet* **6**, 241-9.

Schneider, R. A., Hu, D. and Helms, J. A. (1999). From head to toe: conservation of molecular signals regulating limb and craniofacial morphogenesis. *Cell and Tissue Research* **296**, 103-109.

Scott-Emuakpor, A. B. and Madueke, E. D. (1976). The study of genetic variation in Nigeria. II. The genetics of polydactyly. *Human Heredity* **26**, 198-202.

Shimamura, K. and Rubenstein, J. L. R. (1997). Inductive interactions direct early regionalization of the mouse forebrain. *Development* **124**, 2709-2718.

Shin, S. H., Kogerman, P., Lindstrom, E., Toftgard, R. and Biesecker, L. G. (1999). GLI3 mutations in human disorders mimic Drosophila Cubitus interruptus protein functions and localization. *Proceedings of the National Academy of Sciences of the United States of America* **96**, 2880-2884.

Sills, I. N., Rapaport, R. and Desposito, F. (1994a). Familial Pallister-Hall syndrome. *J Pediatr* **125**, 170-1.

Sills, I. N., Rapaport, R., Desposito, F. and Lieber, C. (1994b). Familial Pallister-Hall syndrome: three affected offspring. *Am J Med Genet* **52**, 251.

Sills, I. N., Rapaport, R., Robinson, L. P., Lieber, C., Shih, L. Y., Horlick, M. N., Schwartz, M. and Desposito, F. (1993). Familial Pallister-Hall syndrome: case report and hormonal evaluation. *Am J Med Genet* **47**, 321-5.

Silver, L. M. (1985). Mouse t haplotypes. *Annu Rev Genet* **19**, 179-208.

Silver, L. M. (1993). The peculiar journey of a selfish chromosome: mouse t haplotypes and meiotic drive. *Trends Genet* **9**, 250-4.

Slaney, S. F., Oldridge, M., Hurst, J. A., Moriss-Kay, G. M., Hall, C. M., Poole, M. D. and Wilkie, A. O. (1996). Differential effects of FGFR2 mutations on syndactyly and cleft palate in Apert syndrome. *Am J Hum Genet* **58**, 923-32.

Sobetzko, D., Eich, G., Kalff-Suske, M., Grzeschik, K. H. and Superti-Furga, A. (2000). Boy with syndactylies, macrocephaly, and severe skeletal dysplasia: Not a new syndrome, but two dominant mutations (GLI3 E543X and COL2A1 G973R) in the same individual. *American Journal of Medical Genetics* **90**, 239-242.

Song, Q. B., Mehler, M. F. and Kessler, J. A. (1998). Bone morphogenetic proteins induce apoptosis and growth factor dependence of cultured sympathoadrenal progenitor cells. *Developmental Biology* **196**, 119-127.

Sun, X., Mariani, F. V. and Martin, G. R. (2002). Functions of FGF signalling from the apical ectodermal ridge in limb development. *Nature* **418**, 501-508.

Sverdrup, A. (1922). Postaxial polydactylism in six generations of a Norwegian family. *J. Genet.* **12**, 217-240.

Tan, S. S., Kalloniatis, M., Sturm, K., Tam, P. P., Reese, B. E. and Faulkner-Jones, B. (1998). Separate progenitors for radial and tangential cell dispersion during development of the cerebral neocortex. *Neuron* **21**, 295-304.

Temtamy, S. A. and McKusick, V. A. (1978). The genetics of hand malformations. New York: Liss.

Theil, T., Alvarez-Bolado, G., Walter, A. and Ruther, U. (1999). Gli3 is required for Emx gene expression during dorsal telencephalon development. *Development* **126**, 3561-3571.

Thien, H., Buscher, D. and Ruther, U. (1996). Cloning and sequence analysis of the murine Gli3 cDNA. *Biochimica Et Biophysica Acta-Gene Structure and Expression* **1307**, 267-269.

Thomas, H. M., Todd, P. J., Heaf, D. and Fryer, A. E. (1994). Recurrence of Pallister-Hall syndrome in two sibs. *J Med Genet* **31**, 145-7.

Tole, S., Ragsdale, C. W. and Grove, E. A. (2000). Dorsoventral patterning of the telencephalon is disrupted in the mouse mutant extra-toes(J). *Dev Biol* **217**, 254-65.

Tomioka, N., Osumi, N., Sato, Y., Inoue, T., Nakamura, S., Fujisawa, H. and Hirata, T. (2000). Neocortical origin and tangential migration of guidepost neurons in the lateral olfactory tract. *Journal of Neuroscience* **20**, 5802-5812.

Trousse, F., Esteve, P. and Bovolenta, P. (2001). BMP4 mediates apoptotic cell death in the developing chick eye. *Journal of Neuroscience* **21**, 1292-1301.

Ventruto, V., Theo, G., Celona, A., Fioretti, G., Pagano, L., Stabile, M. and Cavaliere, M. L. (1980). A and B postaxial polydactyly in two members of the same family. *Clin Genet* **18**, 342-7.

Verloes, A., David, A., Ngo, L. and Bottani, A. (1995a). Stringent delineation of Pallister-Hall syndrome in two long surviving patients: importance of radiological anomalies of the hands. *J Med Genet* **32**, 605-11.

Verloes, A., Narcy, F. and Fallet-Bianco, C. (1995b). Syndromal hypothalamic hamartoblastoma with holoprosencephaly sequence, microphthalmia, pulmonary malformations, radial hypoplasia and mullerian regression: further delineation of a new syndrome? *Clin Dysmorphol* **4**, 33-7.

Vogel, A., Rodriguez, C. and Izpisua-Belmonte, J. C. (1996). Involvement of FGF-8 in initiation, outgrowth and patterning of the vertebrate limb. *Development* **122**, 1737-50.

Vortkamp, A., Franz, T., Gessler, M. and Grzeschik, K. H. (1992). Deletion of Gli3 Supports the Homology of the Human Greig Cephalopolysyndactyly Syndrome (Gcps) and the Mouse Mutant Extra Toes (Xt). *Mammalian Genome* **3**, 461-463.

Vortkamp, A., Gessler, M. and Grzeschik, K. H. (1991). Gli3 Zinc-Finger Gene Interrupted by Translocations in Greig Syndrome Families. *Nature* **352**, 539-540.

Waddington, C. H. (1939). An introduction to modern genetics. London: G. Allen & Unwin ltd.

Wang, B. L., Fallon, J. F. and Beachy, P. A. (2000). Hedgehog-regulated processing of Gli3 produces an anterior/posterior repressor gradient in the developing vertebrate limb. *Cell* **100**, 423-434.

Ware, M. L., Tavazoie, S. F., Reid, C. B. and Walsh, C. A. (1999). Coexistence of widespread clones and large radial clones in early embryonic ferret cortex. *Cereb Cortex* **9**, 636-45.

Wassersug, R. J. (1976). A procedure for differential staining of cartilage and bone in whole formalin-fixed vertebrates. *Stain Technology* **51**, 131-134.

Welscher, P. T., Fernandez-Teran, M., Ros, M. A. and Zeller, R. (2002). Mutual genetic antagonism involving GLI3 and dHAND prepatterns the vertebrate limb bud mesenchyme prior to SHH signaling. *Genes & Development* **16**, 421-426.

Wessling, M., Kalff-Suske, M., Bornholdt, D., Engel, H. and Grzeschik, K. H. (2000a). Functional consequences of GLI3 mutations in human developmental disorders. *Developmental Dynamics* **219**, P31.

Wessling, M., Kalff-Suske, M., Bornholdt, D., Engel, H. and Grzeschik, K. H. (2000b). Functional implications of GLI3 mutations detected in human polydactylies GLI3. *American Journal of Human Genetics* **67**, 2148.

Wild, A., KalffSuske, W., Vortkamp, A., Bornholdt, D. and Grzeschik, K. H. (1997). Point mutations in human GLI3 cause Greig syndrome. *Human Molecular Genetics* **6**, 1979-1984.

Wilkie, A. O., Slaney, S. F., Oldridge, M., Poole, M. D., Ashworth, G. J., Hockley, A. D., Hayward, R. D., David, D. J., Pulleyn, L. J., Rutland, P. et al. (1995). Apert syndrome results from localized mutations of FGFR2 and is allelic with Crouzon syndrome. *Nat Genet* **9**, 165-72.

Williams, P. G., Hersh, J. H., Yen, F. F., Barch, M. J., Kleinert, H. E., Kunz, J. and Kalff-Suske, M. (1997). Greig cephalopolysyndactyly syndrome: altered phenotype of a microdeletion syndrome due to the presence of a cytogenetic abnormality. *Clinical Genetics* **52**, 436-441.

Withers, G. S., Higgins, D., Charette, M. and Banker, G. (2000). Bone morphogenetic protein-7 enhances dendritic growth and receptivity to innervation in cultured hippocampal neurons. *European Journal of Neuroscience* **12**, 106-116.

Woolf, C. M. and Myrianthopoulos, N. C. (1973). Polydactyly in American negroes and whites. *Am J Hum Genet* **25**, 397-404.

Zakany, J., Fromental_Ramain, C., Warot, X. and Duboule, D. (1997). Regulation of number and size of digits by posterior Hox genes: a dose-dependent mechanism with potential evolutionary implications. *Proceedings of the National Academy of Sciences of the United States of America* **94**, 13695-700.

Zeng, X., Goetz, J. A., Suber, L. M., Scott, W. J., Schreiner, C. M. and Robbins, D. J. (2001). A freely diffusible form of Sonic hedgehog mediates long-range signalling. *Nature* **411**, 716-720.

Zuniga, A. and Zeller, R. (1999). Gli3 (Xt) and formin (Id) participate in the positioning of the polarising region and control of posterior limb-bud identity. *Development* **126**, 13-21.

Zuniga, M. B. A., Haramis, A. G. and Zeller, R. (1997). Genetic interaction of Ld and Gli3: Positive and negative regulation controls posterior identities and patterning of the vertebrate limb. *Developmental Biology* **186**, S30-S30.

Appendix A: Culture Reagents

.

Culture Medium

Mix together in a sterile beaker:

Component	Sigma Cat No.	(Final conc.)
100ml F12 (Hams)*	N4888	
100ml Delbeco's modified Eagles' medium (DMEM) *	D5671	
1mg insulin	I6634	(5µg/ml)
2mg apo-transferrin**	T1147	(10µg/ml)
3ml HEPES buffer	H0887	
0.24g Na_2HCO_3	S5761	(0.12g/ml)
3ml antibiotics (Gentamycin + Kanamycin)* **	G1264 + K1377	
2ml putrescene****	P5780	(16.11µg/ml)
20µl progesterone****	P8783	(6.29ng/ml)
20µl Na_2SeO_3****	S5261	(5.2ng/ml)
2ml $_L$-glutamine****	G2128	(25µg/ml)

Notes

* DMEM-F12 components in water:

Inorganic Salts	**(g/liter)**
CaCl2 (anhydrous)	0.11665
CuSO4 (anhydrous)	0.0000008
Fe(NO3)3·9H2O	0.00005
FeSO4·7H2O	0.000417
MgSO4(anhydrous)	0.08495
KCl	0.31180
NaHCO3	1.20000
NaCl	7.00000
Na2HPO4 (anhydrous)	0.07100
NaH2PO4·H2O	0.06250
ZnSO4·7H2O	0.000432

Amino Acids	**(g/liter)**
L-Alanine	0.00445
L-Arginine·HCl	0.14750
L-Asparagine·H2O	0.00750
L-Aspartic Acid	0.00665
L-Cysteine·HCl·H2O	0.01756
L-Cystine·2HCl	0.03129
L-Glutamic Acid	0.00735
L-Glutamine	0.36510
Glycine	0.01875
L-Histidine·HCl·H2O	0.03148
L-Isoleucine	0.05437
L-Leucine	0.05895
L-Lysine·HCl	0.09135
L-Methionine	0.01724
L-Phenylalanine	0.03548
L-Proline	0.01725
L-Serine	0.02625
L-Threonine	0.05355
L-Tryptophan	0.00902
L-Tyrosine·2Na·2H2O	0.05582
L-Valine	0.05285

Vitamins	**(g/liter)**
D-Biotin	0.00000365
Choline Chloride	0.00898
Folic Acid	0.00265
myo-Inositol	0.01261
Nicotinamide	0.00202
D-Pantothenic Acid	0.00224
Pyridoxine·HCl	0.00203
Riboflavin	0.00022
Thiamine·HCl	0.00217
Vitamin B-12	0.00068

Other	**(g/liter)**
D-Glucose	3.15100
HEPES	3.57480
Hypoxanthine	0.00239
Methyl Linoleate	0.000044
Phenol Red, Sodium Salt	0.00810
Putrescine·2HCl	0.00008
Sodium Pyruvate	0.05500
DL-Thioctic Acid	0.000105
Thymidine	0.000365

** ***Transferrin*** is a beta glycoprotein (iron transport protein in the blood). It transports iron to (and possibly within the cell) in culture. It may also have a detoxifying role.

*** ***Antibiotics*** Gentamycin sulphate (100mg)
Kanamycin sulphate (200mg)
Make up to 20ml with double distilled water (sterile), then filter sterilise. Store in 1ml aliquots at –20°C.

**** ***Supplements***

1) 100μM putrescene (161.1mg/100ml in sterile double distilled water, filter sterilise. Store in 4ml aliqouts at –70°C. Putrecene is the decarboxylated product of the amino acid ornithine. It is needed as a precursor for the synthesis of polyamines which are involved in cell growth and proliferation.

2) 20μM progesterone (6.29mg/100ml in ethanol). Store in 1ml and then 50μl aliquots at –70°C

3) 30μM Na_2SeO_3 (5.2mg/100ml in sterile double distilled water, filter sterilise). Store in 1ml and then 50μl aliqouts at –70°C. Selenium is a co-factor of glutathione peroxidase which is located in the cytosol and catalyses the reduction of radicals by the antioxidant glutathione.

4) 0.2M $_L$-glutamine (6.344g/100ml in sterile double distilled water, filter sterilise). Store in 2ml aliqouts at 50μl at –70°C. $_L$-glutamine is a non-essential amino acid which is an important precursor for nucleotide and structural protein synthesis. It is required of $_L$-glutamate and GABA synthesis. At high concentrations is may have neurotoxic side effects.

Appendix B: Primary Culture Density and Viability

Table 1. E16.5 Cell Density and Cell Viability Data.

Day 1

pheno	plating density	no.cells counted	no. of fields	mean cells/field	*S.E.M.*	mean % viable	*S.E.M.*
+/+	1000	3114	23	135	*6.89*	34.1	*2.18*
Xt/+	1000	3358	23	146	*4.93*	45.1	*2.00*
Xt/Xt	1000	3515	23	153	*13.4*	61.6	*2.63*
+/+	2000	6135	25	245	*12.0*	45.5	*3.37*
Xt/+	2000	5318	23	231	*11.5*	61.0	*3.92*
Xt/Xt	2000	5621	21	268	*10.5*	73.4	*1.51*

Day 2

pheno	plating density	total no.cells	no. of fields	mean cells/field	*S.E.M.*	mean % viable	*S.E.M.*
+/+	1000	2049	17	120	*6.85*	1.00	*.445*
Xt/+	1000	2221	17	131	*7.28*	1.90	*1.00*
Xt/Xt	1000	2474	17	146	*11.0*	35.0	*2.60*
+/+	2000	3360	16	210	*8.35*	3.45	*2.77*
Xt/+	2000	3746	16	234	*12.1*	2.45	*1.39*
Xt/Xt	2000	4940	17	291	*16.7*	54.7	*2.70*

Day3

pheno	plating density	total no.cells	no. of fields	mean cells/field	*S.E.M.*	mean % viable	*S.E.M.*
+/+	1000	-	-	-	-	0	*0*
Xt/+	1000	-	-	-	-	0	*0*
Xt/Xt	1000	-	-	-	-	0	*0*
+/+	2000	1925	8	241	*10.3*	1.64	*0.39*
Xt/+	2000	2415	8	302	*19.1*	3.43	*0.43*
Xt/Xt	2000	3608	16	225	*18.2*	18.73	*2.63*

Table 2. *E15.5 Cell density and Cell Viability Data.*

Day 1

pheno	plating density	total no.cells	no. of fields	mean cells/field	*S.E.M.*	mean % viable	*S.E.M.*
+/+	1000	3021	25	121	*6.41*	54.3	*3.63*
Xt/+	1000	5483	45	122	*5.84*	62.3	*2.58*
Xt/Xt	1000	5726	45	127	*8.33*	79.8	*2.49*
+/+	2000	5648	22	257	*12.6*	71.7	*3.47*
Xt/+	2000	10900	43	253	*10.9*	76.2	*4.01*
Xt/Xt	2000	9264	40	231	*10.4*	82.9	*3.25*

Day 2

pheno	plating density	total no.cells	no. of fields	mean cells/field	*S.E.M.*	mean % viable	*S.E.M.*
+/+	1000	1751	13	135	*19.4*	20.5	*11.1*
Xt/+	1000	3289	33	103	*11.2*	22.4	*8.51*
Xt/Xt	1000	4120	33	125	*9.50*	60.4	*8.17*
+/+	2000	3492	17	205	*17.6*	26.7	*12.0*
Xt/+	2000	7192	32	225	*10.9*	39.9	*6.84*
Xt/Xt	2000	10034	40	251	*8.17*	70.9	*5.31*

Day 3

pheno	plating density	total no.cells	no. of fields	mean cells/field	*S.E.M.*	mean % viable	*S.E.M.*
+/+	1000	-	-	-	-	0	*0*
Xt/+	1000	-	-	-	-	0	*0*
Xt/Xt	1000	-	-	-	-	0	*0*
+/+	2000	-	-	-	-	0	*0*
Xt/+	2000	-	-	-	-	0	*0*
Xt/Xt	2000	6064	39	232.4	*10.4*	44.5	*4.56*

Table 3. *E14.5 Cell Density and Viabillity Data.*

Day 1

pheno	plating density	total no.cells	no. of fields	mean cells/field	*S.E.M.*	mean % viable	*S.E.M.*
+/+ Ctx	1000	4535	42	108	*2.89*	54.1	*2.21*
Xt/Xt Ctx	1000	3676	36	102	*4.90*	63.3	*2.66*
+/+ Str	1000	4828	41	118	*6.56*	55.3	*2.81*
+/+ StrCtx	1000	2577	20	129	*8.81*	61.0	*4.29*
Xt/Xt Str	1000	611	6	102	*5.71*	76.3	*3.33*
+/+ Ctx	2000	9213	45	205	*8.03*	72.1	*1.51*
Xt/Xt Ctx	2000	10778	51	211	*6.92*	76.5	*1.02*
+/+ Str	2000	10156	46	221	*9.55*	69.1	*1.64*
+/+ StrCtx	2000	5342	27	198	*14.5*	72.2	*2.06*
Xt/Xt Str	2000	2102	9	234	*13.8*	81.3	*1.06*

Day 2

pheno	plating density	total no.cells	no. of fields	mean cells/field	*S.E.M.*	mean % viable	*S.E.M.*
+/+ Ctx	1000	2134	18	119	*11.1*	36.4	*9.05*
Xt/Xt Ctx	1000	2900	26	112	*8.87*	48.1	*6.58*
+/+ Str	1000	2004	18	111	*9.46*	39.8	*3.60*
+/+ StrCtx	1000	776	10	78	*3.88*	26.6	*3.81*
Xt/Xt Str	1000	1121	8	140	*7.05*	63.0	*4.12*
+/+ Ctx	2000	10662	48	222	*8.47*	55.0	*2.95*
Xt/Xt Ctx	2000	11872	51	233	*8.65*	63.1	*1.27*
+/+ Str	2000	11311	46	246	*14.2*	50.4	*3.33*
+/+ StrCtx	2000	6082	28	217	*14.8*	53.9	*2.65*
Xt/Xt Str	2000	1410	6	235	*20.9*	69.4	*1.21*

Day 3

pheno	plating density	total no.cells	no. of fields	mean cells/field	*S.E.M.*	mean % viable	*S.E.M.*
+/+ Ctx	1000	1286	9	143	*10.8*	9.06	*1.75*
Xt/Xt Ctx	1000	2111	19	111	*8.75*	25.0	*2.96*
+/+ Str	1000	987	9	110	*6.20*	17.0	*1.38*
+/+ StrCtx	1000	-	-	-	-	-	-
Xt/Xt Str	1000	864	8	108	*9.68*	45.5	*2.36*
+/+ Ctx	2000	6536	29	225	*13.7*	41.2	*3.32*
Xt/Xt Ctx	2000	10189	44	232	*10.0*	48.4	*1.90*
+/+ Str	2000	6279	29	217	*13.5*	30.1	*3.57*
+/+ StrCtx	2000	4154	19	219	*16.7*	44.4	*3.41*
Xt/Xt Str	2000	2125	9	236	*14.6*	49.5	*2.87*

Day 4

pheno	plating density	total no.cells	no. of fields	mean cells/field	*S.E.M.*	mean % viable	*S.E.M.*
+/+ Ctx	1000	-	-	-	-	-	-
Xt/Xt Ctx	1000	-	-	-	-	-	-
+/+ Str	1000	-	-	-	-	-	-
+/+ StrCtx	1000	-	-	-	-	-	-
Xt/Xt Str	1000	-	-	-	-	-	-
+/+ Ctx	2000	6168	22	280	*24.7*	20.8	*10.1*
Xt/Xt Ctx	2000	6837	29	236	*14.7*	33.6	*3.29*
+/+ Str	2000	1601	9	178	*29.2*	20.5	*8.34*
+/+ StrCtx	2000	5448	24	227	*19.1*	13.8	*6.83*
Xt/Xt Str	2000	2104	8	263	*23.3*	12.2	*3.12*

Appendix C: *Xt/+* x *Xt/+* Litter Segregations

Xt x Xt Litter Embryo Data

Criteria: 1. Only reliable data to be used - if in doubt then count it out.
2. Only litters larger than 6 embryos used.
3. Only litters >E15.0 used

date	e day	no. in litter	xt/xt	het	wt/wt
07/10/99	16.5	9	1	7	1
07/10/99	16.5	8	1	5	2
29/10/99	18.5	9	3	5	1
29/10/99	16.5	8	1	6	1
29/10/99	15.5	7	1	5	1
21/01/00	15.5	10	4	4	2
08/09/00	16.5	7	2	2	3
08/10/00	18.5	8	5	1	2
26/10/00	20.0	8	3	4	1
26/10/00	18.5	8	1	6	1
26/10/00	19.5	8	3	3	2
20/11/00	16.5	9	2	6	1
22/11/00	15.5	8	3	5	0
11/12/00	16.5	8	3	3	2
11/12/00	20.0	10	1	4	5
25/01/01	20.0	11	4	6	1
02/02/01	20.0	5	2	2	1
22/02/01	15.5	9	2	4	3
24/02/01	15.5	15	2	12	1
28/02/01	15.5	12	2	7	3
28/02/01	15.5	9	2	5	2
08/03/01	20.0	7	0	4	3
18/03/01	15.5	8	3	4	1
18/03/01	16.0	10	5	3	2
05/05/01	15.5	9	2	3	4
06/08/01	15.5	10	2	6	2
06/08/01	15.5	10	1	8	1
06/08/01	19.5	9	2	7	0
06/08/01	16.5	10	3	7	0
17/08/01	16.5	7	0	6	1
31/08/01	15.0	8	2	3	3
31/08/01	17.5	8	1	4	3
08/11/01	15.0	8	4	2	2
08/11/01	16.5	8	1	7	0
19/11/01	15.5	9	1	3	5
07/01/02	20.0	13	4	6	3
22/01/02	15.0	7	4	2	1
sums		327	83	177	67
ratio			1.23	2.64	1

Appendix D: Xt/+ x +/+ Litter Segregations

B.P.	litter no.	litter d.o.b.	total pups	male	female	male xt	male wt	female xt	female wt	total xt	total wt	comments
543	3	03.02.01	11	6	5	4	2	2	3	6	5	
544	3	02.02.01	11	6	5	3	3	5	0	8	3	
544	4	28.02.01	5	2	3	2	0	2	1	4	1	
544	5	21.03.01	10	5	5	3	2	5	0	8	2	
544	6	16.04.01	9	7	2	4	3	0	2	4	5	
547	2	19.03.01	11	8	3	6	2	3	0	9	2	1 missing
547	3	15.04.01	13	9	4	5	4	2	2	7	6	
550	1	16.03.01	8	0	8	0	0	5	3	5	3	
550	8	05.05.01	8	3	5	2	1	4	1	6	2	
550	7	22.07.01	7	5	2	3	2	1	1	4	3	
548	9	30.07.01	9							7	2	
549	6	03.08.01	7							4	3	
552	1	16.08.01	9	5	4	2	2	2	3	4	5	1 missing
553	1	15.08.01	8	3	5	1	2	2	3	3	5	
554	1	16.08.01	7	4	3	1	3	1	2	2	5	
547	0	11.08.01	7							5	2	
552	2	13.09.01	10	7	3	3	4	2	1	5	5	
553	2	12.09.01	11	4	7	2	2	4	3	6	5	
554	2	13.09.01	8	1	7	1	3	0	4	1	7	
551	3	07.10.01	11							6	5	
552	3	09.10.01	9							6	3	
554	3	14.10.01	9	4	5	4	0	1	4	5	4	
553	3	25.10.01	10	5	5	4	1	4	1	8	2	
555	1	26.10.01	6	2	4	0	2	3	1	3	3	
551	5	17.11.01	10	5	5	2	3	2	2	4	6	
552	4	03.11.01	8	3	5	2	1	1	4	3	5	
553	4	20.11.01	10	7	3	3	4	2	1	6	4	
554	4	12.11.01	7							3	4	
555	2	15.11.01	7	6	1	2	4	0	1	2	5	
557	1	06.12.01	8	6	2	5	1	1	1	7	1	
556	2	08.12.01	9							5	4	1 missing
552	5	11.12.01	12	7	5	5	2	1	4	6	6	
555	3	13.12.01	6	2	4	1	1	2	2	3	3	
553	5	17.12.01	8	1	7	1	3	4	0	4	4	
556	3	02.01.02	7							5	2	
557	2	03.01.02	10	5	5	5	0	2	3	7	3	1 missing
552	6	08.01.02	9	5	4	3	2	0	4	3	6	
555	4	10.01.02	8	4	4	1	3	1	3	2	6	
553	6	12.01.02	8	7	1	2	5	0	1	2	6	
556	4	26.01.02	9							6	3	
558	1	28.01.02	6							3	3	
557	3	30.01.02	9							4	5	
553	7	08.02.02	7							5	2	
555	5	08.02.02	6							4	2	
sums			378	144	131	82	67	64	61	210	168	
ratios										1.25	1	

Appendix E: Xt/+ x +/+ Litters Segregated by PTD

High PTD Pairs

B.P.	total xt	total wt
544	24	11
547	21	10
550	15	8
548	7	2
556	16	9
557	18	9
sums	101	49
expected	75	75

chi sqare p= 2.18E-05

total litters = 17
mean litter size = 8.8

No PTD Pairs

B.P.	total xt	total wt
543	6	5
549	4	3
552	27	30
553	34	28
554	11	20
551	10	11
555	14	19
558	3	3
sums	109	119
expected	114	114

chi sqare p= 0.507801

total litters = 27
mean litter size = 8.4

Appendix F: Immunocytochemistry Raw Data

Data from E14.5 Material

experiment	antibody	counter	phenotype	total cells	total pos.	fraction pos.
IM3	MAP2	PZ	Xt/Xt ctx	1816	565	0.311123348
IM3	MAP2	PZ	`+/+ ctx	2214	590	0.266485998
IM3	MAP2	PZ	`+/+ str	3165	1094	0.345655608
IM3	MAP2	JB	`+/+ str	350	76	0.217142857
IM3	b-tubiii	JB	Xt/Xt ctx	1230	241	0.195934959
IM3	b-tubiii	PZ	Xt/Xt ctx	1243	336	0.270313757
IM3	b-tubiii	JB	`+/+ ctx	883	186	0.210645527
IM3	b-tubiii	PZ	`+/+ ctx	1817	252	0.138690149
IM3	b-tubiii	JB	`+/+ str	2211	516	0.233378562
IM3	b-tubiii	PZ	`+/+ str	1203	468	0.389027431
IM3	MASH1	JB+PZ	Xt/Xt ctx	1585	150	0.094637224
IM3	MASH1	JB+PZ	+/+ str	1000	0	0
IM3	MASH1	JB+PZ	+/+ ctx	3065	371	0.121044046
IM3+EXP9	BrDU	JB+PZ	Xt/Xt ctx	4611	353	0.076556062
IM3+EXP9	BrDU	JB+PZ	+/+ ctx	4503	186	0.041305796
IM3+EXP9	BrDU	JB+PZ	+/+ str	4823	332	0.068836824

Data from E15.5 Material

experiment	antibody	counter	phenotype	total cells	total pos.	fraction pos.
IM1	MAP2	JB	Xt/Xt	962	252	0.261954262
IM2	MAP2	JB	Xt/Xt	1742	472	0.270952928
IM2	MAP2	PZ	Xt/Xt	3576	1570	0.439038031
IM1	MAP2	JB	Xt/+	1061	277	0.261074458
IM2	MAP2	JB	Xt/+	2953	734	0.248560786
IM2	MAP2	PZ	Xt/+	1180	426	0.361016949
IM2	MAP2	JB	`+/+	1194	306	0.256281407
IM2	MAP2	PZ	`+/+	3979	1602	0.402613722
IM2	b-tubiii	JB	Xt/Xt	1047	296	0.282712512
IM2	b-tubiii	PZ	Xt/Xt	2268	935	0.412257496
IM2	b-tubiii	JB	Xt/+	1890	400	0.211640212
IM2	b-tubiii	PZ	Xt/+	749	196	0.261682243
IM2	b-tubiii	JB	`+/+	677	148	0.218611521
IM2	b-tubiii	PZ	`+/+	1374	421	0.306404658
IM2	nestin	JB	Xt/Xt	1061	186	0.175306315
IM2	nestin	PZ	Xt/Xt	4452	1105	0.248203055
IM2	nestin	JB	Xt/+	1788	297	0.166107383
IM2	nestin	PZ	`+/+	4353	892	0.20491615
IM2	RC2	JB	Xt/Xt	677	74	0.109305761
IM2	RC2	PZ	Xt/Xt	4973	812	0.163281721
IM2	RC2	JB	Xt/+	941	128	0.136025505
IM2	RC2	JB	`+/+	611	77	0.126022913
IM2	RC2	PZ	`+/+	5441	914	0.167983827